RETINAL CHANGES IN NEUROLOGICAL DISEASES

EDITED BY: Yuyi You, Tim Magnus and Jianhai Du
PUBLISHED IN: Frontiers in Neuroscience

frontiers Research Topics

frontiers

ISSN 1664-8714
ISBN 978-2-88974-493-0
DOI 10.3389/978-2-88974-493-0

About Frontiers

Frontiers is more than just an open-access publisher of scholarly articles: it is a pioneering approach to the world of academia, radically improving the way scholarly research is managed. The grand vision of Frontiers is a world where all people have an equal opportunity to seek, share and generate knowledge. Frontiers provides immediate and permanent online open access to all its publications, but this alone is not enough to realize our grand goals.

Frontiers Journal Series

The Frontiers Journal Series is a multi-tier and interdisciplinary set of open-access, online journals, promising a paradigm shift from the current review, selection and dissemination processes in academic publishing. All Frontiers journals are driven by researchers for researchers; therefore, they constitute a service to the scholarly community. At the same time, the Frontiers Journal Series operates on a revolutionary invention, the tiered publishing system, initially addressing specific communities of scholars, and gradually climbing up to broader public understanding, thus serving the interests of the lay society, too.

Dedication to Quality

Each Frontiers article is a landmark of the highest quality, thanks to genuinely collaborative interactions between authors and review editors, who include some of the world's best academicians. Research must be certified by peers before entering a stream of knowledge that may eventually reach the public - and shape society; therefore, Frontiers only applies the most rigorous and unbiased reviews.
Frontiers revolutionizes research publishing by freely delivering the most outstanding research, evaluated with no bias from both the academic and social point of view. By applying the most advanced information technologies, Frontiers is catapulting scholarly publishing into a new generation.

What are Frontiers Research Topics?

Frontiers Research Topics are very popular trademarks of the Frontiers Journals Series: they are collections of at least ten articles, all centered on a particular subject. With their unique mix of varied contributions from Original Research to Review Articles, Frontiers Research Topics unify the most influential researchers, the latest key findings and historical advances in a hot research area! Find out more on how to host your own Frontiers Research Topic or contribute to one as an author by contacting the Frontiers Editorial Office: frontiersin.org/about/contact

RETINAL CHANGES IN NEUROLOGICAL DISEASES

Topic Editors:
Yuyi You, Macquarie University, Australia
Tim Magnus, University of Hamburg, Germany
Jianhai Du, West Virginia University, United States

Citation: You, Y., Magnus, T., Du, J., eds. (2022). Retinal Changes in Neurological Diseases. Lausanne: Frontiers Media SA. doi: 10.3389/978-2-88974-493-0

Table of Contents

05 ***Editorial: Retinal Changes in Neurological Diseases***
Samridhi Sharma and Yuyi You

07 ***Large-Area Photoreceptor Degeneration Model in Rabbits by Photocoagulation and Oxidative Stress in the Retina***
Zhexuan Wang, Chenli Feng, Ruyi Yang, Tingting Liu, Yin Chen, Aihua Chen, Biao Yan, Yuanzhi Yuan and Jiayi Zhang

19 ***Corrigendum: Large-Area Photoreceptor Degeneration Model in Rabbits by Photocoagulation and Oxidative Stress in the Retina***
Zhexuan Wang, Chenli Feng, Ruyi Yang, Tingting Liu, Yin Chen, Aihua Chen, Biao Yan, Yuanzhi Yuan and Jiayi Zhang

20 ***Foveal Remodeling of Retinal Microvasculature in Parkinson's Disease***
Ane Murueta-Goyena, Maitane Barrenechea, Asier Erramuzpe, Sara Teijeira-Portas, Marta Pengo, Unai Ayala, David Romero-Bascones, Marian Acera, Rocío Del Pino, Juan Carlos Gómez-Esteban and Iñigo Gabilondo

32 ***Brain and Retinal Abnormalities in the 5xFAD Mouse Model of Alzheimer's Disease at Early Stages***
Mengrong Zhang, Liting Zhong, Xiu Han, Guoyin Xiong, Di Xu, Sensen Zhang, Haiyang Cheng, Kin Chiu and Ying Xu

45 ***Optical Coherence Tomography and Visual Evoked Potentials as Prognostic and Monitoring Tools in Progressive Multiple Sclerosis***
Simone Guerrieri, Giancarlo Comi and Letizia Leocani

55 ***Retinal Diseases and Parkinson Disease: A Population-Based Study***
Po-Chih Chen, Chen-Chih Chung, Yun-Yung Cheng, Wan-Ting Chen, Chien-Tai Hong, Lung Chan and Li-Nien Chien

62 ***Characterizing the Retinal Phenotype of the Thy1-h[A30P]α-syn Mouse Model of Parkinson's Disease***
Lien Veys, Joyce Devroye, Evy Lefevere, Lien Cools, Marjan Vandenabeele and Lies De Groef

77 ***Retinal Vasculopathy in Alzheimer's Disease***
Haoshen Shi, Yosef Koronyo, Altan Rentsendorj, Dieu-Trang Fuchs, Julia Sheyn, Keith L. Black, Nazanin Mirzaei and Maya Koronyo-Hamaoui

90 ***Retinal Oxygen Metabolism and Haemodynamics in Patients With Multiple Sclerosis and History of Optic Neuritis***
Martin Kallab, Nikolaus Hommer, Andreas Schlatter, Gabriel Bsteh, Patrick Altmann, Alina Popa-Cherecheanu, Martin Pfister, René M. Werkmeister, Doreen Schmidl, Leopold Schmetterer and Gerhard Garhöfer

99 ***Role of Multifocal Visually Evoked Potential as a Biomarker of Demyelination, Spontaneous Remyelination, and Myelin Repair in Multiple Sclerosis***
Alexandr Klistorner and Stuart L. Graham

109 ***Conditional Deletion of Activating Rearranged During Transfection Receptor Tyrosine Kinase Leads to Impairment of Photoreceptor Ribbon Synapses and Disrupted Visual Function in Mice***
Wei-Hao Peng, Meng-Lin Liao, Wan-Chun Huang, Pei-Kang Liu, Sarah R. Levi, Yun-Ju Tseng, Chia-Ying Lee, Lung-Kun Yeh, Kuan-Jen Chen, Chung-Liang Chien and Nan-Kai Wang

frontiers in Neuroscience

EDITORIAL
published: 14 January 2022
doi: 10.3389/fnins.2021.813044

Editorial: Retinal Changes in Neurological Diseases

Samridhi Sharma[1] *and Yuyi You*[1,2]*

[1] *Faculty of Medicine, Health, and Human Sciences, Macquarie Medical School, Macquarie University, Sydney, NSW, Australia,* [2] *Department of Clinical Medicine, Save Sight Institute, University of Sydney, Sydney, NSW, Australia*

Keywords: retina, optic coherence tomography (OCT), neurodegenerating diseases, imaging, visual pathway, transsynaptic degeneration, non-invasive detection

Editorial on the Research Topic

Retinal Changes in Neurological Diseases

Evidently, retinal manifestations of structural and functional deterioration are interlinked with the development of neurodegenerative disorders. In addition, the presence of retinal vasculopathy is also tightly linked with cognitive deficits in Alzheimer disease (AD) patients and animal models summarized in a review by Shi et al. These retinal changes are clinically measurable using existing non-invasive techniques such as retinal amyloid imaging, pericyte imaging, optical coherence tomography-angiography (OCT-A), electroretinograms, and fundus imaging, and can be used to monitor disease activity of the brain. This prompts the question of whether monitoring retinal changes (functional, vascular, or structural) *via* non-invasive methods can be routinely deployed for the early diagnosis of neurodegenerative disorders. This theme—early detection of neurodegenerative disease by evaluating structural, functional, and vascular changes in the retina—runs through this issue. Zhang et al. establish that the retinal abnormalities in an AD mouse model (5XFAD) precede the abnormalities in the brain and therefore, could be used for AD diagnosis. The study shows that deposition of amyloid-β plaques leads to thickening of the retina with subsequently reduced light responses of retinal ganglion cells (measured with multielectrode-array recording), which is observed to occur before deterioration in cognitive behavior. Similar retinal pathology reflecting alterations in the brain is seen in Parkinson's disease (PD) in a population-based study conducted by Chen et al. They establish that the patients with PD are at higher risk of retinal diseases at the premotor stage than non-PD controls. However, no significant association was identified between optic nerve disease or glaucoma with PD in this study. The observation of retinal pathology reflecting changes in the brain can help serve as a pre-motor biomarker of PD especially if changes are captured by clinically available non-invasive methods. It was interesting to note in the study by Chen et al. that the effects of PD on retinal pathology were reversed after administration of dopamine supplements warranting a further investigation on the role of dopamine in retina revival and restoration.

In congruence to the correlation between retinal diseases and PD, foveal microvascular alterations are also observed in PD patients. Evaluation of the increasing vascular bed surrounding the foveal avascular zone using OCT-A can help to discriminate PD patients with mild cognitive impairment from controls as established by Murueta-Goyena et al. The result of this study also emphasizes the role of vascular pathophysiology in PD which awaits further exploration. Further, the potential of *in vivo* retinal fundus imaging using OCT to non-invasively evaluate vascular and structural changes along with the alterations of oxygen metabolism can be used to assess multiple sclerosis (MS)-related retinal pathology as shown by Kallab et al. The study establishes oxygen metabolism changes in the retina in MS eyes with a history of optic neuritis (ON), but whether these alterations are disease-specific or occur as a consequence of ON warrants further investigation.

OPEN ACCESS

Edited and reviewed by:
Mark P. Burns,
Georgetown University, United States

***Correspondence:**
Yuyi You
yuyi.you@gmail.com

Specialty section:
This article was submitted to Neurodegeneration, a section of the journal Frontiers in Neuroscience

Received: *11 November 2021*
Accepted: *29 November 2021*
Published: *14 January 2022*

Citation:
Sharma S and You Y (2022) Editorial: Retinal Changes in Neurological Diseases. Front. Neurosci. 15:813044. doi: 10.3389/fnins.2021.813044

This research topic collection presents the potential of using non-invasive investigation of retinal changes in predicting the onset of neurodegenerative diseases. These retinal changes may occur as a primary pathology or secondary outcome of transsynaptic changes in neurological disorders (Puthenparampil et al., 2017; Asanad et al., 2020; Sharma et al., 2021). The hierarchy of the visual system is linked with one synapse bridging the anterior and posterior ends of the visual pathway, presenting itself as a model that can be clinically monitored for neuro-structural, functional, and vascular changes in the retina reflecting analogous changes in the brain. A comprehensive review published on this subject by our group details existing clinical scenarios showing the transsynaptic changes in the retina that can be measured clinically to detect and monitor the spread of neurodegeneration (Sharma et al., 2021). The simple hierarchy of the visual pathway can help localize lesions in the posterior pathway for clinical differential diagnosis of neurological diseases. The underlying causes of transsynaptic degeneration are however unknown and offer an unexplored avenue for future research. Studies focused on understanding the cellular and molecular mechanisms driving transsynaptic degeneration in the visual system can help unravel the causes and potential therapeutic targets of neurodegenerative diseases. These investigations can be carried out on animal models described in this research topic collection employing the visual system as a model to understand the spread of neurodegeneration, synaptic dysfunction, and the transmission of β-amyloid and tau plaques in the retina from the brain.

In conclusion, advancements in clinical and lab-based imaging equipment offer easy evaluation of structural, functional, and vascular changes in the retina. Several recent articles have reviewed the potential role of novel retinal imaging techniques such as OCT-A and retinal vascular amyloid imaging in monitoring blood flow and metabolism changes in the retina under disease conditions (Gupta et al., 2021; Kashani et al., 2021; Shi et al.). These findings, however, must be validated by using histopathology to establish the specificity and sensitivity of these proposed imaging methods enabling accurate detection. Further, the clinical utility of retinal imaging in most neurodegenerative diseases is based on case studies and from cross-sectional data derived from subjects in advanced disease stages. This needs to be supplemented with large-scale cohort studies to establish the timeline of the changes in the brain and corresponding retinal changes during disease progression. While brain imaging will remain as a standard confirmatory test for the diagnosis of neurodegenerative diseases, retinal imaging has rapidly emerged as a promising clinical tool for non-invasive detection of disease-specific retinal pathology in numerous neurodegenerative disorders in the brain.

AUTHOR CONTRIBUTIONS

SS wrote the first draft of the manuscript. YY contributed to manuscript revision, read, and approved the submitted version. Both authors contributed to the article and approved the submitted version.

FUNDING

This work was funded by National Multiple Sclerosis Society (Grant no. RG-1907-34571).

REFERENCES

Asanad, S., Fantini, M., Sultan, W., Nassisi, M., Felix, C. M., Wu, J., et al. (2020). Retinal nerve fiber layer thickness predicts CSF amyloid/tau before cognitive decline. *PLoS ONE* 15:e0232785. doi: 10.1371/journal.pone.0232785

Gupta, V. B., Chitranshi, N., Den Haan, J., Mirzaei, M., You, Y., Lim, J. K., et al. (2021). Retinal changes in Alzheimer's disease- integrated prospects of imaging, functional and molecular advances. *Prog. Retin. Eye Res.* 82:100899. doi: 10.1016/j.preteyeres.2020.100899

Kashani, A. H., Asanad, S., Chan, J. W., Singer, M. B., Zhang, J., Sharifi, M., et al. (2021). Past, present and future role of retinal imaging in neurodegenerative disease. *Prog. Retin. Eye Res.* 83:100938. doi: 10.1016/j.preteyeres.2020.100938

Puthenparampil, M., Federle, L., Poggiali, D., Miante, S., Signori, A., Pilotto, E., et al. (2017). Trans-synaptic degeneration in the optic pathway. a study in clinically isolated syndrome and early relapsing-remitting multiple sclerosis with or without optic neuritis. *PLoS ONE* 12:e0183957. doi: 10.1371/journal.pone.0183957

Sharma, S., Chitranshi, N., Wall, R. V., Basavarajappa, D., Gupta, V., Mirzaei, M., et al. (2021). Trans-synaptic degeneration in the visual pathway: neural connectivity, pathophysiology, and clinical implications in neurodegenerative disorders. *Surv. Ophthalmol.* doi: 10.1016/j.survophthal.2021.06.001 [In Press].

Conflict of Interest: The authors declare that the research was conducted in the absence of any commercial or financial relationships that could be construed as a potential conflict of interest.

frontiers in Neuroscience

ORIGINAL RESEARCH
published: 10 June 2021
doi: 10.3389/fnins.2021.617175

Large-Area Photoreceptor Degeneration Model in Rabbits by Photocoagulation and Oxidative Stress in the Retina

Zhexuan Wang[1†], Chenli Feng[1†], Ruyi Yang[1†], Tingting Liu[2], Yin Chen[3], Aihua Chen[3], Biao Yan[1], Yuanzhi Yuan[1*] and Jiayi Zhang[1*]*

[1] State Key Laboratory of Medical Neurobiology, Department of Ophthalmology, MOE Frontiers Center for Brain Science, Zhongshan Hospital, Institutes for Brain Science, Fudan University, Shanghai, China, [2] Department of Ophthalmology, Eye and Ent Hospital of Fudan University, Shanghai, China, [3] Key Laboratory of Brain Functional Genomics, Primate Research Center, East China Normal University, Shanghai, China

OPEN ACCESS

Edited by:
Yuyi You,
Macquarie University, Australia

Reviewed by:
Ilaria Piano,
University of Pisa, Italy
Maria Giuseppina Miano,
Institute of Genetics and Biophysics (CNR), Italy

***Correspondence:**
Biao Yan
biaoyan@fudan.edu.cn
Yuanzhi Yuan
yuan.yuanzhi@zs-hospital.sh.cn
Jiayi Zhang
jiayizhang@fudan.edu.cn

[†] These authors have contributed equally to this work

Specialty section:
This article was submitted to Neurodegeneration, a section of the journal Frontiers in Neuroscience

Received: 14 October 2020
Accepted: 06 May 2021
Published: 10 June 2021

Citation:
Wang Z, Feng C, Yang R, Liu T, Chen Y, Chen A, Yan B, Yuan Y and Zhang J (2021) Large-Area Photoreceptor Degeneration Model in Rabbits by Photocoagulation and Oxidative Stress in the Retina. Front. Neurosci. 15:617175. doi: 10.3389/fnins.2021.617175

Photocoagulation is used for the treatment of retinal ischemic disease. However, due to the invasive nature of photocoagulation and variety of melanin concentrations between individuals, it is challenging to avoid damaging the adjacent photoreceptors and inducing several side effects. Previous studies indicate the role of laser power, duration, and spot size on retinal lesions, but the effect of interspot distance of the laser pulses needs to be considered in panretinal photocoagulation. In this study, we examine different parameters of photocoagulation on lesions of the retina in rabbit, finding that the lesion level of the outer nuclear layer of the retina depended on the pulse duration and laser spot size, and decreasing interspot distance could completely abolish the photoreceptor layer. The degeneration of the photoreceptor by photocoagulation occurred in 24 h and was not restored afterward. We then conducted panretinal photocoagulation in rabbit and found that oxidative stress was decreased in the inner nuclear layer of the retina, and pupillary light reflex and ERG signals were impaired. Our study could provide a rabbit model to explore the mechanism of photoreceptor degeneration and therapies for the side effects after photocoagulation.

Keywords: photocoagulation, light pupillary reflex, rabbit model, oxidative stress, electroretinography

INTRODUCTION

Retinal photocoagulation is considered a gold standard for the therapy of retinal ischemic disease, such as proliferative diabetic retinopathy and retinal vein occlusion (Reddy and Husain, 2018). During photocoagulation, laser light is absorbed by melanin in retinal pigment epithelium (RPE) cells and converted into heat, causing focal coagulation, necrosis, and hemostasis at RPE, Bruch's membrane (BM), and photoreceptor cells (Lock and Fong, 2011; Querques et al., 2018). Therefore, due to the invasive nature of photocoagulation, it also induces serious side effects, including central scotoma, permanent retinal scarring, and loss of visual field and night vision (Pender et al., 1981; Fong et al., 2007). There are some hypotheses offered to explain the mechanism of laser-induced retinal damage (LIRD), including reduction in oxygen consumption, photoablative debulking

of the retina by photocoagulation, and heat-shock protein (HSP) activation (Chhablani et al., 2018). A previous study shows that the RPE cell death after thermal irradiation may take time and mostly undergoes apoptosis, unless cells are immediately killed, but the cellular responses and therapeutic mechanisms are still unclear (Kern et al., 2018).

To minimize the side effects of photocoagulation, selective retinal therapy (SRT) was applied as a new therapeutic laser procedure for retinal diseases (Chhablani et al., 2018). SRT selectively targets RPEs and avoids thermal damage of the adjacent photoreceptors and choriocapillaris, which causes a high peak temperatures around the melanosomes and a low sublethal temperature increase in the adjacent tissue structures (Framme et al., 2004). However, because the melanin concentrations are different among patients or even in regions within an eye and the lesions in RPE are invisible through an ophthalmoscope (Weiter et al., 1986), localized SRT without excessive burning and collateral damage is still challenging. Previous studies indicate the role of laser power, duration, and spot size on retinal lesions (Jain et al., 2008), but during large-area photocoagulation, the effect of the interspot distance of the laser pulses needs to be considered. Meanwhile, the mechanism underlying photoreceptor degeneration after photocoagulation remains unclear. A proper animal model for studying cellular mechanisms would be helpful for further eliminating side effects by SRT.

Due to the convenience of generating transgenic animals, rodents seem to be a good animal model for studying the molecular and cellular mechanisms of photoreceptor degeneration by photocoagulation. However, the anatomical structure and size of human and rodent eyes are significantly different, preventing rodent models from further contributing to translational studies. The anatomy of eyes in nonhuman primates are very similar to that in humans, in particular, the existence of a macular structure, and translational studies often use nonhuman primates for electrophysiological and behavioral experiments (Nishida et al., 2010; Pennesi et al., 2012; Shirai et al., 2016). However, nonhuman primates are expensive and have a long breeding cycle. Despite the lack of macula, the size of eyeballs in rabbits is similar to that of humans (Kondo et al., 2009; Amirpour et al., 2012; Isago et al., 2013; Petrus-Reurer et al., 2018). The surgical tools for human patients in ophthalmology can be used directly in rabbit surgery (Petrus-Reurer et al., 2018), and fundus imaging and optical coherence tomography (OCT) for humans also enable monitoring of the rabbit retina over time (Plaza Reyes et al., 2016; Petrus-Reurer et al., 2017). Furthermore, rabbits are easy to breed and could be a good animal model in studying histological changes and mechanisms after photocoagulation.

In this study, we conducted different parameters of photocoagulation, including duration, spot size, and interspot distance of the laser pulses, and examined retinal lesions by histological approaches, electroretinography, and pupillary light reflex. We also examined the oxidative stress in the retina after photocoagulation at different time points. Our study provides a rabbit model to explore new mechanisms and therapies for the side effects after photocoagulation.

RESULTS

Visualization of Whitening Level and Lesioned Spot Size by Photocoagulation in Fundus Images

The lesion level of the retina in photocoagulation experiments depends on the laser power, pulse duration, spot size, and interspot distances. Previous studies indicate that 100 mW laser power causes retinal whitening but not a ring of edema in rabbits, correlating mainly with damage on the photoreceptors (Jain et al., 2008), so we used 100 mW laser power throughout the experiments. Each laser pulse resulted in a visible bright-color lesioned spot in the fundus images. Retinal whitening level and ring of edema size indicate the intensity of the lesion; increased retinal whitening and a larger ring of edema correspond to a more severe lesion (Jain et al., 2008). As shown in **Figure 1A**, the whitening level of the lesioned spot in the fundus images decreased as the laser spot size increased, indicating that the level of lesion decreased as the size of the laser spot increased. Similar results were obtained in other conditions with different pulse durations (30 ms in **Figure 1B** and 50 ms in **Figure 1C**). The size of the lesioned spot on the retina increased with increasing pulse duration for 200, 300, and 500 μm laser spots (**Figures 1A–D**). These results indicate that the whitening level and lesioned spot size on retinal by photocoagulation was inversely proportional to the size of the laser spot and proportional to the duration of the laser pulse.

The Degree of Retinal Damage Is Proportional to the Duration and Inversely Proportional to the Size of the Laser Spot

To confirm which parameters of photocoagulation induce photoreceptor degeneration, which means the lesioning of the outer nuclear layer (ONL) but not the inner nuclear layer (INL) or ganglion cell layer (GCL), we examined cross-sections of the retina 7 days after photocoagulation using Nissl staining (**Figure 2**). We found that a 200-μm, 20-ms-duration laser spot could induce severe damage of the ONL of the retina and disarrange the structure of the retina. However, when the diameter of the laser spot was 300 μm or 500 μm (100 mW, 20 ms duration), the ONL of the retina was scarcely damaged, and a 200-μm, 30-ms laser spot disrupted the layered structure of the retina, but a 300-μm, 30-ms or 500-μm, 30-ms laser spot only partially damaged the ONL, indicating that these conditions are not efficient for lesioning the entire ONL. Also, a 200-μm, 50-ms laser spot partially damaged the INL of the retina, suggesting that the retinal tissue was over-lesioned. However, the ONL of the retina was eliminated at 300 μm and 500 μm spots (100 mW, 50 ms) without INL damage. These results suggest that the lesion level of the ONL of the retina depends on the pulse duration and laser spot size, and 50 ms, 300 μm and 500 μm laser spots seem to damage the ONL completely but not the INL of the retina.

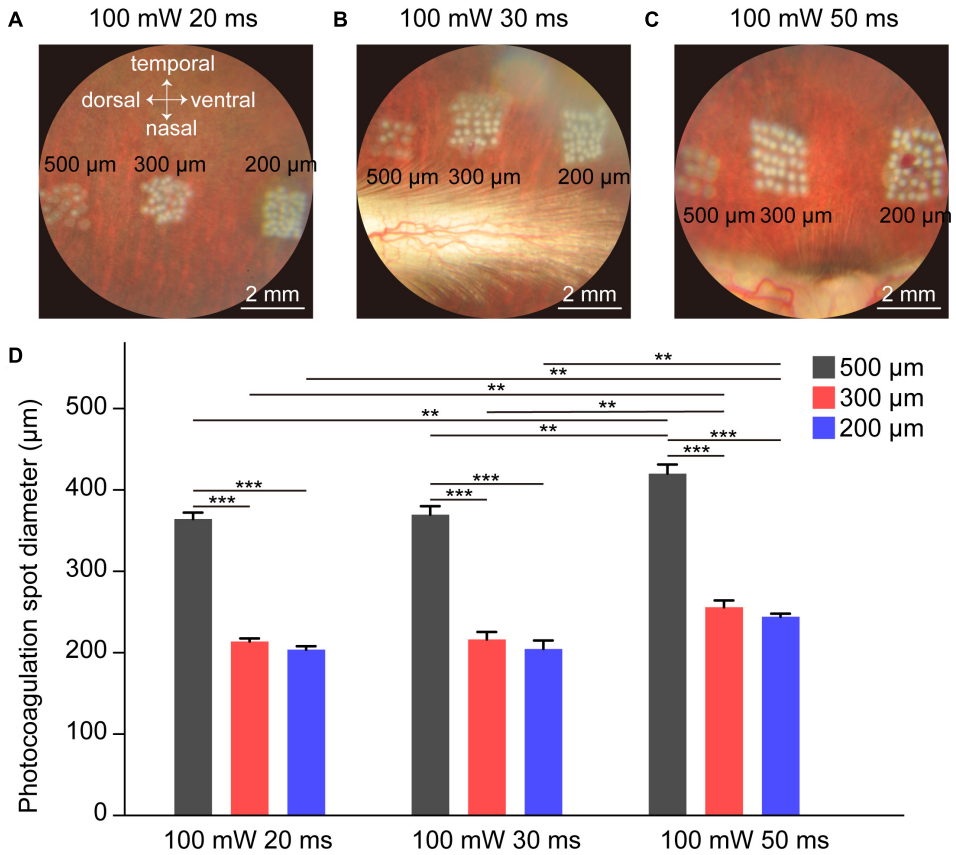

FIGURE 1 | Fundus images of rabbit retina under different photocoagulation conditions 1 h after surgery. **(A–C)** Fundus images of retina after photocoagulation of 200, 300, and 500 μm laser spot size produced by 100 mW laser power and 20 **(A)**, 30 **(B)**, or 50 ms **(C)** pulse duration. Scale bar = 2 mm. **(D)** Lesion diameter on retina by photocoagulation with 200, 300, or 500 μm laser spot size produced by 100 mW laser power and 20, 30, or 50 ms duration (number of spots: $n_{20\ ms/500\ \mu m}$ = 9, $n_{20\ ms/300\ \mu m}$ = 15, $n_{20\ ms/200\ \mu m}$ = 15, $n_{30\ ms/500\ \mu m}$ = 10, $n_{30\ ms/300\ \mu m}$ = 15, $n_{30\ ms/200\ \mu m}$ = 15, $n_{50\ ms/500\ \mu m}$ = 9, $n_{50\ ms/300\ \mu m}$ = 15, $n_{50\ ms/200\ \mu m}$ = 14, Each set of spots comes from one retina). Data were presented as Mean ± SEM. $^{**}P < 0.01$, $^{***}P < 0.001$.

Spatial Distance Between Laser Spots Affected Retinal Damage Level

To examine the photoreceptor degeneration level in the retina by large-area photocoagulation, we used laser spot arrays. Because the magnification of the rabbit eye was 0.66, the size of the laser spot at the retinal plane is different from the sizes of the lesion spots both from our own observation and in the literature (Blumenkranz et al., 2006; Framme et al., 2007). Hence, we next explored how the distance between laser spots affects retinal damage. In **Figure 3**, we conducted histologic analysis 7 days after the photocoagulation surgery using 100-mW laser spots with 50 ms (as used in **Figure 2**). In the first row of **Figure 3**, a 200-μm laser spot with a 0 or 50-μm interspot distance caused severe damage in the INL, ONL, and even GCL of the retina. However, when the interspot distances were increased to 100 or 150 μm, the ONL of the retina was not completely abolished. To optimize the lesion condition, we increased the spot diameter to 300 μm (50 ms duration). In the second row in **Figure 3**, photocoagulation with a 75-μm inter-spot distance led to the disruption of the layered structure in the INL. The level of lesions in the retina decreased with 150- and 225-μm inter-spot distances, but the effect of retinal damage is unstable. When the diameter of the laser spot increased to 500 μm with a 250- or 325-μm interspot distance, the ONL of the retina was not completely eliminated. Laser spots with 500 μm diameter and 0- or 125-μm inter-spot distance completely abolished the photoreceptor layer with intact INL and GCL.

Long-Term Elimination of Photoreceptor Layer by Photocoagulation in Rabbit Retina

We examined the retinal structure and cellular morphological changes after photocoagulation, and found that 1 day after photocoagulation, the photoreceptor of the retina was almost eliminated and the ONL exhibited sparse arrangement. Seven days after photocoagulation, photoreceptor cells were completely eliminated and ONL cells were intact (**Figure 4A**). These data suggest that the degeneration of photoreceptor cells occurred within 24 h after photocoagulation with a few cell remnants and degenerated completely 7 days after photocoagulation. We also used DHE staining to evaluate the level of oxidative stress in retina. For the control group, the DHE fluorescence could

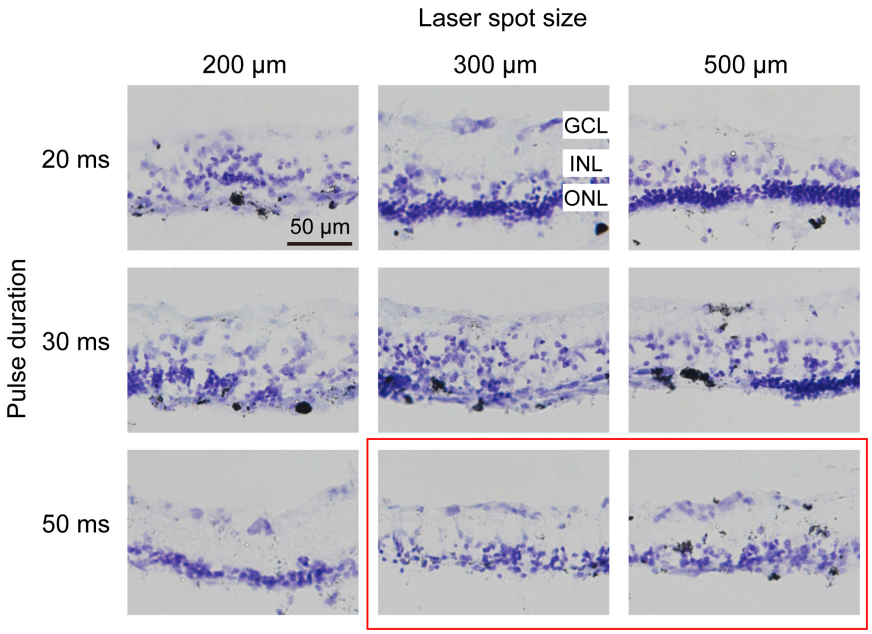

FIGURE 2 | Histomorphology of rabbit retinas 7 days after photocoagulation with 100 mW laser power. Nissl staining of rabbit retina with different pulse durations and laser spot sizes under 100 mW laser power. Each column corresponds to a constant laser spot size, and each row corresponds to a constant pulse duration. The better conditions are circled by the red box. GCL, ganglion cell layer; INL, inner nuclear layer; ONL, outer nuclear layer. Scale bar = 50 μm.

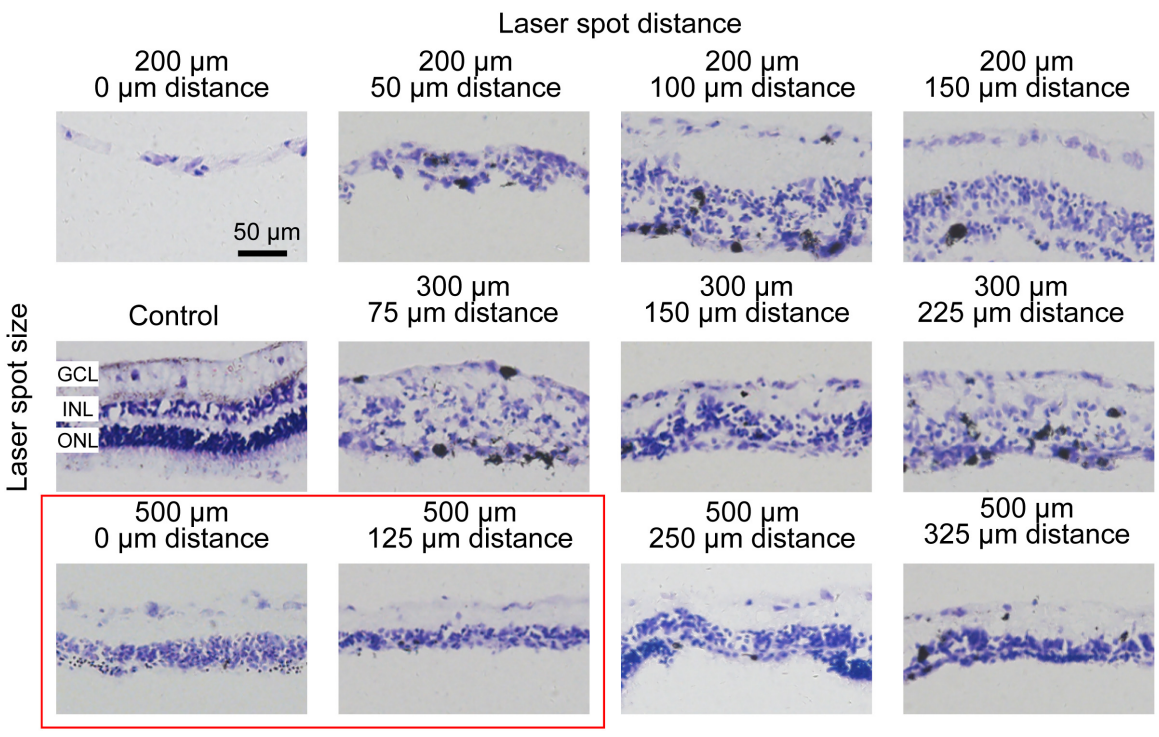

FIGURE 3 | Histomorphology of rabbit retinas 7 days after photocoagulation with 100 mW laser power and 50 ms pulse duration. Histologic images for different laser spot size and distance. The control picture is in the first column and second row. Except for the control picture, each row corresponds to a constant laser spot size, and each column to different laser spot distance. The better conditions are circled by the red box. GCL, ganglion cell layer; INL, inner nuclear layer; ONL, outer nuclear layer. Scale bar = 50 μm.

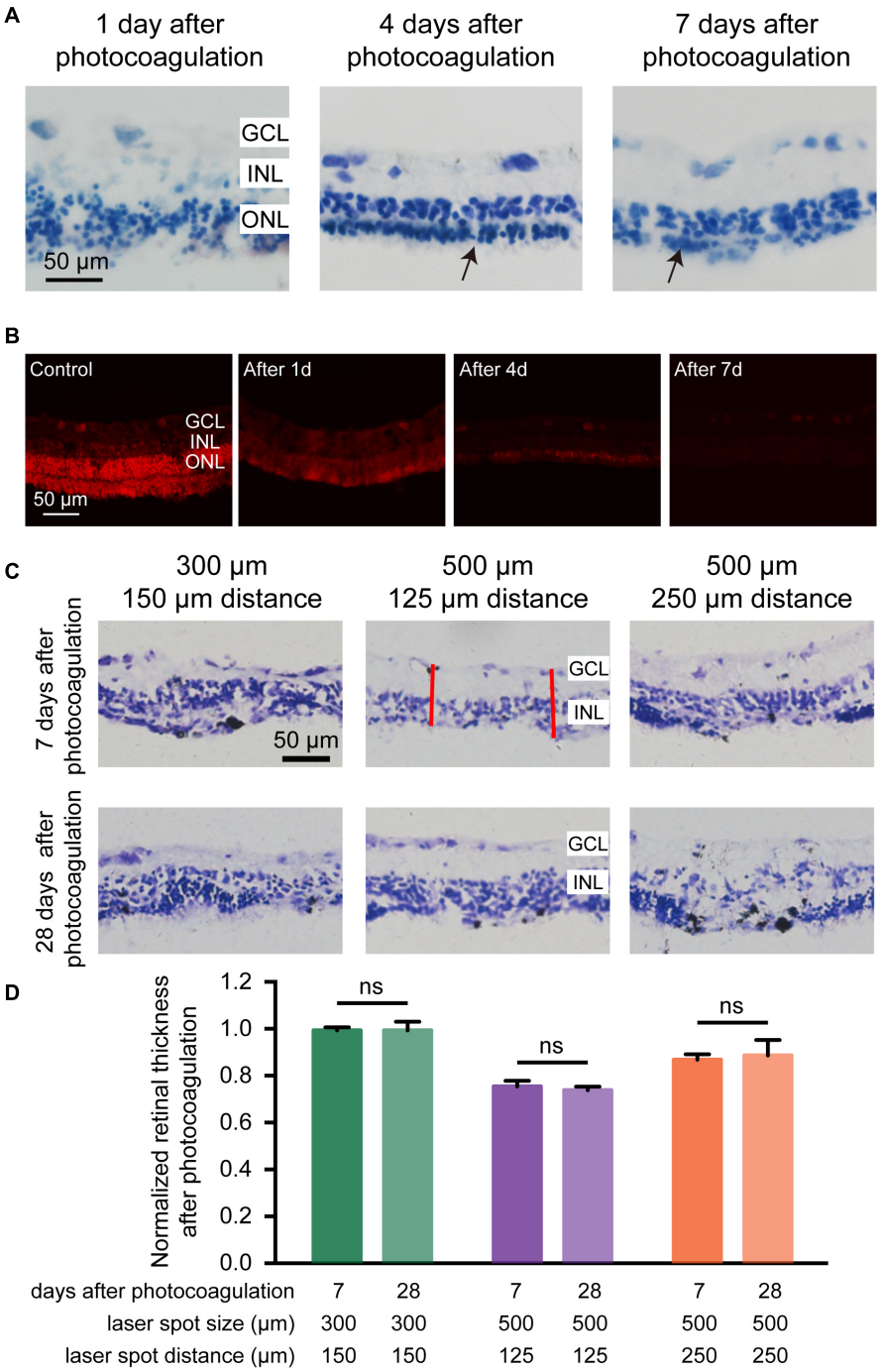

FIGURE 4 | Histomorphology of rabbit retinas and normalized retinal thickness after photocoagulation surgery. **(A)** Histologic images at 1, 4, and 7 days after photocoagulation with 100 mW laser power and 50 ms pulse duration. Histologic images for 500 μm laser spot size and 0 μm laser spot distance. The arrow points to the remnant cells of the ONL. Scale bar = 50 μm. **(B)** DHE staining of control retinal sections and local damage retinal sections at 1, 4, and 7 days after photocoagulation with 100 mW laser power and 50 ms pulse duration. Stained images for 500 μm laser spot size and 0 μm laser spot distance. Scale bar = 50 μm. GCL, ganglion cell layer; INL, inner nuclear layer; ONL, outer nuclear layer. **(C)** Histologic sections of rabbit retinas 7 and 28 days after photocoagulation with 100 mW laser power and 50 ms pulse duration. Histologic images for 300/150, 500/125, and 500/250 μm laser spot size/distance. GCL, ganglion cell layer; INL, inner nuclear layer. Scale bar = 50 μm. The red line represents two locations randomly taken in each section for measuring the thickness of the retina after photocoagulation in the photocoagulation area. **(D)** Normalized photocoagulation retinal thickness in different sections at 7 and 28 days after photocoagulation under the same conditions as in **(A)**. Normalized retinal thickness is the ratio between retinal thickness in photocoagulation area and retinal thickness in nonphotocoagulation area. (7 days after photocoagulation: $n_{300/150\ \mu m} = 8$ slices, $n_{500/125\ \mu m} = 8$ slices, $n_{500/250\ \mu m} = 6$ slices; 28 days after photocoagulation: $n_{300/150\ \mu m} = 5$ slices, $n_{500/125\ \mu m} = 6$ slices, $n_{500/250\ \mu m} = 4$ slices). Data were presented as Mean ± SEM.

be detected in the ONL, GCL, and photoreceptor layer. But the DHE fluorescence appeared decreased 1, 4, and 7 days after photocoagulation (**Figure 4B**), which was similar to the phenomena observed in a previous study (Saenz-de-Viteri et al., 2014). This might be due to the destruction of the mitochondria-rich photoreceptors by the laser treatment causing a decrease in oxygen consumption in the outer retina and allowing oxygen to diffuse from the choroidal circulation to the inner retina, decreasing oxidative stress in the ONL and INL.

We next examined the long-term effects of photocoagulation in the retina. We found that, in the 300-μm diameter/150-μm interspot distance group (100 mW power and 50 ms duration), the thickness of the retinas did not show significant differences between days 7 and 28, and part of the ONL can be observed 28 days after photocoagulation, indicating photoreceptors were not completely removed. In the 500-μm diameter/125-μm interspot distance group, the thicknesses of the retina were similar between days 7 and 28, and both showed abolished ONL and intact INL and GCL. In the 500-μm diameter/250-μm interspot distance group, there were still residual photoreceptors in the ONL on both days 7 and 28 (**Figures 4C,D**). These data suggest that laser pulses with 500-μm diameter and 125-μm interspot distance (100 mW power and 50 ms duration) induced stable photoreceptor degeneration.

Panretinal Photocoagulation in Rabbit Retina With Optimal Parameters

According to the results in **Figure 3**, the optimal parameters for selective damage of the ONL in the rabbit retina were 100 mW, 50 ms pulse duration, 500 μm diameter and 0–125 μm interspot distance. We further conducted photocoagulation on the entire rabbit retina using these parameters. Fundus images showed that the lesioned spots were all connected to each other 7 days after photocoagulation (**Figures 5A,B**). OCT images showed that the signals from the ONL of the rabbit retina were disturbed, but the signal of the INL and the GCL were relatively clear on day 7, indicating that most of the ONL was damaged (**Figures 5C,D**). As expected, Nissl staining showed that the ONL was almost abolished 7 days after photocoagulation (**Figures 5E,F**). The expression of cone outer segment marker PNA could not be observed in the photocoagulated retina, but PKC-α (bipolar cell marker) and ChAT (amacrine cell marker) immunochemistry signals were visible (**Figures 5G,H**). These results show that photocoagulation could induce selective elimination of photoreceptors over a large area.

Disrupted Pupillary Light Reflex and ERG Recording After Panretinal Photocoagulation

Finally, we examined the pupillary light reflex before and after lesions of panretinal photoreceptors by photocoagulation surgery. The pupil constriction ratio was reduced significantly after photocoagulation, indicating that the photoreceptor damage caused the decrease of light response (**Figures 6A,B**). To evaluate the function of retinal neurons after photocoagulation, we performed electroretinogram (ERG) recording at 1, 4, and 7 days after photocoagulation. In control eyes, we could record ERG signals, and the amplitudes of the a-wave has mean values of 261.76 ± 90.73 μV while the b-wave is 538.28 ± 55.71 μV. After photocoagulation, the amplitude of a- and b-waves significantly decreased 1 day after photocoagulation, and the patterns and amplitudes did not show significant changes from days 1 to 7 after photocoagulation (**Figures 6C,D**). These data suggest that the RPE-photoreceptor complex function of the rabbits was obviously damaged on the first day after photocoagulation, and the effect of photocoagulation with the parameters we used may be persistent and stable.

DISCUSSION

In this study, we examined different parameters of photocoagulation in rabbits, which can serve as an effective large animal model for studying cellular mechanisms that come into the retina after photoreceptor degeneration. Prior to the photocoagulation surgery, the laser power and pulse duration need to be calibrated to avoid fundus bleeding due to vascular rupture during the surgery. Consistent with previous results (Jain et al., 2008), the diameter of the lesion spot increases as the pulse duration increases. Jain et al. (2008) report that the diameter of the fundus image of the lesion is larger than the spot size of the laser beam at longer pulse durations.

The level of retinal damage in different rabbit strains could also vary with the same photocoagulation parameters. The most widely used rabbits are pigmented rabbits. McHugh et al. (1995) demonstrate that photocoagulation damage in pigmented rabbits is mainly caused by the absorption of laser energy by melanin in retinal pigment epithelium and choroidal melanocytes, and retinal damage by photocoagulation in albino rabbits is induced by multiple scattering together with absorption within hemoglobin and tissue water. Under the same photocoagulation condition, chorioretinal coagulation in albino rabbits was weaker than that in pigmented rabbits (McHugh et al., 1995). Longer duration and higher power were required to achieve the same coagulation effects in albino rabbits compared with pigmented rabbits (Obana and Miki, 1989). Therefore, the lesion threshold by photocoagulation was lower in pigmented rabbits than in albino rabbits. Moreover, intravenous dye injection, such as indocyanine green (ICG), can enhance the retinal damage level by photocoagulation in rabbits (Suh et al., 1991; Matsumoto et al., 1992). The albino rabbits need less time for recovery of the intraocular pressure after photocoagulation compared with pigmented rabbits (Schubert and Federman, 1989). Therefore, it is necessary to adjust the laser power, pulse duration, and spot size according to the rabbit breeds to achieve the ideal photocoagulation effects. Moreover, pigmented rabbits could effectively absorb laser energy and cause retinal damage, which is more suitable for establishing a rabbit model of photoreceptor damage.

The effectiveness of photocoagulation also depends on the age and metabolic state. Previous studies show that, with increasing age, RPE cells thicken and become heavily loaded with metabolic

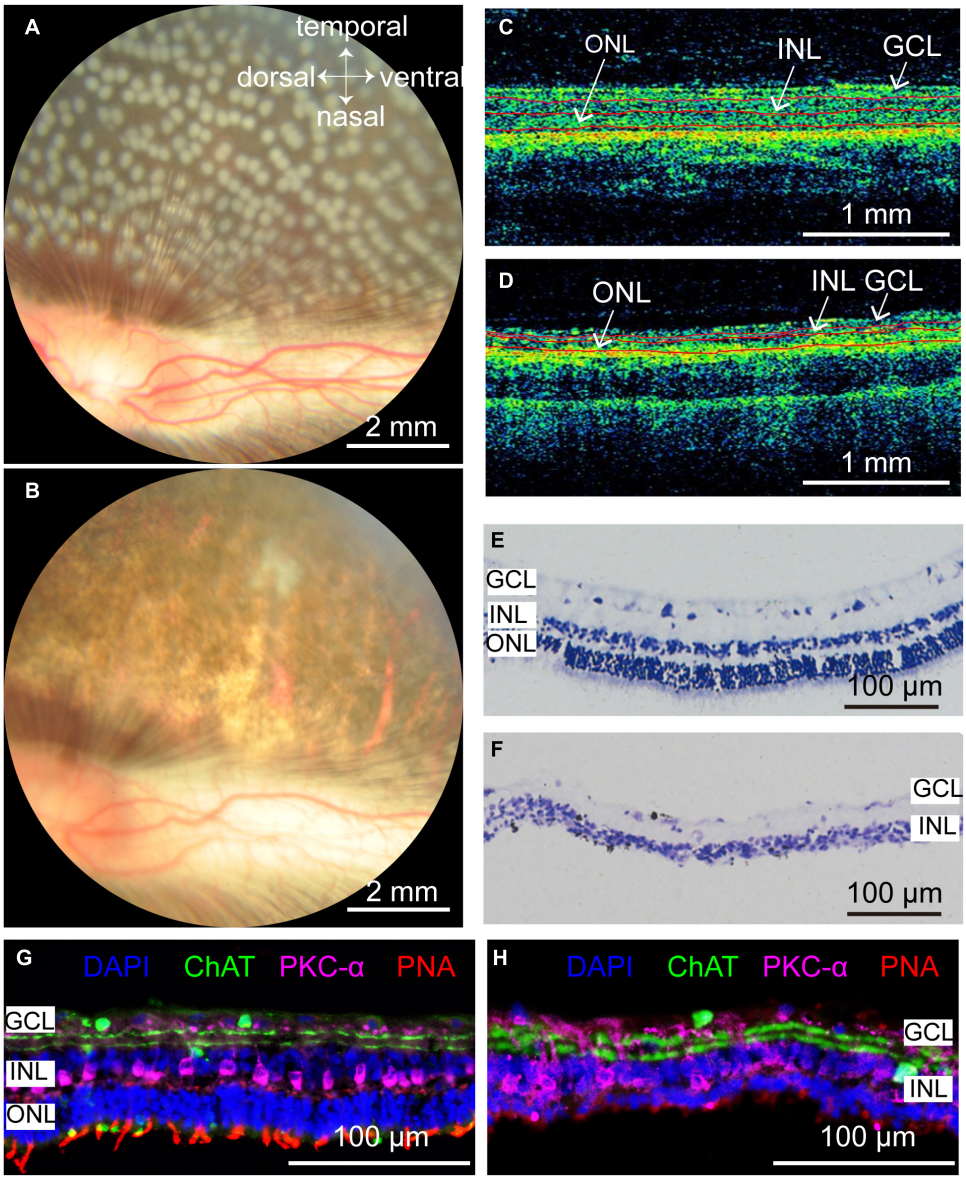

FIGURE 5 | Rabbit retinal photoreceptors across the entire retina were damaged by photocoagulation with 100 mW laser power, 50 ms pulse duration, and 500 μm laser spot size. **(A,B)** Fundus photographs of extensive damage of retinal photoreceptors at 1 h and 7 days after photocoagulation. Scale bar = 2 mm. **(C)** Control OCT image of rabbit retina. Scale bar = 1 mm. **(D)** Example of OCT image of rabbit retina at 7 days after photocoagulation. Scale bar = 1 mm. Red lines in **(C,D)** mark retina stratification. **(E,F)** Histomorphology of control rabbit retina **(E)** and rabbit retina 7 days after photocoagulation **(F)**. Scale bar = 100 μm. **(G,H)** Immunofluorescence staining of control rabbit retina **(G)** and rabbit retina 7 days after photocoagulation **(H)** with cone outer segments marker PNA, bipolar cell marker PKC-α and amacrine cell marker ChAT 7 days after photocoagulation. Scale bar = 100 μm. GCL, ganglion cell layer; INL, inner nuclear layer; ONL, outer nuclear layer.

fatty products (Schraermeyer and Heimann, 1999), and the content of soluble melanin in the pigment epithelium declined with age from 95 μg/mg in the 14–50 year age group to 22 μg/mg dry weight in the over 70 year age group (Schmidt and Peisch, 1986). However, the contents of melanin did not show significant differences between males and females in blue and brown eyes (Menon et al., 1992). Photocoagulation is widely used in the treatment of proliferative diabetic retinopathy. ROS was increased in the retina in diabetic mice compared with control mice, indicating that damage of the retina by photocoagulation might be more severe (Sasaki et al., 2010), and the proliferation and hexagonality of regenerating RPE cells were impaired after photocoagulation, and the regenerated RPE cells lost their original properties in diabetic mice compared with wild-type mice (Jang et al., 2019). Laser-induced choroidal neovascularization was reduced significantly in the laser-injured diabetic mice compared with the laser-injured control mice (Liu et al., 2018).

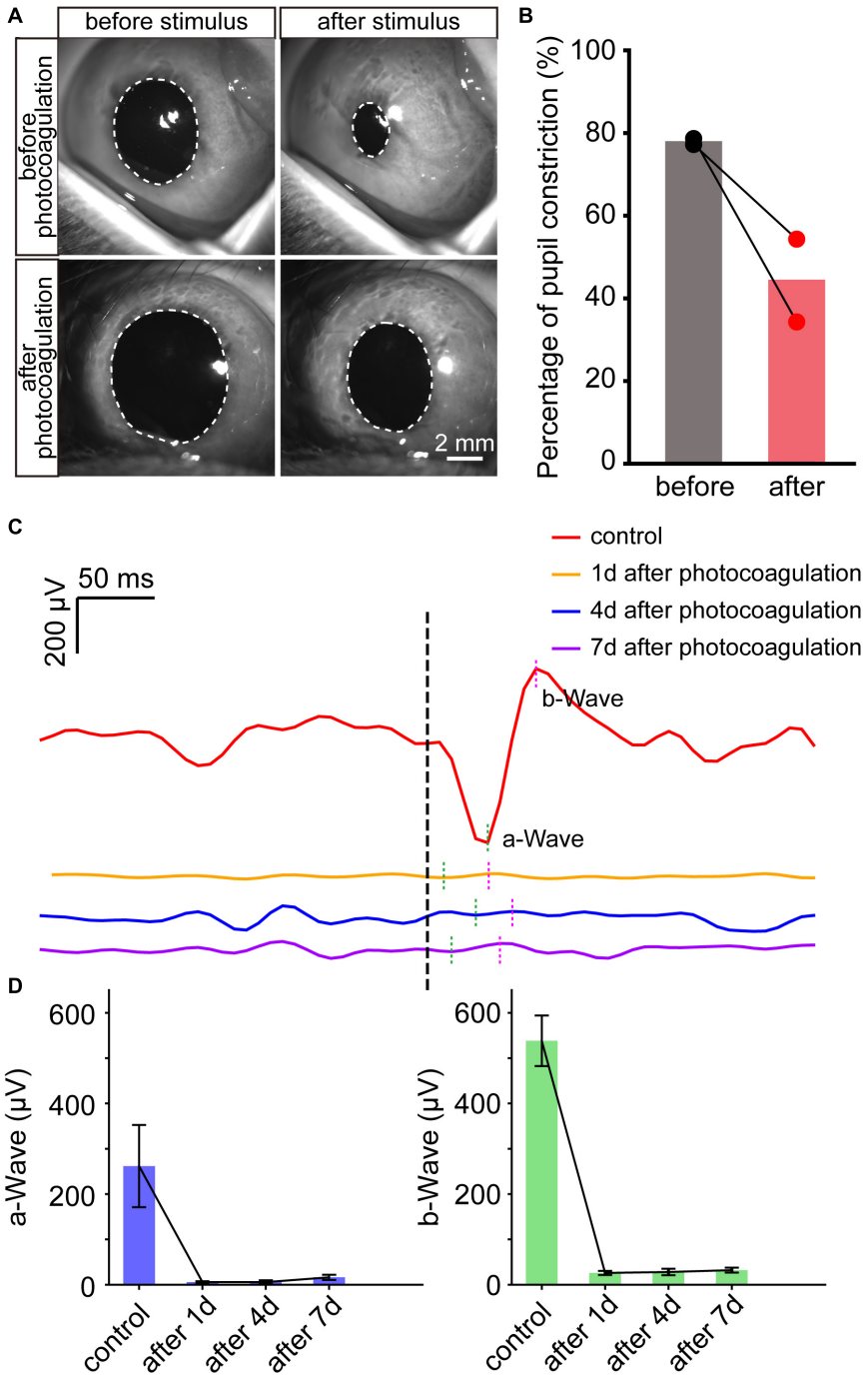

FIGURE 6 | The change of pupillary light reflex and ERG in rabbits before and after photocoagulation. **(A)** The example images of pupillary direct light reflex before (top row) and 3 days after photocoagulation (bottom row) of the same rabbit eye. The position of the white dotted circle is the pupil position. Scale bar = 2 mm. **(B)** Pupil constriction ratio before and 3 days after photocoagulation of rabbits. The pupil constriction ratio is calculated as $(S_0\text{-}S_{min}) / S_0 \times 100\%$, S_{min} is the minimum pupil area under light stimulation, and S_0 is the pupil area of the frame before light is given. **(C)** Sample waveforms of ERG before photocoagulation, 1, 4, and 7 days after photocoagulation. **(D)** Comparison of a- and b-wave amplitudes in eyes before photocoagulation and 1, 4, and 7 days after photocoagulation.

The model established by photocoagulation also has some limitations. First, this model of retinal damage is suitable for pigmented animals because laser light is mainly absorbed by melanin. The photoreceptor degeneration model established by photocoagulation is due to the trauma caused by laser impact, which is different from the progressive, hereditary pathological characteristics of RP and AMD as a result of genetic, environmental, or age-related degeneration. Moreover, the rods

gradually die after progressive atrophy in RP patients, which then leads to the death of the cones, but photocoagulation causes the death of the rods and cones simultaneously, and photocoagulation-induced retinal degeneration occurs almost quickly, which is different from the progressive loss of photoreceptors in retinal degenerative diseases. Due to these limitations of the photoreceptor degeneration model by photocoagulation, the model cannot be used to study the disease progression of typical retinal degenerative diseases, nor is it suitable for studying the treatment of gene therapy, drugs, and chronic nutrition. Nevertheless, this model still has certain actual uses. The model can be used to study the effectiveness of retinal prosthesis and stem cell therapy in photoreceptor degeneration disease, and it may also be used to study the mechanism of cell death caused by oxidative stress.

In transgenic rabbit models of photoreceptor degeneration, the thickness of the ONL of the transgenic rabbit started to decrease at 2 weeks of age. By 48 weeks of age, there was still a little residual ONL of the transgenic rabbit retina. Moreover, 12 out of 80 newborn rabbits are transgenic, and 10 out of 12 survive (Kondo et al., 2009). Hence, transgenic rabbit models are slow and costly. Ahn et al. (2019) establish a local retinal degeneration rabbit model by intravitreal injection of N-methyl-N-nitrosourea (MNU). In the high-dose injection group, loss of the photoreceptor layer occurred 1 month after the injection. However, without vitrectomy, the degree of retinal degeneration is unpredictable. In addition, vitrectomy causes around 30% incidence of cataract, further reducing the success rate. Intravenous injection of IAA in rabbits induced damage in the outer but not the inner segment of the photoreceptors (Yamauchi et al., 2011). In addition, the degree of degeneration was different among animals with the same IAA dose (Liang et al., 2008). In the current study, we demonstrate that the photoreceptor degeneration model established by photocoagulation can stabilize 7 days after surgery, requires no further invasive operations, and the area of degeneration can be precisely controlled.

In summary, we develop and evaluate a reproducible and low-cost photoreceptor degeneration rabbit model by laser photocoagulation, in which selective damage was made to retinal photoreceptors within 7 days. This model can be used to induce local or large-area photoreceptor lesions. Our studies shed light on a convenient model to test potential therapies and mechanisms of cell death for photoreceptor degeneration prior to nonhuman primate studies.

MATERIALS AND METHODS

Animals

A total of 20 healthy male adult Chinchilla Bastard rabbits were used in this study. The rabbits were obtained from Shanghai Songlian Laboratory Animal Co., Ltd. They were housed with a 12-/12-h light/dark cycle, and food and water were available ad libitum. The body weight of a rabbit is between 2.5 and 3.0 kg. All procedures were performed in accordance with the National Institutes of Health Guide for Care and Use of Laboratory Animals and were approved by Animal Care and Use Committee of Shanghai Medical College of Fudan University.

Photocoagulation

Rabbits were anesthetized by a mix of 3% isoflurane (RWD Life Science Co., Shenzhen, China) and oxygen in a gas chamber via a custom-made mask. The position of the rabbit was kept by a custom-made body support during surgery. Before the surgery, the rabbit pupil was fully dilated by two drops of 0.5% phenylephrine hydrochloride and 0.5% tropicamide ophthalmic solution for 20 min. All laser spots were delivered by VISULAS 532s (Carl Zeiss, Dublin, CA, United States) (laser power, 100–200 mW; pulse duration, 20–200 ms; laser spot diameter, 200–500 μm) and focused on the rabbit fundus by a contact lens (Ocular Mainster Focal/Grid Laser Lens, OMRA-S-2).

Fundus Photography and Optical Coherence Tomography

Color fundus photography (CFP) was obtained 1 h and 7 days after laser treatment to evaluate the effect of photocoagulation.

Optical coherence tomography images were obtained before and 7 days after laser treatment to evaluate changes in retinal structure with the Cirrus HD-OCT 4000 (Carl Zeiss Meditec, Inc., Dublin, CA, United States).

Retinal Histology

Rabbits were sacrificed with a lethal dose of sodium pentobarbital under deep anesthesia, and the eyeballs were enucleated afterward. The eye was dissected in Ringer's solution to keep cell viability. Retinal samples for DHE staining were incubated with DHE solution (5 μM) in a light-protected chamber at 37°C for 40 min and immersed for 5 min in 4% paraformaldehyde. Retinal samples for Nissl staining and immunostaining were immersed for 5 min in 4% paraformaldehyde. Then, the retina was dehydrated in graded sucrose solution and embedded in OCT compound (Sakura Finetek, United States). Retinas were sectioned into 14-μm-thick sections.

For immunohistochemistry study, slides were washed three times with 0.05 M tris buffer saline (TBS) for 15 min. After immersing slices in 0.5% Triton-X-100 for 20 min, the slides were incubated in a 10% Donkey serum (Jackson Immunoresearch, United States) blocking solution, with 1% bovine serum albumin (BSA) and 0.05% Triton-X-100. After being incubated with primary antibody (anti-choline acetyltransferase antibody, MILLIPORE (AB144P), 1:200; PNA, Vector (RL1072), 1:500; PKC alpha Monoclonal Antibody, ThermoFisher (MA1-157), 1:100) for 20 h at 4°C, the slides were washed four times for 15 min in 0.05 M TBS and incubated with secondary antibody for 1.5 h at room temperature. After washing the secondary antibody (Donkey anti-Goat conjugated to Alexa Flour 488, 1:200, Jackson ImmunoResearch, United States; Donkey anti-Mouse conjugated to Alexa Flour 647, 1:200, Jackson ImmunoResearch, United States) away with TBS, the slides were covered by 1:3000 DAPI (Sigma, United States) solution for 3 min and washed three times for 10 min with TBS. Finally, the slides were air-dried and cover-slipped.

For Nissl staining, sections washed twice for 2 min by double distilled water and then stained in 0.1 % cresyl violet solution, which was preheated to 37°C for 15 min. After that, the sides were washed in distilled water and differentiated in 30%, 70%, 95%, and absolute ethanol for 30 s, respectively. Finally, the slides were put in Xylol for 30 s and cover-slipped with neutral balsam immediately after air-drying.

For DHE staining, rabbits were anesthetized with isoflurane and then treated with enucleation of eye. The eyeball was dissected in oxygenated Ringer's solution (pH 7.35; oxygenated with 95% O_2 and 5% CO_2) to keep cell viability. Samples were incubated with DHE solution (Beyotime, Shanghai, China, 5 μM/L, dissolved with PBS) in a light-protected chamber at 37°C for 40 min and immersed in 4% formaldehyde for 5 min. For the retina slice staining, 10, 20, and 30% sucrose were used to dehydrate the fixed retina. The retina was embedded in OCT compound (Sakura) and stored at −80°C. Fourteen-micrometer slices were cut (Leica CM 1950, Lecia, Germany) and washed three times for 15 min with 0.05 M TBS to wash away OCT. Slices were air-dried and mounted. The DHE images were obtained by fluorescence imaging microscope (Eclipse Ni, Nikon Inc, Japan).

Pupillary Light Reflex

Rabbits were anesthetized by a mix of isoflurane and oxygen and followed with 30 min dim environment adaptation. Light stimuli provided by white LED was given to one eye and the pupil area was recorded with a near-infrared camera (JAI, Denmark). Each session was recorded for 30 s with a 10-Hz frame, and light stimulus were provided for 10–15 s when recording started for 5 s. Pupil area contraction percentage was calculated as (S0-Smin)/S0 × 100% (Smin: minimum pupil area during light stimulus; S0: pupil area during the dark environment).

ERG Recording

After general anesthesia, compound tropicamide eye drops (Santen Pharmaceutical Co., LTD, Shiga Plant, Japan) were instilled in rabbits' eyes to dilute the pupil, and 0.5% proparacaine hydrochloride eye drops (Alcon, Belgium) were used as corneal surface anesthesia. The circular corneal electrode was placed on the surface of the cornea of the rabbit, and the reference electrode of the silver needle was placed subcutaneously near the eye socket. The ground electrode of the silver needle was inserted subcutaneously into the back of the rabbit's ear. ERG signals were amplified by an amplifier (Brownlee Precision Model 410, United States) at 128 Hz, and bandpass filtered between 1 and 1000 Hz. Light stimuli was applied by white LED and controlled by self-written Arduino code. Each session contains 10 stimuli, which lasts for 200 ms and is separated by 10 to 15 s randomly. The rabbit's cornea was lubricated with 0.3% sodium hyaluronate eye drops (Santen Pharmaceutical Co., LTD, Shiga Plant, Japan) during recordings.

Data Analysis

The pixel size of the spot diameter and retina thickness were measured in imaging-editing software (Adobe Photoshop CC 2018). The pixel-to-μm scale was obtained from the camera manufacturer's software. For the length of spot diameter in the photocoagulation, eight more than clearly visible spots were chosen randomly. The maximum straight-line distance in each spot was manually marked, and the true distance was obtained according to the number of pixels. To calculate the thickness of the retina, two straight lines were manually marked at each region of photocoagulation and nonphotocoagulation, which were chosen randomly. Distance from the GCL to ONL in the nonphotocoagulation region was measured, and the distance from the GCL to the outer layer of the residual retina was measured in the photocoagulation region. The real thickness was estimated according to the mean number of pixels of the straight lines. The thickness of retina was normalized by the mean thickness of the nonphotocoagulation zone. Retinal thickness and spot diameter at each location were expressed as Mean ± Standard Error of Mean (SEM). The pupil area was measured by ImageJ (NIH, United States). Data were analyzed by GraphPad Prism software ver. 6.0c (GraphPad Software Inc., San Diego, CA, United States). P-values $< .05$ were considered statistically significant.

We used self-written python code to analyze the ERG data. The baseline of the ERG is the mean potential of the eye before stimuli during the dark adaption. The amplitude of a- and b-waves is measured from the baseline to the a-wave and the peak of a-wave to the peak of the b-wave, respectively. Each condition was repeated 10 times for each eye, and the average value was taken as the eye's results. We calculated the average values of three eyes from two rabbits as the final results in this experiment.

DATA AVAILABILITY STATEMENT

The original contributions presented in the study are included in the article/supplementary material, further inquiries can be directed to the corresponding author/s.

ETHICS STATEMENT

The animal study was reviewed and approved by Animal Care and Use Committee of Shanghai Medical College of Fudan University.

AUTHOR CONTRIBUTIONS

BY, AC, YY, and JZ conceived the experiments. ZW, CF, RY, YC, and TL conducted the experiments. TL, YC, AC, and YY participated in photocoagulation. CF did fundus photography and OCT scanning. ZW and RY conducted histologic analysis and pupillary light reflex test. ZW, RY, BY, and JZ wrote the manuscript. All authors contributed to the article and approved the submitted version.

FUNDING

This work was supported by the NSF of China (31771195 and 81790640), Shanghai Municipal Science and

Technology Major Project (No. 2018SHZDZX01), ZJLab Key Scientific Technological Innovation research project by Ministry of Education, and Shanghai Health and Family Planning Commission (20184Y0184), and Research and Development Fund of Zhongshan Hospital, 2020ZSFZ19 to CF.

REFERENCES

Ahn, S. M., Ahn, J., Cha, S., Yun, C., Park, T. K., Goo, Y. S., et al. (2019). Development of a Post-vitrectomy Injection of N-methyl-N-nitrosourea as a Localized Retinal Degeneration Rabbit Model. *Exp Neurobiol* 28, 62–73. doi: 10.5607/en.2019.28.1.62

Amirpour, N., Karamali, F., Rabiee, F., Rezaei, L., Esfandiari, E., Razavi, S., et al. (2012). Differentiation of human embryonic stem cell-derived retinal progenitors into retinal cells by Sonic hedgehog and/or retinal pigmented epithelium and transplantation into the subretinal space of sodium iodate-injected rabbits. *Stem Cells Dev.* 21, 42–53. doi: 10.1089/scd.2011.0073

Blumenkranz, M. S., Yellachich, D., Andersen, D. E., Wiltberger, M. W., Mordaunt, D., Marcellino, G. R., et al. (2006). Semiautomated patterned scanning laser for retinal photocoagulation. *Retina* 26, 370–376. doi: 10.1097/00006982-200603000-00024

Chhablani, J., Roh, Y. J., Jobling, A. I., Fletcher, E. L., Lek, J. J., Bansal, P., et al. (2018). Restorative retinal laser therapy: present state and future directions. *Surv. Ophthalmol.* 63, 307–328. doi: 10.1016/j.survophthal.2017.09.008

Fong, D. S., Girach, A., and Boney, A. (2007). Visual side effects of successful scatter laser photocoagulation surgery for proliferative diabetic retinopathy: a literature review. *Retina* 27, 816–824. doi: 10.1097/IAE.0b013e318042d32c

Framme, C., Alt, C., Schnell, S., Sherwood, M., Brinkmann, R., and Lin, C. P. (2007). Selective targeting of the retinal pigment epithelium in rabbit eyes with a scanning laser beam. *Invest Ophthalmol Vis Sci* 48, 1782–1792. doi: 10.1167/iovs.06-0797

Framme, C., Schuele, G., Roider, J., Birngruber, R., and Brinkmann, R. (2004). Influence of pulse duration and pulse number in selective RPE laser treatment. *Lasers. Surg. Med.* 34, 206–215. doi: 10.1002/lsm.20022

Isago, H., Sugano, E., Murayama, N., Tamai, M., and Tomita, H. (2013). Establishment of monocular-limited photoreceptor degeneration models in rabbits. *BMC Ophthalmol.* 13:19. doi: 10.1186/1471-2415-13-19

Jain, A., Blumenkranz, M. S., Paulus, Y., Wiltberger, M. W., Andersen, D. E., Huie, P., et al. (2008). Effect of pulse duration on size and character of the lesion in retinal photocoagulation. *Arch Ophthalmol* 126, 78–85. doi: 10.1001/archophthalmol.2007.29

Jang, S. Y., Cho, I. H., Yang, J. Y., Park, H. Y., Woo, S. E., Madrakhimov, S. B., et al. (2019). The retinal pigment epithelial response after retinal laser photocoagulation in diabetic mice. *Lasers Med Sci* 34, 179–190. doi: 10.1007/s10103-018-2680-9

Kern, K., Mertineit, C. L., Brinkmann, R., and Miura, Y. (2018). Expression of heat shock protein 70 and cell death kinetics after different thermal impacts on cultured retinal pigment epithelial cells. *Exp. Eye Res.* 170, 117–126. doi: 10.1016/j.exer.2018.02.013

Kondo, M., Sakai, T., Komeima, K., Kurimoto, Y., Ueno, S., Nishizawa, Y., et al. (2009). Generation of a transgenic rabbit model of retinal degeneration. *Invest Ophthalmol Vis Sci* 50, 1371–1377. doi: 10.1167/iovs.08-2863

Liang, L., Katagiri, Y., Franco, L. M., Yamauchi, Y., Enzmann, V., Kaplan, H. J., et al. (2008). Long-term cellular and regional specificity of the photoreceptor toxin, iodoacetic acid (IAA), in the rabbit retina. *Vis Neurosci* 25, 167–177. doi: 10.1017/S0952523808080401

Liu, G., Chen, L., Cai, Q., Wu, H., Chen, Z., Zhang, X., et al. (2018). Streptozotocininduced diabetic mice exhibit reduced experimental choroidal neovascularization but not corneal neovascularization. *Mol Med Rep* 18, 4388–4398. doi: 10.3892/mmr.2018.9445

Lock, J. H., and Fong, K. C. (2011). An update on retinal laser therapy. *Clin Exp Optom* 94, 43–51. doi: 10.1111/j.1444-0938.2010.00529.x

Matsumoto, M., Miki, T., Obana, A., Shiraki, K., and Suh, J. H. (1992). Indocyanine green enhanced photocoagulation in the pigmented rabbit. *Nippon Ganka Gakkai Zasshi* 96, 742–748.

McHugh, D., England, C., van der Zypen, E., Marshall, J., Fankhauser, F., and Fankhauser-Kwasnieska, S. (1995). Irradiation of rabbit retina with diode and Nd:YAG lasers. *Br J Ophthalmol* 79, 672–677. doi: 10.1136/bjo.79.7.672

Menon, I. A., Wakeham, D. C., Persad, S. D., Avaria, M., Trope, G. E., and Basu, P. K. (1992). Quantitative determination of the melanin contents in ocular tissues from human blue and brown eyes. *J Ocul Pharmacol* 8, 35–42. doi: 10.1089/jop.1992.8.35

Nishida, K., Kamei, M., Kondo, M., Sakaguchi, H., Suzuki, M., Fujikado, T., et al. (2010). Efficacy of suprachoroidal-transretinal stimulation in a rabbit model of retinal degeneration. *Invest. Ophthalmol. Vis. Sci.* 51, 2263–2268. doi: 10.1167/iovs.09-4120

Obana, A., and Miki, T. (1989). The effect of melanin and hemoglobin on the dye laser photocoagulation in pigmented and albino rabbits. *Nippon Ganka Gakkai Zasshi* 93, 844–851.

Pender, P. M., Benson, W. E., Compton, H., and Cox, G. B. (1981). The effects of panretinal photocoagulation on dark adaptation in diabetics with proliferative retinopathy. *Ophthalmology* 88, 635–638. doi: 10.1016/s0161-6420(81)34977-x

Pennesi, M. E., Neuringer, M., and Courtney, R. J. (2012). Animal models of age related macular degeneration. *Mol. Aspects Med.* 33, 487–509. doi: 10.1016/j.mam.2012.06.003

Petrus-Reurer, S., Bartuma, H., Aronsson, M., Westman, S., Lanner, F., André, H., et al. (2017). Integration of subretinal suspension transplants of human embryonic stem cell-derived retinal pigment epithelial cells in a large-eyed model of geographic atrophy. *Invest. Ophthalmol. Vis. Sci.* 58, 1314–1322. doi: 10.1167/iovs.16-20738

Petrus-Reurer, S., Bartuma, H., Aronsson, M., Westman, S., Lanner, F., and Kvanta, A. (2018). Subretinal transplantation of human embryonic stem cell derived-retinal pigment epithelial cells into a large-eyed model of geographic atrophy. *J. Vis. Exp.* 131:56702. doi: 10.3791/56702

Plaza Reyes, A., Petrus-Reurer, S., Antonsson, L., Stenfelt, S., Bartuma, H., Panula, S., et al. (2016). Xeno-free and defined human embryonic stem cell-derived retinal pigment epithelial cells functionally integrate in a large-eyed preclinical model. *Stem Cell Rep.* 6, 9–17. doi: 10.1016/j.stemcr.2015.11.008

Querques, G., Cicinelli, M. V., Rabiolo, A., de Vitis, L., Sacconi, R., Querques, L., et al. (2018). Laser photocoagulation as treatment of non-exudative age-related macular degeneration: state-of-the-art and future perspectives. *Graefes Arch Clin Exp Ophthalmol* 256, 1–9. doi: 10.1007/s00417-017-3848-x

Reddy, S. V., and Husain, D. (2018). Panretinal Photocoagulation: A Review of Complications. *Semin Ophthalmol* 33, 83–88. doi: 10.1080/08820538.2017.1353820

Saenz-de-Viteri, M., Heras-Mulero, H., Fernández-Robredo, P., Recalde, S., Hernández, M., Reiter, N., et al. (2014). Oxidative stress and histological changes in a model of retinal phototoxicity in rabbits. *Oxid Med Cell Longev* 2014, 637137. doi: 10.1155/2014/637137

Sasaki, M., Ozawa, Y., Kurihara, T., Kubota, S., Yuki, K., Noda, K., et al. (2010). Neurodegenerative influence of oxidative stress in the retina of a murine model of diabetes. *Diabetologia* 53, 971–979. doi: 10.1007/s00125-009-1655-6

Schmidt, S. Y., and Peisch, R. D. (1986). Melanin concentration in normal human retinal pigment epithelium. Regional variation and age-related reduction. *Invest Ophthalmol Vis Sci* 27, 1063–1067.

Schraermeyer, U., and Heimann, K. (1999). Current understanding on the role of retinal pigment epithelium and its pigmentation. *Pigment Cell Res* 12, 219–236. doi: 10.1111/j.1600-0749.1999.tb00755.x

Schubert, H. D., and Federman, J. L. (1989). A comparison of CW Nd:YAG contact transscleral cyclophotocoagulation with cyclocryopexy. *Invest Ophthalmol Vis Sci* 30, 536–542.

Shirai, H., Mandai, M., Matsushita, K., Kuwahara, A., Yonemura, S., Nakano, T., et al. (2016). Transplantation of human embryonic stem cell-derived retinal tissue in two primate models of retinal degeneration. *Proc. Natl. Acad. Sci. U. S. A.* 113, E81–E90. doi: 10.1073/pnas.1512590113

Suh, J. H., Miki, T., Obana, A., Shiraki, K., and Matsumoto, M. (1991). Effects of indocyanine green dye enhanced diode laser photocoagulation in non-pigmented rabbit eyes. *Osaka City Med. J* 37, 89–106.

Weiter, J. J., Delori, F. C., Wing, G. L., and Fitch, K. A. (1986). Retinal pigment epithelial lipofuscin and melanin and choroidal melanin in human eyes. *Invest. Ophthalmol. Vis. Sci.* 27, 145–152.

Yamauchi, Y., Agawa, T., Tsukahara, R., Kimura, K., Yamakawa, N., Miura, M., et al. (2011). Correlation between high-resolution optical coherence tomography (OCT) images and histopathology in an iodoacetic acid-induced model of retinal degeneration in rabbits. *Br J Ophthalmol* 95, 1157–1160. doi: 10.1136/bjo.2010.186718

Conflict of Interest: The authors declare that the research was conducted in the absence of any commercial or financial relationships that could be construed as a potential conflict of interest.

frontiers in Neuroscience

CORRECTION
published: 26 July 2021
doi: 10.3389/fnins.2021.738004

Corrigendum: Large-Area Photoreceptor Degeneration Model in Rabbits by Photocoagulation and Oxidative Stress in the Retina

Zhexuan Wang[1†], Chenli Feng[1†], Ruyi Yang[1†], Tingting Liu[2], Yin Chen[3], Aihua Chen[3], Biao Yan[1], Yuanzhi Yuan[1*] and Jiayi Zhang[1*]*

[1] State Key Laboratory of Medical Neurobiology, Department of Ophthalmology, MOE Frontiers Center for Brain Science, Zhongshan Hospital, Institutes for Brain Science, Fudan University, Shanghai, China, [2] Department of Ophthalmology, Eye and Ent Hospital of Fudan University, Shanghai, China, [3] Key Laboratory of Brain Functional Genomics, Primate Research Center, East China Normal University, Shanghai, China

Keywords: photocoagulation, light pupillary reflex, rabbit model, oxidative stress, electroretinography

OPEN ACCESS

Approved by:
Frontiers Editorial Office, Frontiers Media SA, Switzerland

***Correspondence:**
Biao Yan
biaoyan@fudan.edu.cn
Yuanzhi Yuan
yuan.yuanzhi@zs-hospital.sh.cn
Jiayi Zhang
jiayizhang@fudan.edu.cn

[†] These authors have contributed equally to this work

Specialty section:
This article was submitted to Neurodegeneration, a section of the journal Frontiers in Neuroscience

Received: *08 July 2021*
Accepted: *09 July 2021*
Published: *26 July 2021*

Citation:
Wang Z, Feng C, Yang R, Liu T, Chen Y, Chen A, Yan B, Yuan Y and Zhang J (2021) Corrigendum: Large-Area Photoreceptor Degeneration Model in Rabbits by Photocoagulation and Oxidative Stress in the Retina. Front. Neurosci. 15:738004. doi: 10.3389/fnins.2021.738004

A Corrigendum on

Large-Area Photoreceptor Degeneration Model in Rabbits by Photocoagulation and Oxidative Stress in the Retina

by Wang, Z., Feng, C., Yang, R., Liu, T., Chen, Y., Chen, A., et al. (2021). Front. Neurosci. 15:617175. doi: 10.3389/fnins.2021.617175

In the original article, we neglected to include the funder **Research and Development Fund of Zhongshan Hospital**, **2020ZSFZ19** to **Chenli Feng**.

In the published article, there was an error in affiliation **label for Zhexuan Wang, Chenli Feng and Ruyi Yang**. Instead of "**Zhexuan Wang[1,2†], Chenli Feng[1,2†], Ruyi Yang[1,2†]**", it should be "**Zhexuan Wang[1†], Chenli Feng[1†], Ruyi Yang[1†]**".

The authors apologize for this error and state that this does not change the scientific conclusions of the article in any way. The original article has been updated.

frontiers in Neuroscience

ORIGINAL RESEARCH
published: 12 July 2021
doi: 10.3389/fnins.2021.708700

Foveal Remodeling of Retinal Microvasculature in Parkinson's Disease

*Ane Murueta-Goyena[1,2], Maitane Barrenechea[3], Asier Erramuzpe[3], Sara Teijeira-Portas[1], Marta Pengo[4], Unai Ayala[3], David Romero-Bascones[3], Marian Acera[1], Rocío Del Pino[1], Juan Carlos Gómez-Esteban[1,5,6] and Iñigo Gabilondo[1,5,7]**

[1] Neurodegenerative Diseases Group, Biocruces Bizkaia Health Research Institute, Barakaldo, Spain, [2] Department of Preventive Medicine and Public Health, University of the Basque Country (UPV/EHU), Leioa, Spain, [3] Biomedical Engineering Department, Faculty of Engineering, Mondragon Unibertsitatea (MU-ENG), Mondragon, Spain, [4] Department of Molecular and Translational Medicine, University of Brescia, Brescia, Italy, [5] Neurology Department, Cruces University Hospital, Barakaldo, Spain, [6] Department of Neurosciences, University of the Basque Country (UPV/EHU), Leioa, Spain, [7] Ikerbasque: The Basque Foundation for Science, Bilbao, Spain

Background: Retinal microvascular alterations have been previously described in Parkinson's disease (PD) patients using optical coherence tomography angiography (OCT-A). However, an extensive description of retinal vascular morphological features, their association with PD-related clinical variables and their potential use as diagnostic biomarkers has not been explored.

Methods: We performed a cross-sectional study including 49 PD patients (87 eyes) and 40 controls (73 eyes). Retinal microvasculature was evaluated with Spectralis OCT-A and cognitive status with Montreal Cognitive Assessment. Unified PD Rating Scale and disease duration were recorded in patients. We extracted microvascular parameters from superficial and deep vascular plexuses of the macula, including the area and circularity of foveal avascular zone (FAZ), skeleton density, perfusion density, vessel perimeter index, vessel mean diameter, fractal dimension (FD) and lacunarity using Python and MATLAB. We compared the microvascular parameters between groups and explored their association with thickness of macular layers and clinical outcomes. Data were analyzed with General Estimating Equations (GEE) and adjusted for age, sex, and hypertension. Logistic regression GEE models were fitted to predict diagnosis of PD versus controls from microvascular, demographic, and clinical data. The discrimination ability of models was tested with receiver operating characteristic curves.

Results: FAZ area was significantly smaller in patients compared to controls in superficial and deep plexuses, whereas perfusion density, skeleton density, FD and lacunarity of capillaries were increased in the foveal zone of PD. In the parafovea, microvascular parameters of superficial plexus were associated with ganglion cell-inner plexiform layer thickness, but this was mainly driven by PD with mild cognitive impairment. No such associations were observed in controls. FAZ area was negatively associated with cognition in PD (non-adjusted models). Foveal lacunarity, combined with demographic and clinical confounding factors, yielded an outstanding diagnostic accuracy for discriminating PD patients from controls.

OPEN ACCESS

Edited by:
Yuyi You,
Macquarie University, Australia

Reviewed by:
Alessandro Arrigo,
San Raffaele Hospital (IRCCS), Italy
Dong Ho Park,
Kyungpook National University Hospital, South Korea

***Correspondence:**
Iñigo Gabilondo
igabilon@gmail.com

Specialty section:
This article was submitted to Neurodegeneration, a section of the journal Frontiers in Neuroscience

Received: *12 May 2021*
Accepted: *11 June 2021*
Published: *12 July 2021*

Citation:
Murueta-Goyena A, Barrenechea M, Erramuzpe A, Teijeira-Portas S, Pengo M, Ayala U, Romero-Bascones D, Acera M, Del Pino R, Gómez-Esteban JC and Gabilondo I (2021) Foveal Remodeling of Retinal Microvasculature in Parkinson's Disease. Front. Neurosci. 15:708700. doi: 10.3389/fnins.2021.708700

Conclusion: Parkinson's disease patients displayed foveal microvascular alterations causing an enlargement of the vascular bed surrounding FAZ. Parafoveal microvascular alterations were less pronounced but were related to inner retinal layer thinning. Retinal microvascular abnormalities helped discriminating PD from controls. All this supports OCT-A as a potential non-invasive biomarker to reveal vascular pathophysiology and improve diagnostic accuracy in PD.

Keywords: neurodegeneration, angiography, capillary, density, Parkinson's disease, retina, optical coherence tomography, biomarker

INTRODUCTION

Parkinson's disease (PD) is a progressive neurodegenerative disease characterized by motor impairment, including rest tremor, muscle rigidity, bradykinesia, and postural imbalance. The main hallmark of PD is the accumulation of anomalous α-synuclein deposits within neuronal cytoplasm, presumably resulting in profound loss of neurons, mainly of dopaminergic neurons (Lotharius and Brundin, 2002). The pathological features of PD have also been observed in postmortem retinas (Ortuno-Lizaran et al., 2018), and several *in vivo* cross-sectional studies have reported reduced retinal thickness in PD by means of optical coherence tomography (OCT) (Chrysou et al., 2019). Retinal atrophy seems to be specific to the inner retinal layers, concretely, to macular ganglion cell-inner plexiform complex (GCIPL) around the fovea (Murueta-Goyena et al., 2019), where the largest amount of retinal dopaminergic cells is found (Ortuño-Lizarán et al., 2020). The GCIPL thinning is significantly more pronounced in PD patients over time compared to controls (Murueta-Goyena et al., 2021), but it is present from prodromal stages (Lee et al., 2019a,b), suggesting that an early but active neurodegeneration takes place in PD retina (Murueta-Goyena et al., 2021).

Previous publications have indicated that, in addition to neurodegeneration, the vascular component might be a key contributing factor to the pathogenesis and progression of PD (Bradaric et al., 2012; Guan et al., 2013; Yang et al., 2015). In fact, brain autopsies of PD patients have revealed capillary disruption (Guan et al., 2013), angiogenesis (Bradaric et al., 2012), and small vessel degeneration in substantia nigra, middle frontal cortex and brainstem nuclei (Yang et al., 2015). It has been suggested that retinal vasculature shows similarities with cerebral microcirculation and can be therefore used as a surrogate marker of cerebral microvascular pathology (Patton et al., 2005). Within the retina, blood flow to inner retinal layers comes from capillaries derived from the central retinal artery, whereas outer retinal layers are supplied by choroidal vasculature. Recent advances in OCT technology allow the visualization of retinal vasculature using non-invasive, depth-selective, and high-resolution images. OCT angiography (OCT-A) detects blood flow down to the capillary level by measuring changes in OCT signal in consecutive cross-sectional images taken at the same location and allows a three-dimensional mapping of retinal microvasculature. Studying the morphometric variations of capillary networks in PD might provide key information about the regional neuronal structure, and the basis for investigating retinal vascular morphological features as potential biomarkers of cerebral microcirculation in PD. Although to date few studies have explored retinal vascular alterations in PD using OCT-A, the observations so far support the view that retinal vascular alterations are present in PD (Kromer et al., 2016; Kwapong et al., 2018; Rascunà et al., 2020; Shi et al., 2020; Zou et al., 2020; Robbins et al., 2021).

On the other hand, the relationship between cerebral small vessel disease and cognitive decline is well-established (Zanon Zotin et al., 2021). In PD, cognitive impairment is present in 15 to 40% of patients at diagnosis or early stages of the disease (Aarsland et al., 2009; Pfeiffer et al., 2014), and about 80% of PD patients will progress to dementia, but the rate of disease progression is not uniform across patients (Aarsland et al., 2017). Recent evidence shows that subjects with mild cognitive impairment (MCI) display retinal vascular network impairment (Chua et al., 2020; Criscuolo et al., 2020; Shin et al., 2021). Similarly, it seems that PD patients with GCIPL atrophy might constitute a clinical endophenotype with more pronounced cognitive impairment and worse prognosis (Murueta-Goyena et al., 2019, 2021). However, the relationship between the cognitive status, retinal microvascular parameters and retinal layer thicknesses has not been fully explored in PD patients.

In this study, we aimed to extensively describe retinal vascular morphometric parameters in PD patients using high-resolution Spectralis OCT-A images, in order to verify the presence of microvascular abnormalities in PD compared to controls or specific alterations in PD-MCI compared to PD patients with normal cognition. We also evaluated the association of retinal microvascular parameters with retinal thickness measurements and disease-related clinical variables. Finally, we assessed the diagnostic accuracy of retinal microvascular parameters alone or in combination with the thickness of retinal layers to differentiate PD patients from controls.

MATERIALS AND METHODS

Design and Participants

55 patients with Parkinson's disease (105 eyes) and 48 controls (95 eyes) were initially recruited for the present cross-sectional study from June 2020 to March 2021. We included individuals aged 40 years or older. PD patients were recruited through the outpatient neurology department at Cruces University Hospital and fulfilled PD Parkinson's UK Brain Bank criteria for the

diagnosis of PD before enrollment. Demographic data, disease onset, disease severity and type and dosage of dopaminergic treatment were collected. One experienced neurologist in the field of movement disorders recorded disease onset, Unified Parkinson's Disease Rating Scale (UPDRS) score, and calculated Levodopa Equivalent Daily Dose (LEDD). All patients were studied in an on-state of medication. Control individuals without PD or a history or symptoms of other neurological conditions were also enrolled in the study. Montreal Cognitive Assessment (MoCA) was administered to all participants to evaluate general cognition. A cutoff of 24 was established for determining MCI in this Spanish population (Milani et al., 2018).

All participants completed a comprehensive questionnaire on current comorbidities to check for the following systemic exclusion criteria: severe smoking (>20 cigarettes/day), heavy alcohol use (>4 drinks/day for men or >3 drinks/day for women), diagnosis of any type or grade of diabetes, uncontrolled or resistant elevated blood pressure, history of consumption of drugs or medications known to induce retinal toxicity or cognitive impairment, chronic inflammatory systemic diseases (e.g., lupus erythematosus, sarcoid, Bechet disease), history of brain trauma or central nervous system diseases different from PD. Participants with well-controlled hypertension without complications were included in the study.

PD patients and controls underwent a complete ophthalmologic examination including pupillary reflexes, refraction, visual acuity, color discrimination, slit lamp examination, and spectral domain OCT. Spherical equivalent refractive error above 4.00 diopters or more than 3.00 diopters of astigmatism or any ocular or systemic pathological condition, except PD, influencing retinal OCT measures were considered exclusion criteria. OCT-A images with visually identifiable motion artifacts or incomplete acquisitions were excluded from the analyses.

The study protocol was approved by the regional Basque Clinical Research Ethics Committee. All participants gave written informed consent prior to their participation in the study, in accordance with the tenets of the Declaration of Helsinki.

Spectral Domain Optical Coherence Tomography (OCT)

Macular retinal thickness was assessed using the Spectralis spectral-domain OCT system (HRA2 Acquisition Module version 6.16.6.0, Heidelberg Engineering, Heidelberg, Germany). Macular volumetric scans consisted of 25 single horizontal axial scans (B-scans) covering a 20° × 20° area, with 512 A-scans per B-scan and 49 frames averaged per B-scan. Layer segmentation of the OCT data was performed with the built-in software. All OCT images fulfilled quality control criteria from OSCAR-IB consensus (Tewarie et al., 2012), accounting for Obvious problems (O), poor Signal strength (S), Centration of scan (C), Algorithm failure (A), Retinal pathology other than PD-related (R), Illumination (I), and Beam placement (B).

Macular volumetric scans were exported in raw format (*.vol) and imported into MATLAB 2018b and 2019b (Mathworks, Natick, MA, United States) using the openVolFast.m function of the AURA tools software (Lang et al., 2013). The central point of the macula was determined as the point of minimum thickness after smoothing the thickness map with a circular kernel of 0.05 mm radius (foveaFinder.m function of AURA tools). The thickness values derived from the acquired raster pattern were resampled to a regular grid using cubic interpolation and 0.02 mm spacing between adjacent points. Then, the average thickness within the foveal zone (central 1-mm diameter disc) and parafoveal area (2.5-mm diameter ring adjacent to the foveal zone) were computed by averaging the point-by-point thicknesses in each sector.

The foveal and parafoveal thicknesses were calculated for the following layer complexes: total retinal thickness (Retina), macular nerve fiber layer (mRNFL), ganglion cell-inner plexiform complex (GCIPL), inner nuclear layer (INL), outer plexiform-Henle fiber-outer nuclear layer (OPL-ONL), and the complex including external limiting membrane and photoreceptor inner and outer segments (ELM-IS/OS) (**Figure 1**).

Spectral Domain Optical Coherence Tomography Angiography (OCT-A)

High-resolution acquisition was performed with Spectralis OCT Angiography Module (Heidelberg Engineering, Germany) which offers a lateral resolution of 5.7 μm and an axial resolution of 3.9 μm per pixel, using a scanning area of 10° × 10° and 512 A-scans per B-scan. TruTrack Active Eye Tracking was used to avoid motion artifacts. Superficial and deep vascular plexus complexes of the macula were investigated [superficial vascular complex (SVC) located between the ganglion cell layer and the inner mid-part of inner plexiform layer and deep vascular complex (DVC) located between the outer mid-part of inner plexiform layer and outer plexiform layer]. *En face* images were exported from Spectralis and stored as 768 × 768 pixels jpeg images.

OCT-A Image Processing

MATLAB 2018b and 2019b and Python (v3.8.5) were used to develop image analysis and parameter extraction algorithms. For vascular and foveal feature extraction, *en face* OCT-A images were first cropped to remove the SLO funduscopic image of the periphery. Then, OCT-A images were scaled using X and Y axis scaling parameters from Spectralis OCT-A to obtain images of 1:1 pixel:μm correspondence. We defined the foveal zone as the central 1-mm disc, and the parafovea as the ring surrounding the foveal zone, with an outer diameter of 2.5 mm. The center of the inner 1-mm diameter circle and outer 2.5 mm diameter ring was the centroid of the FAZ in DVC, i.e., the same center location was used in SVC and DVC for calculating microvascular parameters in different concentric regions (**Figure 1**).

For microvascular parameter extraction, OCT-A images were first enhanced using median filtering and later processed with a top-hat filter to improve the contrast in the image. The images were binarized using adaptive thresholding. In SVC, a separate binarization algorithm was applied based on Otsu's threshold to segment large blood vessels. By subtracting large

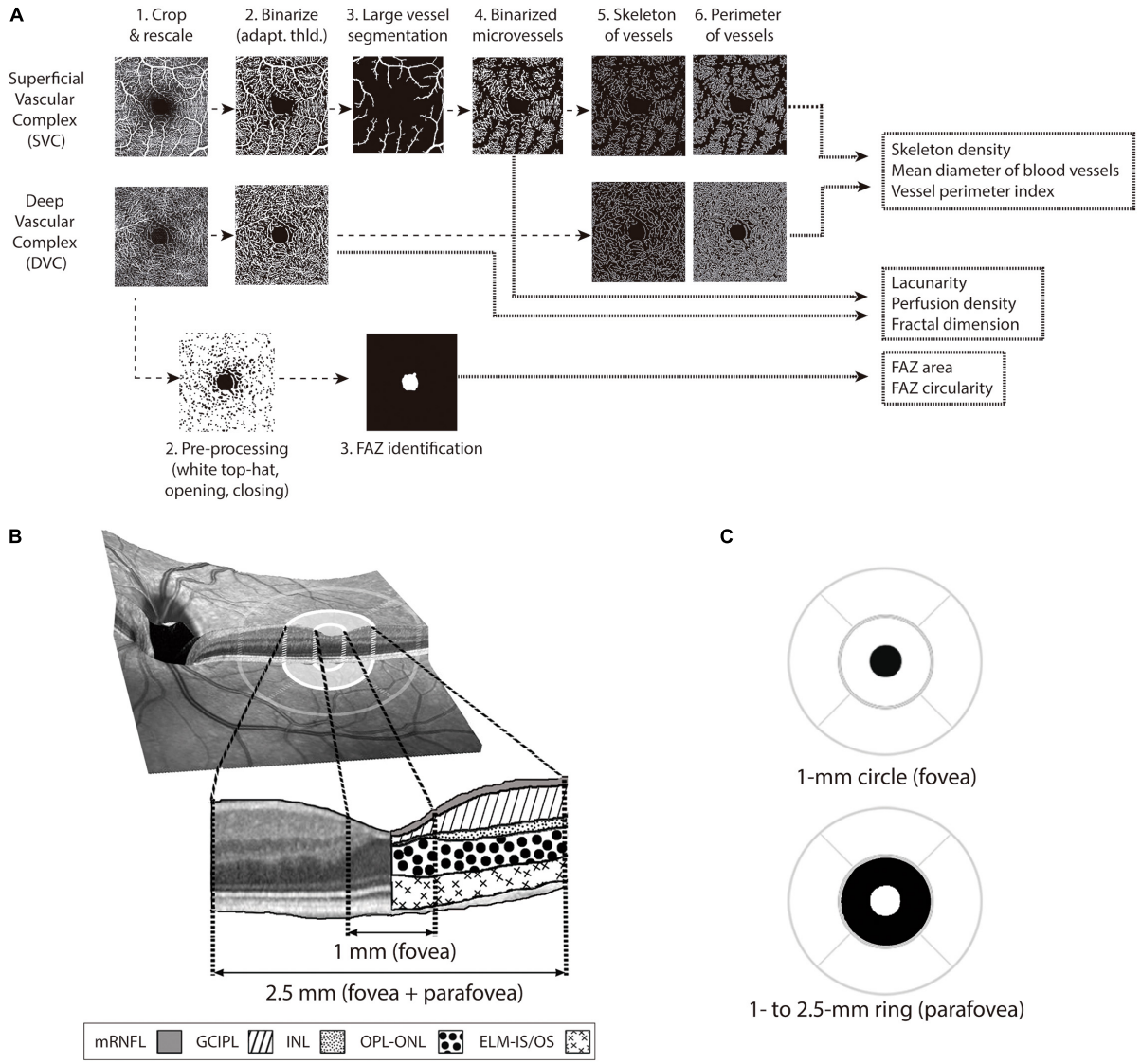

FIGURE 1 | OCT-A image processing pipeline and evaluated retinal layers and regions for OCT and OCT-A images. The analysis protocol of the OCT-A images **(A)** was different for the superficial vascular complex (SVC) and for the deep vascular complex (DVC) (see "Materials and Methods" for more details). Both SVC and DVC images were cropped & rescaled (1) and binarized with an adaptive threshold ("adapt. thld.") (2). In SVC images, after being binarized, the large vessels were segmented (3) and the microvessels were binarized (4). With binarized SVC microvessel and binarized DVC images, images for vessel skeleton (5) and perimeters (6) were obtained. From the vessel skeleton images, the "skeleton density" was quantified, from vessel perimeter images the "vessel perimeter index" was computed and from the combination of vessel skeleton and perimeter images, the "mean diameter of blood vessels" was computed. From the binarized images of SVC and DVC, the parameters "Lacunarity," "Perfusion density," and "Fractal dimension" were calculated. Finally, the cropped & rescaled DVC images were pre-processed with white top-hat and opening/closing to segment the foveal avascular zone (FAZ) mask, from which "FAZ area" and "FAZ circularity" were computed. The layers of the retina that were segmented from the OCT images **(B)** were macular retinal nerve fiber layer (mRNFL), ganglion cell-inner plexiform layer complex (GCIPL), inner nuclear layer (INL), outer plexiform layer, Henle fibers, and outernuclear layer complex (OPL-ONL) and the complex including external limiting membrane and internal andouter segments of photoreceptors (ELM-IS/OS). The mean thickness of the mentioned layers was obtained for two macular regions **(B,C)**: the foveal region (central circle of 1 mm in diameter) and the parafoveal ring (centered in the fovea and delimited by circles with an inner diameter of 1-mm and outer diameter of 2.5 mm). For both regions, the mean thicknesses of the mentioned retinal layers and the described OCT-A parameters were calculated.

vessel segmentation to the binarized OCT-A images, we obtained SVC microvasculature. As the OCT-A detects blood flow down to the capillary level by measuring the changes in OCT signal in consecutive cross-sectional images, the whiteness of the binarized images reflects the probability of perfusion. This allowed us to calculate microvascular perfusion density as the ratio between the number of white pixels of the binarized image and the total number of pixels in the region of interest. The binarized images of the microvasculature were further processed to extract the skeleton of the vasculature using a built-in function in MATLAB. Furthermore, a Canny edge detector was implemented to detect the borders of the vasculature. From these images, we computed

the following microvascular parameters: skeleton density as the number of pixels of the skeleton divided by the number of pixels in the region, the vessel perimeter index (Alam et al., 2017), mean vessel diameter (Alam et al., 2017), the fractal dimension (FD) estimated with Hausdorff (Box-counting) method (Harrar and Hamami, 2007) and lacunarity with gliding box method (Tolle et al., 2008). The lacunarity parameter used herein refers to the calculation of lacunarity using a box-size of 512 pixels, which represents a relative box-size of 0.1741 with respect to the rescaled binarized image. These parameters were extracted in the foveal zone and the parafovea. FD, lacunarity and perfusion density were dimensionless, skeleton density and vessel perimeter index were measured in 1/mm (length per unit of area) and mean vessel diameter in μm.

For foveal avascular zone (FAZ) parameter extraction, FAZ was first segmented using a parameterized version of Díaz et al. (2019). The process consisted of a top hat transform for image enhancement, Canny edge detection processing (including a Gaussian filter), and the application of opening and closing morphological operations to remove noise and fill holes. The FAZ area (mm^2) was measured, and the circularity was calculated with the following formula: 4π (area/perimeter^2).

Statistical Analysis

Statistical analysis was done in R (version 3.6.1) and RStudio (version 1.2.1335). Group differences of demographic categorical variables were tested using Chi square test. Quantitative variables were described using mean and standard deviation. Normality of data was visually inspected and tested with Shapiro-Wilks. Group comparisons of normally distributed variables were done with *T*-test and non-normally distributed data assessed with Mann Whitney *U*-test. The analyses of OCT and OCT-A parameters were conducted using generalized estimating equation (GEE) models with an exchangeable working correlation structure to account for correlation between the two eyes from a single participant. Effect sizes were calculated with Cohen's d. To test the diagnostic ability of OCT-A parameters alone or in combination with demographic or retinal thickness variables, we fitted logistic GEE models and their predictive ability was tested in ROC curves, using fitted values as predictors. For this, we first fitted the null model including age, sex, and hypertension as *a priori* confounders, and then added retinal variables for the full model. The differences in goodness-of-fit between models were tested with Wald test. All GEE analyses were performed with geepack package and ROC curves calculated with pROC package. *p-values* lower than 0.05 were considered statistically significant.

RESULTS

A total of 87 eyes from 49 PD patients and 73 eyes from 40 controls were analyzed after removing the acquisitions with visually identifiable motion artifacts, incomplete acquisitions or eyes presenting ocular exclusion criteria.

The demographics and clinical characteristics of participants are listed in **Table 1**. There were no statistically significant differences in age, but the proportion of females was larger in the control group. The mean disease duration was 7.1 ± 4.1 years (range 0.4 to 19.4 years), and the mean UPDRS motor score was 27.7 ± 7.7 (range, 9 to 54). The cognitive status was similar between PD and controls, but the proportion of subjects with MCI was larger in PD group. In PD patients, MoCA score presented a mild correlation with motor deficits ($r = -0.292$, $p = 0.04$). The frequency of well-controlled hypertension was comparable in both groups.

PD patients were further divided into two groups: PD patients with MCI (PD-MCI) ($n = 18$) and PD patients with normal cognition (PD-NC) ($n = 31$). The mean age of PD-MCI was 67.1 ± 8.9 years and in PD-NC it was 63.1 ± 6.9 years ($p = 0.11$). Disease duration was comparable among both groups (PD-MCI 6.3 ± 4.4 vs. PD-NC 7.5 ± 4.0, $p = 0.3$). The proportion of females was also similar in both groups (PD-MCI 38.9% and PD-NC 32.2%, $p = 0.9$), as well as the proportion of patients with well-controlled hypertension (PD-MCI 16.6% and PD-NC 22.2%, $p = 0.7$).

Comparison of Microvascular Parameters Between PD Patients and Controls

Comparing PD patients and controls, significant differences were found in FAZ area in SVC ($p = 0.004$) and DVC ($p < 0.001$) with a medium to large effect size, but not in FAZ circularity. After controlling for *a priori* confounders (i.e., age, sex, and hypertension), FAZ area remained significantly smaller in PD patients compared to controls in both SVC and DVC (estimate −0.1 μm, adjusted $p = 0.004$ in SVC and $p = 0.014$ in DVC) (**Table 2**).

When analyzing differences in microvascular parameters between PD patients and controls, skeleton density, perfusion density and vessel perimeter of PD patients were increased in the foveal zone, with statistically significant differences compared

TABLE 1 | Demographics and clinical characteristics of participants.

	PD	Control	*p*-value
n	49	40	
Age (years)	64.6 (7.9)	62.1 (8.0)	0.2
Sex (female n, %)	16 (34.7%)	27 (67.5%)	<0.001
MoCA	24.4 (4.1)	25.7 (2.5)	0.3
MCI (n, %)	18 (36.7%)	6 (15%)	0.03
Hypertension (n, %)	12 (24.5%)	7 (17.5%)	0.59
Disease Duration (years)	7.1 (4.1)	–	
UPDRS I	2.0 (1.5)	–	
UPDRS II	10.8 (4.0)	–	
UPDRS III	27.7 (7.7)	–	
UPDRS IV	4.0 (2.9)	–	
LEDD (mg)	647.5 (364.6)	–	

Categorical data are expressed as number and percentage, whereas quantitative data is expressed as mean (standard deviation). The proportion of participants with well-controlled or benign hypertension is provided for each group. LEDD, Levodopa Equivalent Daily Dose; MCI, Mild Cognitive Impairment; MoCA, Montreal Cognitive Assessment; n, sample size; PD, Parkinson's disease; UPDRS, Unified Parkinson's disease Rating Scale.

to controls (**Figure 2**). Moreover, PD eyes showed increased FD and lacunarity of both complexes in the foveal zone. Adjusted GEE models showed that the SVC lacunarity and FD, and DVC lacunarity, skeleton density and perfusion density were significantly different between groups (**Table 2**), being the effect size particularly large for lacunarity. On the other hand, the parafoveal lacunarity in the retina of PD patients was significantly decreased in SVC and significantly increased in DVC (GEE, $p < 0.001$), but no differences were observed in the remaining parafoveal microvascular parameters.

Retinal Thicknesses and Its Association With Microvascular Parameters

Multivariate GEE adjusted for age, sex and hypertension showed no significant differences in retinal thickness or its layers between PD patients and controls.

In the foveal zone, FAZ area was negatively associated with GCIPL and INL thickness in both PD patients and controls ($p < 0.001$), and no significant associations were found with ELM-IS/OS thickness in any group. These results suggest that the foveal microvasculature significantly contributes to OCT thickness measurement of inner retinal layers in normal and pathological conditions. In a similar fashion, in both groups, skeleton density, perfusion density, FD, and vessel perimeter of both plexuses were positively associated with the thickness of inner retinal layers (GCIPL and INL), but not with ELM-IS/OS.

However, a unique positive association was found in PD patients between microvascular parameters and OPL-ONL in the fovea. Concretely, FAZ areas in SVC and DVC were negatively associated, and skeleton density, perfusion density, and vessel perimeter of both plexuses were positively associated with OPL-ONL thickness, indicating that increased capillary bed in the fovea was related to OPL-ONL thickening. Also, foveal lacunarity of DVC was associated with GCIPL, INL and OPL-ONL thinning in PD patients, but not in controls.

In the parafovea of PD patients, a positive association was found between some microvascular parameters of the SVC, including skeleton density, perfusion density, FD and vessel perimeter with parafoveal GCIPL thickness (GEE, adjusted p-values: 0.014, 0.006, <0.001, and 0.013, respectively), but not with the thickness of the remaining retinal layer complexes. No such significant associations were found in control participants. None of the microvascular parameters of DVC were associated with retinal thicknesses in the parafovea.

Retinal Parameters in PD Patients With Mild Cognitive Impairment

We also tested whether differences in microvascular parameters could be detected between PD patients with and without MCI. Some of such parameters tended to be lower in PD-MCI compared to PD-NC patients, like DVC lacunarity in the foveal zone or SVC skeleton density in the parafovea, but the differences did not reach statistical significance (**Table 3**). FAZ area was larger and FAZ circularity was decreased in PD-MCI patients, and both parameters were significantly different in SVC compared to PD-NC patients.

On the other hand, we observed that in PD-MCI retinal thickness was 6 μm lower in the parafovea and 9 μm lower in the foveal zone compared to PD-NC patients. Most of the parafoveal retinal thickness decrease in PD-MCI was accounted for changes in GCIPL (absolute difference of 4 μm). Contrarily, in the foveal zone, the GCIPL only accounted for a third part of the total retinal thinning (3 μm thinner), whereas foveal OPL-ONL thickness accounted for the rest (6 μm lower in PD-MCI vs. PD-NC, GEE, $p = 0.047$). However, none of these differences

TABLE 2 | Foveal microvascular changes in PD.

		PD	Control	Cohen's *d*	Univariatep-value	Multivariate *p*-value
FAZ area (mm^2)	SVC	0.669 ± 0.214	0.824 ± 0.292	0.61	**0.004**	**0.004**
	DVC	0.401 ± 0.181	0.544 ± 0.198	0.75	**<0.001**	**0.014**
FAZ circularity	SVC	0.187 ± 0.038	0.194 ± 0.029	0.21	0.280	0.686
	DVC	0.257 ± 0.045	0.271 ± 0.043	0.32	0.067	0.210
Lacunarity	SVC	6.0 ± 0.4	5.7 ± 0.4	0.75	**<0.001**	**<0.001**
	DVC	12.8 ± 0.7	9.8 ± 3.2	1.30	**<0.001**	**<0.001**
Fractal Dimension	SVC	1.42 ± 0.05	1.37 ± 0.09	0.69	**0.008**	**0.027**
	DVC	1.49 ± 0.04	1.47 ± 0.04	0.50	**0.030**	0.127
Perfusion Density	SVC	0.14 ± 0.04	0.11 ± 0.05	0.66	**0.009**	0.112
	DVC	0.22 ± 0.04	0.20 ± 0.05	0.44	**0.020**	**<0.001**
Skeleton Density (1/mm)	SVC	6.0 ± 1.9	4.8 ± 2.2	0.58	0.052	0.650
	DVC	8.6 ± 1.9	7.6 ± 1.8	0.54	**0.034**	**0.002**
Vessel Perimeter Index (1/mm)	SVC	17.1 ± 4.8	13.6 ± 5.6	0.67	**0.006**	0.210
	DVC	27.6 ± 5.2	23.6 ± 5.6	0.74	**0.003**	0.541
Vessel Diameter (μm)	SVC	23.3 ± 1.6	23.7 ± 2.1	0.21	0.160	0.056
	DVC	26.1 ± 2.1	25.8 ± 2.0	0.15	0.320	0.944

Microvascular parameters are expressed as mean ± standard deviation for each group. Cohen's d represents the effect size. p-values were obtained with GEE. Multivariate p-values are adjusted for age, sex, and hypertension. Significant results are highlighted in bold. Microvascular parameters without units are dimensionless. DVC, deep vascular complex; FAZ, foveal avascular zone; PD, Parkinson's disease; SVC, superficial vascular complex.

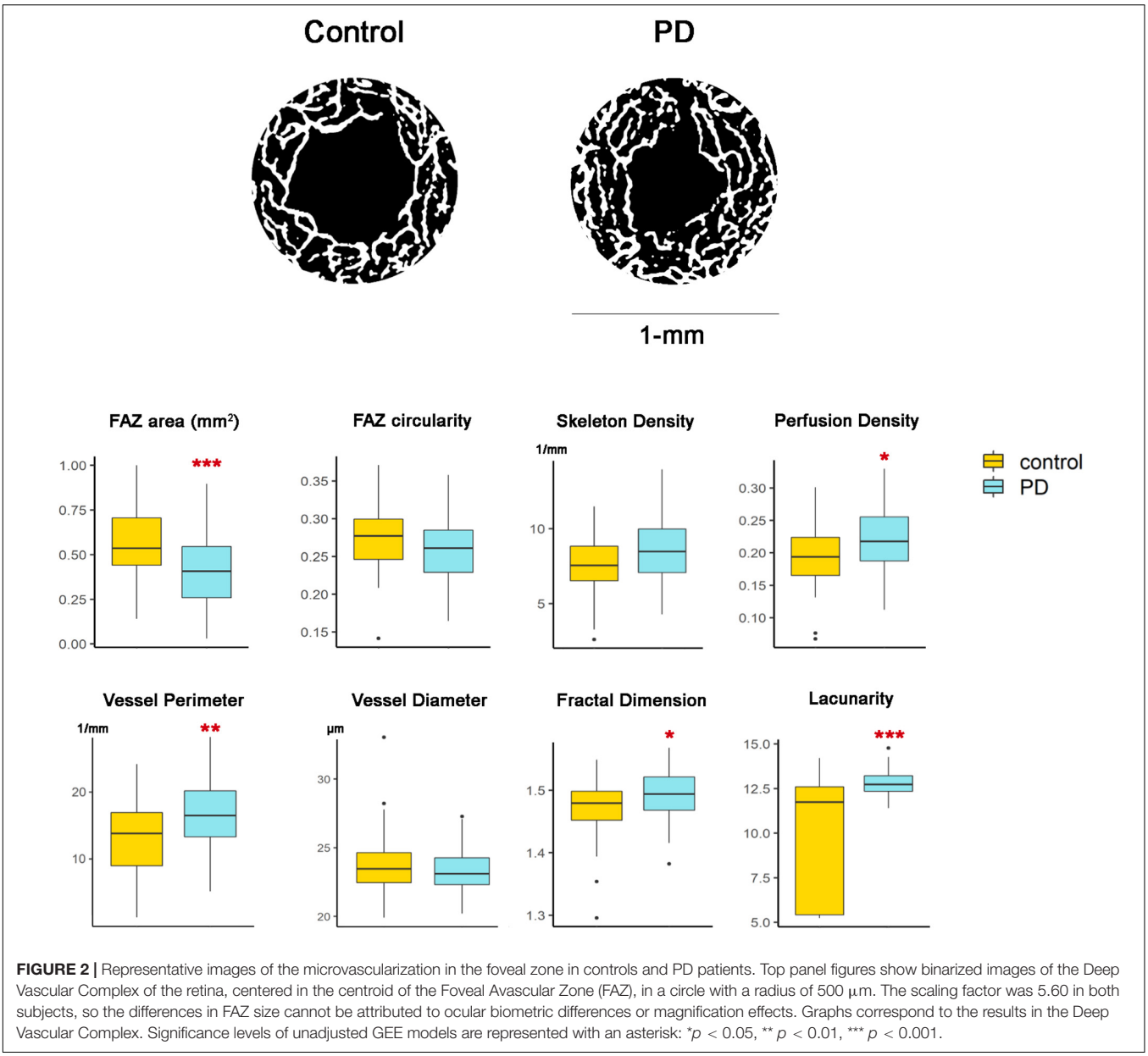

FIGURE 2 | Representative images of the microvascularization in the foveal zone in controls and PD patients. Top panel figures show binarized images of the Deep Vascular Complex of the retina, centered in the centroid of the Foveal Avascular Zone (FAZ), in a circle with a radius of 500 µm. The scaling factor was 5.60 in both subjects, so the differences in FAZ size cannot be attributed to ocular biometric differences or magnification effects. Graphs correspond to the results in the Deep Vascular Complex. Significance levels of unadjusted GEE models are represented with an asterisk: *$p < 0.05$, **$p < 0.01$, ***$p < 0.001$.

reached statistical significance after controlling for the effect of age, sex, and hypertension (**Table 3**).

Interestingly, we observed that parafoveal GCIPL thickness was significantly associated with parafoveal microvascular parameters in SVC, including skeleton density, perfusion density, fractal dimension, lacunarity and vessel perimeter, but only in PD-MCI and not in PD-NC.

Association Between Microvascular Parameters and Clinical Outcomes

In PD patients, FAZ area and circularity of SVC were significantly associated with MoCA scores (GEE, $p = 0.028$, $p = 0.036$, respectively), but not with disease duration or UPDRS III scores. However, the relationship between superficial FAZ parameters and cognitive function lost significance when controlling for the effect of covariates. None of the remaining foveal or parafoveal microvascular parameters yielded significant associations with disease duration, motor impairment or cognitive outcomes.

Diagnostic Accuracy of Macular Parameters

To test the diagnostic ability of OCT-A parameters alone or in combination with demographic, clinical, or retinal thickness variables, we fitted multivariable logistic GEE models and their predictive ability was tested in ROC curves. We first fitted the null model including age, sex, and hypertension as the *a priori* confounders. This yielded an area under the curve (AUC) of 0.691 (95% CI, 0.601 – 0.772). Then, we included

TABLE 3 | Microvascular and thickness parameters in PD patients with and without MCI.

		PD-MCI	PD-NC	Cohen's *d*	GEE *p*-value
n		18	31		
FAZ area (mm^2)	SVC	0.73 ± 0.20	0.63 ± 0.21	0.49	0.049
	DVC	0.43 ± 0.17	0.38 ± 0.18	0.29	–
FAZ circularity	SVC	0.17 ± 0.02	0.20 ± 0.04	0.95	0.001
	DVC	0.25 ± 0.05	0.26 ± 0.04	0.22	–
Microvascular parameters					
Fovea					
Fractal Dimension	SVC	1.40 ± 0.05	1.42 ± 0.05	0.40	–
	DVC	1.49 ± 0.04	1.50 ± 0.04	0.25	–
Lacunarity	SVC	6.02 ± 0.32	6.03 ± 0.48	0.02	–
	DVC	12.59 ± 0.63	12.91 ± 0.66	0.50	–
Skeleton Density (1/mm)	SVC	11.8 ± 1.5	11.7 ± 1.2	0.07	–
	DVC	12.0 ± 1.2	12.1 ± 1.3	0.08	–
Perfusion Density	SVC	0.28 ± 0.04	0.27 ± 0.03	0.28	–
	DVC	0.31 ± 0.02	0.32 ± 0.02	0.50	–
Parafovea					
Fractal Dimension	SVC	1.63 ± 0.02	1.63 ± 0.01	0	–
	DVC	1.69 ± 0.01	1.69 ± 0.01	0	–
Lacunarity	SVC	1.04 ± 0.01	1.04 ± 0.01	0	–
	DVC	10.98 ± 0.24	11.14 ± 0.24	0.67	–
Skeleton Density (1/mm)	SVC	11.4 ± 1.4	11.8 ± 1.3	0.30	–
	DVC	13.4 ± 1.2	13.5 ± 1.2	0.08	–
Perfusion Density	SVC	0.24 ± 0.02	0.24 ± 0.02	0.00	–
	DVC	0.35 ± 0.01	0.35 ± 0.01	0.00	–
Thickness (μm)					
Fovea					
Retina		277.1 ± 19.1	286.3 ± 18.2	0.49	0.045
GCIPL		36.0 ± 7.7	39.4 ± 7.9	0.44	–
INL		19.4 ± 6.1	21.0 ± 5.9	0.27	–
OPL-ONL		117.2 ± 13.7	123.3 ± 8.4	0.54	0.047
ELM-IS/OS		49.6 ± 6.2	49.1 ± 4.9	0.09	–
Parafovea					
Retina		339.4 ± 14.8	345.9 ± 13.3	0.46	–
GCIPL		92.0 ± 8.5	96.3 ± 7.2	0.55	0.039
INL		40.7 ± 2.8	40.7 ± 4.3	0	–
OPL-ONL		104.7 ± 8.1	106.1 ± 6.6	0.19	–
ELM-IS/OS		44.2 ± 3.5	44.0 ± 3.0	0.06	–

Data are expressed as mean ± standard deviation for each group. Cohen's d represents the effect size. p-values were obtained with univariate GEE. P-values are only provided for significant results. DVC, deep vascular complex; ELM-IS/OS, macular complex including external limiting membrane and inner and outer segments of photoreceptors; FAZ, foveal avascular zone; GCIPL, ganglion cell-inner plexiform complex; INL, inner nuclear layer; OPL-ONL, complex including the outer plexiform and outer nuclear layers; PD-MCI, Patients with Parkinson's disease and Mild Cognitive Impairment; PD-NC, patients with Parkinson's disease and normal cognition; SVC, superficial vascular complex.

single microvascular parameters that differed most between PD patients and controls, including FAZ area, foveal skeleton density, perfusion density and lacunarity (both plexuses), foveal FD in SVC and parafoveal lacunarity (both plexuses). Each model was then compared to the null with Wald test to test whether microvascular parameters significantly contributed to diagnostic accuracy. From this, we observed that 3 parameters significantly contributed to the model, providing excellent diagnostic accuracies (AUC > 0.8). These parameters were the lacunarity in DVC fovea (AUC = 0.852, 95% CI 0.79 – 0.92), lacunarity in DVC parafovea (AUC = 0.838, 95% CI 0.77 – 0.90) and lacunarity in SVC parafovea (AUC = 0.835, 95% CI 0.77 – 0.90) (**Figure 3**). Further adding retinal thicknesses of the parafovea or central macula or combining different microvascular parameters did not significantly improve the classification performance.

DISCUSSION

In the present study, we observed retinal capillary alterations in the central macula of PD patients. The area of the FAZ in both superficial and deep vascular plexuses was significantly smaller in PD patients compared to controls. In line with this finding, the perfusion and density of capillaries in the foveal zone was greater in PD patients, mainly in deep vascular plexus, suggesting an enlarged vascular bed surrounding FAZ. Moreover, fractal dimension and lacunarity of capillaries were greater in this region reflecting the increased vascular complexity and heterogeneity in PD fovea. Remodeling of foveal capillary bed was associated with increased OPL-ONL thickness in PD patients. Even though we failed to find differences in microvascular density or perfusion in the parafovea, parafoveal lacunarity significantly differed between patients and controls. Interestingly, parafoveal microvascular parameters on the superficial vascular complex were associated with GCIPL thickness in PD patients, but not in controls, and these associations were mainly driven by PD-MCI. Our results demonstrate that retinal microvascular alterations in PD are mainly restricted to the fovea, and that the parafoveal GCIPL atrophy in PD-MCI is associated with the superficial vascular supply.

Previous studies have explored retinal vascular alterations in PD. The first study analyzing retinal vascular changes in PD was conducted using fluorescein angiography (FA) (Miri et al., 2015). Although the resolution for fine capillary vessels of retinal FA is somewhat limited, these authors found a shrinking of FAZ in PD patients compared to controls, which is in line with the results of the current study using OCT-A images and improved algorithms to enhance the visualization of capillaries around the FAZ. Furthermore, we found that the decrease in FAZ area was accompanied by an increase in microvascular parameters in the foveal zone, like skeleton and perfusion density, fractal dimension or lacunarity. This contrasts with the results of Zou et al. who found less vessel length and perfusion in the central macula of PD patients and no changes in FAZ area (Zou et al., 2020), and with the results of Rascunà et al. who did not find vascular density changes in the foveal zone of early PD patients (Rascunà et al., 2020). Some of these differences might be attributed to smaller sample sizes, differences in disease stage of patients and study design flaws of previous studies.

The first study using OCT-A in PD was published in 2018, where Kwapong et al. (2018) nicely described a decrease in

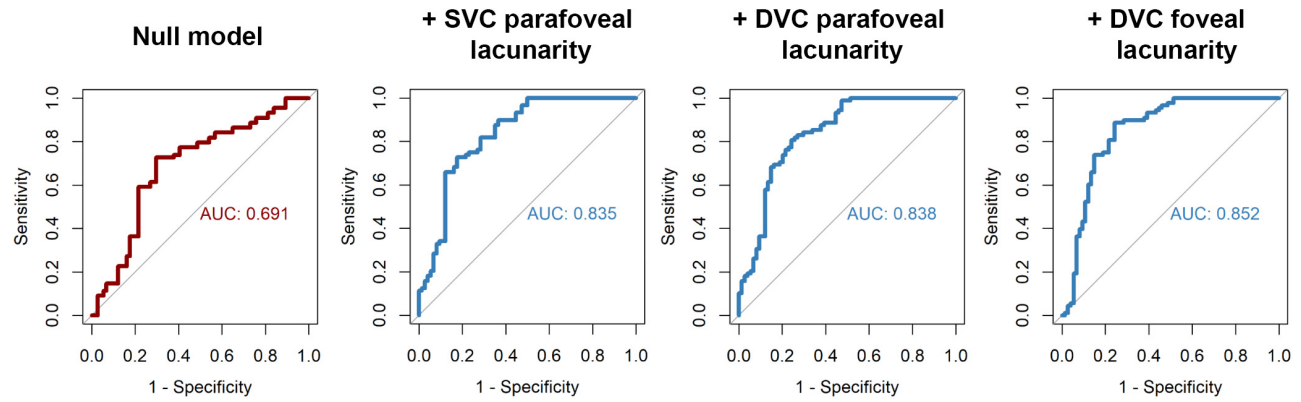

FIGURE 3 | Receiver operating characteristic (ROC) curves for testing the diagnostic accuracy of microvascular parameters. Fitted values resulting from logistic regression were used as classifiers. ROC curve for the null model is shown in red, in which confounding demographical and clinical variables were used as independent factors, including age, sex, and hypertension. In blue, ROC curves of regression models that were significantly different from null (Wald test) after adding single microvascular parameters to the model. AUC, area under the curve; DVC, deep vascular complex; SVC, superficial vascular complex.

parafoveal microvascular density of superficial vascular complex in PD and its relationship with GCIPL thickness decrease. Similar results were reported by Shi et al. (2020). Nonetheless, none of these authors explored microvascular alterations in the foveal zone, where the fundamental microvascular alterations occur according to the present study. They did neither control for the inter-eye correlation in statistical analyses, possibly increasing the rate of false positive findings in the parafovea. In our study, we used GEE models to control for this effect, and did not find significant changes in the parafoveal skeleton or perfusion density. Nonetheless, part of their results coincides with ours, as we also found an association between the parafoveal microvascular density and GCIPL thickness, even after adjusting for confounding variables. Similarly, Rascunà et al. (2020), did not observe significant differences in the parafoveal microvascular density between early PD patients and controls but did find a correlation of inner retinal layer thickness and microvascular density. However, these correlations were mostly restricted to the foveal zone, and in the present study, we showed that such associations were not specific to PD, as they were also observed in controls. More recently, Robbins et al. (2021) used larger sample sizes, including 124 eyes of 69 PD patients and 248 eyes of 137 controls, concluding that retinal superficial capillary vessel density and perfusion density around the foveal zone are decreased in PD compared to age and sex-matched control participants, but no correlation analyses with retinal thickness were performed. Intriguingly, we observed that the association between parafoveal GCIPL thickness and microvascular parameters in PD was mainly driven by PD-MCI patients, whose parafoveal GCIPL was significantly reduced compared to PD-NC patients. As far as we know, this is the first study that classifies PD patients into subgroups in an attempt to unravel OCT-A differences between clinical endophenotypes. Even though few significant differences were found, PD-MCI tended to display larger FAZ areas and less FAZ circularity than PD-NC. Future studies with larger sample sizes might confirm this trend.

To date, few studies have assessed retinal vascular descriptors beyond density that can be useful for increasing the information obtainable from OCT-A images. Fractal dimension is a widely known parameter for describing shape or texture, and determines the complexity of an image. Two studies calculated FD of the retinal vasculature of PD patients finding contradictory results. Miri et al. (2015) did not find differences using FA, whereas Shi et al. (2020) reported decreased FD in the parafoveal superficial and deep vascular plexuses using OCT-A. This contrasts with our results, as we did not find differences in FD in the parafoveal region, but the FD within the foveal zone was significantly increased in PD patients. On the other hand, lacunarity is a feature descriptor that determines the heterogeneity of an image and complements FD. Lacunarity expresses patchiness or inhomogeneity of an image, and since it is not predicated on fractality, it may be particularly useful for characterizing the texture of retinal microvasculature. Indeed, in our study lacunarity was the parameter that differed most between patients and controls. The lacunarity within the foveal zone was significantly higher in PD patients compared to controls, even after adjusting for age, sex, and hypertension, suggesting that the distribution of capillaries was more heterogeneous in this region, with larger dispersion of gap sizes. The parafoveal lacunarity was greater in DVC in both PD patients and controls, as this plexus contains irregularly distributed vascular loops and vascular branches extending from a central seed point, notably increasing image heterogeneity (Hirano et al., 2018). Still, in the present work this parameter was also found to be significantly higher in PD patients compared to controls.

Moreover, lacunarity yielded the best diagnostic accuracy. Many efforts are being devoted to the identification and characterization of PD biomarkers. Notwithstanding the progress made so far, reliable biomarkers are still lacking. In this work, we showed that foveal lacunarity could be a promising biomarker for differentiating patients from controls, as a significantly greater AUC was achieved after adding this parameter to the null model that controlled for confounding variables

like age, sex, and hypertension. In a previous study of Zou et al. (2020), similar AUCs were obtained after combining OCT-A and OCT parameters. However, these authors only accounted for capillary length and density, and no further microvascular parameters were considered. In our study, the combination of microvascular and structural modifications did not increase the classification accuracy, and lacunarity could be considered as a single imaging biomarker for discriminating patients from controls. The differences in microvascular imaging parameters between PD patients and controls, and the lack of association between these parameters with disease duration or severity, further support OCT-A as a useful diagnostic marker.

An important aspect to consider for the comparability of OCT-A studies is the critical contribution of technical differences among OCT-A devices. The definition of the delimiting boundaries of retinal vascular plexuses determines the tissue and associated vasculature that is represented in two-dimensional *en face* images. It is known that the location of these boundaries varies among OCT-A devices and limits the comparability of OCT-A studies (Li et al., 2018). So far, 2 OCT-A devices have been used to explore the vascular changes in PD, namely, AngioVue XR Avanti (Optovue Inc, Fremont, California, United States) and AngioPlexTM OCTA system (Cirrus; Zeiss, Dublin). In both devices, the intermediate capillary plexus (ICP) defined by Campbell et al. (2017) is considered to be part of SVC, whereas in Spectralis OCT-A the ICP pertains to DVC. Also, the axial resolution is similar among the 3 OCT-A devices (5 μm), but the lateral resolution of the OCT beam of Spectralis is much higher (5.7 μm) than the other two (15 μm). This is especially important considering that the average diameter of small capillaries is about 8 μm (Tan et al., 2012). Therefore, Spectralis OCT-A enables a more precise detection and more confident evaluation of vascular abnormalities at capillary level. As far as we know, this is the first study using Spectralis OCT-A in PD, and the mere use of this device could account for some of the contradictory results of our work compared to previous literature in PD.

The pathophysiological mechanisms driving retinal microvascular changes in PD are still unknown. In autopsy brains of PD patients, increased angiogenesis has been observed (Bradaric et al., 2012) with abnormally fragmented capillaries (Guan et al., 2013), increased expression of vascular endothelial growth (VEGF) receptors (Wada et al., 2006), and the formation of string vessels (Yang et al., 2015), supporting vascular events as a contributing factor to the PD pathophysiology. Concretely, string vessels are remnants of capillary vessels with no function in blood flow, and are triggered by factors that promote angiogenesis, like VEGF (Brown, 2010). As retinal and brain microvasculature share similarities, string vessel formation in the foveal zone could account for the current results. This hypothesis is partially supported by a recent in-vitro study that has demonstrated how degenerating retinal ganglion cells release VEGF to drive their own survival (Froger et al., 2020). Moreover, we observed that the relationship between microvascular parameters and OPL-ONL thickness in the fovea was exclusively present in PD patients, even though no significant thickness changes were detected between PD patients and controls in this area. It might be that the activation of VEGF receptor could not only promote pro-angiogenic effects, but also a microinflammation of the outer layers (Uemura et al., 2021). However, the mechanistic basis of microvascular retinal changes cannot be inferred from clinical studies.

Furthermore, the axons of retinal ganglion cells exit the eye to form the optic nerve, optic chiasm, and optic tract, which in turn synapse with other neurons in the lateral geniculate nucleus that extend through the optic radiations to the occipital lobe. Previous studies have observed morphometric abnormalities of the intracranial visual pathway structures in drug-naïve early PD patients, including decreased volume of chiasmatic area, and reduced white matter concentration and diffusivity in optic radiations (Arrigo et al., 2017). In future studies, it would be interesting to acknowledge not only whether the retinal microvascular alterations are associated to intracranial morphometric and functional changes, but also related to extracranial pathology, like pathology of carotid arteries.

Lastly, it is worth mentioning that the involvement of the eye in PD goes beyond the retina. In the last years, it has been demonstrated that PD patients show profound alterations of corneal innervation with decreased density of corneal subbasal nerve fibers and branches, and increased number of beadings (Arrigo et al., 2018; Ulusoy and Ulusoy, 2020). Probably, this denervation is responsible for the defective lacrimal reflex, and the subsequent dry eye signs and symptoms that are commonly reported in the literature (Biousse et al., 2004; Ekker et al., 2017).

One limitation of the current study was that the automatic segmentation of vascular plexuses near the fovea might not be completely accurate, as at this region the vascular plexuses converge into a single plexus around the FAZ, and DVC might be added to SVC in the fovea (Spaide and Curcio, 2017). However, we observed that microvascular changes in both plexuses were in line, but quantitative measurements should be interpreted with caution. Moreover, to find a tradeoff between the speed of acquisition and the resolution, the size of the field of view from the current OCT-A system was smaller than in previous studies. Nonetheless, we expected that macular changes in PD were predominantly restricted to the most central areas. Also, the cutoff for MCI was defined using MoCA scores, but future studies should rely on a comprehensive set of neuropsychological tests to refine the classification of PD patients. Several microvascular parameters were compared between PD patients and controls, and p-values were not corrected for multiple comparisons due to the exploratory nature of these analyses, and this remains a limitation of the current study. Finally, we did not account for all the potential confounding variables, such as smoking, intraocular pressure or axial length, although the effects of the latter were mitigated by scaling the OCT-A images. Future studies will benefit from using larger sample sizes to control for the effect of these factors in multivariable regression analyses.

In conclusion, the identification of biomarkers for PD is a mainstream in clinical research to forestall the progression of PD. Early retinal abnormalities in PD could permit a fast, non-invasive, and cost-effective imaging of surrogate markers. Our results support retinal vascular alterations detectable by OCT-A, mainly in the foveal zone, and as far as we know,

our study is the first to describe changes in retinal vessel lacunarity in PD as a potential diagnostic biomarker of PD. Also, we indicate that PD patients with MCI might represent a clinical subtype in which retinal small vessel disease is related to retinal atrophy, although this working hypothesis needs to be tested in future studies. It is important to acknowledge the technical properties and limitations of each OCT-A device to ensure optimal interpretation of the obtained results in the clinical setting. The standardization of OCT-A vascular plexuses segmentation, the extraction and analysis of common vascular parameters and increasing the speed and resolution of acquisitions will enable a more precise description of retinal microvascular variations in PD. Without limiting the foregoing, vascular alterations in PD might need to be corroborated in postmortem retinas using histochemistry.

DATA AVAILABILITY STATEMENT

The raw data supporting the conclusions of this article will be made available by the authors, without undue reservation.

ETHICS STATEMENT

The studies involving human participants were reviewed and approved by the CEIm de Euskadi (Comité de Ética de la Investigación con medicamentos). Osasun saila/Departamento de Salud. Eusko Jaurlaritza/Gobierno Vasco. C/Donostia-San Sebastián, 1 – 01010 Vitoria-Gasteiz. The patients/participants provided their written informed consent to participate in this study.

AUTHOR CONTRIBUTIONS

AM-G and IG conceptualized and designed the study. MB contributed to the implementation of the research. AE, UA, and DR-B processed imaging data. AM-G analyzed the data. ST-P collected imaging data and managed the project. JG-E recruited participants and collected neurological data. MA and RD collected cognitive data. AM-G wrote the manuscript with assistance from IG. All authors reviewed and contributed to the article and approved the submitted version.

FUNDING

This study was partially co-funded by the Instituto de Salud Carlos III through the projects PI14/00679 and PI16/00005 (co-funded by European Regional Development Fund/European Social Fund "A way to make Europe"/"Investing in your future"), and by the Department of Health of the Basque Government through the projects "2019111100" and "2020333033".

ACKNOWLEDGMENTS

We thank all the patients and participants involved in the study.

REFERENCES

Aarsland, D., Bronnick, K., Larsen, J. P., Tysnes, O. B., and Alves, G. (2009). Cognitive impairment in incident, untreated Parkinson disease: the Norwegian ParkWest study. *Neurology* 72, 1121–1126. doi: 10.1212/01.wnl.0000338632.00552.cb

Aarsland, D., Creese, B., Politis, M., Chaudhuri, K. R., Ffytche, D. H., Weintraub, D., et al. (2017). Cognitive decline in Parkinson disease. *Nat. Rev. Neurol.* 13, 217–231. doi: 10.1038/nrneurol.2017.27

Alam, M., Thapa, D., Lim, J. I., Cao, D., and Yao, X. (2017). Quantitative characteristics of sickle cell retinopathy in optical coherence tomography angiography. *Biomed. Opt. Exp.* 8, 1741–1753. doi: 10.1364/BOE.8.001741

Arrigo, A., Calamuneri, A., Milardi, D., Mormina, E., Rania, L., Postorino, E., et al. (2017). Visual system involvement in patients with newly diagnosed Parkinson disease. *Radiology* 285, 885–895. doi: 10.1148/radiol.2017161732

Arrigo, A., Rania, L., Calamuneri, A., Postorino, E. I., Mormina, E., Gaeta, M., et al. (2018). Early corneal innervation and trigeminal alterations in Parkinson disease: a pilot study. *Cornea* 37, 448–454.

Biousse, V., Skibell, B. C., Watts, R. L., Loupe, D. N., Drews-Botsch, C., and Newman, N. J. (2004). Ophthalmologic features of Parkinson's disease. *Neurology* 62, 177–180. doi: 10.1212/01.Wnl.0000103444.45882.D8

Bradaric, B. D., Patel, A., Schneider, J. A., Carvey, P. M., and Hendey, B. (2012). Evidence for angiogenesis in Parkinson's disease, incidental lewy body disease, and progressive supranuclear palsy. *J. Neural. Transm.* 119, 59–71. doi: 10.1007/s00702-011-0684-8

Brown, W. R. (2010). A review of string vessels or collapsed, empty basement membrane tubes. *J. Alzheimers Dis.* 21, 725–739. doi: 10.3233/jad-2010-100219

Campbell, J. P., Zhang, M., Hwang, T. S., Bailey, S. T., Wilson, D. J., Jia, Y., et al. (2017). Detailed vascular anatomy of the human retina by projection-resolved optical coherence tomography angiography. *Sci. Rep.* 7:42201. doi: 10.1038/srep42201

Chrysou, A., Jansonius, N. M., and van Laar, T. (2019). Retinal layers in Parkinson's disease: a meta-analysis of spectral-domain optical coherence tomography studies. *Parkinson. Relat. Disord.* 64, 40–49. doi: 10.1016/j.parkreldis.2019.04.023

Chua, J., Hu, Q., Ke, M., Tan, B., Hong, J., Yao, X., et al. (2020). Retinal microvasculature dysfunction is associated with Alzheimer's disease and mild cognitive impairment. *Alzheimers Res. Ther.* 12:161. doi: 10.1186/s13195-020-00724-0

Criscuolo, C., Cennamo, G., Montorio, D., Carotenuto, A., Strianese, A., Salvatore, E., et al. (2020). Assessment of retinal vascular network in amnestic mild cognitive impairment by optical coherence tomography angiography. *PLoS One* 15:e0233975. doi: 10.1371/journal.pone.0233975

Díaz, M., Novo, J., Cutrín, P., Gómez-Ulla, F., Penedo, M. G., and Ortega, M. (2019). Automatic segmentation of the foveal avascular zone in ophthalmological OCT-A images. *PLoS One* 14:e0212364. doi: 10.1371/journal.pone.0212364

Ekker, M. S., Janssen, S., Seppi, K., Poewe, W., de Vries, N. M., Theelen, T., et al. (2017). Ocular and visual disorders in Parkinson's disease: common but frequently overlooked. *Parkinson. Relat. Disord.* 40, 1–10. doi: 10.1016/j.parkreldis.2017.02.014

Froger, N., Matonti, F., Roubeix, C., Forster, V., Ivkovic, I., Brunel, N., et al. (2020). VEGF is an autocrine/paracrine neuroprotective factor for injured retinal ganglion neurons. *Sci. Rep.* 10:12409. doi: 10.1038/s41598-020-68488-z

Guan, J., Pavlovic, D., Dalkie, N., Waldvogel, H. J., O'Carroll, S. J., Green, C. R., et al. (2013). Vascular degeneration in 'disease. *Brain Pathol.* 23, 154–164. doi: 10.1111/j.1750-3639.2012.00628.x

Harrar, K., and Hamami, L. (2007). "The box counting method for evaluate the fractal dimension in radiographic images," in *Proceedings of the 6th WSEAS International Conference on Circuits, Systems, Electronics,Control & Signal Processing*, Cairo.

Hirano, T., Chanwimol, K., Weichsel, J., Tepelus, T., and Sadda, S. (2018). Distinct retinal capillary plexuses in normal eyes as observed in optical coherence tomography angiography axial profile analysis. *Sci. Rep.* 8:9380. doi: 10.1038/s41598-018-27536-5

Kromer, R., Buhmann, C., Hidding, U., Keseru, M., Keseru, D., Hassenstein, A., et al. (2016). Evaluation of retinal vessel morphology in patients with Parkinson's disease using optical coherence tomography. *PLoS One* 11:e0161136. doi: 10.1371/journal.pone.0161136

Kwapong, W. R., Ye, H., Peng, C., Zhuang, X., Wang, J., Shen, M., et al. (2018). Retinal microvascular impairment in the early stages of parkinson's disease. *Invest. Ophthalmol. Vis. Sci.* 59, 4115–4122. doi: 10.1167/iovs.17-23230

Lang, A., Carass, A., Hauser, M., Sotirchos, E. S., Calabresi, P. A., Ying, H. S., et al. (2013). Retinal layer segmentation of macular OCT images using boundary classification. *Biomed. Opt. Exp.* 4, 1133–1152. doi: 10.1364/BOE.4.001133

Lee, J. Y., Ahn, J., Oh, S., Shin, J. Y., Kim, Y. K., Nam, H., et al. (2019a). Retina thickness as a marker of neurodegeneration in prodromal lewy body disease. *Mov. Disord.* 35, 349–354. doi: 10.1002/mds.27914

Lee, J. Y., Ahn, J., Yoon, E. J., Oh, S., Kim, Y. K., and Jeon, B. (2019b). Macular ganglion-cell-complex layer thinning and optic nerve integrity in drug-naïve Parkinson's disease. *J. Neural. Transm.* 126, 1695–1699. doi: 10.1007/s00702-019-02097-7

Li, X.-X., Wu, W., Zhou, H., Deng, J.-J., Zhao, M.-Y., Qian, T.-W., et al. (2018). A quantitative comparison of five optical coherence tomography angiography systems in clinical performance. *Int. J. Ophthalmol.* 11, 1784–1795. doi: 10.18240/ijo.2018.11.09

Lotharius, J., and Brundin, P. (2002). Pathogenesis of parkinson's disease: dopamine, vesicles and α-synuclein. *Nat. Rev. Neurosci.* 3, 932–942. doi: 10.1038/nrn983

Milani, S. A., Marsiske, M., Cottler, L. B., Chen, X., and Striley, C. W. (2018). Optimal cutoffs for the montreal cognitive assessment vary by race and ethnicity. *Alzheimers Dement.* 10, 773–781. doi: 10.1016/j.dadm.2018.09.003

Miri, S., Shrier, E. M., Glazman, S., Ding, Y., Selesnick, I., Kozlowski, P. B., et al. (2015). The avascular zone and neuronal remodeling of the fovea in Parkinson disease. *Ann. Clin. Transl. Neurol.* 2, 196–201. doi: 10.1002/acn3.146

Murueta-Goyena, A., Del Pino, R., Galdós, M., Arana, B., Acera, M., Carmona-Abellán, M., et al. (2021). Retinal thickness predicts the risk of cognitive decline in parkinson disease. *Ann. Neurol.* 89, 165–176. doi: 10.1002/ana.25944

Murueta-Goyena, A., Del Pino, R., Reyero, P., Galdos, M., Arana, B., Lucas-Jimenez, O., et al. (2019). Parafoveal thinning of inner retina is associated with visual dysfunction in Lewy body diseases. *Mov. Disord.* 34, 1315–1324. doi: 10.1002/mds.27728

Ortuno-Lizaran, I., Beach, T. G., Serrano, G. E., Walker, D. G., Adler, C. H., and Cuenca, N. (2018). Phosphorylated alpha-synuclein in the retina is a biomarker of Parkinson's disease pathology severity. *Mov. Disord.* 33, 1315–1324. doi: 10.1002/mds.27392

Ortuño-Lizarán, I., Sánchez-Sáez, X., Lax, P., Serrano, G. E., Beach, T. G., Adler, C. H., et al. (2020). Dopaminergic retinal cell loss and visual dysfunction in parkinson disease. *Ann. Neurol.* 88, 893–906. doi: 10.1002/ana.25897

Patton, N., Aslam, T., Macgillivray, T., Pattie, A., Deary, I. J., and Dhillon, B. (2005). Retinal vascular image analysis as a potential screening tool for cerebrovascular disease: a rationale based on homology between cerebral and retinal microvasculatures. *J. Anat.* 206, 319–348. doi: 10.1111/j.1469-7580.2005.00395.x

Pfeiffer, H. C., Løkkegaard, A., Zoetmulder, M., Friberg, L., and Werdelin, L. (2014). Cognitive impairment in early-stage non-demented Parkinson's disease patients. *Acta Neurol. Scand.* 129, 307–318. doi: 10.1111/ane.12189

Rascunà, C., Russo, A., Terravecchia, C., Castellino, N., Avitabile, T., Bonfiglio, V., et al. (2020). Retinal thickness and microvascular pattern in early Parkinson's disease. *Front. Neurol.* 11:533375. doi: 10.3389/fneur.2020.533375

Robbins, C. B., Thompson, A. C., Bhullar, P. K., Koo, H. Y., Agrawal, R., Soundararajan, S., et al. (2021). Characterization of retinal microvascular and choroidal structural changes in Parkinson disease. *JAMA Ophthalmol.* 139, 182–188. doi: 10.1001/jamaophthalmol.2020.5730

Shi, C., Chen, Y., Kwapong, W. R., Tong, Q., Wu, S., Zhou, Y., et al. (2020). CHARACTERIZATION BY FRACTAL DIMENSION ANALYSIS OF THE RETINAL CAPILLARY NETWORK IN PARKINSON DISEASE. *Retina* 40, 1483–1491. doi: 10.1097/iae.0000000000002641

Shin, J. Y., Choi, E. Y., Kim, M., Lee, H. K., and Byeon, S. H. (2021). Changes in retinal microvasculature and retinal layer thickness in association with apolipoprotein E genotype in Alzheimer's disease. *Sci. Rep.* 11:1847. doi: 10.1038/s41598-020-80892-z

Spaide, R. F., and Curcio, C. A. (2017). Evaluation of segmentation of the superficial and deep vascular layers of the retina by optical coherence tomography angiography instruments in normal eyes. *JAMA Ophthalmol.* 135, 259–262. doi: 10.1001/jamaophthalmol.2016.5327

Tan, P. E., Yu, P. K., Balaratnasingam, C., Cringle, S. J., Morgan, W. H., McAllister, I. L., et al. (2012). Quantitative confocal imaging of the retinal microvasculature in the human retina. *Invest. Ophthalmol. Vis. Sci.* 53, 5728–5736. doi: 10.1167/iovs.12-10017

Tewarie, P., Balk, L., Costello, F., Green, A., Martin, R., Schippling, S., et al. (2012). The OSCAR-IB consensus criteria for retinal OCT quality assessment. *PLoS One* 7:e34823. doi: 10.1371/journal.pone.0034823

Tolle, C. R., McJunkin, T. R., and Gorsich, D. J. (2008). An efficient implementation of the gliding box lacunarity algorithm. *Phys. D Nonlin. Phenom.* 237, 306–315. doi: 10.1016/j.physd.2007.09.017

Uemura, A., Fruttiger, M., D'Amore, P. A., De Falco, S., Joussen, A. M., Sennlaub, F., et al. (2021). VEGFR1 signaling in retinal angiogenesis and microinflammation. *Prog. Retin. Eye Res.* 100954. doi: 10.1016/j.preteyeres.2021.100954 [Epub ahead of print].

Ulusoy, E. K., and Ulusoy, D. M. (2020). Evaluation of corneal sublayers thickness and corneal parameters in patients with Parkinson's disease. *Int. J. Neurosci.* 1–7. doi: 10.1080/00207454.2020.1761353 [Epub ahead of print].

Wada, K., Arai, H., Takanashi, M., Fukae, J., Oizumi, H., Yasuda, T., et al. (2006). Expression levels of vascular endothelial growth factor and its receptors in Parkinson's disease. *Neurorep.* 17, 705–709. doi: 10.1097/01.wnr.0000215769.71657.65

Yang, P., Pavlovic, D., Waldvogel, H., Dragunow, M., Synek, B., Turner, C., et al. (2015). String vessel formation is increased in the brain of Parkinson disease. *J. Parkinsons Dis.* 5, 821–836. doi: 10.3233/jpd-140454

Zanon Zotin, M. C., Sveikata, L., Viswanathan, A., and Yilmaz, P. (2021). Cerebral small vessel disease and vascular cognitive impairment: from diagnosis to management. *Curr. Opin. Neurol.* 34, 246–257. doi: 10.1097/wco.0000000000000913

Zou, J., Liu, K., Li, F., Xu, Y., Shen, L., and Xu, H. (2020). Combination of optical coherence tomography (OCT) and OCT angiography increases diagnostic efficacy of Parkinson's disease. *Quant. Imaging Med. Surg.* 10, 1930–1939. doi: 10.21037/qims-20-460

Conflict of Interest: The authors declare that the research was conducted in the absence of any commercial or financial relationships that could be construed as a potential conflict of interest.

frontiers in Neuroscience

ORIGINAL RESEARCH
published: 23 July 2021
doi: 10.3389/fnins.2021.681831

Brain and Retinal Abnormalities in the 5xFAD Mouse Model of Alzheimer's Disease at Early Stages

Mengrong Zhang[1†], Liting Zhong[1†], Xiu Han[1], Guoyin Xiong[2], Di Xu[1], Sensen Zhang[1], Haiyang Cheng[1], Kin Chiu[2,3] and Ying Xu[1,4,5*]*

[1] Guangdong-Hongkong-Macau Institute of Central Nervous System Regeneration, Jinan University, Guangzhou, China, [2] Department of Ophthalmology, LKF Faculty of Medicine, The University of Hong Kong, Hong Kong SAR, China, [3] State Key Laboratory of Brain and Cognitive Sciences, The University of Hong Kong, Hong Kong SAR, China, [4] Key Laboratory of Central Nervous System Regeneration, Jinan University, Ministry of Education, Guangzhou, China, [5] Co-Innovation Center of Neuroregeneration, Nantong University, Jiangsu, China

One of the major challenges in treating Alzheimer's disease (AD) is its early diagnosis. Increasing data from clinical and animal research indicate that the retina may facilitate an early diagnosis of AD. However, a previous study on the 5xFAD (a fast AD model), showing retinal changes before those in the brain, has been questioned because of the involvement of the retinal degeneration allele $Pde6b^{rd1}$. Here, we tested in parallel, at 4 and 6 months of age, both the retinal and the brain structure and function in a 5xFAD mouse line that carries no mutation of rd1. In the three tested regions of the 5xFAD brain (hippocampus, visual cortex, and olfactory bulb), the Aβ plaques were more numerous than in wild-type (WT) littermates already at 4 months, but deterioration in the cognitive behavioral test and long-term potentiation (LTP) lagged behind, showing significant deterioration only at 6 months. Similarly in the retina, structural changes preceded functional decay. At 4 months, the retina was generally normal except for a thicker outer nuclear layer in the middle region than WT. At 6 months, the visual behavior (as seen by an optomotor test) was clearly impaired. While the full-field and pattern electroretinogram (ERG) responses were relatively normal, the light responses of the retinal ganglion cells (measured with multielectrode-array recording) were decreased. Structurally, the retina became abnormally thick with few more Aβ plaques and activated glia cells. In conclusion, the timeline of the degenerative processes in the retina and the brain is similar, supporting the use of non-invasive methods to test the retinal structure and function to reflect changes in the brain for early AD diagnosis.

Keywords: Alzheimer's disease, retinal ganglion cell, multielectrode array, long-term potentiation, photoreceptor

OPEN ACCESS

Edited by:
Jianhai Du,
West Virginia University, United States

Reviewed by:
Saravanan Kolandaivelu,
West Virginia University Hospitals, United States
Ilaria Piano,
University of Pisa, Italy

****Correspondence:***
Ying Xu
xuying@jnu.edu.cn
Kin Chiu
datwai@hku.hk

† These authors have contributed equally to this work

Specialty section:
This article was submitted to Neurodegeneration, a section of the journal Frontiers in Neuroscience

Received: *17 March 2021*
Accepted: *16 June 2021*
Published: *23 July 2021*

Citation:
Zhang M, Zhong L, Han X, Xiong G, Xu D, Zhang S, Cheng H, Chiu K and Xu Y (2021) Brain and Retinal Abnormalities in the 5xFAD Mouse Model of Alzheimer's Disease at Early Stages. Front. Neurosci. 15:681831. doi: 10.3389/fnins.2021.681831

INTRODUCTION

Alzheimer's disease (AD) is a progressive, age-related neurodegenerative disorder that causes memory loss and a decline in cognitive function in patients. It is characterized by abnormal accumulation of beta-amyloid (Aβ) plaques and neurofibrillary tangles in the central nervous system, which cause selective loss in neurons and synaptic connections (Huang and Jiang, 2009). As the current standard tests including testing Aβ biomarkers by positron emission tomography and cerebrospinal fluid assays are invasive and expensive (Sutphen et al., 2014), early diagnosis of AD remains a challenge for its treatment.

Increasing data from clinical and animal research indicate that retina may serve as a window for early diagnostic of AD. Several changes were reported in AD patients' vision; these include decrease in visual acuity, contrast sensitivity, color discrimination, pattern electroretinogram (pERG) response, and defects in the visual fields. Morphological changes were also shown with optical coherence tomography (OCT) scanning, and these include a thinning of the retinal nerve fiber layer (RNFL) and a deficit in the retinal vasculature [reviewed in Chiquita et al. (2019)]. Visual and morphological deficits including a decrease in pERG response, presence of Aβ and Tau tangles in retina, thinning of RNFL and ganglion cell layers, loss of ganglion cell numbers, and reactive gliosis [reviewed in Chiquita et al. (2019)] were reported in different transgenic AD animal models at various degrees. Furthermore, simultaneous examinations of the retina and brain pathologies are limited, and hence, the correlation of the time course of retinal pathology and brain degeneration remained unclear.

The 5xFAD mice is a good model with emphasis on the overaccumulation of Aβ with marked AD symptoms seen in behavioral tests by the age of 6 months (Oakley et al., 2006). Using this model, it has been reported that the Aβ deposits in the retina appears as early as 1.5M (Pogue et al., 2015), and retinal light responses and visual acuity decays earlier than the cognitive deficit (Criscuolo et al., 2018). However, the 5xFAD mice used in these studies contained Pde6b^{rd1} mutation that cause rods to die; hence, the effect of the 5xFAD mutations could not be isolated. Therefore, it is important to reassess the progressive retinal degeneration that is caused by Aβ overaccumulation. Work done by Lim et al. (2020) found abnormal retinal structure and function at age of 6, 12, and 17 months. These retinal degenerative processes were progressive and associated with amyloid pathology patterns similar to that of the brain. However, it remained unclear whether the retina shows abnormalities at an early stage of AD or even precedes the brain degeneration in this non-Pde6b^{rd1} 5xFAD mice. Therefore, the goal of this study was to investigate the progressive changes in the retinal structure and function of 5xFAD mice with no mutation of rd1 and to compare them with Aβ-related pathologies in the brain.

MATERIALS AND METHODS

Animals

Transgenic mice with 5xFAD mutations [B6.Cg-Tg (APPSwFlLon, PSEN1*M146L*L286V) 6799Vas/Mmjax] (Oakley et al., 2006) were purchased from Jackson Lab (MMRRC stock no. 34848) with no retinal degeneration allele Pde6b^{rd1}. 5xFAD transgenic mice overexpress both mutant human APP (695) with the Swedish (K670N, M671L), Florida (I716V), and London (V717I) Familial Alzheimer's Disease (FAD) mutations and human PS1 harboring two FAD mutations, M146L and L286V, under transcriptional control of the neural-specific mouse Thy1 promoter (Oakley et al., 2006). C57BL/6J female mice were purchased from Guangdong Medical Lab Animal Center to be bred to 5xFAD to maintain the colony. Hemizygous 5xFAD mice and non-transgenic wild-type littermates were used. All animals were kept under standard laboratory conditions with 12-h/12-h light/dark cycles and were supplied with regular food and water. All animal procedures were performed according to the ARRIVE guidelines and were approved by competent ethics committee at Jinan University. All efforts were taken to minimize the number of animals used and their suffering.

Morris Water Maze Test

A water tank 70 cm in diameter and 35 cm in height was filled with water to 16.5 cm at 22–25°C. The pool was divided into four equal quadrants. A 4×4-cm^2 white escape platform was placed 5 cm beneath the water at the center of the fourth quadrant. During four consecutive days of training session, mice were placed into the pool and allowed to search for the platform for 60 s for four trials (once from each quadrant) with at least 10-min interval. Animals were guided to the platform if they could not find it within 60 s, in which case the latency was recorded as 60 s. On the fifth day, the platform was removed from the pool, and mice were allowed to swim freely in the pool for 60 s. Times of animals traversing the original platform position and the time spent in the target quarter were measured to evaluate the working memory of the animal. Data were recorded with a video camera and analyzed using EthoVision XT 7.0 (Noldus, Wageningen, the Netherlands). Animals that refused to swim were excluded from the experiments.

Visual Behavioral Tests

The day after the water maze test, the visual performance of these mice was tested by a black–white transition system and then an optokinectic system. The black–white transition system measures the ability of animal to tell luminance. As we previously described (Zhang et al., 2017), an animal was placed at the center of the white chamber that was connected with the black chamber and was able to move freely between these two chambers. The time at which the animal stayed in the black chamber was recorded by Noldus EthoVision XT 8.0 software.

Optomotor system measured the visual acuity of the animal. Briefly, dark-adapted mice were placed on a pedestal located at the center of an enclosure formed by four video monitors that displayed the stimulus gratings. Vertical sine wave gratings (100% contrast) written in MATLAB (MathWorks, Natick, MA, USA) were projected on the computer monitors and rotated at the speed of 12°/s with increasing spatial frequencies of 0.1, 0.2, 0.3, 0.35, 0.4, 0.45, 0.5, and 0.6 cycle/degree. For each spatial frequency, the grating was rotated clockwise for 1 min and then counterclockwise for another 1 min. Animals reflexively track the gratings by head movements as long as they could follow them. The head movements were videotaped, and the maximal spatial frequency at which an optokinetic response could be followed was recorded as the visual acuity of the animal.

Electroretinogram

After behavioral tests, mice were dark adapted for 4 h, and the electroretinogram of mice was measured to test retinal function with a RETI-scan system (Roland Consult, RETI-scan, Heidelberger, Germany) as we previously described (Zhang et al., 2017; Liu et al., 2018). Briefly, mice were anesthetized with tribromoethanol (0.14 ml/10 g bodyweight of 1.25% solution)

and placed on a heated platform (37°C) under dim red light. Pupils were dilated with phenylephrine HCl (0.5%) and tropicamide (0.5%). ERGs were recorded with gold-plated wire loop electrodes contacting the corneal surface as the active electrode. Stainless steel needle electrodes were inserted in the skin near the eye and in the tail serving as reference and ground leads, respectively. Dark-adapted animals were stimulated with full-field green flashes of graded intensities of 0.01, 0.1, and 3.0 cd/m^2 by Ganzfied stimulator. Then, mice were light adapted for 5 min under bright green background (20 cd/m^2), and photopic responses to green flashes of 3.0 and 10.0 cd/m^2 were recorded. ERG data were collected with RETI-scan system at a sampling rate of 2 kHz and analyzed with the RETIport software (Roland) after 50 Hz low-pass filtering. To isolate the oscillatory response (OPs), a 100-Hz high-pass filter was further applied. The a-wave amplitude was measured from baseline to the first negative peak, and the b-wave amplitude was measured from a-wave trough to the next positive peak. Photopic negative response (PhNR) was measured as the amplitude of the negative peak following b-wave relative to the baseline. To measure the amplitude of OPs, the voltage difference between the second negative peak (N2) to positive peak (P2) and between the third negative peak (N3) to positive peak (P3) were measured. For each animal, the average response of the two eyes was taken as one data point. To further evaluate the function of retinal ganglion cells, some mice were tested with patterned ERG projected by a flat LED screen (Roland). The pattern consisted of a horizontal grating (with 0.5°/cycle and 99% contrast) and a flicker checkerboard (horizontal grating size, 2°50″; checkerboard size, 4°15″; flickering frequency, 1.0 Hz). The animal was tilted with the left eye covered and the right eye directly facing the center of the screen at the distance of 26 cm for the recording after photopic ERG recording. The sampling rate was 1 kHz, and 200 trails were recorded and averaged. The pERG waveform is characterized by a small initial negative wave N1, followed by a large positive wave P1, and then a second negative wave N2. The amplitude of P1-N2 peak was measured to evaluate pERG.

Multielectrode Array Recording From Retina and Data Collection

To examine the light response of single ganglion cell, multielectrode array (MEA) recording was performed on whole-mount retinas as we previously described (Liu et al., 2018; Bao et al., 2019). Briefly, mice were dark adapted for 3 h before euthanization, and a small piece of retina (∼2×2 mm^2) from whole-mount regions avoiding main blood vessels was pressed down on an 8×8 MEA array (with electrodes of 20 μm in diameter spaced 100 μm apart; P210A, Japan) by a platinum ring to obtain a close contact between the ganglion cells and the electrodes. The MEA array with the retina was transferred to the recording stage, connected to the amplifier (MED64 amplifier; Alpha MED Scientific, Inc., Osaka, Japan), and perfused continuously with the oxygenated AMES solution at a rate of 3 ml/min at ∼32°C. After dark adaptation in a light-tight enclosure for over 30 min, retinas were stimulated with a white light-emitting diode (LEDWE-15; Thorlabs, Newton, NJ, USA) with the stimulation intensity and duration controlled by the main amplifier (MED64; Alpha MED Scientific, Inc.). The LED gave a full-field flash focused onto the photoreceptor layer of the retina. The flash protocol consisted of a 2-s light ON with a saturating intensity of 3.6×10^7 photons/μm^2/s, followed by an 8-s light OFF, and repeated 30 times.

The MEA system with MED64 amplifier (Japan) and Mobius software (MED64, Japan) was used for recording and filtering spike trains from each of the electrode in the array. Extracellular spikes were bandpass filtered between 100 and 5,000 Hz, digitized at a rate of 20 kHz, and subsequently analyzed offline.

To identify responses from each individual cell, the MEA data were processed offline using a spike sorter software (Offline Sorter, Plexon Inc., Dallas, TX, USA) as previously described (Liu et al., 2018). Sorted spikes were then exported to Spike2 (version 8, CED, UK), MATLAB (MathWorks), and R software (version 3.3.0) to get the peristimulus time histograms (PSTHs) and raster plots of individual cells with a 10-ms bin width. Light responses were measured as the average spike rate during the first 2 s of light onset (ON) or offset (OFF) or the average of both ON and OFF (for ON–OFF), subtracted by the spontaneous spiking (average response within 2 s before light onset).

LTP Recordings With Microelectrode Array

LTP was recorded from CA3–CA1 regions of hippocampal slices from 6-month-old 5xFAD and WT mice. Briefly, a mouse was decapitated under isoflurane anesthesia; then, the brain was quickly dissected and placed in ice-cold oxygenated (95% O_2/5% CO_2) sucrose cutting solution (containing in mM: 40 NaCl, 4 KCl, 26 $NaHCO_3$, 1.25 NaH_2PO_4, 0.5 $CaCl_2$,7 $MgCl_2$, 10 D-glucose, and 150 sucrose, pH 7.4, 330 mOsmol). Slices were then cut into 300 μm thickness with a Vibratome (VT1000S; Leica, Wetzlar, Germany) and maintained at room temperature for at least 1 h in the oxygenated artificial cerebrospinal fluid (ACSF) (comprising in mM: 125 NaCl, 3.5 KCl, 26 $NaHCO_3$, 1.2 NaH_2PO_4, 2.4 $CaCl_2$, 1.3 $MgCl_2$, 25 D-glucose, pH 7.35, 310 mOsmol). Then, a single slice was transferred to an 8×8 MEA array (with electrodes of 50 μm in diameter spaced 200 μm apart; Japan), pressed down by a nylon mesh, and continually perfused with oxygenated ACSF buffer (flowrate, 3 ml/min) at 34°C. One of the microelectrodes under the apical dendritic region of CA3 was selected for stimulating the Schaffer collateral pathway. A biphasic electric current (ranging from −10 to 40 pA) of 0.20 ms was given every 20 s at the stimulus intensity sufficient to elicit 30–50% maximal extracellular field excitatory postsynaptic potential (fEPSP) recorded from other electrodes. After establishing a stable baseline for at least 15 min, three repeated theta-burst stimulations (TBSs) were applied. Each TBS contained 10 trains of four 100-Hz pulses at 5 Hz, and TBS was repeated three times with a 20-s interval. After the TBS stimuli, fEPSP were recorded every 20 s for another 45 min. The peak amplitudes of the fEPSPs were measured by the MED64 Mobius software.

For both retinal and brain slice recording, at the end of recording, the position of the tissue on the array was verified under a dissecting microscope, and a bright field image was taken with a digital camera (Mshot Image Analysis System; MC16, Guangzhou, China).

Tissue Processing and Immunocytochemistry

Animals were killed by anesthetic overdose with tribromoethanol, and eyes were enucleated and fixed in 4% paraformaldehyde (PFA) for 30 min at 4°C. Following fixation, the eyes were rinsed in 0.01 M phosphate buffered saline (PBS), cryoprotected overnight at 4°C in 0.01 M PBS containing 30% sucrose, and embedded in optimal cutting temperature compound (OCT; Tissue Tek, Torrance, CA, USA). Retinas were cryosectioned through the optic disk (OD) longitudinally at a thickness of 15 μm, and sections were mounted on glass slides for future process.

For brain tissue collection, brains were removed and washed in PBS three times with 1 min each time, then fixed in 4% paraformaldehyde (PFA) for 24 h at room temperature (RT). Then, brains were rinsed in PBS, cryoprotected in 0.01 M PBS containing 10, 20, 30, and 40% sucrose at 4°C overnight for each concentration before embedded in OCT. Brain were cryosectioned into sagittal slices at a thickness of 20 μm, and sections were mounted on glass slides for future process.

For immunochemical staining, both eyes and brain sections were washed three times for 5 min with 0.1% Triton X-100 in PBS (0.1% PBST) and incubated in 0.3% PBST containing 3% normal donkey serum (NDS), 1% bovine serum albumin (BSA), and 0.3% Triton X-100 for 1 h at RT, then incubated with primary antibodies overnight at 4°C. After thorough washes with 0.1% PBST, retinal or brain sections were incubated with secondary antibodies for 1 h at RT. Sections were then washed, mounted, and sealed under coverslips. For 4′,6-diamidino-2-phenylindole (DAPI) staining, sections were incubated with DAPI (1:1,000, Electron Microscopy Sciences, Hatfield, PA, USA) for 5 min at room temperature, then washed before mounting.

The primary antibodies used were rat anti-glial fibrillary acidic protein (anti-GFAP) (1:500, 13-0300, Thermo Fisher, Waltham, USA), rabbit anti-Iba1 (1:1,000, 019-19741, Wako, Osaka, Japan); anti-Brn3A (1:500, ab81213, Abcam, Cambridge, UK) and Aβ 1-42 antibody (1:1,000, Cat. # AB5078P, Millipore, Burlington, USA). Secondary antibodies used were donkey-antirabbit or goat-antirat IgG (conjugated to Alexa 488 or 594; 1:1,000, Invitrogen, Waltham, USA).

To calculate the thickness of each retinal layer, retinal slices were stained with Hematoxylin and Eosin (HE) Staining Kit (G1120, Solarbio, Beijing, China) according to the provided protocol. To stain for senile plaques, brain sections were rehydrated and dehydrated in distilled water for 2 min. Then, they were incubated with thioflavin solution (1% in DDW) for 5 min. Slices were immersed in 70% alcohol for 5 min and washed with distilled water two times before mounted.

Image Collection and Processing

Fluorescent or immunostaining images were captured using a Zeiss LSM700 confocal microscope or fluorescent microscope (Carl Zeiss, Oberkochen, Germany). To measure the survival of retinal ganglion cells, Brn3a-positive cells were counted on whole-mount retina from 12 regions (field size, 200×200 μm) distributed at a distance of 300, 1,000, and 1,700 μm from the optic disk for each quadrant of the retina, and the average density of RGCs over 12 regions was calculated. To measure the Iba1 expression, the number of Iba-1-positive cells were counted from the middle region on the whole-mount retina at the size of 320×320 μm. For all retinal slices, to ensure analysis of the same eccentricity for different retinas, images were taken from regions 1–1.2 mm from the optic disk. To measure the thickness of each layer of retina, a line was drawn from the left, right, and center of each HE staining image, and the length of three lines were measured and averaged as one data point for the image. To measure the fluorescent intensity of GFAP, retinal sections from different groups were processed simultaneously with the same procedure and imaging parameters; the mean fluorescent intensity in the inner retinal region (INL, IPL, and GCL) was measured by Zen software (Zeiss, Germany), then normalized to the mean of WT at the same age. To quantify the number of Aβ in brain regions, the hippocampal area (HP, 1,500×2,250 μm), visual cortex (VC, 1,100×850 μm), and ventro-posterior of olfactory bulb (OB, 1,100×850 μm) were imaged and analyzed from the sagittal plane.

Image J software (NIH, Bethesda, MD, USA) was applied for analyzing all the measurements. For each retina and brain slice, data from three to five images was averaged to provide one data point; these were then averaged for all retinas to provide the average of each group. For a better display of the images in the figures, intensity enhancement was applied by Photoshop (Adobe Inc., San Jose, USA) with the same adjustment.

Statistical Analysis

All data are expressed as mean ± SEM. Student's *t*-test or two-way ANOVA with Sidak's *post-hoc* tests was performed with GraphPad 7 (GraphPad Software, San Diego, CA, USA) depending on the number of groups to compare. $p < 0.05$ were considered statistically significant, and $p < 0.01$ were highly significant. Unless otherwise stated, the "n" indicates the total number of mice examined for each group.

RESULTS

5xFAD Mice Demonstrate a Deficit in Working Memory and Hippocampal LTP at 6 Months

In order to identify the behavioral changes in our 5xFAD mice, we first performed a Morris water maze test for cognitive performance. Mice were tested at the ages of 4 and 6 months (examples of the moving traces at 6 months are shown in **Figure 1A**). During trial days, both WT mice and 5xFAD showed a decrease in the escape latency, but the latency of 5xFAD mice decreased more slowly than WT ($p < 0.05$ for 4 months and $p < 0.001$ for 6 months, two-way ANOVA) (**Figure 1B**). On the test day, 5xFAD mice trans-passed the platform region at a lower frequency than WT ($p = 0.4$ for 4 months, $p < 0.05$ for 6 months, **Figure 1C**). This result indicates a deficit in spatial working memory in 5xFAD at 6 months.

After the water maze test, to determine whether the memory impairment of 5xFAD mice was also observed at the level of

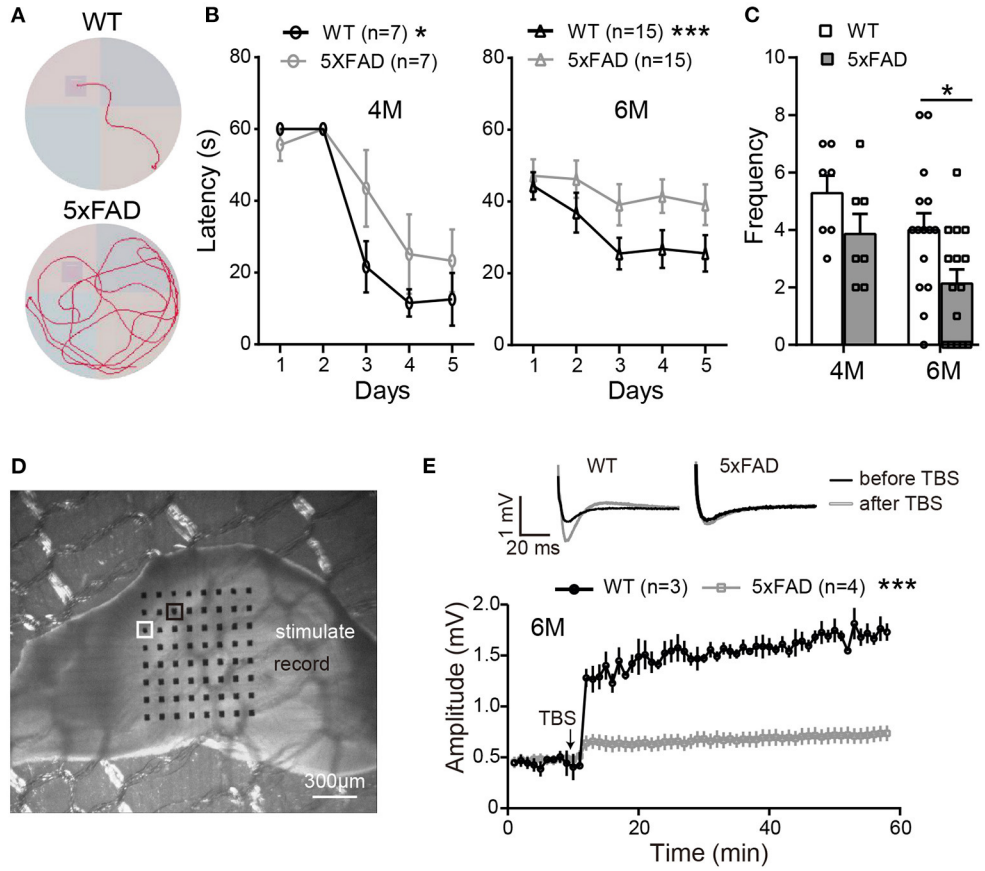

FIGURE 1 | The working memory and LTP deficiency in 5xFAD mice. **(A)** Swimming traces of a WT and 5xFAD mice in the water maze, with the hidden platform in the upper-left quadrant. **(B)** The latency for mice to reach the platform during the first 5 days of trials at 4 and 6 months. **(C)** The frequency of mice crossing the platform region on the test day. 5xFAD mice at 6 months took longer time to locate the platform during the trial day and crossed the platform region less frequently than WT. **(D)** Illustration of a mouse hippocampus slice placed on the 8×8 multielectrode array. One of the electrodes (white squared) was used to apply the electric stimuli; the other electrodes recorded the evoked field potential; the electrode squared in black, which gave the best response, was selected for data analysis. **(E)** Average changes in the amplitude of the evoked post-synaptic potential (EPSP) within 45 min after the theta-burst stimulation (TBS) in WT and 5xFAD mice. Typical EPSP of a WT and 5xFAD mice before (black line) and after (gray line) TBS stimulation at an expanded time scale are shown above. n, number of experimental animals. Data shown as mean ± SEM. *$p < 0.05$; ***$p < 0.001$; two-way ANOVA.

neuronal networks, we carried out hippocampal LTP recordings from the same batch of mice. Stimulating the Schaffer collaterals of CA3 elicited excitatory postsynaptic potentials (EPSPs) in the CA1 area (**Figures 1D,E**). After stable baseline recording in hippocampal slices of WT mice, a theta burst stimulation (TBS) induced long-term potentiation of EPSP in CA1 area. This LTP effect was hardly observed in 5xFAD mice at 6 months (**Figure 1E**).

Aβ Plaque Deposits Are Detected in the Brain of 5xFAD at 4 Months

After identifying the memory and LTP deficits in 5xFAD, we tested the expression of Aβ plaques in different brain regions using thioflavine S staining. The staining showed that there were obvious Aβ plaques in the olfactory bulb (OB), the visual cortex (VC), and the hippocampus (HP) of 5xFAD mice at both 4 and 6 months (**Figures 2A,B**, with enlarged areas shown in **Figures 2C,D**), while no plaques were found in WT controls. The number of plaques in each brain region of 5xFAD was significantly higher than that in WT (**Figure 2E**). Interestingly, in the olfactory bulb of 5xFAD mice, the accumulation of Aβ plaque was more gradual as it increased from 4 to 6 months (21.9 ± 1.5 vs. 73.0 ± 5.0, $p < 0.001$), while the number in the hippocampal region and the visual cortex was already high at 4 months and then remained stable or increased slowly (**Figure 2E**).

The Visual Behavior of 5xFAD Mice Is Impaired at 6 Months

After confirming the AD symptoms in the brain of 5xFAD mice, we wondered whether the visual system had similar deficits. We examined the visual system by optokinetic behavior and electroretinogram recordings and then by histological examinations.

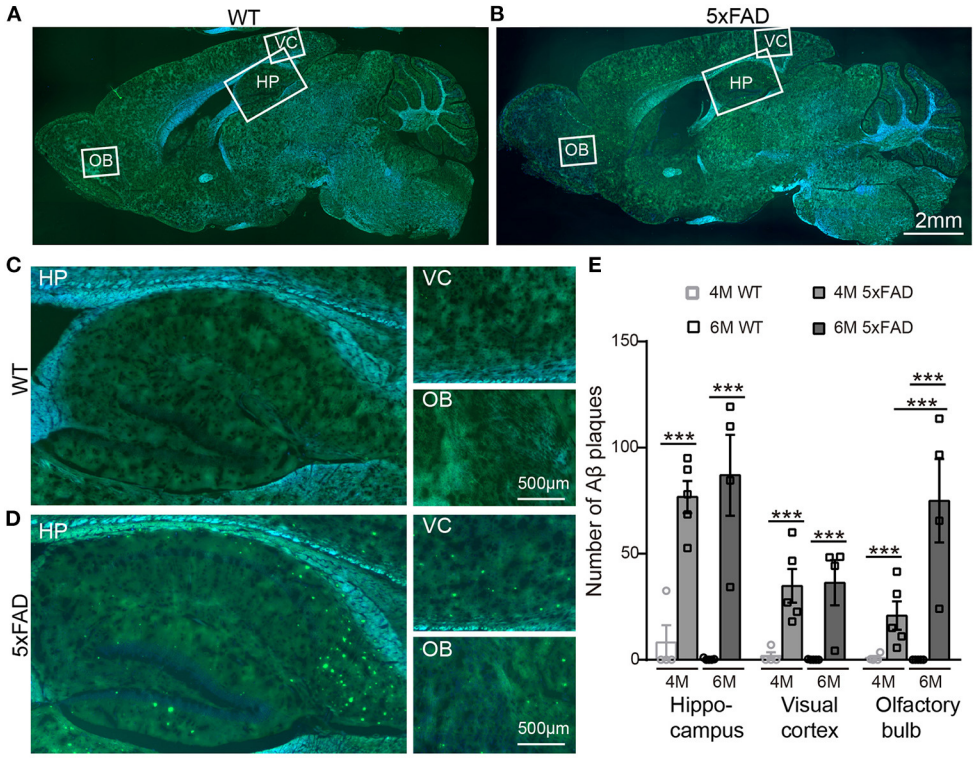

FIGURE 2 | Aβ plaques appear in various brain regions of 5xFAD mice already at 4 months. **(A,B)** Images of brain slices stained with thioflavine S (green) that labels Aβ plaques from a **(A)** WT and **(B)** 5xFAD mice. Brain regions including olfactory bulb (OB), hippocampus (HP), and visual cortex (VC) were enlarged in Panels **(C)** and **(D)**, respectively, for WT and 5xFAD. **(E)** Number of Aβ plaques in different brain regions of WT and 5xFAD at 4 and 6 months. At 4 months, 5xFAD mice have more Aβ plaques in the brain than WT. Data shown as mean ± SEM. ***$p < 0.001$, two-way ANOVA test.

The optokinetic system tests the ability of a mouse to track rotating gratings with its head (**Figure 3A**). The visual acuity (i.e., the highest spatial frequency of the grating that can induce the optokinetic reflex in mice) of the 5xFAD mouse decreased compared to WT, and the difference reached significance at 6 months (0.32 ± 0.03 c/d vs. 0.41 ± 0.02 c/d in WT, $p < 0.05$) but not at 4 months (**Figure 3B**).

The ability of a mouse to tell luminance was tested with a black/light transition box. The 5xFAD mice tended to spend shorter time than WT control in the black chamber, but the difference did not reach statistical significance at 6 months (5xFAD: 174 ± 23 s in black box, $n = 4$; WT: 208 ± 19 s, $n = 6$; not shown).

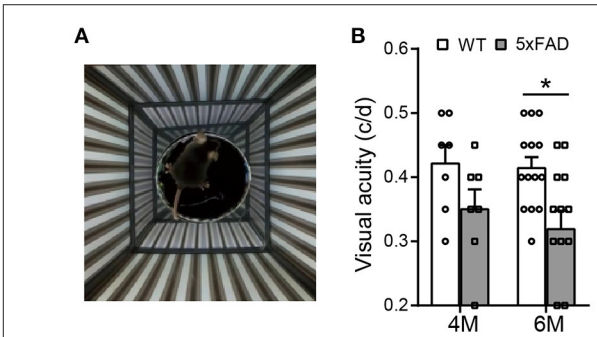

FIGURE 3 | The visual acuity is impaired in 5xFAD mice at 6 months. **(A)** Illustration of the optokinetic system that measures the mouse visual acuity. Visual acuity is the maximum spatial frequency of the moving gratings that a mouse can track with its head movement. **(B)** Scattered plot of the visual acuity of 5xFAD and WT at 4 and 6 months. The visual acuity of 5xFAD was lower than that of WT both at 4 months and at 6 months, and the difference reached significance at 6 months. Data shown as mean ± SEM. *$p < 0.05$, two-way ANOVA.

Rod and Cone Light Responses Are Normal in 5xFAD Mice

The deficit in the above visual behavior indicates a deficit either in the retina or the retina-to-superior colliculus pathway (or both). Thus, we next evaluated the retinal function by full-field ERG recording. Under dark adaptation (scotopic conditions), both WT and 5xFAD mice responded well to flashes of increasing intensities (0.01, 0.1, and 3.0 cd s/m^2) (**Figure 4A**). The amplitude of the a- and b-waves were similar between 5xFAD and WT at both 4 and 6 months (**Figures 4B,C**), indicating that the rod-to-rod bipolar pathway is normal in 5xFAD. We next light adapted the mice (photopic condition) and recorded cone responses. Again, the b-wave amplitude was similar between

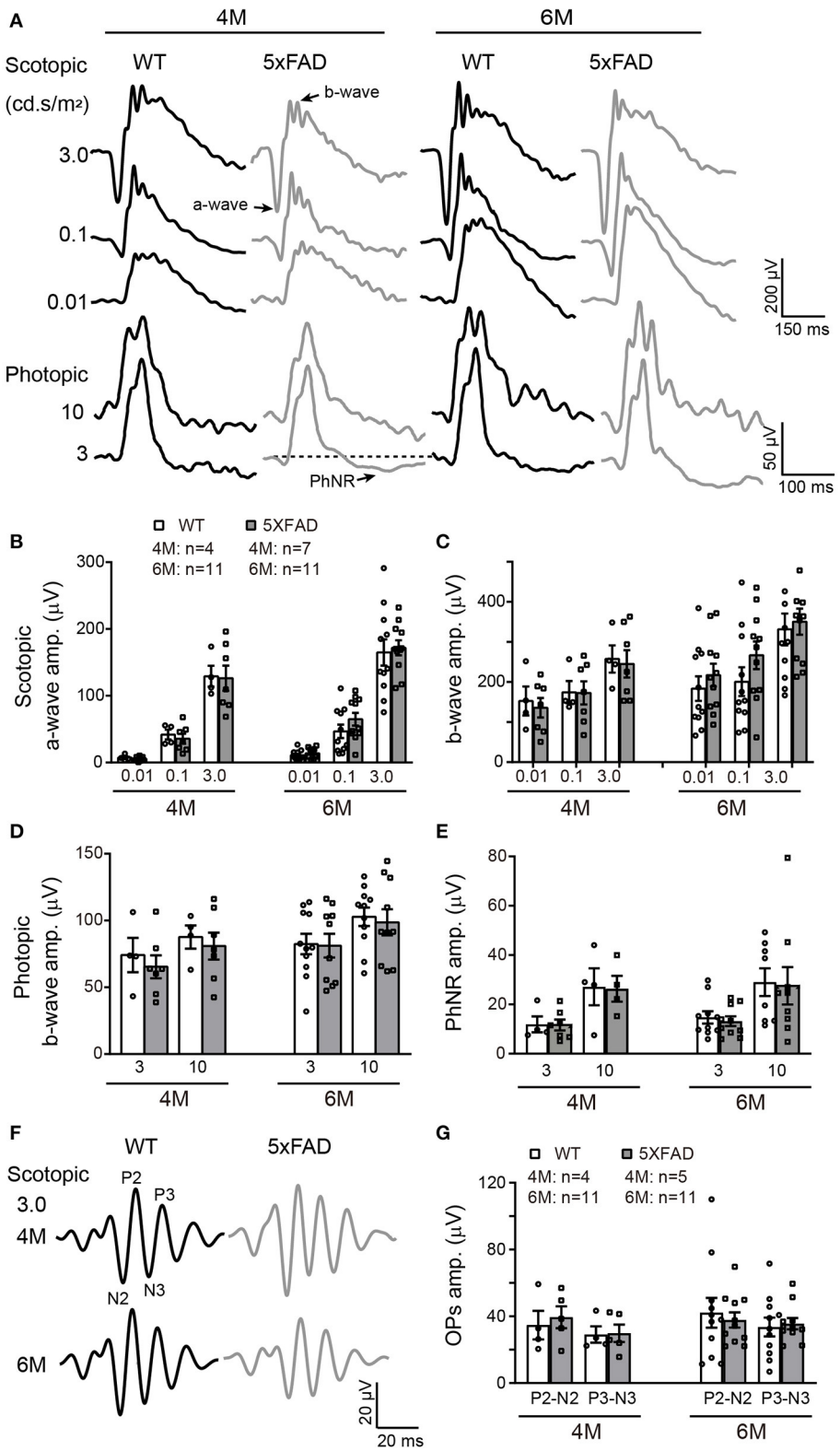

FIGURE 4 | The light responses of the first and second order retinal neurons are normal in 5xFAD. **(A)** Example ERG traces from a WT and 5xFAD mice at age of 4 and 6 months under dark adaptation (scotopic) and light adaptation (photopic). **(B,C)** Scattered plot of the amplitude of **(B)** a-wave and **(C)** b-wave under scotopic condition. **(D,E)** Scattered plots of the amplitude of **(D)** b-wave and **(E)** PhNR under photopic condition. **(F)** Example OPs traces to flash of 3.0 cd s/m^2 under scotopic condition. **(G)** Scattered plots of the amplitude of P2-N2 and P3-N3. Data shown as mean ± SEM.

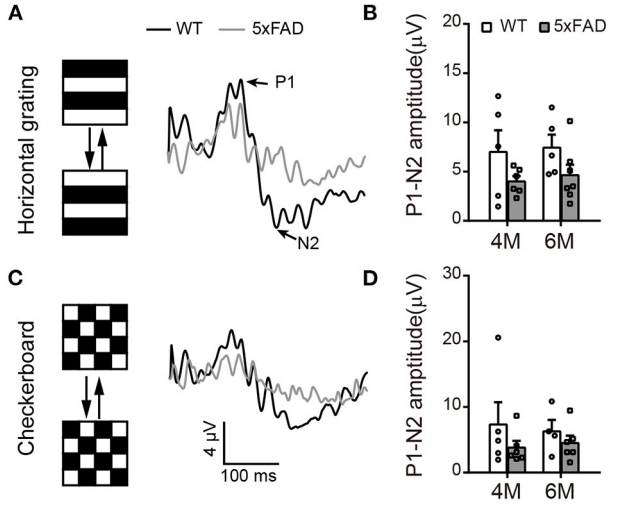

FIGURE 5 | Pattern ERG response tend to decrease in 5xFAD. **(A,C)** Example traces of pattern ERG responses to **(A)** horizontal gratings or **(C)** checkerboard from a WT and 5xFAD mice. **(B,D)** Scattered plots of the P1-N2 amplitudes under stimuli of **(B)** horizontal gratings or **(D)** checkerboard. Data shown as mean ± SEM.

5xFAD and WT at 4 and 6 months (**Figures 4A,D**), indicating that the light response of cones and bipolar cells are also normal in the 5xFAD mouse. The time-to-peak of a- and b-waves under both scotopic and photopic conditions were also similar between 5xFAD and WT (data not shown).

The light responses of amacrine cells were also evaluated by the oscillatory response (OPs) using ERG recordings. 5xFAD mice showed a normal OPs response as did WT at both 4 and 6 months (**Figure 4F**), and the amplitudes of P2-N2 and P3-N3 were similar to WT (**Figure 4G**).

The Light Response of Retinal Ganglion Cell Is Reduced in 5xFAD

To check the light response of retinal ganglion cells, we first used ERG and measured the amplitude of the photopic negative response (PhNR, a negative wave that follows the b-wave under light adaptation) to full-field stimuli. The PhNR response was similar between 5xFAD and WT at both 4 and 6 months, with similar amplitude and time to peak (**Figure 4E**). Similar results were obtained with responses to pattern ERG, which is more sensitive (Liu et al., 2014). For that, we used patterned stimuli including horizontal grating and checkerboard (**Figures 5A,C**). Under both stimuli, 5xFAD mice tended to have smaller P1-N2 amplitude, but there was no significant difference (**Figures 5B,D**).

We further analyzed the light responses of individual ganglion cells by multielectrode array recordings. An example of a flattened retina mounted on 8×8 MEA array, and the spike responses recorded in each channel are shown in **Figures 6A,B**. Both WT and 5xFAD RGCs fired strongly in response to light stimuli (**Figure 6C**). Comparing the average light response within the 2-s flashes showed a significant decrease in 5xFAD at 6 months (to 52% of WT, $p < 0.001$) but not at 4 months (**Figure 6D**). Similar changes were observed in the peak firing rate (4 months: 100.8% of WT, $p = 0.97$; 6 months: 89% of WT, $p < 0.001$, data not shown). While the light responses were not much affected at 4 months, the spontaneous frequency of 5xFAD started to decrease significantly compared with WT already at 4 months (59% of WT at 4 months and 65% of WT at 6 months, $p < 0.001$) (**Figure 6E**).

Retinal Ganglion Cells Appear Normal in 5xFAD Retina at 6 Months With a Few Aβ Plaques

As the function of ganglion cells in 5xFAD mice declined, we further examined the survival rate of RGCs by Brn3a staining on the whole-mount retina. The number of RGCs was counted for three eccentricities; for each eccentricity, we counted and averaged the numbers from four quadrants of the whole-mount retina (**Figure 7A**, enlarged area shown in **Figure 7B**). For each eccentricity, the number of RGCs in 5xFAD and WT at 4 months and 6 months was similar (**Figures 7A,B,D**).

We have also stained the retinas for Aβ plaque deposits with an Aβ1-42 antibody. For both WT and 5xFAD, staining in whole-mount retinas revealed only few Aβ plaques (red dots pointed by white arrows in **Figure 7A**). In retinal slices, however, a few Aβ deposits were observed also in the inner and outer retinal layers of 5xFAD mice but not that of WT (the sampled region was 1 mm from the optic disk) (**Figure 7C**). Counting the number of Aβ deposits in these retinal slices showed that 5xFAD retina has accumulated significantly more Aβ deposits than the WT controls (2.0 ± 0.2 accumulated from three retinal slices for each animal vs. 1.0 ± 0.2 in WT, $p < 0.05$) (**Figure 7E**).

The Retina Becomes Abnormally Thick in 5xFAD Mice

While examining the Aβ plaques, we noticed that the 5xFAD retina appeared thicker and less organized. We have therefore further examined the structure of the retinal layers. Using DAPI staining, we measured the thickness of each retinal layer from the center to periphery, with examples of images collected from the middle region (800–1,000 μm away from the optic disk center) shown in **Figure 8A**. At 4 months, all retinal layers except ONL in 5xFAD were as normal as WT (top panel, **Figure 8B**). For the ONL in 5xFAD, the thickness tended to increase from the center to middle region, then dropped in the peripheral region, and the difference from WT reached significance at the middle region of the retina. At the age of 6 months, all retinal layers of 5xFAD were thicker than WT, with regional limited thicker ONL, OPL, and INL, but a widespread thicker IPL, thus a general thicker retina from center-to-peripheral regions (bottom panel, **Figure 8B**).

Retinal Glial Cells in Retina of 5xFAD at 6 Months Are Activated

Since pathological changes often accompany inflammation, we next examined retinal inflammation using the indicator of reactive gliosis in microglia and Muller cells.

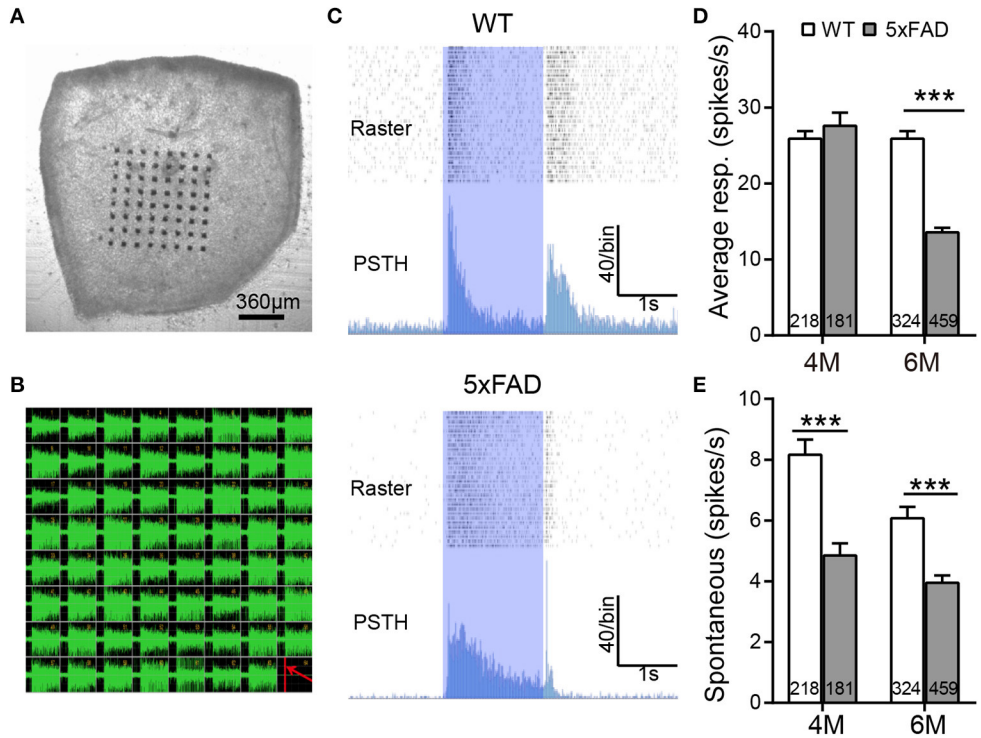

FIGURE 6 | The light response of individual ganglion cells is reduced in 5xFAD mice at 6 months. **(A)** Illustration of an isolated retinal tissue placed on an 8×8 multielectrode array. **(B)** Spikes recorded from each electrode in response to a saturated flash (light intensity (4.68×10^7 photons/μm^2/s) whose onset is indicated by a red line in the lower right corner of the array. **(C)** Examples of spiking responses from WT and 5xFAD RGCs. For each cell, the top panel shows a raster plot from 30 repeats, and the bottom panel shows the corresponding PSTH. The 2-s light stimuli are indicated as blue regions. **(D)** Average firing rate of RGCs within the 2-s light stimuli was significantly reduced at 6 months in 5xFAD. **(E)** Spontaneous firing was greatly decreased in 5xFAD mice at both 4 and 6 months. The numbers within the bars represent the number of responsive cells recorded from retinas of three animals. ***$p < 0.001$, two-way ANOVA.

In WT retina, microglia cells stained with Iba1 showed a resting state with small somas and many elongated protrusions extending around the soma. In 5xFAD retina, the appearance of the microglia cells was different at 6 months, with often shorter and less organized branches (**Figure 9A**), and the number significantly increased at 6 months (32.4 ± 3.7 vs. 22.3 ± 2.6 per 320×320 μm for WT, $p < 0.01$) (**Figure 9B**), indicating an active state. In WT retina, GFAP in Muller cells was limited to the end feet in the inner limiting layer, showing a resting state. In 5xFAD retina, the GFAP remained in the end feet area at 4 months, but at 6 months, the GFAP positive staining appeared in many processes that cross the retina (**Figure 9C**). The fluorescent intensity of GFAP in the inner retinal layers (INL, IPL, and GCL layers) increased significantly at 6 months ($p < 0.01$) (**Figure 9D**). We therefore conclude that glial cells in 5xFAD retinas are being activated at 6 months.

DISCUSSION

In this study, we examined the retinal structure and function of 5xFAD mice carrying no rd1 mutation and compared the temporal changes with the brain. Obvious retinal pathologies including thickening of retina, reactive gliosis, and few but significantly increased Aβ plaques were identified at 6 months old. An abnormal thickening of the outer nuclear layer was noticed already at 4 months. Functionally, full-field ERG and pERG remained normal, but visual acuity and light responses of individual RGCs were reduced at 6 months. In comparison, numerous Aβ plaques appeared in different regions of the brain at 4 months, but the working memory and hippocampal LTP significantly decayed only at 6 months. Thus, the timeline of retinal abnormality coincides with the progress of brain degeneration.

As early symptoms of AD include functional deficit of smell and vision, olfactory and vision biomarkers are suggested to serve as noninvasive biomarkers to diagnose dementia (Romano et al., 2021). In AD patients or AD mice, beta-amyloid deposition is found in the olfactory bulb [reviewed by Dibattista et al. (2020)]. In the 5xFAD mice, besides hippocampal region, we also found an accumulation of Aβ in the olfactory bulb and visual cortex, confirming the AD pathology in various brain regions in 5xFAD mice. But unlike visual cortex and hippocampus, the rise in Aβ deposition in the olfactory bulb was initially slow, and it kept on rising from 4 to 6 months. This suggests that the progression of AD pathology in olfactory bulb develops more slowly than

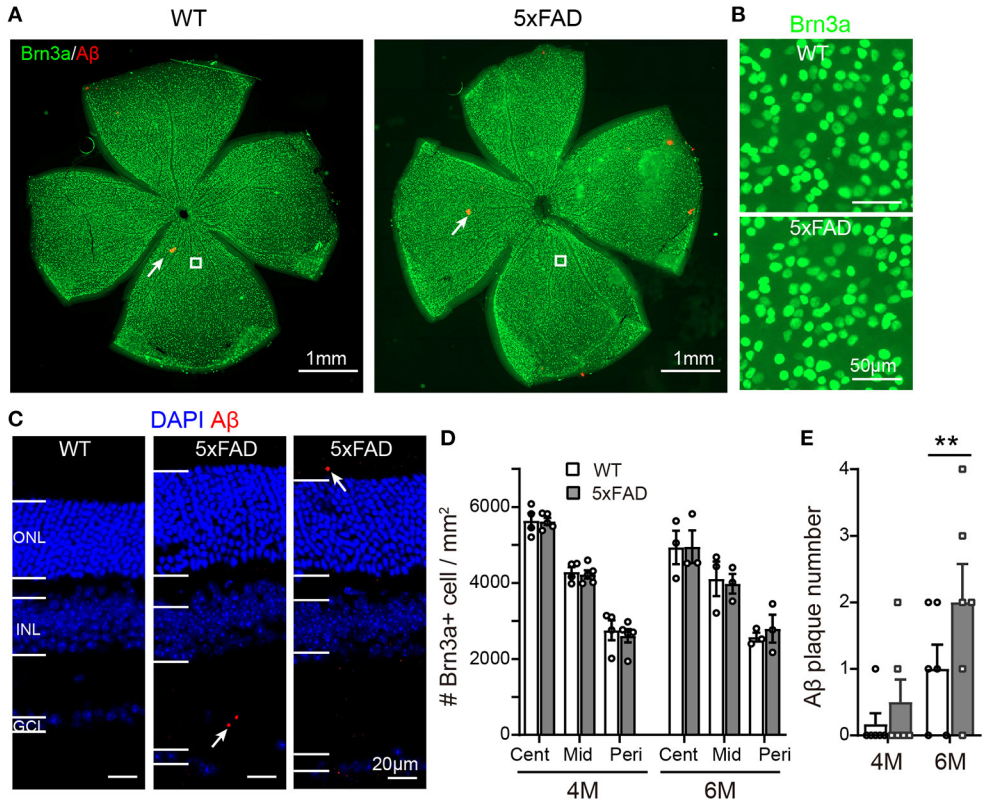

FIGURE 7 | Density of retinal ganglion cells is normal in 5xFAD but a few Aβ plaques emerge in retina at 6 months. **(A)** Example of Brn3a staining of RGCs (green) and Aβ plaque deposition (red, examples indicated by white arrows) from a whole mount retina of a WT and 5xFAD mice at 6 months; the white square from similar eccentricity is shown in Panel **(B)** at higher magnification. **(C)** Images of retinal slices stained with DAPI and Aβ plaque deposition (red, points by white arrow). **(D)** Scattered plot of the Brn3a-positive cell density in whole mount retina at central (cent), middle (mid), and peripheral (peri) regions (corresponding to 300, 1,000, and 1,700 μm away from the center of the optic disk, respectively). The RGCs density in 5xFAD is similar to that of WT at both 4 and 6 months. **(E)** Scattered plot of Aβ plaque number in retinal slices (accumulated from three slices for each animal). $^{**}p < 0.01$; two-way ANOVA.

other two brain regions. Indeed, a slower decay of the volume of olfactory bulb than hippocampus at the early and middle stages of AD was reported in rTg510 mice, another AD mice model (Kim et al., 2017). In another study on 5xFAD mice, an intact olfactory memory from 3 to 15 months of age was reported (O'Leary et al., 2020). Whether olfactory system decay differentially from hippocampus and visual system in AD mice may need further study, but it is not the main focus of current study.

Consistent with other reports, we found normal full-field ERG responses in 5xFAD both at 4 and 6 months, indicating unaffected photoreceptors and bipolar cells (Criscuolo et al., 2018; Lim et al., 2020). Regarding RGCs, we did not find an impairment of the amplitude of PhNR or pERG, which represents a compound light response of all RGCs (Porciatti, 2007; Chrysostomou and Crowston, 2013). However, those methods may not be as sensitive as the pSTR used by Lim et al., who reported a decreased amplitude of pSTR at 6 months on the same mouse line (Lim et al., 2020). This finding is consistent with our MEA data, which showed a reduced light response in RGCs in 5xFAD by 6 months and also a reduced spontaneous firing at 4 months. The dysfunction of RGCs was also reported in AD patient (Parisi et al., 2001). The response of amacrine cell, indicated by OPs, remained normal in 5xFAD as in WT. Thus, the reduction in ganglion cell activity found with MEA recordings probably depends on direct changes within these cells rather than abnormal transmission from their upstream cells.

Morphologically, instead of observing retinal thinning as in other reports on animals (Liu et al., 2009; Georgevsky et al., 2019) and AD patients [reviewed in Chiquita et al. (2019)], we found an abnormal thickening of the 5xFAD retina at 6 months, and the ONL was thicker already at 4 months. The seemingly different results are likely due to the different age used in these reports. In AD patients, the reduction in the retinal neve fiber layer (RNFL) is reported in patients showing mild to severe cognitive impairment (Paquet et al., 2007; Gao et al., 2015), while no difference or even thicker inner retina (especially IPL) in preclinical AD patients was also reported (Snyder et al., 2016; van de Kreeke et al., 2019). Consistent with the results from preclinical AD patient, Lim et al. observed a thickening of IPL at 6 months only, but not at a later stage (Lim et al., 2020) in 5xFAD mice, while RNFL layer decreased since 6 months. In other animal models such as Tg2576 mice (Liu et al., 2009),

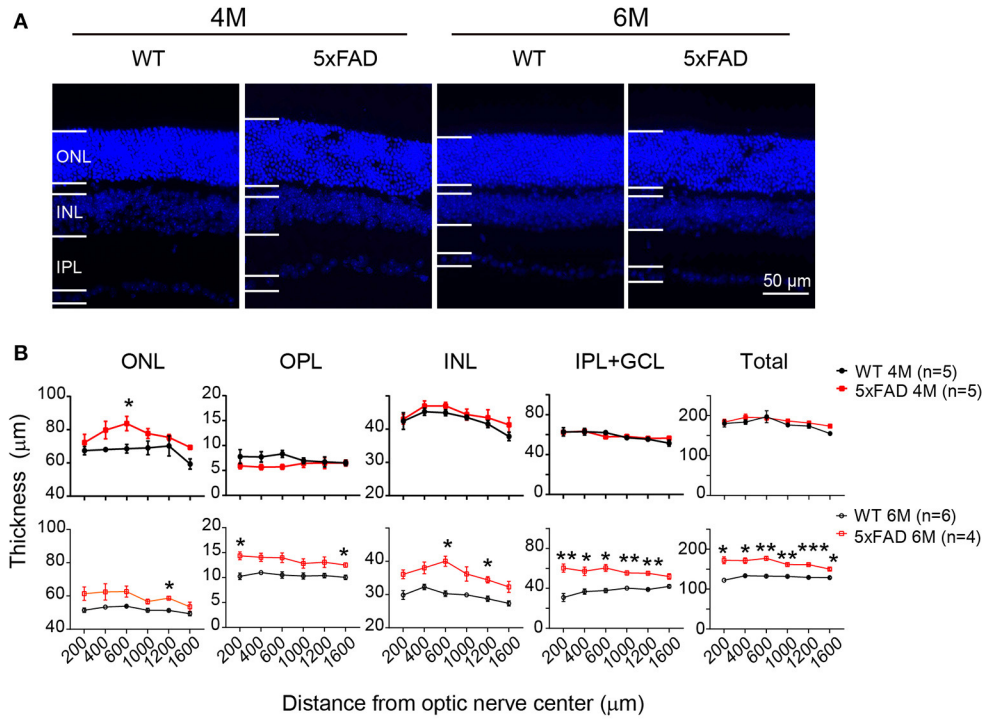

FIGURE 8 | Retina is abnormally thick in 5xFAD mice already at 4 months. **(A)** Images of DAPI staining of retinal slices from a WT and 5xFAD mice at 4 and 6 months. **(B)** Retinal thickness from the center to periphery for ONL, OPL, INL, and IPL with GCL layers and the total thickness at 4 months (top panel) and 6 months (bottom panel). The retina of 5xFAD mice is thicker than that of WT at 6 months. ONL, outer nuclear layer; INL, inner nuclear layer; GCL, ganglion cell layer. Data shown as mean ± SEM. $^{*}p < 0.05$, $^{**}p < 0.01$; $^{***}p < 0.001$, two-way ANOVA with repetitive measurement. n, number of animals tested.

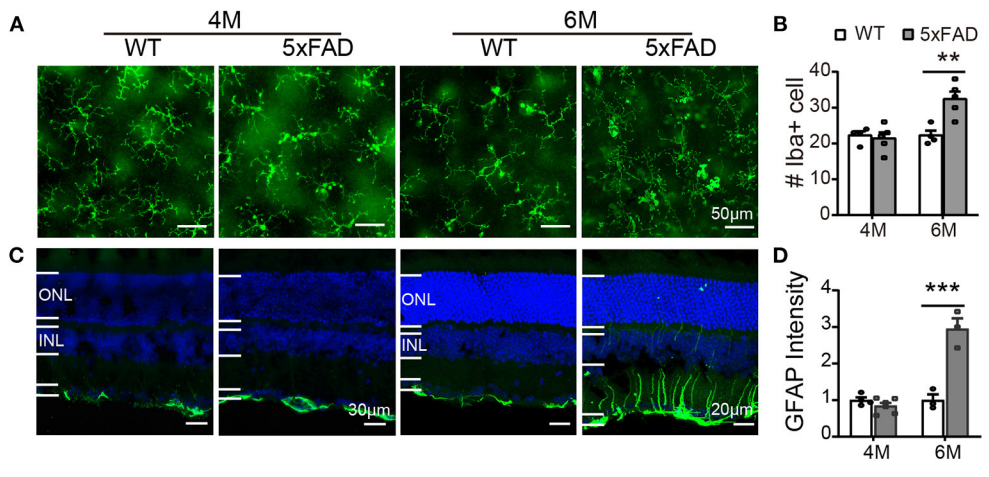

FIGURE 9 | Reactive gliosis happens in 5xFAD at 6 months. **(A)** Images of Iba1 staining (green) on whole mount retinas of WT and 5xFAD mice at 4 and 6 months. **(B)** Number of Iba1+ cells on retina (an image size of 320×320 μm). **(C)** Images of GFAP staining (green) on retinal sections of WT and 5xFAD mice at both ages. Note the difference in scale. **(D)** The GFAP intensity in the inner retina, normalized to the WT control. ONL, outer nuclear layer; INL, inner nuclear layer; GCL, ganglion cell layer. Data shown as mean ± SEM. $^{**}p < 0.01$; $^{***}p < 0.001$, two-way ANOVA.

3xTg mice (Song et al., 2020), and APP1/PS1 (Georgevsky et al., 2019), a thinning of the retinal layers was reported at late stages, but in an earlier study, using APP1/PS1 mice up to 12M, no retinal pathology was observed (Chidlow et al., 2017). The early thickening of the retina we observed in 5xFAD may be related to the inflammation that happened around 6 months or edema. Therefore, at the initial time, there might be edematous change before any detectable functional change. Future experiment using

OCT system to check the retinal thickness in alive 5xFAD mice at early stages would help for early non-invasive diagnostic. Indeed, we were collecting a series of OCT scanning of 5xFAD retina together with its littermate at various time points (as early as 3M) to access this possibility. It may be puzzling that the ERG waves in 5xFAD mice were normal in spite of abnormal retinal thickness. This may be due to the full-field flash we applied, since full-field flash ERG averages responses all over the retina and may not be able to detect regional difference. Future experiment using multifocal ERG may help to identify any regional response abnormalities that may be correlated with the outer retinal structure.

In both AD patients and animal models, Aβ plagues were present in the retina (Koronyo-Hamaoui et al., 2011) [also see review Chiquita et al. (2019)]. Consistent with these reports, we found more Aβ plagues in 5xFAD retina than in WT, although the number of Aβ plagues was rather low even at 6 months, especially when compared with those in brain regions. In the other line of 5xFAD that carries rd1 mutation, Aβ present in the retina as early as 1.5M (Pogue et al., 2015). The earlier presence of Aβ in the retina may be due to the pathology caused by the rd1 mutation. Interestingly, besides 5xFAD, we also noticed a few Aβ staining on WT retina, and this was also mentioned by Barton et al. (2021) when they used inhalable thioflavin S (Barton et al., 2021). They also reported a significant association of Aβ deposits with RGCs. In 5xFAD mice (without rd1 mutation) age 6 months and older, extracellular Aβ plagues were found in ONL, INL, IPL, and GCL of the retina (Habiba et al., 2020). Consistent with this, in our study, we noticed that the few Aβ plagues appeared in the inner retinal layers as well as the outer retina. While Aβ plagues do accumulate in the retina, their accumulation may be too little to cause the abnormally thick retina we saw in 5xFAD. We believe that global inflammation (especially in the IPL where microglia got activated) may be the main reason at this age. In older animals, when numerous Aβ aggregates starts to appear in the retina, degradation of cells and synaptic proteins may happen and cause retinal degeneration. Indeed, Habiba et al. (2020) reported an increased number of Aβ plagues in aging 5xFAD mice at 12 and 17M, and the retina degenerated with age (Habiba et al., 2020). Currently, it is not known whether the synaptic proteins degrade in the aging 5xFAD mice as Aβ plague accumulates; further experiments on older AD mice may be needed to check this.

Using the same mouse line of 5xFAD carrying no rd1 mutation, Lim et al. (2020) found deficits in retinal function and structure at 6 months, the earliest time point they assessed. We also noticed retinal deficits at 6 months and further extended their study by exploring an earlier time point at 4 months. The retinal structure and function were in general normal at 4 months except a thickening of the outer nuclear layer in the middle region. The pathology in retina does not happen earlier than the pathology in brain, bringing the concern of using retinal pathology as an early preclinical marker of cortical and behavioral changes. However, obvious retinal deficits were noticed at 6 months when working memory and LTP significantly decay, so retinal abnormality in this line of 5xFAD concurred with brain degeneration. Thus, we suggest that using retinal pathology to reflect the changes in the brain is still the right way for AD diagnostic and evaluation of the treatment effects.

DATA AVAILABILITY STATEMENT

The raw data supporting the conclusions of this article will be made available by the authors, without undue reservation.

ETHICS STATEMENT

The animal study was reviewed and approved by the ethics committee at Jinan University.

AUTHOR CONTRIBUTIONS

YX and KC designed the study. MZ carried out the major experiments including LTP recording, MEA recording, immunostaining, pattern ERG recording, behavioral tests, and data analysis. LZ and GX carried out the full-field ERG recording and analyzed the ERG data. XH, HC, SZ, and DX assisted the experiment and data analysis. MZ and YX wrote the manuscript and KC edited it. All authors contributed to manuscript revision, read, and approved the submitted version.

FUNDING

This project was supported by Midstream Research Programme for Universities (MRP-092-17x) to KC, Guangdong Grant Key Technologies for Treatment of Brain Disorders, China (2018B030332001) to YX, and Guangzhou Key Projects of Brain Science and Brain-Like Intelligence Technology (20200730009) to YX.

ACKNOWLEDGMENTS

We would like to thank Noga Vardi for advices and proofreading of the manuscript.

REFERENCES

Bao, Y. Q., Liu, F., Liu, X. B., Huang, M., He, L. M., Ramakrishna, S., et al. (2019). Methyl 3,4-dihydroxybenzoate protects retina in a mouse model of acute ocular hypertension through multiple pathways. *Exp. Eye Res.* 181, 15–24. doi: 10.1016/j.exer.2019.01.010

Barton, S. M., To, E., Rogers, B. P., Whitmore, C., Uppal, M., Matsubara, J. A., et al. (2021). Inhalable thioflavin S for the detection of amyloid beta deposits in the retina. *Molecules* 26:835. doi: 10.3390/molecules26040835

Chidlow, G., Wood, J. P., Manavis, J., Finnie, J., and Casson, R. J. (2017). Investigations into retinal pathology in the early stages of a mouse model of Alzheimer's disease. *J. Alzheimers Dis.* 56, 655–675. doi: 10.3233/JAD-160823

Chiquita, S., Rodrigues-Neves, A. C., Baptista, F. I., Carecho, R., Moreira, P. I., Castelo-Branco, M., et al. (2019). The retina as a window or mirror of the

brain changes detected in Alzheimer's disease: critical aspects to unravel. *Mol. Neurobiol.* 56, 5416–5435. doi: 10.1007/s12035-018-1461-6

Chrysostomou, V., and Crowston, J. G. (2013). The photopic negative response of the mouse electroretinogram: reduction by acute elevation of intraocular pressure. *Investig. Ophthalmol. Vis. Sci.* 54, 4691–4697. doi: 10.1167/iovs.13-12415

Criscuolo, C., Cerri, E., Fabiani, C., Capsoni, S., Cattaneo, A., and Domenici, L. (2018). The retina as a window to early dysfunctions of Alzheimer's disease following studies with a 5xFAD mouse model. *Neurobiol. Aging* 67, 181–188. doi: 10.1016/j.neurobiolaging.2018.03.017

Dibattista, M., Pifferi, S., Menini, A., and Reisert, J. (2020). Alzheimer's disease: what can we learn from the peripheral olfactory system? *Front. Neurosci. Switz.* 14:440. doi: 10.3389/fnins.2020.00440

Gao, L., Liu, Y., Li, X., Bai, Q., and Liu, P. (2015). Abnormal retinal nerve fiber layer thickness and macula lutea in patients with mild cognitive impairment and Alzheimer's disease. *Arch. Gerontol. Geriatr.* 60 162–167. doi: 10.1016/j.archger.2014.10.011

Georgevsky, D., Retsas, S., Raoufi, N., Shimoni, O., and Golzan, S. M. (2019). A longitudinal assessment of retinal function and structure in the APP/PS1 transgenic mouse model of Alzheimer's disease. *Transl. Neurodegener.* 8:30. doi: 10.1186/s40035-019-0170-z

Habiba, U., Merlin, S., Lim, J. K. H., Wong, V. H. Y., Nguyen, C. T. O., Morley, J. W., et al. (2020). Age-specific retinal and cerebral immunodetection of amyloid-beta plaques and oligomers in a rodent model of Alzheimer's disease. *J. Alzheimers Dis.* 76, 1135–1150. doi: 10.3233/JAD-191346

Huang, H. C., and Jiang, Z. F. (2009). Accumulated amyloid-beta peptide and hyperphosphorylated tau protein: relationship and links in Alzheimer's disease. *J. Alzheimers Dis.* 16, 15–27. doi: 10.3233/JAD-2009-0960

Kim, J., Choi, I. Y., Duff, K. E., and Lee, P. (2017). Progressive pathological changes in neurochemical profile of the hippocampus and early changes in the olfactory bulbs of tau transgenic mice (rTg4510). *Neurochem. Res.* 42, 1649–1660. doi: 10.1007/s11064-017-2298-5

Koronyo-Hamaoui, M., Koronyo, Y., Ljubimov, A. V., Miller, C. A., Ko, M. K., Black, K. L., et al. (2011). Identification of amyloid plaques in retinas from Alzheimer's patients and noninvasive *in vivo* optical imaging of retinal plaques in a mouse model. *Neuroimage 54(Suppl.* 1), S204–S217. doi: 10.1016/j.neuroimage.2010.06.020

Lim, J. K. H., Li, Q. X., He, Z., Vingrys, A. J., Chinnery, H. R., Mullen, J., et al. (2020). Retinal functional and structural changes in the 5xFAD mouse model of Alzheimer's disease. *Front. Neurosci.* 14:862. doi: 10.3389/fnins.2020.00862

Liu, B., Rasool, S., Yang, Z., Glabe, C. G., Schreiber, S. S., Ge, J., et al. (2009). Amyloid-peptide vaccinations reduce {beta}-amyloid plaques but exacerbate vascular deposition and inflammation in the retina of Alzheimer's transgenic mice. *Am. J. Pathol.* 175, 2099–2110. doi: 10.2353/ajpath.2009.090159

Liu, F., Zhang, J., Xiang, Z., Xu, D., So, K. F., Vardi, N, et al. (2018). Lycium barbarum polysaccharides protect retina in rd1 mice during photoreceptor degeneration. *Invest. Ophthalmol. Vis Sci.* 59, 597–611. doi: 10.1167/iovs.17-22881

Liu, Y., McDowell, C. M., Zhang, Z., Tebow, H. E., Wordinger, R. J., and Clark, A. F. (2014). Monitoring retinal morphologic and functional changes in mice following optic nerve crush. *Investig. Ophthalmol. Vis. Sci.* 55, 3766–3774. doi: 10.1167/iovs.14-13895

Oakley, H., Cole, S. L., Logan, S., Maus, E., Shao, P., Craft, J., et al. (2006). Intraneuronal beta-amyloid aggregates, neurodegeneration, and neuron loss in transgenic mice with five familial Alzheimer's disease mutations: potential factors in amyloid plaque formation. *J. Neurosci.* 26, 10129–10140. doi: 10.1523/JNEUROSCI.1202-06.2006

O'Leary, T. P., Stover, K. R., Mantolino, H. M., Darvesh, S., and Brown, R. E. (2020). Intact olfactory memory in the 5xFAD mouse model of Alzheimer's disease from 3 to 15 months of age. *Behav. Brain Res.* 393:112731. doi: 10.1016/j.bbr.2020.112731

Paquet, C., Boissonnot, M., Roger, F., Dighiero, P., Gil, R., and Hugon, J. (2007). Abnormal retinal thickness in patients with mild cognitive impairment and Alzheimer's disease. *Neurosci. Lett.* 420, 97–99. doi: 10.1016/j.neulet.2007.02.090

Parisi, V., Restuccia, R., Fattapposta, F., Mina, C., Bucci, M. G., and Pierelli, F. (2001). Morphological and functional retinal impairment in Alzheimer's disease patients. *Clin. Neurophysiol.* 112, 1860–1867. doi: 10.1016/S1388-2457(01)00620-4

Pogue, A. I., Dua, P., Hill, J. M., and Lukiw, W. J. (2015). Progressive inflammatory pathology in the retina of aluminum-fed 5xFAD transgenic mice. *J. Inorg. Biochem.* 152, 206–209. doi: 10.1016/j.jinorgbio.2015.07.009

Porciatti, V. (2007). The mouse pattern electroretinogram. *Doc. Ophthalmol.* 115, 145–153. doi: 10.1007/s10633-007-9059-8

Romano, R. R., Carter, M. A., and Monroe, T. B. (2021). Narrative review of sensory changes as a biomarker for Alzheimer's disease. *Biol. Res. Nurs.* 23, 223–230. doi: 10.1177/1099800420947176

Snyder, P. J., Johnson, L. N., Lim, Y. Y., Santos, C. Y., Alber, J., Maruff, P., et al. (2016). Nonvascular retinal imaging markers of preclinical Alzheimer's disease. *Alzheimers Dement. (Amst.)* 4, 169–178. doi: 10.1016/j.dadm.2016.09.001

Song, G., Steelman, Z. A., Finkelstein, S., Yang, Z., Martin, L., Chu, K. K., et al. (2020). Multimodal coherent imaging of retinal biomarkers of Alzheimer's disease in a mouse model. *Sci. Rep.* 10:7912. doi: 10.1038/s41598-020-64827-2

Sutphen, C. L., Fagan, A. M., and Holtzman, D. M. (2014). Progress update: fluid and imaging biomarkers in Alzheimer's disease. *Biol. Psychiatry* 75, 520–526. doi: 10.1016/j.biopsych.2013.07.031

van de Kreeke, J. A., Nguyen, H. T., den Haan, J., Konijnenberg, E., J., Tomassen, den Braber, A., et al. (2019). Retinal layer thickness in preclinical Alzheimer's disease. *Acta Ophthalmol.* 97, 798–804. doi: 10.1111/aos.14121

Zhang, J., Xu, D., Ouyang, H., Hu, S., Li, A., Luo, H., et al. (2017). Neuroprotective effects of methyl 3,4 dihydroxybenzoate in a mouse model of retinitis pigmentosa. *Exp. Eye Res.* 162, 86–96. doi: 10.1016/j.exer.2017.07.004

Conflict of Interest: The authors declare that the research was conducted in the absence of any commercial or financial relationships that could be construed as a potential conflict of interest.

Publisher's Note: All claims expressed in this article are solely those of the authors and do not necessarily represent those of their affiliated organizations, or those of the publisher, the editors and the reviewers. Any product that may be evaluated in this article, or claim that may be made by its manufacturer, is not guaranteed or endorsed by the publisher.

frontiers in Neuroscience

REVIEW
published: 05 August 2021
doi: 10.3389/fnins.2021.692599

Optical Coherence Tomography and Visual Evoked Potentials as Prognostic and Monitoring Tools in Progressive Multiple Sclerosis

Simone Guerrieri[1,2], *Giancarlo Comi*[2,3]* *and Letizia Leocani*[1,2]*

[1] *Experimental Neurophysiology Unit, San Raffaele Hospital, Institute of Experimental Neurology (INSPE), Milan, Italy,* [2] *Vita-Salute San Raffaele University, Milan Italy,* [3] *Casa di Cura del Policlinico, Milan, Italy*

Understanding the mechanisms underlying progression and developing new treatments for progressive multiple sclerosis (PMS) are among the major challenges in the field of central nervous system (CNS) demyelinating diseases. Over the last 10 years, also because of some technological advances, the visual pathways have emerged as a useful platform to study the processes of demyelination/remyelination and their relationship with axonal degeneration/protection. The wider availability and technological advances in optical coherence tomography (OCT) have allowed to add information on structural neuroretinal changes, in addition to functional information provided by visual evoked potentials (VEPs). The present review will address the role of the visual pathway as a platform to assess functional and structural damage in MS, focusing in particular on the role of VEPs and OCT, alone or in combination, in the prognosis and monitoring of PMS.

Keywords: multiple sclerosis, progressive multiple sclerosis, visual pathway, visual evoked potentials, optical coherence tomography

OPEN ACCESS

Edited by:
Yuyi You,
Macquarie University, Australia

Reviewed by:
Dong Ho Park,
Kyungpook National University Hospital, South Korea
Alexandr Klistorner,
Sydney Hospital, Australia

***Correspondence:**
Giancarlo Comi
comi.giancarlo@unisr.it
Letizia Leocani
leocani.letizia@hsr.it

Specialty section:
This article was submitted to Neurodegeneration, a section of the journal Frontiers in Neuroscience

Received: *08 April 2021*
Accepted: *07 June 2021*
Published: *05 August 2021*

Citation:
Guerrieri S, Comi G and Leocani L (2021) Optical Coherence Tomography and Visual Evoked Potentials as Prognostic and Monitoring Tools in Progressive Multiple Sclerosis. Front. Neurosci. 15:692599. doi: 10.3389/fnins.2021.692599

BACKGROUND

The Challenge of Progressive Multiple Sclerosis

Multiple sclerosis (MS) is a chronic inflammatory, immune-mediated disease of the central nervous system (CNS; Ontaneda and Fox, 2015), characterized by demyelination, axonal loss, and neurodegeneration. Although the pathophysiology underlying the different phenotypes still needs to be clarified, four main clinical courses of the disease have been identified: relapsing–remitting MS (RRMS; characterized by clearly defined neurological exacerbations with full or incomplete recovery, in the presence of dissemination in space and time of the inflammatory process among the CNS), clinically isolated syndrome (CIS; a first neurological episode suggestive of MS, but formal criteria of dissemination in time are not fulfilled), secondary progressive MS (SPMS; defined retrospectively by the occurrence of gradual disability worsening with or without occasional relapses, minor remissions, and plateaus, following an initial RRMS course), and primary progressive MS (PPMS; characterized by progressive accumulation of disability from disease onset with occasional plateaus, temporary minor improvements, or acute relapses still consistent with the definition; Lublin and Reingold, 1996; Lublin et al., 2014). The MS courses can be further qualified by the presence/absence of disease activity [presence of relapses and/or magnetic resonance imaging (MRI) activity – i.e., gadolinium-enhancing lesions or

new/unequivocally enlarging T2 hyperintense lesions] and by the disability state: worsening, improving, or stable (Lublin et al., 2014).

The pathological key features underlying the clinical expression of the disease can be depicted as a spectrum, ranging from waves of acute focal inflammation in RRMS to predominant neurodegenerative features with concomitant chronic compartmentalized inflammation in progressive multiple sclerosis (PMS) (Lassmann et al., 2007; Giovannoni et al., 2016).

During the past decades, a major progress has been made in understanding disease mechanisms in RRMS, with inflammation and subsequent focal demyelination with breakdown of the blood–brain barrier representing the main driver of clinical disease in this subset of patients. This knowledge has led to the development of anti-inflammatory and immunomodulatory treatments that effectively reduce the severity and frequency of new demyelinating episodes (Diebold and Derfuss, 2016). In PMS, instead, focal disruption of the blood–brain barrier is less common, and widespread degeneration of the white and gray matter variably combined with slow expansion of chronically active lesions are the pathological hallmarks (Lassmann, 2017). Several and non-necessarily exclusive mechanisms have been proposed to explain the pathogenesis of PMS (i.e., compartmentalized ongoing chronic inflammation, chronic inflammation leading to inflammation-independent neurodegeneration, and primary neurodegeneration amplified by concurrent independent inflammation), with SPMS and PPMS course likely sharing similar pathophysiological features (Confavreux and Vukusic, 2006; Trapp and Nave, 2008; Frischer et al., 2009; Lassmann et al., 2012). Fundamental pathogenetic pathways responsible of clinical progression, however, still remain unidentified, with no available accurate preclinical model reproducing this stage of the disease. The approval of Ocrelizumab for active PPMS and SPMS treatment (Montalban et al., 2017), and of Siponimod for active SPMS by EMA and for relapsing MS by FDA (Kappos et al., 2018), represent important encouraging novelties, but the tangible real-world impact of these molecules has still to be assessed especially in the absence of overt inflammation (Montalban et al., 2017; Kappos et al., 2018). Unfortunately, previous studies exploring neuroprotective strategies have failed; however, some positive results have recently emerged from phase III clinical trials and are now under exploration in definite clinical trials (Ontaneda et al., 2015; Sorensen et al., 2020). Moreover, the process of discovery of new therapeutic targets for PMS is a priority of the International Progressive MS Alliance (2021), a multistakeholder initiative promoted by International Federation of Multiple Sclerosis and MS patient associations.[1]

The Visual Pathway as a Model of Brain Damage in Multiple Sclerosis

In order to succeed in the challenge represented by PMS, our ability to early detect the pathological processes on the stage will be of fundamental importance. At present, diagnosis of PMS is mainly retrospective since imaging methods as well as other biomarkers to catch or predict progression are not well established (Correale et al., 2017). There is an unmet need for new strategies to identify inflammation/demyelination and particularly neurodegeneration in a subclinical phase, with consequent prompt interventions aimed to prevent disability to occur for our patient.

Emerging evidence suggests that the visual system may play an important role in this game (Martinez-Lapiscina et al., 2014). The visual pathway is in fact frequently involved in MS, with visual dysfunction that is not only common but also highly relevant (Fisher et al., 2006; Heesen et al., 2008; Chatziralli et al., 2012). Furthermore, the visual pathway may represent a model of both acute focal CNS damage [through acute optic neuritis (ON) and retinal periphlebitis] (Albrecht et al., 2007; Siger et al., 2008), as well as a model of chronic, diffuse CNS involvement (through chronic retinopathy, optic neuropathy, and *trans*-synaptic degeneration). The ongoing pathological processes can be accurately evaluated due to the availability of highly sensitive imaging [i.e., MRI or optical coherence tomography (OCT)] and electrophysiological [i.e., visual evoked potentials (VEPs) and electroretinography (ERG)] tests. The combination of these techniques allows to describe the interactions between the different processes at play (such as inflammation, demyelination, and axonal and neuronal loss) *in vivo* and in a non-invasive way, features that identify the visual pathway as an elective platform to differentiate MS pathophysiology from other inflammatory conditions of the CNS (Vabanesi et al., 2019), as well as a reliable model to monitor the disease and to test new neuroprotective or regenerative therapies in the context of clinical trials (Fisher et al., 2006; Heesen et al., 2008; Chatziralli et al., 2012; Martinez-Lapiscina et al., 2014; Villoslada, 2016).

Optical coherence tomography in MS has been widely used to measure in particular retinal nerve fiber layer (RNFL) and ganglion cell–inner plexiform layer (GCIPL) thickness as markers of neuroaxonal loss, allowing to detect subclinical neurodegeneration (Petzold et al., 2010; Alonso et al., 2018; Costello and Burton, 2018). RNFL and GCIPL thickness have been correlated with tests of visual function (Pulicken et al., 2007; Pueyo et al., 2008; Zaveri et al., 2008), with global disability scores such as Expanded Disability Status Scale (EDSS; Albrecht et al., 2007; Siger et al., 2008), with functional measures as those provided by VEPs (Klistorner et al., 2008; Pueyo et al., 2008; Di Maggio et al., 2014), but also with cerebral and optic nerve MRI parameters (Trip et al., 2006; Grazioli et al., 2008; Siger et al., 2008), as well as with fluid biomarkers such as serum neurofilament light chain concentration (Tavazzi et al., 2020). Most of the evidence available in the field is actually related to the RRMS course, with neuroretinal atrophy being associated with disease activity (Pisa et al., 2017), but with the possibility to detect RNFL and GCIPL thinning over time in MS patients with progression independent of relapse activity (PIRA; Bsteh et al., 2020; Pisa et al., 2020). Cross-sectional RNFL, total macular volume (TMV), and GCIPL thickness measures independently predicted long-term disability in large cohorts of predominately RRMS patients (Martinez-Lapiscina et al., 2016; Rothman et al., 2019; Lambe et al., 2021), while the application of mathematical models has suggested RNFL evolution, resulting from a mix of

[1] www.progressivemsalliance.org

inflammatory and degenerative processes, to accurately reflect disability progression over time (Montolío et al., 2019).

More recently, other retinal layers have also received attention as possible biomarkers in MS: in particular, inner nuclear layer (INL) consists of a network of bipolar, amacrine, and horizontal cells; despite some signs of atrophy have been described on histopathology at this level in MS (Green et al., 2010), *in vivo* studies did not show an extensive INL atrophy as in the case of RNFL and GCIPL, even after ON (Seigo et al., 2012; Syc et al., 2012). Pathology studies have identified inflammation and microglial activation within the inner retina in MS patients (Green et al., 2010), and *in vivo* observations also suggest INL as a possible biomarker of inflammation within the CNS, with increased INL thickness reflecting a condition of retinal inflammation, which parallels brain inflammatory activity in MS: microcystic macular edema (MME) within this layer has in fact been described to be associated with ON and disability; furthermore, increased INL thickness has been associated with a greater risk of developing new T2 or gadolinium-enhancing lesions and of new relapses (Saidha et al., 2012; Balk et al., 2019); finally, successful response to disease-modifying treatments (DMTs) has been associated with a sustained reduction of INL volume (Knier et al., 2016). Other authors, however, have postulated the possibility for INL thickening (and MME in particular) to be related to vitreomacular tractions, Müller cell pathology, subclinical uveitis, or retinal periphlebitis, conditions possibly found in association with MS (Kerrison et al., 1994; Chen and Gordon, 2005). Significant correlations between INL thickening and RNFL/GCIPL thinning have been also described: according to this evidence, it has been speculated that INL enlargement is related to structural changes in other retinal layers (as the result of the opposing tractions between inner limiting and Bruch's membranes), being therefore compensatory in nature (Kaushik et al., 2013).

MRI can be used to identify inflammation (lesion load on T2-weighted images and gadolinium-enhancing lesions on T1-contrast sequences), but also (with 3D high-resolution T1-weighted images) to quantify regional atrophy along the visual pathway, such as optic nerve atrophy after ON, of the lateral geniculate nucleus (LGN) at the thalamic level and of the visual cortex (Gabilondo et al., 2014). Other MRI parameters such as the magnetization transfer ratio (MTR) and the diffusion-weighted imaging (DWI) are sensitive to microstructural damage, allowing to characterize demyelination and axonal damage along the visual pathway, with an association with visual function measures (Melzi et al., 2007; Naismith et al., 2010; Kolbe et al., 2012). In the following sections, possible relations between OCT-VEPs parameters and MRI data have been assessed; however, an extensive dissertation of MRI findings and their implications in PMS is beyond the purpose of the present review.

Among functional techniques, traditional full-field VEPs (ff-VEPs) can be performed as an indicator of demyelination/remyelination, expressed by latency delay/shortening of the major component P100, with potential diagnostic, prognostic, and monitoring roles in MS (Comi et al., 1999; Leocani et al., 2018). In addition, multifocal techniques (mf-VEPs) allow to assess conduction for separate portions of the visual field, providing information about local signals of small areas occupying up to 24 central degrees of the visual field, with the possibility to detect mild abnormal local responses and scotomas (Klistorner et al., 2008).

Starting from this background, in this article, we wanted to assess the real value of the visual pathway as a specific biomarker of functional and structural damage in PMS patients, focusing in particular on VEPs and OCT use as possible prognostic and monitoring tools.

EVIDENCE ACQUISITION

We searched PubMed up to March 15, 2021, using the following terms: "Progressive Multiple Sclerosis and Visual Evoked Potentials," "Progressive Multiple Sclerosis and Optical Coherence Tomography," "Optical Coherence Tomography and Disability and Multiple Sclerosis," and "Visual Evoked Potentials and Disability and Multiple Sclerosis."

VISUAL EVOKED POTENTIALS IN PMS

There is little specific information about VEPs in PMS, and especially PPMS, because many studies on VEPs in MS were performed prior to the current classification of disease courses (Lublin et al., 2014).

Currently available data on ff-VEPs sensitivity mainly derive from studies assessing the role of a multimodal neurophysiological assessment in MS cohorts, including subsets of PMS patients. Leocani et al. (2006) performed a study in which, among the others, 41 PMS patients (13 PPMS and 28 SPMS) underwent multimodal evoked potentials including ff-VEPs, with high rates of visual conduction impairment in both subgroups (92.3% for PPMS and 85.7% for SPMS), significantly more elevated than the abnormalities recorded among the RRMS cohort (77.4%; Leocani et al., 2006). These findings were consistent with those deriving from other previous experiences: in a small Japanese cohort of 11 PPMS patients, higher frequencies of VEPs abnormality were reported in comparison with 35 RRMS patients (Kira et al., 1993). In a similar way, data extrapolated from a European cohort of 156 PPMS patients showed a delay of conduction along the visual pathway in 105 out of 131 subjects (80%) who had undergone ff-VEP examination (Stevenson et al., 1999); VEP studies in PMS patients are summarized in **Table 1**. The high frequency of abnormal ff-VEPs in PPMS, asymptomatic in the vast majority of the cases, allowed to reveal a clinically unsuspected spatial dissemination of the disease, and ff-VEPs were therefore once included among PPMS diagnostic criteria (Thompson et al., 2000). Multifocal VEP is a new technique that provides high sensitivity and specificity in detecting abnormalities in visual function in MS patients (Laron et al., 2009); however, no specific information exploring their role in PMS is currently available in literature to the knowledge of the authors.

Backner et al. (2019) analyzed the relations between different vision-related measures, including ff-VEPs, in PMS. In particular,

TABLE 1 | Studies assessing visual evoked potentials (VEPs) in progressive multiple sclerosis (PMS).

Study	Technique	Cohort	Main findings
Leocani et al., 2006	ff-VEPs	43 RRMS, 28 SPMS, 13 PPMS	VEPs abnormalities significantly more frequent in PMS (92.3% PPMS and 85.7% SPMS) than in RRMS (77.4%)
Kira et al., 1993	ff-VEPs	35 RRMS, 11 PPMS (japanese)	VEPs abnormalities more frequent in PPMS compared to RRMS patients
Stevenson et al., 1999	ff-VEPs	131 PPMS	Visual conduction delay in 105/131 (80%) PPMS patients

ff-VEPs, full-field visual evoked potentials; RRMS, relapsing–remitting multiple sclerosis; SPMS, secondary progressive multiple sclerosis; PPMS, primary progressive multiple sclerosis.

they reported data related to a cohort of 48 PMS patients (classified as 18 progressive with relapses, 21 SPMS, and nine PPMS) who had been enrolled in a longitudinal mesenchymal stem cell therapy study (NCT02166021), conducted at the Hadassah-Hebrew University Medical Center. Significant inverse correlations were found between motion perception tests [object for motion (OFM) and number for motion (NFM)] and ff-VEPs latency in eyes with previous ON and their fellow eyes, in the presence of preserved visual acuity (VA), thus confirming previous evidences suggesting that dynamic visual functions may reflect myelination levels along the visual pathway (Raz et al., 2014). Considering instead functional and structural measures, a correlation between ff-VEPs latency on the one hand and RNFL thickness as well as optic radiation lesion load on the other was described in non-ON eyes of the same cohort of patients enrolled in the NCT02166021 trial (Berman et al., 2020). In this regard, Davies et al. (1998) had previously reported optic nerve lesion length and area [detected by MRI on the short tau inversion recovery (STIR) sequence], to significantly correlate with ff-VEP latency prolongation in a cohort of 25 SPMS patients, only four of whom had a history of acute ON.

When considering the specific prognostic role of VEPs in PMS, available data are even more limited. Sater et al. (1999) proposed ff-VEPs as a tool to assess disease progression in addition to standard disability-based endpoints: obtaining serial VEPs and MRI scans from 11 PMS patients over a 1.5-year period, they found in fact no significant change in disability as measured by EDSS and Ambulation Index, nor in MRI T2 plaque burden, in the presence, however, of a significant progression of the P100 latency over time (Sater et al., 1999). More recently, Schlaeger et al. (2014) prospectively investigated the role of VEPs in the context of a multimodal evoked potential assessment as possible predictors of disease course in a small cohort of PPMS patients; they found that a multimodal evoked potential score correlated with disability in these patients, also allowing some prediction of the course of the disease.

OPTICAL COHERENCE TOMOGRAPHY IN PMS

Several studies over the last 15 years examined cross-sectionally the pattern of retinal axonal loss (expressed by RNFL measurement at a peripapillary level), across the different MS clinical subtypes also including subsets of PMS patients, often coming to partially contrasting conclusions. As a premise, it is important to notice that early studies measured RNFL thickness through time-domain OCT devices (TD-OCT), while more recent experiences have been made with next-generation OCT based on spectral-domain technology (SD-OCT). This innovation allowed not only to increase speed acquisition but also to improve resolution power and reproducibility; segmentation algorithms also differ between TD-OCT and SD-OCT devices; therefore, results obtained with different OCT generations are not interchangeable and directly comparable (Bock et al., 2010).

In 2007, Pulicken et al. (2007) obtained RNFL thickness measures using a TD-OCT device (OCT-3, Zeiss Meditec) on a cohort of 135 RRMS, 16 SPMS, and 12 PPMS patients, as well as in 47 healthy controls: the three subgroups of MS patients all showed decreased RNFL values in comparison with controls; compared with RRMS, both SPMS and PPMS patients revealed a trend toward thinner RNFL values although in the absence of a statistical significance, probably due to the small number of PMS patients included in the study. In 2008, Henderson et al. (2008) performed a similar study (using TD-OCT Stratus, Zeiss Meditec) on 27 SPMS and 23 PPMS patients, with the former but not the latter showing reduced RNFL thickness values when compared with 20 healthy controls, in the absence of significant differences between the two PMS subgroups when age-adjusted regression coefficient of RNFL thickness was directly compared (although in the presence of lower values among SPMS patients); significant correlations between RNFL values and VA measures were also reported, especially in the PPMS cohort. In another study using the same TD-OCT device (Stratus) published in 2010, Siepman et al. (2010) reported no statistically significant difference in terms of mean RNFL thickness comparing 26 RRMS and 29 PPMS patients. In 2012, Gelfand et al. (2012) published retinal imaging data obtained in 60 SPMS and 33 PPMS patients, using a new SD-OCT device (Spectralis, Heidelberg Engineering): the authors reported similar RNFL thickness values between SPMS and PPMS patients examining eyes without previous ON, with TMV slightly lower in the PPMS group. These results were consistent with those published by Albrecht et al. (2012), including 41 SPMS and 12 PPMS patients: using the same Spectralis device, the authors reported significant RNFL thinning compared with healthy controls for both subgroups, although a direct comparison between different PMS subsets was not performed. Another coeval work performed with Spectralis on a German cohort of 414 MS patients (308 RRMS, 65 SPMS, and 41 PPMS) and 94 healthy controls reported significant differences in terms of RNFL thickness only between RRMS and SPMS patients after adjusting for clinical–demographic parameters (such as age,

gender, and disease duration), while the PPMS subgroup did not differ from neither RRMS nor SPMS cohorts; a different pattern was obtained for TMV measures, for which a significant reduction was found in both SPMS and PPMS subgroups when compared with RRMS patients (Oberwahrenbrock et al., 2012). Data deriving from a Dutch cohort of 230 MS patients (including 61 SPMS and 29 PPMS), despite being obtained with the same SD-OCT (Spectralis), depicted another different situation: the authors found SPMS to show significant RNFL thickness reduction in comparison with PPMS but not RRMS patients, with PPMS subgroup showing the highest absolute values (Balk et al., 2014). Finally, in a recently published work, Jankowska-Lech et al. (2019; using SD-OCT Topcon OCT 1000 Mark II, Topcon) compared 26 RRMS with 22 PMS patients, finding significantly decreased RNFL thickness values in the latter subgroup only when taking into account also eyes with previous ON. The contrasting results emerging from the studies listed above may be partly related to the different techniques employed, with new SD-OCT showing higher resolution power, image quality, and reproducibility than the older TD-OCT devices (Bock et al., 2010); however, due to the relatively small sample sizes provided across the different studies, RNFL inter-individual variability among general and MS population, as well as the possibility of primary retinal pathology in a subset of MS patients, may have also played a role (Kallenbach and Frederiksen, 2007; Petzold et al., 2010; Serbecic et al., 2010; Saidha et al., 2011).

In more recent years, thanks to the availability of new commercial software allowing retinal automated segmentation, increasing attention has been directed toward the analysis of other retinal strata (particularly GCIPL) measured on macular scans; initial specific information is becoming available also for PMS cohorts. Some of the studies previously described already took into account these aspects: Albrecht et al. (2012) performed a manual segmentation of macular scans, reporting reduced GCIPL values in both SPMS and PPMS patients compared with controls; in PPMS subgroup, a significant reduction of the INL was also reported but not confirmed after the exclusion from the analysis of eyes with previous ON. Balk et al. (2014), using instead an automated software program, showed GCIPL to be significantly reduced among PPMS patients when compared with SPMS, also in the absence of previous ON history. Another work published in 2017 using SD-OCT (Cirrus 5000, Zeiss Meditec) compared 29 PMS with 84 RRMS patients, showing in the former subgroup significantly reduced thickness values not only for GCIPL but also when considering outer plexiform layer (OPL); included patients, however, were of non-Caucasian origin (Behbehani et al., 2017). Cross-sectional OCT studies assessing retinal layers in PMS are summarized in **Table 2**.

Researchers also focused on exploring the relation between retinal measures and clinical parameters; available data, however, are often non-specific for PMS, with major contributions (relative to visual function and global disability measures) deriving from some of the studies previously reported. Henderson et al. (2008) found a relationship between VA (both high- and low-contrast tests) and RNFL thickness in their PMS cohort, with particularly robust data in PPMS patients, as also suggested by

TABLE 2 | Cross-sectional OCT studies assessing retinal layers in PMS.

Study	Device	Cohort	Main findings
Pulicken et al., 2007	TD-OCT (OCT-3, Zeiss Meditec)	1 3 5 R RMS, 16 SPMS, 12 PPMS, 47 HC	RNFLt reduced in MS groups compared to HC; statistical trend indicating thinner RNFLt in SPMS and PPMS compared to RRMS
Henderson et al., 2008	TD-OCT (Stratus, Zeiss Meditec)	2 7 SPMS, 23 PPMS, 20 HC	Mean RNFLt reduced in SPMS (but not PPMS) compared to HC
Siepman et al., 2010	TD-OCT (Stratus, Zeiss Meditec)	26 RRMS, 10 SPMS, 29 PPMS	Mean RNFLt no statistically different between RRMS and PPMS patients
Gelfand et al., 2012	SD-OCT (Spectralis, Heidelberg Engineering)	4 5 CIS, 403 RRMS, 60 SPMS, 33 PPMS, 53 HC	Mean RNFLt similar in SPMS and PPMS patients in non-ON eyes; TMV slighlty lower in PPMS group
Albrecht et al., 2012	SD-OCT (Spectralis, Heidelberg Engineering)	4 2 RRMS, 41 SPMS, 12 PPMS, 95 HC	Mean RNFLt and GCIPLt reduction in both SPMS and PPMS compared to HC; INLt reduction only in PPMS in comparison to HC
Oberwahrenbrock et al., 2012	SD-OCT (Spectralis, Heidelberg Engineering)	308 RRMS, 65 SPMS, 41 PPMS, 94 HC	Mean RNFLt lower in SPMS (but not PPMS) compared to RRMS; TMV reduced in both SPMS and PPMS compared to RRMS
Balk et al., 2014	SD-OCT (Spectralis, Heidelberg Engineering)	140 RRMS, 61 SPMS, 29 PPMS, 63 HC	Mean RNFLt, GCIPLt and INLt reduction in SPMS compared with PPMS but not RRMS considering non-ON eyes; highest absolute values in PPMS
Behbehani et al., 2017	SD-OCT (Cirrus 5000, Zeiss Meditec)	84 RRMS, 29 PMS, 38 HC (non-caucasian)	Mean RNFLt, GCIPLt and OPLt reduced in PMS compared to RRMS patients
Jankowska-Lech et al., 2019	SD-OCT (OCT 1000 Mark II, Topcon)	26 RRMS, 22 PMS, 31 HC	Mean RNFLt reduced in PMS compared to RRMS patients only when taking into account ON eyes

TD-OCT, time domain–optical coherence tomography; SD-OCT, spectral domain–optical coherence tomography; CIS, clinically isolated syndrome; RRMS, relapsing–remitting multiple sclerosis; SPMS, secondary progressive multiple sclerosis; PPMS, primary progressive multiple sclerosis; HC, healthy controls; RNFLt, retinal nerve fiber layer thickness; TMV, total macular volume; GCIPLt, ganglion cells–inner plexiform layer thickness; INLt, inner nuclear layer thickness; OPLt, outer plexiform layer thickness; ON, optic neuritis.

the observation (with SD-OCT Spectralis) of a significant relation between low-contrast VA and GCIPL thickness in another cohort of 25 PPMS patients (Poretto et al., 2017). The same authors, however, did not identify any significant relation between RNFL thickness and disease duration, duration of the progressive phase, nor with EDSS (Henderson et al., 2008). A lack of a correlation between RNFL thickness and EDSS has been also reported with SD-OCT Spectralis in a cohort of 28 non-Caucasian SPMS patients (Yousefipour et al., 2016). Siepman et al. (2010) reported instead similar relations between RNFL thickness and VA, also pointing out a negative correlation with EDSS in eyes without previous ON; data, however, were referred to the entire study cohort of 26 RRMS and 29 PPMS patients. Albrecht et al. (2012) expanded this analysis in their cohort of 95 MS patients (including 41 SPMS and 12 PPMS) observing EDSS to correlate also with macular thickness and OPL, interestingly with a positive correlation in this latter case. Behbehani et al. (2017) reported instead an inverse correlation between ONL thickness and EDSS in 29 PMS patients. No significant correlation with RNFL (measured with Spectralis) was instead identified when considering motion perception tests, which appear to be mainly related to myelination status along the visual pathway more than to axonal loss (Backner et al., 2019). Finally, considering the possible relation between OCT measures and other clinical parameters, Coric et al. (2018) analyzed with Spectralis a cohort of 217 MS patients (including a remarkable percentage of PMS patients – 56 SPMS and 28 PPMS, respectively) describing cognitively impaired patients to have significantly reduced RNFL and GCIPL values.

Moving to assess the relation between OCT and other instrumental parameters, in 2007, Gordon-Lipkin et al. (2007) had already described RNFL thickness (measured with OCT-3) to correlate with brain atrophy in 40 MS patients (20 RRMS and 20 PMS), although this association appeared to be driven by the RRMS subset and by cerebrospinal fluid more than white or gray matter volume. In another cohort of 25 PPMS patients (assessed with Spectralis), RNFL thickness revealed to be associated with thalamus and visual cortex volume, while GCIPL values were associated with cortical lesion load; the authors suggested retrograde *trans*-synaptic degeneration and/or a common pathophysiologic process affecting both the brain and the retina as possible explanations (Petracca et al., 2017). Data deriving from a recent Italian retrospective study including a cohort of 84 PMS patients also revealed increased values of INL thickness in a subset of patients who had shown MRI activity during the year before OCT assessment (Spectralis), proposing INL evaluation as a possible surrogate marker of disease activity also among progressive patients (Cellerino et al., 2019). Saidha et al. (2015) explored the relation between SD-OCT (Cirrus 4000, Zeiss Meditec) and MRI parameters longitudinally in the context of a 4-year study including 107 MS patients: the authors described RNFL and GCIPL thinning to be significantly associated with whole-brain, and gray and white matter atrophy, pointing out a stronger relation in the subset of 36 PMS patients. However, data extrapolated from a randomized placebo-controlled trial testing the possible role of lipoic acid in SPMS showed only modest correlations between RNFL and cortical gray matter atrophy in a subset of 51 patients with OCT (Cirrus 5000) and MRI longitudinal data available, with no significant results for GCIPL (Winges et al., 2019). In the SPRINT MS phase II clinical trial, however, ibudilast significantly reduced over 2 years the progression of brain atrophy compared with placebo in PMS patients; this positive result was supported by a trend for a lower RNFL thickness reduction in ibudilast-treated patients (Fox et al., 2018). Finally, OCT parameters have been also analyzed in association with other functional instrumental techniques: in particular, a correlation between RNFL thickness and ff-VEPs latency has been identified in PMS patients considering eyes without ON history (Backner et al., 2019).

The evolution over time of OCT parameters has also started to be explored in different subsets of MS patients, but conclusive specific data for PMS are still lacking. In a work published

TABLE 3 | Longitudinal OCT studies assessing retinal layers in PMS.

Study	Device	Cohort	Follow-up	Main findings
Talman et al., 2010	TD-OCT (OCT-3, Zeiss Meditec)	299 MS (84% RRMS)	1.5 years (range 0.5–4.5)	RNFLt reduction as a function of time (average −2.9 μm at 2–3 years and −6.1 μm at 3–4.5 years) in some patients with MS, even in the absence of aON
Henderson et al., 2010	TD-OCT (Stratus, Zeiss Meditec)	18 SPMS, 16 PPMS, 18 HC	1.5 years (range 1.1–2.4)	No significant RNFLt reduction over time in patients and controls. TMV decline in both groups, with no between-group differences
Balk et al., 2016	SD-OCT (Spectralis, Heidelberg Engineering)	7 CIS, 89 RRMS, 26 SPMS, 13 PPMS, 16 HC	2 years	RNFLt and GCIPLt reductions more pronounced early in the course of disease (higher atrophy rate in RRMS than SPMS patients)
Winges et al., 2019	SD-OCT (Cirrus 5000, Zeiss Meditec)	51 SPMS	2 years	RNFL (−0.31 μm/year) and GCIPL (−0.29 μm/year) atrophy rates similar in aON and nON eyes; RNFLt > 75 μm associated with higher (−0.85 μm/year) rate
Sotirchos et al., 2020	SD-OCT (Cirrus HD-OCT, Zeiss Meditec)	178 RRMS, 186 PMS, 66 HC	3.7 years (IQ range 2.0–5.9)	PMS phenotype associated with faster RNFLt (−0.34 %/year) and GCIPLt (−0.27 %/year) reduction; no significant impact determined by DMTs

TD-OCT, time domain–optical coherence tomography; SD-OCT, spectral domain–optical coherence tomography; CIS, clinically isolated syndrome; RRMS, relapsing–remitting multiple sclerosis; SPMS, secondary progressive multiple sclerosis; PPMS, primary progressive multiple sclerosis; HC, healthy controls; RNFLt, retinal nerve fiber layer thickness; TMV, total macular volume; GCIPLt, ganglion cells–inner plexiform layer thickness; aON, acute optic neuritis; nON, non-optic neuritis; DMTs, disease-modifying treatments.

in 2010, Talman et al. (2010) followed up (mean 18 months, range 6 months–4.5 years) 299 MS patients (84% with RRMS phenotype) with TD-OCT (OCT-3): the authors described progressive RNFL thinning as a function of time. In contrast with this finding, Henderson et al. (2010) using Stratus TD-OCT did not find any significant change of RNFL thickness over time in a small cohort of 34 PMS patients (18 SPMS and 16 PPMS) who were followed up for a median interval of 1.5 years. Balk et al. (2016) performed another study enrolling 135 MS patients (including 26 SPMS and 13 PPMS), who have been assessed with SD-OCT (Spectralis) over a 2-year period: the authors showed RNFL and GCIPL thinning to be significantly related to disease duration (with thinning rate becoming smaller in the presence of longer disease duration), and consistently, they found RNFL and GCIPL atrophy rate to be higher in RRMS than SPMS patients; such a relation was not identified for INL. Longitudinal data over 2 years relative to the cohort of 51 SPMS patients enrolled in the lipoic acid trial showed annualized RNFL and GCIPL atrophy rates (−0.31 and −0.29 μm/year, respectively) to not differ between eyes with and without previous ON history; however, a baseline RNFL thickness higher than 75 μm was associated with a greater (−0.85 μm/year) annualized atrophy rate (Winges et al., 2019). Only very recently Sotirchos et al. (2020) published a significant OCT longitudinal study including a cohort of 178 RRMS and 186 PMS patients who were followed up with serial OCT scans (performed with Cirrus SD device) for a median of 3.7 years: independently from age, PMS phenotype was found to be associated with faster mean annualized percent changes for both RNFL (−0.34%/year) and GCIPL (−0.27%/year), and possibly also for INL and ONL, with no significant impact determined by disease-modifying therapies; the relation between retinal layers atrophy rates and disability progression over time, however, has not been extensively assessed. Longitudinal OCT studies assessing evolution over time of retinal layers in PMS are summarized in **Table 3**.

CONCLUDING REMARKS

Optic pathway offers the unique opportunity to combine functional and structural measures: given the demonstrated correlations between optic nerve and brain damage (as revealed by MRI), it represents an attractive CNS area of interest to monitor MS evolution, as well as the response to DMTs, particularly in PMS. On the one hand, VEP studies, albeit in the presence of limited specific information, suggested a significant functional involvement of the visual pathway in PMS, in the presence of a relation with dynamic visual function measures and with a possible prognostic contribution on progression, in the context of a multimodal assessment of evoked responses. On the other hand, OCT studies, although in the presence of some contrasting results, highlighted a significant retinal neuro-axonal loss in PMS compared with HC but also RRMS patients, in the presence of possible, although non-linear, cross-sectional and longitudinal relations with measures of visual and global disability. Significant relations have been also identified in PMS between retinal neuro-axonal architecture and structural measures of brain atrophy provided by MRI; more recently, INL has been proposed as a marker of neuroinflammation also in the progressive phase of the disease. Our exploration of the literature, however, appears to highlight a lack of studies specifically combining a functional exploration of the visual pathway with a morphological description of the retina in PMS patients, with a still open possibility to better characterize the relation between demyelination and neurodegeneration in the progressive phase of the disease. To validate the use of VEPs and OCT in PMS, it is mandatory to recruit large cohorts of patients in the context of multicenter studies, longitudinally followed to define the correlations with clinically relevant visual parameters from the one side (i.e., contrast sensitivity measures) and with global disability measures on the other. Of great value could be also studies comparing combined OCT and VEPs data with conventional and advanced MRI techniques. A better knowledge in the field would be of fundamental importance in a near future, in order to identify the most suitable biomarkers to assess the efficacy of possible neuroprotective and remyelinating strategies aimed to contrast irreversible disability accrual affecting PMS patients.

AUTHOR CONTRIBUTIONS

All listed authors have made a substantial, direct and intellectual contribution to the present work, and approved it for publication. In particular, SG performed literature search and wrote the first draft of the manuscript. LL and GC completed bibliography and revised the manuscript.

REFERENCES

Albrecht, P., Frohlich, R., Hartung, H. P., Kieseier, B. C., and Methner, A. (2007). Optical coherence tomography measures axonal loss in multiple sclerosis independently of optic neuritis. *J. Neurol.* 254, 1595–1596. doi: 10.1007/s00415-007-0538-3

Albrecht, P., Ringelstein, M., Muller, A. K., Keser, N., Dietlein, T., Lappas, A., et al. (2012). Degeneration of retinal layers in multiple sclerosis subtypes quantified by optical coherence tomography. *Mult. Scler.* 18, 1422–1429. doi: 10.1177/1352458512439237

Alonso, R., Gonzalez-Moron, D., and Garcea, O. (2018). Optical coherence tomography as a biomarker of neurodegeneration in multiple sclerosis: a review. *Mult. Scler. Relat. Disord.* 22, 77–82. doi: 10.1016/j.msard.2018.03.007

Backner, Y., Petrou, P., Glick-Shames, H., Raz, N., Zimmermann, H., Jost, R., et al. (2019). Vision and vision-related measures in progressive multiple sclerosis. *Front. Neurol.* 10:455. doi: 10.3389/fneur.2019.00455

Balk, L. J., Cruz-Herranz, A., Albrecht, P., Arnow, S., Gelfand, J. M., Tewarie, P., et al. (2016). Timing of retinal neuronal and axonal loss in MS: a longitudinal OCT study. *J. Neurol.* 263, 1323–1331. doi: 10.1007/s00415-016-8127-y

Balk, L. J., Coric, D., Knier, B., Zimmermann, H. G., Behbehani, R., Alroughani, R., et al. (2019). Retinal inner nuclear layer volume reflects inflammatory disease activity in multiple sclerosis; a longitudinal OCT study. *Mult. Scler. J. Exp. Transl. Clin.* 5:2055217319871582. doi: 10.1177/2055217319871582

Balk, L. J., Tewarie, P., Killestein, J., Polman, C. H., Uitdehaag, B., and Petzold, A. (2014). Disease course heterogeneity and OCT in multiple sclerosis. *Mult. Scler.* 20, 1198–1206. doi: 10.1177/1352458513518626

Behbehani, R., Abu Al-Hassan, A., Al-Salahat, A., Sriraman, D., Oakley, J. D., and Alroughani, R. (2017). Optical coherence tomography segmentation analysis in relapsing remitting versus progressive multiple sclerosis. *PLoS One* 12:e0172120. doi: 10.1371/journal.pone.0172120

Berman, S., Backner, Y., Krupnik, R., Paul, F., Petrou, P., Karussis, D., et al. (2020). Conduction delays in the visual pathways of progressive multiple sclerosis patients covary with brain structure. *Neuroimage* 221:117204. doi: 10.1016/j.neuroimage.2020.117204

Bock, M., Brandt, A. U., Dörr, J., Pfueller, C. F., Ohlraun, S., Zipp, F., et al. (2010). Time domain and spectral domain optical coherence tomography in multiple sclerosis: a comparative cross-sectional study. *Mult. Scler.* 16, 893–896. doi: 10.1177/1352458510365156

Bsteh, G., Hegen, H., Altmann, P., Auer, M., Berek, K., Di Pauli, F., et al. (2020). Retinal layer thinning is reflecting disability progression independent of relapse activity in multiple sclerosis. *Mult. Scler. J. Exp. Transl. Clin.* 6:2055217320966344. doi: 10.1177/2055217320966344

Cellerino, M., Cordano, C., Boffa, G., Bommarito, G., Petracca, M., Sbragia, E., et al. (2019). Relationship between retinal inner nuclear layer, age, and disease activity in progressive MS. *Neurol. Neuroimmunol. Neuroinflamm.* 6:e596. doi: 10.1212/NXI.0000000000000596

Chatziralli, I. P., Moschos, M. M., Brouzas, D., Kopsidas, K., and Ladas, I. D. (2012). Evaluation of retinal nerve fibre layer thickness and visual evoked potentials in optic neuritis associated with multiple sclerosis. *Clin. Exp. Optom.* 95, 223–228. doi: 10.1111/j.1444-0938.2012.00706.x

Chen, L., and Gordon, L. K. (2005). Ocular manifestations of multiple sclerosis. *Curr. Opin. Ophthalmol.* 16, 315–320. doi: 10.1097/01.icu.0000179804.49842.e2

Comi, G., Leocani, L., Medaglini, S., Locatelli, T., Martinelli, V., Santuccio, G., et al. (1999). Measuring evoked responses in multiple sclerosis. *Mult. Scler.* 5, 263–267. doi: 10.1177/135245859900500412

Confavreux, C., and Vukusic, S. (2006). Natural history of multiple sclerosis: a unifying concept. *Brain* 129(Pt 3), 606–616. doi: 10.1093/brain/awl007

Coric, D., Balk, L. J., Verrijp, M., Eijlers, A., Schoonheim, M. M., Killestein, J., et al. (2018). Cognitive impairment in patients with multiple sclerosis is associated with atrophy of the inner retinal layers. *Mult. Scler.* 24, 158–166. doi: 10.1177/1352458517694090

Correale, J., Gaitan, M. I., Ysrraelit, M. C., and Fiol, M. P. (2017). Progressive multiple sclerosis: from pathogenic mechanisms to treatment. *Brain* 140, 527–546. doi: 10.1093/brain/aww258

Costello, F., and Burton, J. M. (2018). Retinal imaging with optical coherence tomography: a biomarker in multiple sclerosis? *Eye Brain* 10, 47–63. doi: 10.2147/EB.S139417

Davies, M. B., Williams, R., Haq, N., Pelosi, L., and Hawkins, C. P. (1998). MRI of optic nerve and postchiasmal visual pathways and visual evoked potentials in secondary progressive multiple sclerosis. *Neuroradiology* 40, 765–770. doi: 10.1007/s002340050681

Di Maggio, G., Santangelo, R., Guerrieri, S., Bianco, M., Ferrari, L., Medaglini, S., et al. (2014). Optical coherence tomography and visual evoked potentials: which is more sensitive in multiple sclerosis? *Mult. Scler.* 20, 1342–1347. doi: 10.1177/1352458514524293

Diebold, M., and Derfuss, T. (2016). Immunological treatment of multiple sclerosis. *Semin. Hematol.* 53(Suppl. 1), S54–S57. doi: 10.1053/j.seminhematol.2016.04.016

Fisher, J. B., Jacobs, S. L., Markowitz, D. A., Galetta, C. E., Volpe, N. J., Nano-Schiavi, M. L., et al. (2006). Relation of visual function to retinal nerve fiber layer thickness in multiple sclerosis. *Ophthalmology* 113, 324–332. doi: 10.1016/j.ophtha.2005.10.040

Fox, R. J., Coffey, C. S., Conwit, R., Cudkowicz, M. E., Gleason, T., Goodman, A., et al. (2018). Phase 2 trial of ibudilast in progressive multiple sclerosis. *N. Engl. J. Med.* 379, 846–855. doi: 10.1056/NEJMoa1803583

Frischer, J. M., Bramow, S., Dal-Bianco, A., Lucchinetti, C. F., Rauschka, H., Schmidbauer, M., et al. (2009). The relation between inflammation and neurodegeneration in multiple sclerosis brains. *Brain* 132(Pt 5), 1175–1189. doi: 10.1093/brain/awp070

Gabilondo, I. E., Martinez-Lapiscina, H., Martinez-Heras, E., Fraga-Pumar, E., Llufriu, S., Ortiz, S., et al. (2014). Trans-synaptic axonal degeneration in the visual pathway in multiple sclerosis. *Ann. Neurol.* 75, 98–107. doi: 10.1002/ana.24030

Gelfand, J. M., Goodin, D. S., Boscardin, W. J., Nolan, R., Cuneo, A., and Green, A. J. (2012). Retinal axonal loss begins early in the course of multiple sclerosis and is similar between progressive phenotypes. *PLoS One* 7:e36847. doi: 10.1371/journal.pone.0036847

Giovannoni, G., Butzkueven, H., Dhib-Jalbut, S., Hobart, J., Kobelt, G., Pepper, G., et al. (2016). Brain health: time matters in multiple sclerosis. *Mult. Scler. Relat. Disord.* 9(Suppl. 1), S5–S48. doi: 10.1016/j.msard.2016.07.003

Gordon-Lipkin, E., Chodkowski, B., Reich, D. S., Smith, S. A., Pulicken, M., Balcer, L. J., et al. (2007). Retinal nerve fiber layer is associated with brain atrophy in multiple sclerosis. *Neurology* 69, 1603–1609. doi: 10.1212/01.wnl.0000295995.46586.ae

Grazioli, E., Zivadinov, R., Weinstock-Guttman, B., Lincoff, N., Baier, M., Wong, J. R., et al. (2008). Retinal nerve fiber layer thickness is associated with brain MRI outcomes in multiple sclerosis. *J. Neurol. Sci.* 268, 12–17. doi: 10.1016/j.jns.2007.10.020

Green, A. J., McQuaid, S., Hauser, S. L., Allen, I. V., and Lyness, R. (2010). Ocular pathology in multiple sclerosis: retinal atrophy and inflammation irrespective of disease duration. *Brain* 133(Pt 6), 1591–1601. doi: 10.1093/brain/awq080

Heesen, C., Bohm, J., Reich, C., Kasper, J., Goebel, M., and Gold, S. M. (2008). Patient perception of bodily functions in multiple sclerosis: gait and visual function are the most valuable. *Mult. Scler.* 14, 988–991. doi: 10.1177/1352458508088916

Henderson, A. P., Trip, S. A., Schlottmann, P. G., Altmann, D. R., Garway-Heath, D. F., Plant, G. T., et al. (2008). An investigation of the retinal nerve fibre layer in progressive multiple sclerosis using optical coherence tomography. *Brain* 131(Pt 1), 277–287. doi: 10.1093/brain/awm285

Henderson, A. P., Trip, S. A., Schlottmann, P. G., Altmann, D. R., Garway-Heath, D. F., Plant, G. T., et al. (2010). A preliminary longitudinal study of the retinal nerve fiber layer in progressive multiple sclerosis. *J. Neurol.* 257, 1083–1091. doi: 10.1007/s00415-010-5467-x

International Progressive MS Alliance (2021). *What We Do*. Available online at: https://www.progressivemsalliance.org/what-we-do (accessed March 22, 2021).

Jankowska-Lech, I., Wasyluk, J., Palasik, W., Terelak-Borys, B., and Grabska-Liberek, I. (2019). Peripapillary retinal nerve fiber layer thickness measured by optical coherence tomography in different clinical subtypes of multiple sclerosis. *Mult. Scler. Relat. Disord.* 27, 260–268. doi: 10.1016/j.msard.2018.11.003

Kallenbach, K., and Frederiksen, J. (2007). Optical coherence tomography in optic neuritis and multiple sclerosis: a review. *Eur. J. Neurol.* 14, 841–849. doi: 10.1111/j.1468-1331.2007.01736.x

Kappos, L., Bar-Or, A., Cree, B. A. C., Fox, R. J., Giovannoni, G., Gold, R., et al. (2018). Siponimod versus placebo in secondary progressive multiple sclerosis (EXPAND): a double-blind, randomised, phase 3 study. *Lancet* 391, 1263–1273. doi: 10.1016/S0140-6736(18)30475-6

Kaushik, M., Yu Wang, C., Barnett, M. H., Garrick, R., Parratt, J., Graham, S. L., et al. (2013). Inner nuclear layer thickening is inversley proportional to retinal ganglion cell loss in optic neuritis. *PLoS One* 8:e78341. doi: 10.1371/journal.pone.0078341

Kerrison, J. B., Flynn, T., and Green, W. R. (1994). Retinal pathologic changes in multiple sclerosis. *Retina* 14, 445–451. doi: 10.1097/00006982-199414050-00010

Kira, J., Tobimatsu, S., Goto, I., and Hasuo, K. (1993). Primary progressive versus relapsing remitting multiple sclerosis in Japanese patients: a combined clinical, magnetic resonance imaging and multimodality evoked potential study. *J. Neurol. Sci.* 117, 179–185. doi: 10.1016/0022-510x(93)90171-t

Klistorner, A., Arvind, H., Nguyen, T., Garrick, R., Paine, M., Graham, S., et al. (2008). Axonal loss and myelin in early ON loss in postacute optic neuritis. *Ann. Neurol.* 64, 325–331. doi: 10.1002/ana.21474

Knier, B., Schmidt, P., Aly, L., Buck, D., Berthele, A., Mühlau, M., et al. (2016). Retinal inner nuclear layer volume reflects response to immunotherapy in multiple sclerosis. *Brain* 139, 2855–2863. doi: 10.1093/brain/aww219

Kolbe, S. C., Marriott, M., Walt, A., Fielding, J., Klistorner, A., Mitchell, P. J., et al. (2012). Diffusion tensor imaging correlates of visual impairment in multiple sclerosis and chronic optic neuritis. *Invest. Ophthalmol. Vis. Sci.* 53, 825–832. doi: 10.1167/iovs.11-8864

Lambe, J., Fitzgerald, K. C., Murphy, O. C., Filippatou, A. G., Sotirchos, E. S., Kalaitzidis, G., et al. (2021). Association of spectral-domain OCT with long-term disability worsening in multiple sclerosis. *Neurology* 96, e2058–e2069. doi: 10.1212/WNL.0000000000011788

Laron, M., Cheng, H., Zhang, B., Schiffman, J. S., Tang, R. A., and Frishman, L. J. (2009). Assessing visual pathway function in multiple sclerosis patients with multifocal visual evoked potentials. *Mult. Scler.* 15, 1431–1441. doi: 10.1177/1352458509350470

Lassmann, H. (2017). Targets of therapy in progressive MS. *Mult. Scler.* 23, 1593–1599. doi: 10.1177/1352458517729455

Lassmann, H., Bruck, W., and Lucchinetti, C. F. (2007). The immunopathology of multiple sclerosis: an overview. *Brain Pathol.* 17, 210–218. doi: 10.1111/j.1750-3639.2007.00064.x

Lassmann, H., van Horssen, J., and Mahad, D. (2012). Progressive multiple sclerosis: pathology and pathogenesis. *Nat. Rev. Neurol.* 8, 647–656. doi: 10.1038/nrneurol.2012.168

Leocani, L., Guerrieri, S., and Comi, G. (2018). Visual evoked potentials as a biomarker in multiple sclerosis and associated optic neuritis. *J. Neuroophthalmol.* 38, 350–357. doi: 10.1097/WNO.0000000000000704

Leocani, L., Rovaris, M., Boneschi, F. M., Medaglini, S., Rossi, P., Martinelli, V., et al. (2006). Multimodal evoked potentials to assess the evolution of multiple sclerosis: a longitudinal study. *J. Neurol. Neurosurg. Psychiatry* 77, 1030–1035. doi: 10.1136/jnnp.2005.086280

Lublin, F. D., and Reingold, S. C. (1996). Defining the clinical course of multiple sclerosis: results of an international survey. National Multiple Sclerosis Society (USA) Advisory Committee on clinical trials of new agents in multiple sclerosis. *Neurology* 46, 907–911. doi: 10.1212/wnl.46.4.907

Lublin, F. D., Reingold, S. C., Cohen, J. A., Cutter, G. R., Sørensen, P. S., Thompson, A. J., et al. (2014). Defining the clinical course of multiple sclerosis: the 2013 revisions. *Neurology* 83, 278–286. doi: 10.1212/WNL.0000000000000560

Martinez-Lapiscina, E. H., Arnow, S., Wilson, J. A., Saidha, S., Preiningerova, J. L., Oberwahrenbrock, T., et al. (2016). Retinal thickness measured with optical coherence tomography and risk of disability worsening in multiple sclerosis: a cohort study. *Lancet Neurol.* 15, 574–584. doi: 10.1016/S1474-4422(16)00068-5

Martinez-Lapiscina, E. H., Sanchez-Dalmau, B., Fraga-Pumar, E., Ortiz-Perez, S., Tercero-Uribe, A. I., Torres-Torres, R., et al. (2014). The visual pathway as a model to understand brain damage in multiple sclerosis. *Mult. Scler.* 20, 1678–1685. doi: 10.1177/1352458514542862

Melzi, L., Rocca, M. A., Bianchi-Marzoli, S., Falini, A., Vezzulli, P., Ghezzi, A., et al. (2007). A longitudinal conventional and magnetization transfer magnetic resonance imaging study of optic neuritis. *Mult. Scler.* 13, 265–268. doi: 10.1177/1352458506071212

Montalban, X., Hauser, S. L., Kappos, L., Arnold, D. L., Bar-Or, A., Comi, G., et al. (2017). Ocrelizumab versus placebo in primary progressive multiple sclerosis. *N. Engl. J. Med.* 376, 209–220. doi: 10.1056/NEJMoa1606468

Montolío, A., Cegoñino, J., Orduna, E., Sebastian, B., Garcia-Martin, E., and Pérez Del Palomar, A. (2019). A mathematical model to predict the evolution of retinal nerve fiber layer thinning in multiple sclerosis patients. *Comput. Biol. Med.* 111:103357. doi: 10.1016/j.compbiomed.2019.103357

Naismith, R. T., Xu, J., Tutlam, N. T., Scully, P. T., Trinkaus, K., Snyder, A. Z., et al. (2010). Increased diffusivity in acute multiple sclerosis lesions predicts risk of black hole. *Neurology* 74, 1694–1701. doi: 10.1212/WNL.0b013e3181e042c4

Oberwahrenbrock, T., Schippling, S., Ringelstein, M., Kaufhold, F., Zimmermann, H., Keser, N., et al. (2012). Retinal damage in multiple sclerosis disease subtypes measured by high-resolution optical coherence tomography. *Mult. Scler. Int.* 2012:530305. doi: 10.1155/2012/530305

Ontaneda, D., and Fox, R. J. (2015). Progressive multiple sclerosis. *Curr. Opin. Neurol.* 28, 237–243. doi: 10.1097/WCO.0000000000000195

Ontaneda, D., Fox, R. J., and Chataway, J. (2015). Clinical trials in progressive multiple sclerosis: lessons learned and future perspectives. *Lancet Neurol.* 14, 208–223. doi: 10.1016/S1474-4422(14)70264-9

Petracca, M., Cordano, C., Cellerino, M., Button, J., Krieger, S., Vancea, R., et al. (2017). Retinal degeneration in primary-progressive multiple sclerosis: a role for cortical lesions? *Mult. Scler.* 23, 43–50. doi: 10.1177/1352458516637679

Petzold, A., de Boer, J. F., Schippling, S., Vermersch, P., Kardon, R., Green, A., et al. (2010). Optical coherence tomography in multiple sclerosis: a systematic review and meta-analysis. *Lancet Neurol.* 9, 921–932. doi: 10.1016/S1474-4422(10)70168-X

Pisa, M., Guerrieri, S., Di Maggio, G., Medaglini, S., Moiola, L., Martinelli, V., et al. (2017). No evidence of disease activity is associated with reduced rate of axonal retinal atrophy in MS. *Neurology* 89, 2469–2475. doi: 10.1212/WNL.0000000000004736

Pisa, M., Ratti, F., Vabanesi, M., Radaelli, M., Guerrieri, S., Moiola, L., et al. (2020). Subclinical neurodegeneration in multiple sclerosis and neuromyelitis optica spectrum disorder revealed by optical coherence tomography. *Mult. Scler.* 26, 1197–1206. doi: 10.1177/1352458519861603

Poretto, V., Petracca, M., Saiote, C., Mormina, E., Howard, J., Miller, A., et al. (2017). A composite measure to explore visual disability in primary progressive multiple sclerosis. *Mult. Scler. J. Exp. Transl. Clin.* 3:2055217317709620.

Pueyo, V., Martin, J., Fernandez, J., Almarcegui, C., Ara, J., Egea, C., et al. (2008). Axonal loss in the retinal nerve fiber layer in patients with multiple sclerosis. *Mult. Scler.* 14, 609–614. doi: 10.1177/1352458507087326

Pulicken, M., Gordon-Lipkin, E., Balcer, L. J., Frohman, E., Cutter, G., and Calabresi, P. A. (2007). Optical coherence tomography and disease subtype in multiple sclerosis. *Neurology* 69, 2085–2092. doi: 10.1212/01.wnl.0000294876.49861.dc

Raz, N., Hallak, M., Ben-Hur, T., and Levin, N. (2014). Dynamic visual tests to identify and quantify visual damage and repair following demyelination in optic neuritis patients. *J. Vis. Exp.* 86:e51107. doi: 10.3791/51107

Rothman, A., Murphy, O. C., Fitzgerald, K. C., Button, J., Gordon-Lipkin, E., Ratchford, J. N., et al. (2019). Retinal measurements predict 10-year disability in multiple sclerosis. *Ann. Clin. Transl. Neurol.* 6, 222–232. doi: 10.1002/acn3.674

Saidha, S., Al-Louzi, O., Ratchford, J. N., Bhargava, P., Oh, J., Newsome, S. D., et al. (2015). Optical coherence tomography reflects brain atrophy in multiple sclerosis: a four-year study. *Ann. Neurol.* 78, 801–813. doi: 10.1002/ana.24487

Saidha, S., Sotirchos, E. S., Ibrahim, M. A., Crainiceanu, C. M., Gelfand, J. M., Sepah, Y. J., et al. (2012). Microcystic macular oedema, thickness of the inner nuclear layer of the retina, and disease characteristics in multiple sclerosis: a retrospective study. *Lancet Neurol.* 11, 963–972. doi: 10.1016/S1474-4422(12)70213-2

Saidha, S., Syc, S. B., Ibrahim, M. A., Eckstein, C., Warner, C. V., Farrell, S. K., et al. (2011). Primary retinal pathology in multiple sclerosis as detected by optical coherence tomography. *Brain* 134(Pt 2), 518–533. doi: 10.1093/brain/awq346

Sater, R. A., Rostami, A. M., Galetta, S., Farber, R. E., and Bird, S. J. (1999). Serial evoked potential studies and MRI imaging in chronic progressive multiple sclerosis. *J. Neurol. Sci.* 171, 79–83. doi: 10.1016/s0022-510x(99)00255-5

Schlaeger, R., D'Souza, M., Schindler, C., Grize, L., Kappos, L., and Fuhr, P. (2014). Electrophysiological markers and predictors of the disease course in primary progressive multiple sclerosis. *Mult. Scler.* 20, 51–56. doi: 10.1177/1352458513490543

Seigo, M. A., Sotirchos, E. S., Newsome, S., Babiarz, A., Eckstein, C., Ford, E., et al. (2012). In vivo assessment of retinal neuronal layers in multiple sclerosis with manual and automated optical coherence tomography segmentation techniques. *J. Neurol.* 259, 2119–2130. doi: 10.1007/s00415-012-6466-x

Serbecic, N., Aboul-Enein, F., Beutelspacher, S. C., Graf, M., Kircher, K., Geitzenauer, W., et al. (2010). Heterogeneous pattern of retinal nerve fiber layer in multiple sclerosis. High resolution optical coherence tomography: potential and limitations. *PLoS One* 5:e13877. doi: 10.1371/journal.pone.0013877

Siepman, T. A., Bettink-Remeijer, M. W., and Hintzen, R. Q. (2010). Retinal nerve fiber layer thickness in subgroups of multiple sclerosis, measured by optical coherence tomography and scanning laser polarimetry. *J. Neurol.* 257, 1654–1660. doi: 10.1007/s00415-010-5589-1

Siger, M., Dziegielewski, K., Jasek, L., Bieniek, M., Nicpan, A., Nawrocki, J., et al. (2008). Optical coherence tomography in multiple sclerosis: thickness of the retinal nerve fiber layer as a potential measure of axonal loss and brain atrophy. *J. Neurol.* 255, 1555–1560. doi: 10.1007/s00415-008-0985-5

Sorensen, P. S., Fox, R. J., and Comi, G. (2020). The window of opportunity for treatment of progressive multiple sclerosis. *Curr. Opin. Neurol.* 33, 262–270. doi: 10.1097/WCO.0000000000000811

Sotirchos, E. S., Gonzalez Caldito, N., Filippatou, A., Fitzgerald, K. C., Murphy, O. C., Lambe, J., et al. (2020). Progressive multiple sclerosis is associated with faster and specific retinal layer atrophy. *Ann. Neurol.* 87, 885–896. doi: 10.1002/ana.25738

Stevenson, V. L., Miller, D. H., Rovaris, M., Barkhof, F., Brochet, B., Dousset, V., et al. (1999). Primary and transitional progressive MS: a clinical and MRI cross-sectional study. *Neurology* 52, 839–845. doi: 10.1212/wnl.52.4.839

Syc, S. B., Saidha, S., Newsome, S. D., Ratchford, J. N., Levy, M., Ford, E., et al. (2012). Optical coherence tomography segmentation reveals ganglion cell layer pathology after optic neuritis. *Brain* 135, 521–533. doi: 10.1093/brain/awr264

Talman, L. S., Bisker, E. R., Sackel, D. J., Long, D. A. Jr., Galetta, K. M., Ratchford, J. N., et al. (2010). Longitudinal study of vision and retinal nerve fiber layer thickness in multiple sclerosis. *Ann. Neurol.* 67, 749–760. doi: 10.1002/ana.22005

Tavazzi, E., Jakimovski, D., Kuhle, J., Hagemeier, J., Ozel, O., Ramanathan, M., et al. (2020). Serum neurofilament light chain and optical coherence tomography measures in MS: a longitudinal study. *Neurol. Neuroimmunol. Neuroinflamm.* 7:e737. doi: 10.1212/NXI.0000000000000737

Thompson, A. J., Montalban, X., Barkhof, F., Brochet, B., Filippi, M., Miller, D. H., et al. (2000). Diagnostic criteria for primary progressive multiple sclerosis: a position paper. *Ann. Neurol.* 47, 831–835.

Trapp, B. D., and Nave, K. A. (2008). Multiple sclerosis: an immune or neurodegenerative disorder? *Annu. Rev. Neurosci.* 31, 247–269. doi: 10.1146/annurev.neuro.30.051606.094313

Trip, S. A., Schlottmann, P. G., Jones, S. J., Li, W. Y., Garway-Heath, D. F., Thompson, A. J., et al. (2006). Optic nerve atrophy and retinal nerve fibre layer thinning following optic neuritis: evidence that axonal loss is a substrate of MRI-detected atrophy. *Neuroimage* 31, 286–293. doi: 10.1016/j.neuroimage.2005.11.051

Vabanesi, M., Pisa, M., Guerrieri, S., Moiola, L., Radaelli, M., Medaglini, S., et al. (2019). In vivo structural and functional assessment of optic nerve damage in neuromyelitis optica spectrum disorders and multiple sclerosis. *Sci. Rep.* 9:10371. doi: 10.1038/s41598-019-46251-3

Villoslada, P. (2016). Neuroprotective therapies for multiple sclerosis and other demyelinating diseases. *Mult. Scler. Demyelinating Disord.* 1:1. doi: 10.1186/s40893-016-0004-0

Winges, K. M., Murchison, C. F., Bourdette, D. N., and Spain, R. I. (2019). Longitudinal optical coherence tomography study of optic atrophy in secondary progressive multiple sclerosis: results from a clinical trial cohort. *Mult. Scler.* 25, 55–62. doi: 10.1177/1352458517739136

Yousefipour, G., Hashemzahi, Z., Yasemi, M., and Jahani, P. (2016). Findings of optical coherence tomography of retinal nerve fiber layer in two common types of multiple sclerosis. *Acta Med. Iran.* 54, 382–390.

Zaveri, M. S., Conger, A., Salter, A., Frohman, T. C., Galetta, S. L., Markowitz, C. E., et al. (2008). Retinal imaging by laser polarimetry and optical coherence tomography evidence of axonal degeneration in multiple sclerosis. *Arch. Neurol.* 65, 924–928. doi: 10.1001/archneur.65.7.924

Conflict of Interest: The authors declare that the research was conducted in the absence of any commercial or financial relationships that could be construed as a potential conflict of interest.

Publisher's Note: All claims expressed in this article are solely those of the authors and do not necessarily represent those of their affiliated organizations, or those of the publisher, the editors and the reviewers. Any product that may be evaluated in this article, or claim that may be made by its manufacturer, is not guaranteed or endorsed by the publisher.

frontiers in Neuroscience

ORIGINAL RESEARCH
published: 30 August 2021
doi: 10.3389/fnins.2021.679092

Retinal Diseases and Parkinson Disease: A Population-Based Study

Po-Chih Chen[1,2†], Chen-Chih Chung[1,2,3†], Yun-Yung Cheng[1], Wan-Ting Chen[4], Chien-Tai Hong[1,2], Lung Chan[1,2†] and Li-Nien Chien[4,5*†]*

[1] Department of Neurology, Shuang-Ho Hospital, Taipei Medical University, New Taipei City, Taiwan, [2] Department of Neurology, School of Medicine, College of Medicine, Taipei Medical University, Taipei City, Taiwan, [3] Graduate Institute of Biomedical Informatics, Taipei Medical University, Taipei City, Taiwan, [4] School of Health Care Administration, College of Management, Taipei Medical University, Taipei City, Taiwan, [5] Health and Clinical Research Data Center, Office of Data, Taipei Medical University, Taipei City, Taiwan

OPEN ACCESS

Edited by:
Yuyi You,
Macquarie University, Australia

Reviewed by:
Petr A. Slominsky,
National Research Center "Kurchatov Institute," Russia
M. Heather West Greenlee,
Iowa State University, United States

***Correspondence:**
Lung Chan
cjustinmd@gmail.com
Li-Nien Chien
lnchien@tmu.edu.tw

[†] These authors have contributed equally to this work

Specialty section:
This article was submitted to Neurodegeneration, a section of the journal Frontiers in Neuroscience

Received: *11 March 2021*
Accepted: *30 July 2021*
Published: *30 August 2021*

Citation:
Chen P-C, Chung C-C, Cheng Y-Y, Chen W-T, Hong C-T, Chan L and Chien L-N (2021) Retinal Diseases and Parkinson Disease: A Population-Based Study. Front. Neurosci. 15:679092. doi: 10.3389/fnins.2021.679092

Introduction: Patients with Parkinson disease (PD) tend to have ophthalmic symptoms. Retinal diseases are associated with central nervous system diseases, especially neurodegenerative diseases. Here, we investigated the association of retinal diseases with PD, especially the temporal relationship before and after PD diagnosis.

Methods: Data were obtained from the National Health Insurance Research Database of Taiwan. In total, 21,845 patients with newly diagnosed PD were matched with four controls each on the basis of propensity score. This study was bidirectional. A case–control study evaluated the adjusted odds ratio (aOR) of retinal disease before PD diagnosis by using conditional logistic regression. Furthermore, a cohort study evaluated the adjusted subdistribution hazard ratio (aSHR) for new-onset retinal and optic nerve diseases after PD diagnosis by using competing risk analysis. The association between PD with optic nerve diseases and glaucoma (another common ophthalmic diseases with the consequence of retinal dysfunction) were also analyzed as reference.

Results: In the case–control study, PD was found to be significantly comorbid with recent and remote retinal disease [recent: $\leq$ 5 years, aOR: 1.12, 95% confidence interval (CI): 1.03–1.23; remote: $>$ 5 years, aOR: 1.18, 95% CI: 1.04–1.34]. No similar association was identified between optic nerve disease or glaucoma with PD. In the cohort study, patients with PD were found to have a low risk of retinal disease in short-term ($\leq$ 5 years, aSHR: 0.81, 95% CI: 0.71–0.93) and long-term ($>$ 5 years, aSHR: 0.82, 95% CI: 0.72–0.93) follow-up.

Conclusion: The study findings demonstrated that patients with prediagnostic PD were at greater risk of retinal disease than non-PD participants, but the risk reversed afterward. Thus, retinal disease may be a premotor manifestation of PD, and there may be some possible effect of dopamine supplements on retina.

Keywords: retina, Parkinson's disease, population-based, cohort study, dopamine

INTRODUCTION

Parkinson disease (PD) is the second most common neurodegenerative disease worldwide, with an estimated incidence of 15–328 per 100,000 individuals and prevalence of 15–12,500 per 100,000 individuals. The disease prevalence has been increasing over time, affecting roughly 2.5 million patients in 1990 and 6.1 million patients (5.0–7.3) in 2016 (GBD 2016 Parkinson's Disease Collaborators, 2018). Among PD risk factors, age is the most important and un-modified. With progress in the domains of public health and medicine as well as increased life expectancy (Christensen et al., 2009) among the general population, the number of patients with PD will likely continue to increase in the future.

Motor symptoms in PD are characteristic and include resting tremor, bradykinesia, postural instability, and freezing phenomenon. Non-motor symptoms at various stages of PD include ophthalmologic symptoms and disorders (Borm et al., 2020), mood disorders and affective apathy, anhedonia and depression, cognitive dysfunction, complex behavioral disorders, and hallucinations (Poewe, 2008).

Despite advances in technology and modern medicine, the actual mechanism of PD remains obscure. The disease is characterized by dopaminergic neuron depletion and abnormal intracellular α-synuclein aggregation in Lewy bodies. Both environmental (Klingelhoefer and Reichmann, 2015) and genetic factors (Koros et al., 2017), such as neuroinflammation, mitochondrial dysfunction (Rocha et al., 2018), and characteristics of the brain–gut axis, appear to be associated with PD pathogenesis, although none of them can explain the disease phenomenon completely.

Dopaminergic neuron depletion, associated with the shortage of dopamine up to approximately 70%, results in the manifestation of clinical motor symptoms of PD (Engelender and Isacson, 2017). Dopamine is a neurotransmitter with key roles in not only the central nervous system (CNS) but also the gastrointestinal system (Glavin and Szabo, 1990), immune response mediation (Matt and Gaskill, 2020), light adaptation (Flood et al., 2018), and eye growth (Stone et al., 1989).

Visual disturbances are prominent at all PD stages (Satue et al., 2017), with up to 82% of patients reporting dry eyes, blepharitis, double vision, or visual hallucination (Borm et al., 2020). The shortage and depletion of dopamine have been associated with the retinal degeneration and denervation of the visual cortex or adjacent regions in animal studies and clinical studies involving patients with PD (Phillipson et al., 1987; Weil et al., 2016). In an animal study, dopaminergic treatment preserved visual function (Pardue and Allen, 2018). However, levodopa and dopamine agonists used in the treatment of PD are associated with ocular and visual adverse effects (Armstrong, 2017; Daggumilli et al., 2019).

Given the high prevalence of ophthalmologic symptoms in patients with PD (Satue et al., 2017) and the possible role of dopamine in retinal functions, we investigated the association of retinal diseases with PD. To test the role of dopamine as a premotor PD biomarker and avoid the possible bias introduced by dopaminergic medications, we conducted case–control and cohort studies using patient data from the National Health Insurance Research Database (NHIRD). The bidirectional approach helped assess the risk of newly diagnosed retinal disease before and after PD diagnosis. To minimize the potential of identifying retinal diseases secondary to glaucoma or optic nerve disease, a prevalent disease in the elderly population, we analyzed the risk of glaucoma and optic nerve diseases in parallel for the purpose of comparison (Weinreb et al., 2014).

MATERIALS AND METHODS

Data Source

Patient data were obtained from the NHIRD, which is maintained by the National Health Insurance (NHI) Administration (NHIA) of Taiwan. The NHIRD is a nationwide claims-based database of those insured under the NHI program, which is a compulsory insurance program that has been providing coverage for most of the health care services in Taiwan and almost 30,000 prescription medications since 1995. In this study, we used data collected between 2000 and 2017, and data collected after 2000 were used because electronic claims data were incomplete during the initial phases of NHI implementation. The NHIRD includes information on disease diagnoses [coded according to the *International Classification of Diseases, Ninth Revision, Clinical Modification* (ICD-9-CM) before 2016 and according to ICD-10 thereafter], treatment procedures, service dates, prescribed medications (classified according to the Anatomical Therapeutic Chemical Classification System for Medications), reimbursement amounts, patient demographic information, and patient- and provider-encrypted identifiers. To verify the accuracy of diagnoses and treatment rationales, the NHIA routinely samples a portion of the NHI claims and penalizes hospitals and clinics if they determine unnecessary medical treatment has been provided.

Study Population

Patients with newly diagnosed PD were defined as those who had at least two diagnostic claims (ICD-9-CM: 332.0) and prescription claims for dopaminergic agents between 2004 and 2013. It had been validated that the diagnostic accuracy of this inclusion criteria was 94.8% (Lee et al., 2013). The index date of PD was defined as the date of first PD diagnosis, hereafter referred to as the index PD. Patients aged < 45 years or who had a history of stroke or prior treatment with an antipsychotic drug before the index PD were excluded to avoid the possibility of misclassification of secondary parkinsonism. In addition, patients with a history of thyroid disease were excluded, as thyroid dysfunction (ICD-9-CM: 240–246) may be directly associated with ophthalmic diseases. The same exclusion criteria were used for control participants.

Propensity Score Matching

Matching aims to reduce potential selection bias in observational studies. Propensity score (PS) matching (PSM) is frequently used to control for confounding factors that inevitably occur in studies investigating the effect of exposures on an outcome.

In PSM, study and control groups sharing similar propensity scores are matched. The weighted value reveals the risk of a participant for the outcome of interest according to underlying characteristics that predispose them to that outcome irrespective of the exposure of interest. In this study, the PS was measured on the basis of hypertension (HTN, ICD-9-CM: 401–405), diabetes mellitus (DM, ICD-9-CM: 250), hyperlipidemia (ICD-9-CM: 272), chronic heart failure (CHF, ICD-9-CM: 428), coronary artery disease (CAD, ICD-9-CM: 410–414), chronic lung disease (ICD-9-CM: 415–417, 490–496, and 500–508), renal disease (ICD-9-CM: 580–589), and inflammatory diseases (ICD-9-CM: 710, 714). The selection of these factors was based on their association with retinal and optic nerve diseases. Control participants without PD were assigned an index date of pseudo-PD diagnosis corresponding to the index PD of their matched patients. Each patient with PD was matched with four control participants without PD based on age, sex, pseudo diagnostic year, and the PS using a caliper with a width of 0.1; consequently, the two cohorts had similar baseline characteristics but differed in PD diagnosis.

Main Outcome

Both patients with PD and control participants were tracked or followed up for their risk of retinal and optic nerve diseases according to the study design. Patients with retinal diseases (ICD-9-CM: 361–363 except 363.4–363.7) were defined as those who first had at least two diagnostic claims corresponding with the fundus examination. In the cohort study, retinal disease risk was measured after the index PD or pseudo-PD diagnosis. Hereditary retinal disease (ICD-9-CM: 362.7) were excluded. Optic nerve disease was defined as the presence of two disease diagnostic claim (ICD-9-CM: 377) and traumatic optic nerve disease (ICD-9-CM:377.3) was excluded. Glaucoma was defined as the presence of disease diagnosis (ICD-9-CM:365) and medication treatment. The detailed disease diagnostic codes are presented in **Supplementary Table 1**. The selection process is presented in **Figure 1**.

Statistical Analysis

Baseline characteristics were analyzed using the standardized mean difference (SMD). An SMD of > 0.1 indicated non-negligible differences between the groups. The case–control study evaluated the adjusted odds ratio (aOR) of retinal disease before PD diagnosis by using conditional logistic regression, and the cohort study evaluated the adjusted subdistribution hazard ratio (aSHR) of new-onset retinal and optic nerve diseases after PD diagnosis by using competing risk analysis. Competing risk model analyses were applied to estimate the absolute relative retinal disease risks because the participants had a high mortality risk. The follow-up period for each patient ranged from the index PD or pseudo-PD diagnosis to the date of retinal and optic nerve disease diagnosis, death, or the end of the observation period (December 31, 2017). All analyses were performed using SAS/STAT version 9.4 (SAS Institute Inc., Cary, NC, United States) and STATA 14 (Stata Corp., LP, College Station, TX, United States). A p-value of < 0.05 was considered significant.

RESULTS

Figure 1 is the flow chart detailing the selection of patients with PD. Overall, 21,845 patients with newly diagnosed PD and 87,380 non-PD PS-matched control participants for comparison were included. No differences were present in age or sex between the groups (**Table 1**). Comorbidities, including DM, hyperlipidemia, CHF, CAD, chronic lung disease, renal disease, and inflammatory diseases, were well-matched between the PD and non-PD control groups.

The overall risk of retinal disease was significantly increased in the PD group (aOR: 1.14, 95% CI: 1.06–1.23, $p < 0.001$) compared with the non-PD group before PD diagnosis. The significantly increased risk was consistent following separation of the premotor stage into recent ($\leq$ 5 years; aOR: 1.12, 95% CI: 1.03–1.23) and remote ($>$ 5 years; aOR: 1.18, 95% CI: 1.04–1.34) periods. The increased risk was not evident in the diagnosis of optic nerve disease or glaucoma, other common ophthalmic diseases with the consequence of retinal disease, between the groups before PD diagnosis (**Table 2** and **Supplementary Tables 2**, **3**).

Regarding the follow-up cohort, we excluded participants with a diagnosis of any ophthalmologic disorder before PD diagnosis to focus on newly diagnosed retinal diseases after PD diagnosis. The results demonstrated a significant reduction in the hazard ratio of newly diagnosed retinal disease (aSHR: 0.77, 95% CI: 0.70–0.85, $p < 0.001$), and the reduced risk remained significant in short-term ($\leq$ 5 years; aSHR: 0.81, 95% CI: 0.71–0.93) and long-term ($>$ 5 years; aSHR: 0.82, 95% CI: 0.72–0.93) follow-up. Regarding optic nerve disease, the overall hazard ratio was not different between PD and non-PD (aSHR: 0.91, 95% CI: 0.67–1.23, $p = 0.540$). For the glaucoma, the overall hazard ratio was significantly reduced (aSHR: 0.87, 95% CI: 0.78–0.97, $p = 0.010$) but was identical between PD and non-PD groups at short-term ($\leq$ 5 years) follow-up and significantly lower only in the PD group at long-term ($>$ 5 year) follow-up (**Table 3** and **Supplementary Tables 4**, **5**).

DISCUSSION

The present study demonstrated that patients with PD are at higher risk of retinal disease at the premotor PD stage than non-PD controls, although the hazard ratio reversed markedly in the follow-up period. This contrasting association was not observed between PD and optic nerve disease or glaucoma, other common age-related ophthalmic diseases. This discrepancy in the temporal relationship between the two diseases may hint that retinal disease is a premotor manifestation of PD, and the possible effect of dopamine supplements on retina.

Anosmia is a well-recognized non-motor symptom of the premotor PD stage (Iannilli et al., 2017), and the degeneration of the olfactory bulb is found to occur before the loss of dopaminergic neurons in the midbrain. Similar to the olfactory bulb, the optic nerve and retina are considered to be extension of the CNS (London et al., 2013). Dopamine is endogenously

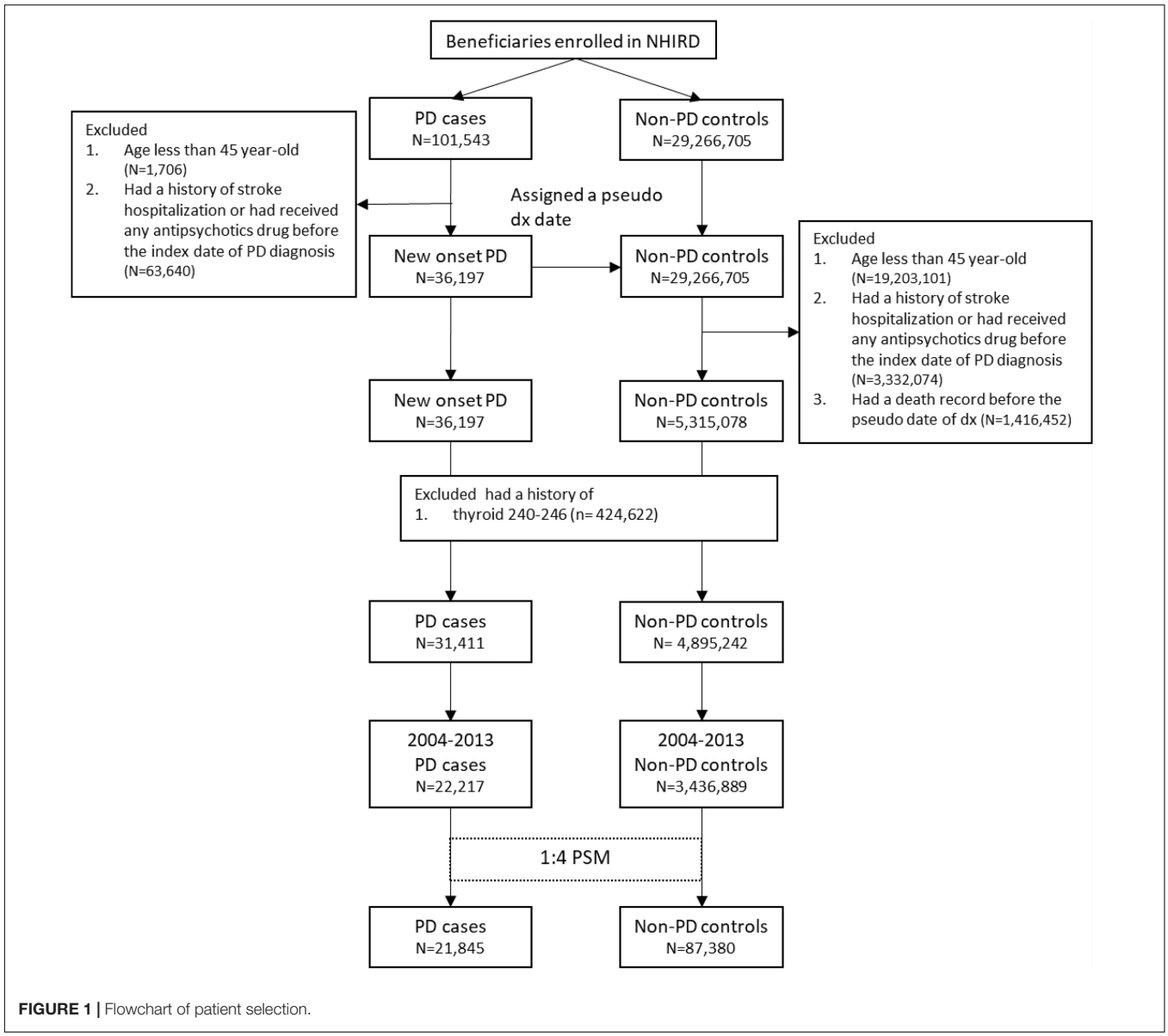

FIGURE 1 | Flowchart of patient selection.

found in and essential for the functioning of the retina, although disorders of these structures are markedly underestimated in patients with PD. Pathological α-synuclein aggregation and deposits have been noted in retinal cells in postmortem patients with PD (Veys et al., 2019). Thinning of the retinal nerve fiber layers, a measure of the integrity of the retinal ganglion cell axon, has been found in PD, and macular thickness has also been reported to be reduced (Altintaş et al., 2008). The association between PD with retinal disease suggest possible explanation that dopaminergic deficiency is harmful for the retina of key to maintain structural integrity (Witkovsky, 2004). Applying dopamine was found to be effective in slowing retinal degeneration in some preclinical studies and clinical trials (Zhou et al., 2017) and the possible benefit of dopamine supplement on restoring visual and neuronal function were the stimulation of the secretion of pigment epithelium derived factor, and anti-angiogenesis (Review by Pardue and Allen, 2018). The present study used a bidirectional approach to successfully distinguish the reverse association between the two diseases; our approach is superior to previous cross-sectional, case–control studies because it could discern the temporal relationship and avoid the bias from dopaminergic supplements.

Glaucoma is widely recognized as an age-related disease and a leading cause of retinal and optic nerve disease. The present study did not find an increased risk of glaucoma for patients with PD in the prediagnostic stage, and this excluded the possible bias of increased risk of retinal and optic nerve disease secondary to uncontrolled glaucoma. Regarding the follow-up period for patients with PD, we found a significant reduction of the hazard ratio of newly diagnosed glaucoma. Previous studies have shown the effects of a dopamine receptor agonist in decreasing intraorbital pressure over several hours

TABLE 1 | Baseline characteristics of participants with PD versus non-PD before and after PSM.

	Before matching					After matching				
	Non-PD		PD		SMD	Non-PD		PD		SMD
	n	(%)	n	(%)		n	(%)	n	(%)	
Sample size	3,436,889		22,217			87,380		21,845		
Male	1,917,573	(55.8)	13,139	(59.1)	0.068	51,712	(59.2)	12,928	(59.2)	<0.001
Age, years										
Mean (SD)	57.67	(10.44)	72.05	(9.89)	1.414	71.89	(9.82)	71.89	(9.82)	<0.001
45–64	2,639,180	(76.8)	4,857	(21.9)	1.315	19,386	(22.2)	4,847	(22.2)	<0.001
65+	797,709	(23.2)	17,360	(78.1)	1.315	67,994	(77.8)	16,998	(77.8)	<0.001
Year of diagnosis										
2004–2005	651,760	(19.0)	4,306	(19.4)	0.011	16,936	(19.4)	4,234	(19.4)	<0.001
2006–2007	698,620	(20.3)	4,558	(20.5)	0.005	17,884	(20.5)	4,471	(20.5)	<0.001
2008–2009	698,440	(20.3)	4,474	(20.1)	0.005	17,568	(20.1)	4,392	(20.1)	<0.001
2010–2011	693,020	(20.2)	4,470	(20.1)	0.001	17,620	(20.2)	4,405	(20.2)	<0.001
2012–2013	695,049	(20.2)	4,409	(19.8)	0.009	17,372	(19.9)	4,343	(19.9)	<0.001
Comorbidities										
HTN	732,817	(21.3)	11,127	(50.1)	0.629	46,891	(53.7)	10,796	(49.4)	0.085
DM	332,270	(9.7)	4,687	(21.1)	0.321	17,404	(19.9)	4,552	(20.8)	0.023
Hyperlipidemia	353,140	(10.3)	4,036	(18.2)	0.227	13,730	(15.7)	3,950	(18.1)	0.063
CHF	32,781	(1.0)	898	(4.0)	0.199	3,427	(3.9)	819	(3.7)	0.009
CAD	179,610	(5.2)	3,902	(17.6)	0.396	14,913	(17.1)	3,713	(17.0)	0.002
Chronic lung disease	145,698	(4.2)	2,682	(12.1)	0.289	10,953	(12.5)	2,520	(11.5)	0.031
Renal disease	51,413	(1.5)	1,107	(5.0)	0.198	3,893	(4.5)	1,038	(4.8)	0.014
Inflammatory disease	27,063	(0.8)	338	(1.5)	0.069	984	(1.1)	324	(1.5)	0.031
Statin prescription	59,571	(4.6)	2,108	(9.5)	0.190	7,577	(8.7)	2,057	(9.4)	0.026
Average clinic visits/year	10.32	(11.83)	23.65	(17.49)	0.893	21.86	(15.93)	22.79	(15.94)	0.058

Standardized mean difference (SMD) indicates the variable difference in means or proportions divided by standard error; imbalance defined as absolute value > 0.1. PD, Parkinson disease; PSM, propensity score matching; HTN, hypertension; DM, diabetes mellitus; CHF, congestive heart failure; CAD, coronary heart disease.

TABLE 2 | The aOR of retinal disease, optic nerve disease and glaucoma among the study participants in the case–control study.

	PD	Non-PD	aOR (95% CI)	*p*-value
Participants	21,845	87,380		
Retinal disease, n (%)				
Overall	972 (4.4)	3,428 (3.9)	1.14 (1.06–1.23)	<0.001
Recent (≤5 years)	654 (3.0)	2,344 (2.7)	1.12 (1.03–1.23)	0.011
Remote (>5 years)	318 (1.5)	1,084 (1.2)	1.18 (1.04–1.34)	0.011
Optic Nerve disease, n (%)				
Overall	86 (0.4)	275 (0.3)	1.25 (0.98–1.60)	0.069
Recent (≤5 years)	60 (0.3)	211 (0.2)	1.14 (0.85–1.51)	0.379
Remote (>5 years)	26 (0.1)	64 (0.1)	1.63 (1.03–2.58)	0.036
Glaucoma, n (%)				
Overall	1,363 (6.2)	5,157 (5.9)	1.06 (1.00–1.13)	0.057
Recent (≤5 years)	695 (3.2)	2,645 (3.0)	1.05 (0.97–1.15)	0.234
Remote (>5 years)	668 (3.1)	2,512 (2.9)	1.07 (0.98–1.16)	0.146

aOR, adjusted odds ratio; PD, Parkinson disease; CI, confidence interval.

(Pescosolido et al., 2013), but there is scant evidence of a more prolonged effect. We speculate that supplementation with dopaminergic agents may lower the incidence of glaucoma in patients with PD in the long-term, although further studies must investigate the actual mechanism through which this could be achieved.

To the best of our knowledge, this is the first study to elucidate the association of retinal disease with PD using a bidirectional approach and the first to identify a discrepancy in risk based on temporal association. The main strengths of our study are attributable to the characteristics of the cohort. The NHIRD contains comprehensive data on a nationwide

TABLE 3 | The aSHR of retinal disease, optic nerve disease and glaucoma among participants in the cohort study.

	PD	Non-PD	aOR (95% CI)	*p*-value
Retinal disease, n/N (%)				
Overall	446/11,184 (4.3)	2,465/45,986 (5.7)	0.77 (0.70–0.85)	<0.001
Short-term (≤5 years)	216/11,184 (1.9)	1,137/45,986 (2.5)	0.81 (0.71–0.93)	0.003
Long-term (>5 years)	230/7,928 (2.9)	1,328/35,308 (3.8)	0.82 (0.72–0.93)	0.003
Optic nerve disease, n/N (%)				
Overall	50/11,184 (0.4)	226/45,986 (0.5)	0.91 (0.67–1.23)	0.540
Short-term (≤5 years)	23/11,184 (0.2)	105/45,986 (0.2)	0.94 (0.60–1.47)	0.770
Long-term (>5 years)	27/8,086 (0.3)	1,231/36,193 (0.3)	1.05 (0.70–1.60)	0.799
Glaucoma, n/N (%)				
Overall	340/11,184 (3.0)	1,611/45,986 (3.5)	0.87 (0.78–0.97)	0.010
Short-term (≤5 years)	216/11,184 (1.9)	880/45,986 (1.9)	1.04 (0.90–1.20)	0.567
Long-term (>5 years)	124/7,924 (1.6)	731/35,500 (2.1)	0.75 (0.62–0.89)	0.001

aSHR, adjusted subdistribution hazard ratio; PD, Parkinson disease; CI, confidence interval.

population (> 99% of Taiwan's population), and these data have been collected for over two decades. Typically, the diagnosis of PD and retinal and optic nerve disease is made by specialists. Because we used the NHIRD, we were able to take advantage of data encompassing long prediagnostic and follow-up periods before and after PD diagnosis. Moreover, the data were free from the false recall concern, which is a common concern in most case–control studies, and the percentage of loss to follow-up in the cohort was low. Despite these advantages, the present study has certain limitations. First, the NHIRD does not have information regarding family history of PD, environmental factors, or occupational factors, all of which may affect the incidence of retinal degeneration or PD. To minimize potential bias, we excluded patients diagnosed with PD before 45 years of age, but this exclusion criterion could not eliminate all genetic-related PD. Second, the severity of retinal and optic nerve disease was not documented in the NHIRD, which limits further analysis of the diseases with PD risk. Third, although the finding of significant risk reduction of retinal disease after the diagnosis of PD, as the nature of epidemiological study, it was not able to clearly delineate the causal relationship between dopamine supplement with the risk reduction, which may need more studies to confirm. Lastly, in the NHIRD, there was no information abouts the motor symptoms and motor subtypes of PD, which limited the possibility of further subgroup analysis.

In conclusion, the study demonstrated that patients with PD are at a greater risk of retinal disease at the prediagnostic stage, even more than 5 years in advance of diagnosis, than are non-PD individuals. By contrast, the risk of retinal disease after PD diagnosis decreased significantly compared with the control group, implying the possible effect from dopaminergic supplements. Further large-scale prospective studies investigating retinal and optic nerve disease as a premotor predictive biomarker for PD are warranted.

DATA AVAILABILITY STATEMENT

The raw data supporting the conclusions of this article will be made available by the authors, without undue reservation.

ETHICS STATEMENT

This study was approved by the Joint Institutional Review Board of Taipei Medical University (approval N202101060). Confidentiality was ensured by adhering to data regulations of the Health and Welfare Data Science Center (HWDC), Ministry of Health and Welfare, Executive Yuan, Taiwan. To protect patient privacy, individual identifiers are encrypted before the HWDC releases patient-level data to investigators, which they do only for research purposes. Therefore, the requirement for informed consent from study participants was exempted by the Joint Institutional Review Board. All study methods were in accordance with guidelines approved by the Joint Institutional Review Board and aforementioned governmental regulations.

AUTHOR CONTRIBUTIONS

L-NC, LC, and C-TH: conceptualization, formal analysis, writing—review and editing. P-CC, C-CC, Y-YC, W-TC, LC, and L-NC: data curation. P-CC, C-CC, Y-YC, W-TC, and C-TH: methodology. LC and L-NC: supervision and validation. C-CC: visualization. P-CC, C-CC, and Y-YC: writing—original draft. All authors contributed to the article and approved the submitted version.

FUNDING

This study was funded by the Shuang Ho Hospital, Taipei Medical University (109TMU-SHH-19).

SUPPLEMENTARY MATERIAL

The Supplementary Material for this article can be found online at: https://www.frontiersin.org/articles/10.3389/fnins.2021.679092/full#supplementary-material

REFERENCES

Altintaş, O., Işeri, P., Ozkan, B., and Cağlar, Y. (2008). Correlation between retinal morphological and functional findings and clinical severity in Parkinson's disease. *Doc. Ophthalmol.* 116, 137–146. doi: 10.1007/s10633-007-9091-8

Armstrong, R. A. (2017). Visual dysfunction in Parkinson's disease. *Int. Rev. Neurobiol.* 134, 921–946. doi: 10.1016/bs.irn.2017.04.007

Borm, C. D. J. M., Visser, F., Werkmann, M., de Graaf, D., Putz, D., Seppi, K., et al. (2020). Seeing ophthalmologic problems in Parkinson disease: results of a visual impairment questionnaire. *Neurology* 94, e1539–e1547. doi: 10.1212/WNL.0000000000009214

Christensen, K., Doblhammer, G., Rau, R., and Vaupel, J. W. (2009). Ageing populations: the challenges ahead. *Lancet* 374, 1196–1208. doi: 10.1016/S0140-6736(09)61460-4

Daggumilli, S., Vanathi, M., Ganger, A., Goyal, V., and Tandon, R. (2019). Corneal evaluation in patients with parkinsonism on long-Term Amantadine Therapy. *Cornea* 38, 1131–1136. doi: 10.1097/ICO.0000000000001951

Engelender, S., and Isacson, O. (2017). The threshold theory for Parkinson's disease. *Trends Neurosci.* 40, 4–14. doi: 10.1016/j.tins.2016.10.008

Flood, M. D., Moore-Dotson, J. M., and Eggers, E. D. (2018). Dopamine D1 receptor activation contributes to light-adapted changes in retinal inhibition to rod bipolar cells. *J. Neurophysiol.* 120, 867–879. doi: 10.1152/jn.00855.2017

GBD 2016 Parkinson's Disease Collaborators (2018). Global, regional, and national burden of Parkinson's disease, 1990-2016: a systematic analysis for the Global Burden of Disease Study 2016. *Lancet Neurol.* 17, 939–953. doi: 10.1016/S1474-4422(18)30295-3

Glavin, G. B., and Szabo, S. (1990). Dopamine in gastrointestinal disease. *Dig. Dis. Sci.* 35, 1153–1161. doi: 10.1007/BF01537589

Iannilli, E., Stephan, L., Hummel, T., Reichmann, H., and Haehner, A. (2017). Olfactory impairment in Parkinson's disease is a consequence of central nervous system decline. *J. Neurol.* 264, 1236–1246.

Klingelhoefer, L., and Reichmann, H. (2015). Pathogenesis of Parkinson disease–the gut-brain axis and environmental factors. *Nat. Rev. Neurol.* 11, 625–636. doi: 10.1038/nrneurol.2015.197

Koros, C., Simitsi, A., and Stefanis, L. (2017). Genetics of Parkinson's disease: genotype-phenotype correlations. *Int. Rev. Neurobiol.* 132, 197–231. doi: 10.1016/bs.irn.2017.01.009

Lee, Y. C., Lin, C. H., Wu, R. M., Lin, M. S., Lin, J. W., Chang, C. H., et al. (2013). Discontinuation of statin therapy associates with Parkinson disease: a population-based study. *Neurology* 81, 410–416. doi: 10.1212/WNL.0b013e31829d873c

London, A., Benhar, I., and Schwartz, M. (2013). The retina as a window to the brain-from eye research to CNS disorders. *Nat. Rev. Neurol.* 9, 44–53. doi: 10.1038/nrneurol.2012.227

Matt, S. M., and Gaskill, P. J. (2020). Where is dopamine and how do immune cells see it?: Dopamine-mediated immune cell function in health and disease. *J. Neuroimmune Pharmacol.* 15, 114–164.

Pardue, M. T., and Allen, R. S. (2018). Neuroprotective strategies for retinal disease. *Prog. Retin. Eye Res.* 65, 50–76. doi: 10.1016/j.preteyeres.2018.02.002

Pescosolido, N., Parisi, F., Russo, P., Buomprisco, G., and Nebbioso, M. (2013). Role of dopaminergic receptors in glaucomatous disease modulation. *Biomed Res. Int.* 2013:193048. doi: 10.1155/2013/193048

Phillipson, O. T., Kilpatrick, I. C., and Jones, M. W. (1987). Dopaminergic innervation of the primary visual cortex in the rat, and some correlations with human cortex. *Brain Res. Bull.* 18, 621–633. doi: 10.1016/0361-9230(87)90132-8

Poewe, W. (2008). Non-motor symptoms in Parkinson's disease. *Eur. J. Neurol.* 15(Suppl. 1), 14–20. doi: 10.1111/j.1468-1331.2008.02056.x

Rocha, E. M., De Miranda, B., and Sanders, L. H. (2018). Alpha-synuclein: pathology, mitochondrial dysfunction and neuroinflammation in Parkinson's disease. *Neurobiol. Dis.* 109, 249–257. doi: 10.1016/j.nbd.2017.04.004

Satue, M., Rodrigo, M. J., Obis, J., Vilades, E., Gracia, H., Otin, S., et al. (2017). Evaluation of progressive visual dysfunction and retinal degeneration in patients with Parkinson's disease. *Invest. Ophthalmol. Vis. Sci.* 58, 1151–1157.

Stone, R. A., Lin, T., Laties, A. M., and Iuvone, P. M. (1989). Retinal dopamine and form-deprivation myopia. *Proc. Natl. Acad. Sci. U.S.A.* 86, 704–706. doi: 10.1073/pnas.86.2.704

Veys, L., Vandenabeele, M., Ortuño-Lizarán, I., Baekelandt, V., Cuenca, N., Moons, L., et al. (2019). Retinal α-synuclein deposits in Parkinson's disease patients and animal models. *Acta Neuropathol.* 137, 379–395. doi: 10.1007/s00401-018-01956-z

Weil, R. S., Schrag, A. E., Warren, J. D., Crutch, S. J., Lees, A. J., and Morris, H. R. (2016). Visual dysfunction in Parkinson's disease. *Brain*139, 2827–2843. doi: 10.1093/brain/aww175

Weinreb, R. N., Aung, T., and Medeiros, F. A. (2014). The pathophysiology and treatment of glaucoma: a review. *JAMA* 311, 1901–1911. doi: 10.1001/jama.2014.3192

Witkovsky, P. (2004). Dopamine and retinal function. *Doc. Ophthalmol.* 108, 17–40. doi: 10.1023/b:doop.0000019487.88486.0a

Zhou, X., Pardue, M. T., Iuvone, P. M., and Qu, J. (2017). Dopamine signaling and myopia development: What are the key challenges. *Prog. Retin. Eye Res.* 61, 60–71. doi: 10.1016/j.preteyeres.2017.06.003

Conflict of Interest: The authors declare that the research was conducted in the absence of any commercial or financial relationships that could be construed as a potential conflict of interest.

frontiers in Neuroscience

ORIGINAL RESEARCH
published: 07 September 2021
doi: 10.3389/fnins.2021.726476

Characterizing the Retinal Phenotype of the Thy1-h[A30P]α-syn Mouse Model of Parkinson's Disease

*Lien Veys[1,2], Joyce Devroye[1,2], Evy Lefevere[1,2], Lien Cools[1,2], Marjan Vandenabeele[1,2] and Lies De Groef[1,2]**

[1] Research Group of Neural Circuit Development and Regeneration, Department of Biology, KU Leuven, Leuven, Belgium,
[2] Department of Biomedical Sciences, Leuven Brain Institute, Leuven, Belgium

Despite decades of research, disease-modifying treatments of Parkinson's disease (PD), the second most common neurodegenerative disease worldwide, remain out of reach. One of the reasons for this treatment gap is the incomplete understanding of how misfolded alpha-synuclein (α-syn) contributes to PD pathology. The retina, as an integral part of the central nervous system, recapitulates the PD disease processes that are typically seen in the brain, and retinal manifestations have emerged as prodromal symptoms of the disease. The timeline of PD manifestations in the visual system, however, is not fully elucidated and the underlying mechanisms are obscure. This highlights the need for new studies investigating retinal pathology, in order to propel its use as PD biomarker, and to develop validated research models to investigate PD pathogenesis. The present study pioneers in characterizing the retina of the Thy1-h[A30P]α-syn PD transgenic mouse model. We demonstrate widespread α-syn accumulation in the inner retina of these mice, of which a proportion is phosphorylated yet not aggregated. This α-syn expression coincides with inner retinal atrophy due to postsynaptic degeneration. We also reveal abnormal retinal electrophysiological responses. Absence of selective loss of melanopsin retinal ganglion cells or dopaminergic amacrine cells and inflammation indicates that the retinal manifestations in these transgenic mice diverge from their brain phenotype, and questions the specific cellular or molecular alterations that underlie retinal pathology in this PD mouse model. Nevertheless, the observed α-syn accumulation, synapse loss and functional deficits suggest that the Thy1-h[A30P]α-syn retina mimics some of the features of prodromal PD, and thus may provide a window to monitor and study the preclinical/prodromal stages of PD, PD-associated retinal disease processes, as well as aid in retinal biomarker discovery and validation.

Keywords: retina, visual system, alpha-synuclein, transgenic mouse model, Parkinson's disease

OPEN ACCESS

Edited by:
Yuyi You,
Macquarie University, Australia

Reviewed by:
Thierry Baron,
Laboratoire de Lyon, Agence Nationale de Sécurité Sanitaire de l'Alimentation, de l'Environnement et du Travail (ANSES), France
Jürgen Winkler,
University of Erlangen Nuremberg, Germany

***Correspondence:**
Lies De Groef
lies.degroef@kuleuven.be

Specialty section:
This article was submitted to Neurodegeneration, a section of the journal Frontiers in Neuroscience

Received: *16 June 2021*
Accepted: *19 August 2021*
Published: *07 September 2021*

Citation:
Veys L, Devroye J, Lefevere E, Cools L, Vandenabeele M and De Groef L (2021) Characterizing the Retinal Phenotype of the Thy1-h[A30P]α-syn Mouse Model of Parkinson's Disease. Front. Neurosci. 15:726476. doi: 10.3389/fnins.2021.726476

Abbreviations: α-syn, Alpha-synuclein; α-syn mice, Thy1-h[A30P]α-syn mice; AQP4, Aquaporin 4; ChAT, Choline acetyltransferase; CNS, Central nervous system; ERG, Electroretinography; DAPI, 4′,6-diamidino-2-phenylindole; GCL, Ganglion cell layer; GFAP, Glial fibrillary acidic protein; Iba-1, Ionized calcium-binding adapter molecule 1; INL, Inner nuclear layer; IPL, Inner plexiform layer; NFL, Nerve fiber layer; OP, Oscillatory potential; p-α-syn, Phosphorylated serine-129 α-syn; pSTR, Positive scotopic threshold response; RGC, Retinal ganglion cell; TH, Tyrosine hydroxylase; ThioS, Thioflavin S; WT, Wild type.

INTRODUCTION

Despite decades of research, disease-modifying treatments of Parkinson's disease (PD), the second most common neurodegenerative disease worldwide, remain out of reach (Guo et al., 2018; Veys et al., 2019). It has been suggested that one of the principal reasons for this treatment gap is the lack of accurate and timely diagnosis. Traditionally, diagnosis is based on the cardinal motor symptoms of PD (tremor, rigidity, bradykinesia, and postural instability), which only arise years after a long non-symptomatic phase during which a large proportion of the dopaminergic cells in the substantia nigra are lost (Jankovic, 2008). In order to preserve brain function, therapies -and hence diagnosis- should be focused on the preclinical (asymptomatic) and prodromal (early symptomatic) stages (Forsaa et al., 2010; Mahlknecht et al., 2015; Hustad and Aasly, 2020). In 2017, new diagnostic criteria for PD have been defined by the International Parkinson Disease and Movement Disorders Society (Postuma and Berg, 2017; Marsili et al., 2018), whereby the probability of an individual to develop PD is now calculated based on several predictors, such as age, environmental predictors, prodromal signs, genetic risk variables, and biomarker testing (Postuma et al., 2016). Constant updating of these diagnostic criteria is required as more insights into early stage PD emerge (Postuma and Berg, 2017).

The retina has become a target organ in the search for early biomarkers, relevant diagnostic criteria and techniques that are amenable to population-wide patient screening and disease monitoring. As an integral part of the central nervous system (CNS), the eye can be considered a window to the brain. The visual pathway has shown to be an excellent model system to gain insight into classical neurodegenerative diseases, as both retina and brain are often affected by these diseases and share disease processes (e.g., neurodegeneration, inflammation, aggregation of misfolded proteins, mitochondrial dysfunction; Armstrong, 2009; Martínez-Lapiscina et al., 2014; Rahimi et al., 2015; Veys et al., 2019; Kashani et al., 2021). Therefore, it is not surprising that in many PD patients, one or more visual symptoms are described, such as decreased visual acuity, spatial contrast sensitivity, and color vision (Price et al., 1992; Archibald et al., 2011; Armstrong, 2011; Bodis-Wollner, 2013; Guo et al., 2018). Retinal dysfunction at least partially contributes to these deficits (Bertrand et al., 2012; Mazzarella and Cole, 2016). This is corroborated by retinal imaging via optical coherence tomography (OCT) and with electroretinography (ERG) measurements, which revealed, respectively, retinal nerve fiber layer (NFL), ganglion cell layer (GCL), inner plexiform layer (IPL), and inner nuclear layer (INL) thinning (Shrier et al., 2012; Adam et al., 2013; London et al., 2013; Spund et al., 2013; Lee et al., 2014; Bodis-Wollner et al., 2014b; Boeke et al., 2016; Aydin et al., 2018; Matlach et al., 2018); and abnormalities of the photopic b-wave, scotopic oscillatory potentials (OPs), and P50 component of the pattern ERG in PD patients (Nightingale et al., 1986; Gottlob et al., 1987; Burguera et al., 1990; Ikeda et al., 1994; Peppe et al., 1992, 1995, 1998; Langheinrich et al., 2000; Sartucci et al., 2006; Garcia-Martin et al., 2014; Nowacka et al., 2015; Kashani et al., 2021). Histopathological studies have revealed pathological manifestations that may underlie these changes in *in vivo* measures, including a reduction in dopamine levels in the retina (Nguyen-Legros, 1988; Harnois and Di Paolo, 1990; Chorostecki et al., 2015), reduced density and complexity of dopaminergic neurons (Ortuño-Lizarán et al., 2020) and melanopsin-positive retinal ganglion cells (RGCs; Ortuno-Lizaran et al., 2018b), and, finally, the presence of alpha-synuclein (α-syn) and phosphorylated (S129) α-syn (p-α-syn) inclusions in the retina (Beach et al., 2014; Ho et al., 2014; Bodis-Wollner et al., 2014a; Ortuno-Lizaran et al., 2018a; Veys et al., 2019). Importantly, p-α-syn deposits in the retina accumulate in parallel with the brain, already during the prodromal stage of PD, and are associated with PD severity (Ortuno-Lizaran et al., 2018a). This reinforces that retinal biomarkers have a high potential for PD diagnosis and disease monitoring.

Further research into the (temporal) relationship between retinal biomarker alterations and neurodegenerative changes in the brain is needed, however, for retinal biomarkers to be adopted in the clinic. Longitudinal and prospective studies in PD patients and patients at risk of developing PD will be essential to assess the value of retinal biomarkers for PD (Kashani et al., 2021). Animal models of PD, on the other hand, can support these studies, by providing a framework in which the correlation between retinal biomarkers and disease manifestations can be explored and novel insights into the molecular and cellular changes underlying the retinal manifestations of PD can be obtained (Santano et al., 2011; Normando et al., 2016; Price et al., 2016; Mammadova et al., 2018, 2021; Veys et al., 2019). Altogether, the wide availability of technologies for non-invasive high-resolution ocular imaging, such as OCT, is a clear advantage over current brain imaging techniques (De Groef and Cordeiro, 2018) and, collectively, visual function measures, ERG, and retinal imaging could offer a multimodal biomarker approach for PD diagnosis, stratification, and monitoring (Guo et al., 2018; Turcano et al., 2018; Veys et al., 2019).

In this study, we aim to fill the need for well-characterized preclinical models to study retinal alternations in PD. We characterized the retinal phenotype of the Thy1-h[A30P]α-syn mouse model, by studying α-syn accumulation, neurodegeneration, inflammation, synaptic integrity, and retinal function. The brain phenotype of this mouse model has been studied before, yet the retinal phenotype remains untouched (Kahle et al., 2000; Neumann et al., 2002; Freichel et al., 2007; Ekmark-Lewen et al., 2018). Here, we used *in vivo* retinal imaging and electrophysiology measurements with high clinical translatability, combined with *post mortem* histological studies, to map the timeline of retinal disease manifestations in these mice.

MATERIALS AND METHODS

Animals

Thy1-h[A30P]α-syn mice (C57BL/6 background, RRID:MGI:2652214) and corresponding wild type (WT) controls, were bred under standard laboratory conditions (Kahle et al., 2000). Both female and male mice were used at 4, 8, 12, 15, and 18 months of age. All experiments were

performed according to the European directive 2010/63/EU and in compliance with protocols approved by the KU Leuven institutional ethical committee.

(Immuno)histochemistry

Prior to eye dissection, mice were euthanized by an intraperitoneal injection of 60 mg/kg sodium pentobarbital (Dolethal, Vetoquinol) followed by transcardial perfusion with saline and 4% paraformaldehyde (PFA). Next, eyes were either fixed in 1% PFA for 4 h at 4°C and embedded in paraffin, or in 4% PFA for 1 h at RT for wholemount preparations. The latter were post-fixed for 1 h in 4% PFA for another hour.

Seven-micrometer sagittal paraffin sections were deparaffinized and stained with hematoxylin (Sigma) and eosin (Sigma) and mounted with Distyrene Plasticizer Xylene mounting medium (Sigma). For Thioflavin S histological staining, sections were stained for 5 min with Thioflavin S (Sigma, 1/200 in 1:1 distilled water and ethanol) and mounted with mowiol (Sigma). For immunohistochemistry, sections were incubated overnight with one or two of the following primary antibodies: human specific α-syn (1/5000; Millipore, clone Syn211 [36-008] RRID:AB_310817), α-syn (1/1000; produced and kindly provided by V. Baekelandt, KU Leuven, for double staining with p-α-syn), p-α-syn (1/5000; Elan Pharmaceuticals), p62 (1/200; Proteintech [#55274-1-AP], RRID:AB_11182278), Brn3a (1/750; Santa Cruz Biotechnology, c-20 [#sc-31984], RRID:AB_2167511), tyrosine hydroxylase (TH; 1/1000; Millipore [#AB152], RRID:AB_390204), choline acetyltransferase (ChAT; 1/100; Millipore [#AB144P], RRID:AB_2079751), VGLUT1 (1/1000, Synaptic Systems [#135 302], RRID:AB_887877), Prox1 (1/500; Biolegend [PCB-238C]), Homer1 (1/500; Synaptic Systems [#160 003], RRID:AB_887730), glial fibrillary acidic protein (GFAP; 1/1000; Dako [#Z0334], RRID:AB_10013382), or aquaporin 4 (AQP4; 1/10000; Alomone labs [AQP-004], RRID:AB_2039734). For α-syn, Brn3a, TH, ChAT, Prox1, and Homer1, antigen retrieval with heated citrate buffer (20 min, 95°C) was used, while no antigen retrieval treatment was used for VGLUT1 and proteinase K (5 min, 20 μg/ml, Qiagen) antigen retrieval was used for GFAP stainings. Fluorescent labeling was performed using an Alexa-488 labeled secondary antibody (Invitrogen) for Brn3a, TH, ChAT, Prox1, VGLUT1, and GFAP staining, or with a fluorescein or cyanine 3 tyramid signal amplification kit (PerkinElmer) for p-α-syn, α-syn, and Homer1 stainings. Finally, slides were counterstained with 4′,6-diamidino-2-phenylindole and mounted with mowiol.

For wholemount immunohistochemistry, tissue permeabilization was achieved by a freeze-thaw step (15 min, −80°C), followed by overnight incubation with one of the following primary antibodies: p-α-syn (1/5000; Elan Pharmaceuticals), TH (1/1000; Millipore [#AB152], RRID:AB_390204), melanopsin (1/5000; Advanced Targeting Systems [#AB-N38], RRID:AB_1608077), or ionized calcium-binding adapter molecule 1 (Iba-1; 1/1000; Wako [#019-19741], RRID:AB_839504). Subsequently, fluorescent labeling was performed using an Alexa-488 labeled secondary antibody (Invitrogen) and wholemounts were mounted with mowiol.

Image Analysis

Imaging was performed using a FV1000 confocal or FV1000-M multiphoton microscope (Olympus) or a conventional epifluorescence microscope (DM6, Leica).

Image analyses were performed with Fiji software (Schindelin et al., 2012). For retinal wholemounts, the entire perimeter of the wholemount was outlined and its area measured prior to analysis. For sections, five sections per mouse were investigated, including the central section containing the optic nerve head, and the sections located 210 and 420 μm anterior/posterior. On each section, analysis was done over a distance of 300 μm at four locations per section. For α-syn, TH and GFAP, the immunopositive area was measured in the inner retina (from the retinal NFL until the INL included), while for AQP4 both the outer retina (from OPL to ONL) and inner retina were measured and for VGLUT1 and Homer1, only the IPL was included (Van Hove et al., 2020). For cell counting, both on wholemounts and sections, Fiji "Cell Counter" plugin was used. Microglia density and morphology were quantified as described in Davis et al. (2017) on projection images of z-stack (step size 1.5 μm) pictures of Iba-1 stained wholemounts (Davis et al., 2017).

Optical Coherence Tomography

Optical coherence tomography imaging was performed as described before (Sergeys et al., 2019; Vandenabeele et al., 2021). Briefly, after pupil dilatation with tropicamide (0.5%, Tropicol, Théa), the retina of anesthetized animals was imaged (1000 A-scans, 100 B-scans, 1.4 × 1.4 mm, Bioptigen Envisu R2200). Retinal layer thickness was measured using InVivoVue Diver (v 3.0.8, Bioptigen) software, at 16 locations in the central retina spaced around the optic nerve head, and averaged per mouse.

Electroretinography

Electroretinography was performed as described before (Sergeys et al., 2019; Vandenabeele et al., 2021). Full-field flash dark-adapted electroretinograms were measured at increasing flash intensities of 0.003, 0.01, 0.1, 1, 2.5, and 7.5 cd^*s/m^2. Electroretinograms were analyzed using Espion software (v6.59.9, Diagnosys), as shown in **Supplementary Figure 1**. To analyze the OPs on the rising part of the b-wave, a band pass filter (75–300 Hz) was used. The positive scotopic threshold response (pSTR) was measured at 1×10^{-4} cd^*s/m^2. 1 week after baseline ERG or pSTR measurement, mice were intraperitoneally injected with benserazide hydrochloride (12.5 g/kg, Sigma) and L-DOPA (25 g/kg, Sigma) 50′ and 30′ prior to ERG/pSTR measurement, respectively.

Statistical Analysis

Statistical analyses were performed using GraphPad Prism (v8.4.3, GraphPad, RRID:SCR_002798). The number of animals (n) used is depicted on the figures and the statistical analyses are indicated in the figure legends. Data are presented as mean ± SEM. Differences were considered statistically significant for two-sided p-values < 0.05 ($^*p < 0.05$; $^{**}p < 0.01$; $^{***}p < 0.001$; and $^{****}p < 0.0001$).

RESULTS

Retinal Accumulation of (Phosphorylated) α-syn in Thy1-h[A30P]α-syn Mice

α-syn expression, phosphorylation, and aggregation was studied in the retina of WT and Thy1-h[A30P]α-syn mice (α-syn mice) of various ages, using (immuno)stainings for transgenic human α-syn, phosphorylated (serine-129) α-syn (p-α-syn; detecting both human and rodent α-syn), thioflavin S (ThioS) and p62. Conform with previously published data of Veys et al. (2019), hα-syn expression was observed in neuronal cell bodies in the GCL, in neurites in the retinal NFL and IPL and in dispersed cell bodies in the INL of 4-, 8-, 12-, 15-, and 18-month-old Thy1-h[A30P]α-syn mice (**Figures 1A–F,T**; Veys et al., 2019). The hα-syn positive cell types in the inner retina comprise RGCs, as shown by double staining with Brn3a (**Figure 1U**), and amacrine cells, based on their morphology and location (**Figures 1V–X**). Furthermore, the accumulation of hα-syn in dopaminergic, (nor)adrenergic, cholinergic, or AII amacrine cells was ruled out based on the lack of colocalization with TH, ChAT, and Prox1 positive cells, respectively (**Figures 1V–X**; Müller et al., 2017). Quantitative analysis of the hα-syn fluorescent area did not reveal any progressive changes in hα-syn expression in the inner retina of α-syn mice with aging (**Figure 1M**). Next, a fraction of α-syn was phosphorylated, most prominently in cell bodies and neurites in the GCL (**Figures 1G–L,S,T**), and this did not change with age (**Figure 1N**), not even in end-stage diseased animals with severe signs of hind limb paralysis (data not shown). At 18 months of age, only 34 ± 8% of strongly α-syn positive cells in the GCL also contained p-α-syn. Finally, we assessed p62 and ThioS labeling to investigate α-syn ubiquitination and aggregation, respectively. At 18 months of age, no p62 accumulation nor relocalization were observed in the retina of α-syn mice as compared to WT mice (**Figures 1Q,R**), and no ThioS positive aggregates were found in the retina of transgenic nor WT animals (**Figures 1O,P**). Of note, although no accumulation of ThioS-positive or p62-positive cellular inclusions was detted in the Thy1-h[A30P]α-syn PD mouse model, we cannot exclude that oligomeric, prefibrillar, or non-fibril α-syn conformers contribute to the retinal phenotype observed in these mice (Lashuel et al., 2013; Roberts and Brown, 2015; Cascella et al., 2021). This needs to be explored in follow-up studies.

Altogether, these data show that, while both α-syn overexpression and phosphorylation are present in the retina of Thy1-h[A30P]α-syn mice already at a young age, α-syn aggregation and ubiquitination do not manifest.

Synaptic Degeneration in the Retina of Old Thy1-h[A30P]α-syn Mice

Spectral domain OCT was applied in a longitudinal *in vivo* experiment to measure the thickness of the retinal layers in α-syn mice and WT controls, early in their life (4 and 8 months) and at 12, 15, and 18 months of age (**Figures 2A,B,D–F**). At 4 months of age, a minor yet significant thickening of the photoreceptor layer (PL) was found in the α-syn mice ($p = 0.0023$; **Figure 2A**). This difference in retinal thickness persisted at 12, 15, and 18 months ($p = 0.0009$, $p = 0.0130$, and $p = 0.0122$; **Figures 2C–G**). Furthermore, at 12 months, α-syn mice also displayed thinning of the IPL, which persisted at 15 and 18 months ($p = 0.0034$ at 12 months, $p = 0.0336$ at 15 months, $p = 0.0444$ at 18 months; **Figures 2C–G**).

As retinal thinning is typically a sign of neurodegeneration, we next performed a more in-depth analysis of different subpopulations of inner retinal neurons at 15 months of age to clarify the origin of the observed IPL thinning. Given that the IPL consists of neurites emerging from cell bodies in both the GCL and INL, cell density was assessed in these layers on hematoxylin and eosin-stained sections. No overt neurodegeneration was seen in α-syn mice (**Figure 2H**). Additionally, a detailed analysis of disease-relevant neuronal subtypes, also at 15 months of age, revealed that cell numbers of intrinsically photosensitive RGCs (melanopsin positive) in the GCL and of dopaminergic (TH positive) amacrine cells in the INL (**Figures 2I–N**) were not affected. However, IPL thinning may also occur due to dendrite or synapse loss, a pathological process that is known to precede loss of neuronal cell bodies. In line with the preservation of dopaminergic cell bodies (cfr. above), we found that the dopaminergic plexus of the retina, measured as the TH-immunopositive area in the inner retina, was unaltered in α-syn mice of 15 months of age (**Figures 2O–Q**). However, taking a closer look at the synaptic integrity of the IPL, via immunostainings with the established pre- and postsynaptic markers VGLUT1 and Homer1, we revealed loss of postsynaptic contacts yet preservation of the presynaptic terminals in 15-month-old transgenic mice (**Figures 2R–W**). Altogether, these findings suggest that synaptic degeneration in the retina underlies the observed IPL thinning.

Electrophysiological Changes in the Retina of Thy1-h[A30P]α-syn Mice With Aging

In a next series of experiments, we sought to further identify the neuronal cell types that are affected in the α-syn mouse and to establish whether neuronal dysfunction can be detected already at younger ages compared to the OCT thinning that only become apparent at 12 months. Indeed, neuronal death is often preceded by functional changes, and these prodromal manifestations of the disease are of particular interest for biomarker development (Nowacka et al., 2015; Barber et al., 2017; Turcano et al., 2018; Hustad and Aasly, 2020). First, OPs as a read-out for amacrine cell function, were assessed. Already at 4 months, the area under the curve was larger in α-syn mice as compared to WT animals for high intensity light stimuli (2.5 cd^*s/m^2: $p = 0.0137$; 7.5 cd^*s/m^2: $p = 0.0094$), and this effect persisted in older transgenic animals of 8 (1 cd^*s/m^2: $p = 0.0191$; 2.5 cd^*s/m^2: $p = 0.0452$; 7.5 cd^*s/m^2: $p = 0.0050$), 12 (1 cd^*s/m^2: $p = 0.0034$; 2.5 cd^*s/m^2: $p = 0.0039$; 7.5 cd^*s/m^2: $p = 0.0023$), and 18 months of age (1 cd^*s/m^2: $p = 0.0001$; **Figures 3A,B** and **Supplementary Figure 1F**). Second, we measured RGC function via the pSTR. Not yet at 4 months, but at 8, 12, and 18 months, the pSTR latency time was shorter in α-syn mice as compared to WT controls

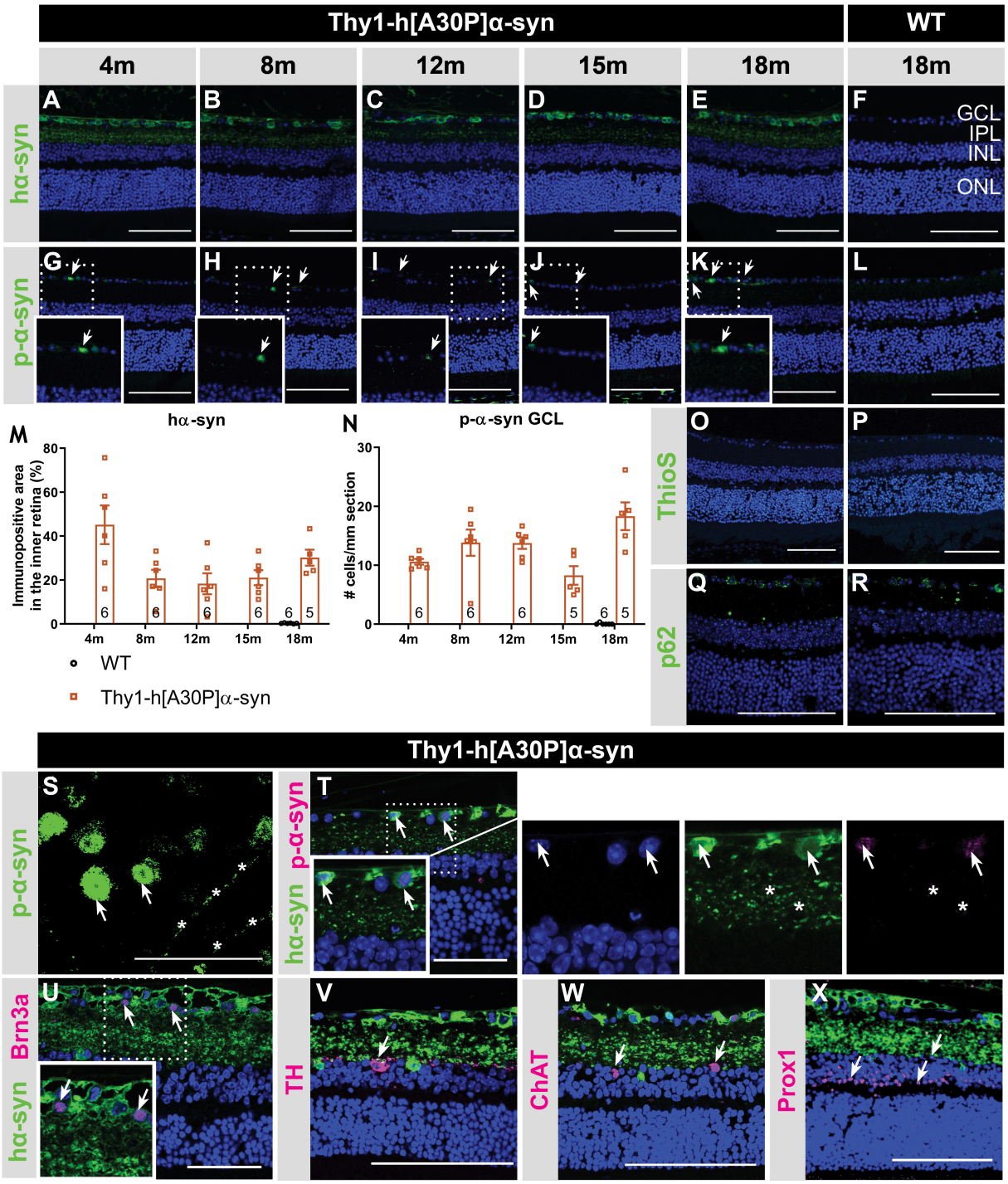

FIGURE 1 | Inner retinal hα-syn expression is accompanied by α-syn phosphorylation, yet no ThioS positive aggregation or p62 accumulation, in the retina of Thy1-h[A30P]α-syn mice. Representative images of hα-syn immunostainings **(A–E)**; p-α-syn immunostainings **(G–K)**; and ThioS staining **(O)** on retinal sections of α-syn mice at 4, 8, 12, 15 and 18 months of age. **(F,L,P)** No staining was observed in the WT controls, at any age (only 18 months shown here). **(M,N)** Quantitative analysis of the hα-syn fluorescent area and counting of the p-α-syn positive cells did not reveal an increase of hα-syn expression in the inner retina or p-α-syn cell density in α-syn mice with age. **(O,P)** No ThioS positive inclusions were found in the retina of transgenic nor wild type animals in any of the age groups. **(Q,R)** No difference in retinal p62 accumulation or localization was detected between transgenic and wild type animals at 18 months of age. **(S)** p-α-syn immunostaining on a retinal wholemount of an α-syn mouse showed p-α-syn localization in cell bodies (arrows) and neurites (asterisks). **(T)** Double staining of hα-syn with p-α-syn revealed clear colocalization. **(U–X)** Double staining of hα-syn with Brn3a, TH, ChAT and Prox1 revealed expression of Brn3a in hα-syn positive cells, yet no colocalization in dopaminergic and cholinergic cells. Scale bar: 100 μm **(A–R, V–X)** or 50 μm **(S–U)**; GCL, ganglion cell layer; INL, inner nuclear layer; IPL, inner plexiform layer; and ONL, outer nuclear layer.

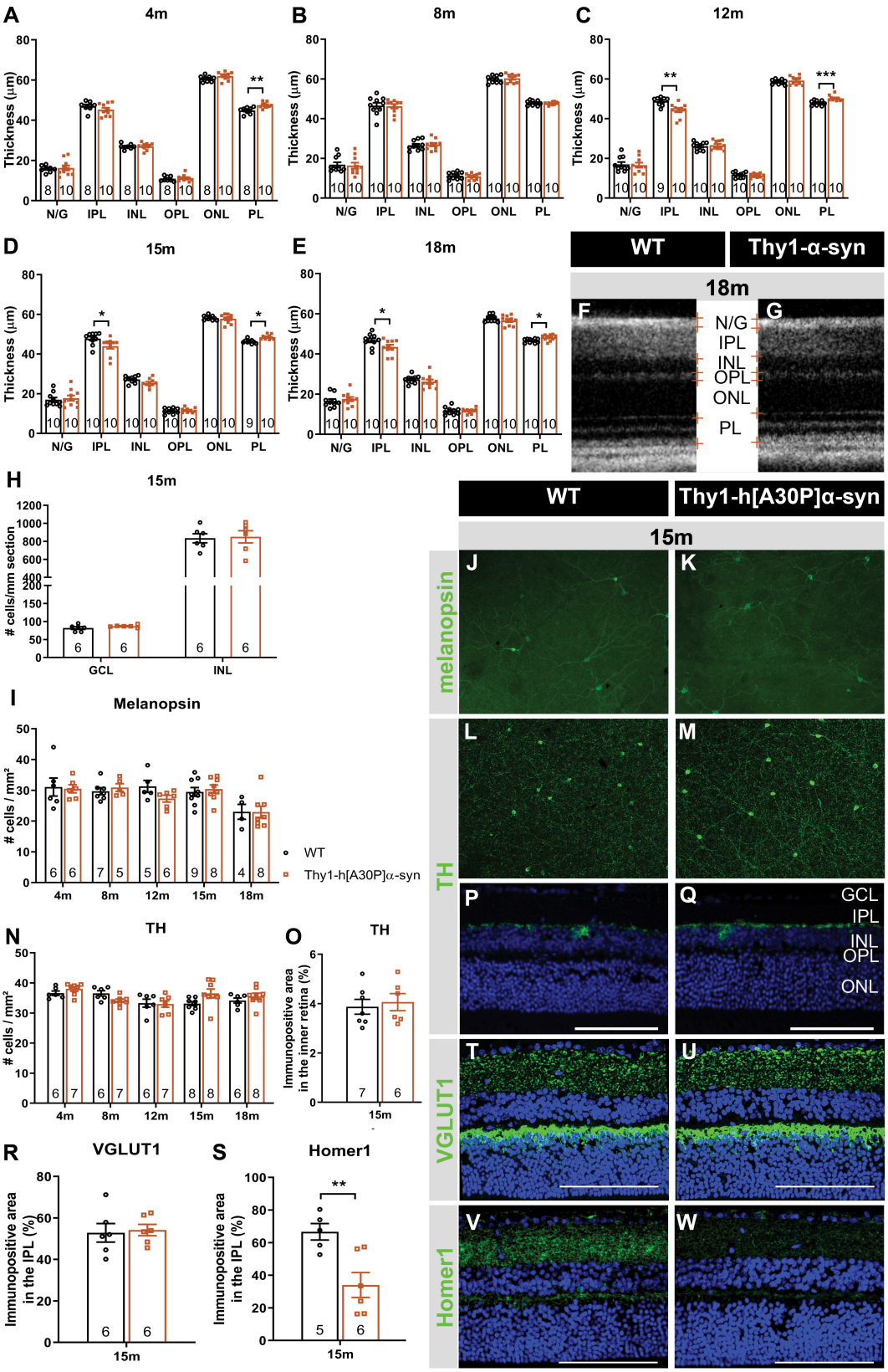

FIGURE 2 | Continued

FIGURE 2 | Outer retinal thickening and inner retinal thinning, associated with loss of postsynaptic labeling, in Thy1-h[A30P]α-syn mice. **(A–E)** Longitudinal OCT measurements in 4- **(A)**, 8- **(B)**, 12- **(C)**, 15- **(D)**, and 18-month-old **(E–G)** mice, revealed significant differences in retinal layer thickness between α-syn and WT mice of 4 months (PL thickening), 15 months (PL thickening and IPL thinning), and 12 and 18 months of age (PL thickening and IPL thinning). **(H)** Cell counts on hematoxylin and eosin-stained sections in the GCL and in the INL did not reveal significant differences between transgenic animals and WT controls at 15 months of age. **(I–W)** Representative images of retinal wholemounts stained for melanopsin **(J,K)** and TH **(L,M)**, and of retinal sections stained for TH **(P,Q)**, VGLUT1 **(T,U)**, and Homer-1 **(V,W)**, of 15-month-old α-syn and WT mice. Counting the number of melanopsin- **(I)** and TH- **(N)** positive cells on retinal wholemounts revealed no significant differences between transgenic and WT animals. No significant differences were uncovered in TH plexus **(O)** and VGLUT1 **(R)** immunopositive area, yet a strong decrease of the Homer1 **(S)** signal was seen. Scale bar: 100 μm; Two-Way ANOVA with Tukey multiple comparisons *post hoc* test **(I–N)**. Unpaired *t*-test (per retinal layer; **A–F,O,R,S**): $^{*}p < 0.05$; $^{**}p < 0.01$; and $^{***}p < 0.001$. N/G, retinal nerve fiber layer + GCL; GCL, ganglion cell layer; INL, inner nuclear layer; IPL, inner plexiform layer; ONL, outer nuclear layer; OPL, outer plexiform layer; and PL, photoreceptor layer.

($p = 0.0082$ at 8 months, $p = 0.0119$ at 12 months, and $p = 0.0006$ at 18 months; **Figures 3D–F** and **Supplementary Figure 1G**). *a*- and *b*-wave measurements were unaltered, indicating normal functioning of the photoreceptors, bipolar cells, and Müller glia (**Supplementary Figures 1B–E**).

In PD patients, visual defects have been attributed to malfunctioning of the dopaminergic retinal neurons -which constitute a subtype of amacrine cells-, which is supported by the fact that ERG abnormalities can be alleviated by L-DOPA treatment (Ikeda et al., 1994; Djamgoz et al., 1997; Peppe et al., 1998; Turcano et al., 2018). Hence, we assessed the effect of systemic L-DOPA treatment 30 min prior to the ERG measurement in a second, independent study. We found that L-DOPA did not fully reverse the effects of genotype on the OPs in 8-month-old mice, nor the pSTR latency in 18-month-old mice (**Figures 3C,F**). These findings are in line with the absence of dopaminergic degeneration as observed in the immunohistological studies (*cfr*. above). Overall, ERG changes in the α-syn mice suggest that amacrine cells and RGCs become dysfunctional with age, yet TH immunostainings showed that it is unlikely that a selective loss of dopaminergic neurons underlies this phenotype.

No Signs of Neuroinflammation in the Retina of Thy1-h[A30P]α-syn Mice

Previous studies demonstrated that α-syn triggers neuroinflammation, and that, in turn, inflammation increases α-syn phosphorylation and pathology in synucleinopathies (Lee et al., 2010; Tansey and Goldberg, 2010; Ramirez et al., 2017; Ferreira and Romero-Ramos, 2018). Furthermore, retinal inflammation has been linked to both swelling of the outer retina and ERG deviations, and may therefore underlie -at least in part- the OCT and ERG abnormalities that we observed in the Thy1-h[A30P]α-syn mice (Mirza and Jampol, 2013; Petzold, 2016; Pisa et al., 2021; Xia et al., 2021). Hence, we next investigated macroglia and microglia reactivity and water homeostasis in the retina. First, Müller glia and astrocytes were investigated. Analysis of GFAP immunostainings on retinal cross-sections of α-syn versus WT mice did not reveal differences in immunofluorescent area at 4, 8, 12, 15, and 18 months of age and radial fiber density at 15 months of age between the two genotypes, although an expected aging effect was present (**Figures 4A–D**). Second, the cause of outer retinal swelling was further investigated by measuring the expression of AQP4 (**Figures 4G,H**). AQP4 is a water channel expressed by the Müller glia, of which differences in expression levels and cellular localization have been linked to retinal edema and neuroinflammation (Amann et al., 2016). In AD patients, it was found to be overexpressed in the brain and associated with blood-brain barrier disruption (Foglio and Luigi Fabrizio, 2010; Fukuda and Badaut, 2012). However, no genotypic difference in immunofluorescent area nor localization in the inner versus outer retinal layers was revealed in mice of 15 months old (**Figures 4E,F**). Third, microgliosis was investigated on retinal wholemounts stained for Iba-1 (**Figures 4J,K,M,N**). Cell density did not differ in transgenic versus WT mice at any of the selected ages (**Figure 4I**). Furthermore, we investigated cell morphology, to probe for changes in soma roundness as a sign of microglia reactivity (Davis et al., 2017). However, no difference in cell body roundness of Iba-1^{+} cells was observed between the two genotypes (**Figure 4L**). In conclusion, this data suggests that retinal inflammation nor edema underlie the OCT and ERG abnormalities that we observed in the α-syn mice.

DISCUSSION

In recent years, neurodegenerative disease research is increasingly focusing on the pre- and early symptomatic stages of disease, when the cascade of neurodegenerative events has only just started and a sufficiently large pool of neurons still remains that can be rescued with disease-modifying treatments to preserve brain function. To identify and take opportunity of this early time window for treatment, however, novel biomarkers and inexpensive, minimally invasive, and widely available screening and diagnostic tests are needed. These may be found in the retina. As an integral part of the CNS, the retina recapitulates many of the PD-related neurodegenerative process in the brain. Indeed, a multitude of OCT and ERG studies has shown that neuronal dysfunction and degeneration affects the retina of PD patients (Garcia-Martin et al., 2014; Boeke et al., 2016; Aydin et al., 2018; Veys et al., 2019). Furthermore, accumulating evidence of retinal dopamine deficits and α-syn misfolding suggest that this is the result of the same disease processes that also drive neurodegeneration in the brain (Guo et al., 2018; Ortuno-Lizaran et al., 2018a; Veys et al., 2019; Ortuño-Lizarán et al., 2020). It remains to be explored, however, what the correlation between the PD manifestations in the brain and retina is, and whether the mechanisms behind these manifestations are the same. A deeper understanding of this will be essential for the rational use of retinal biomarkers for

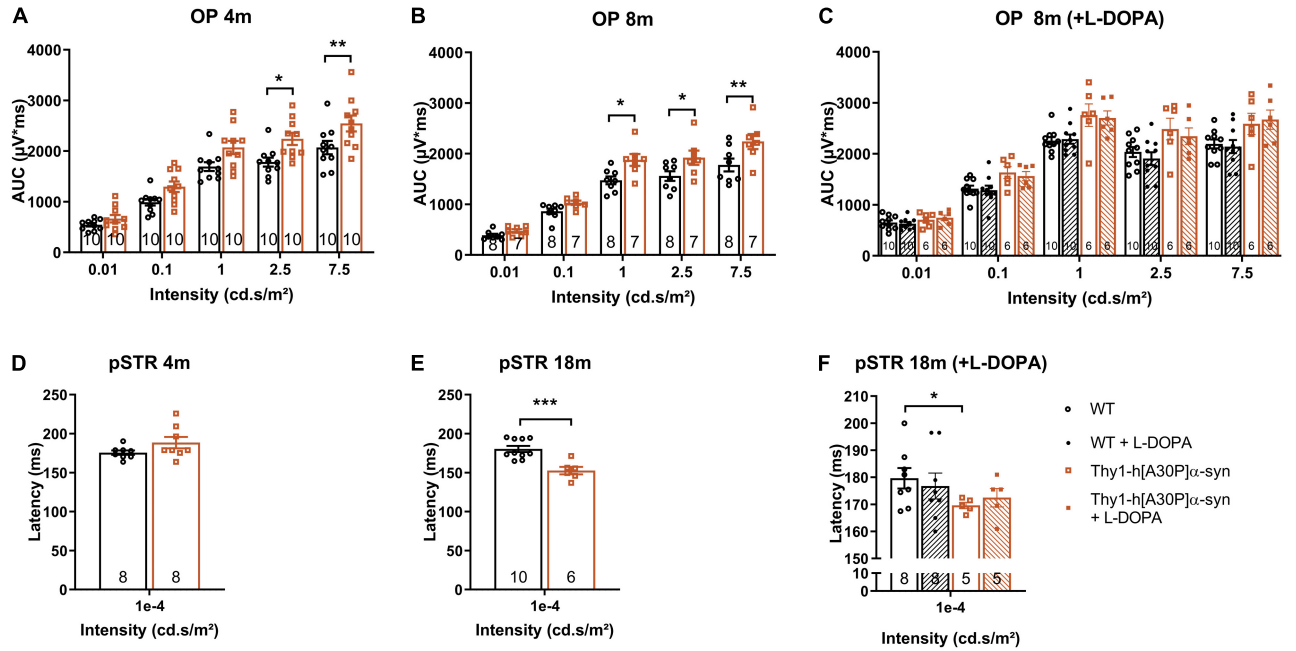

FIGURE 3 | Electrophysiological changes in the retina of older Thy1-h[A30P]α-syn mice cannot be alleviated by L-DOPA treatment. ERG was used to measure the electrophysiological responses of different retinal cell types. **(A,B)** Quantification of the OPs, measured as the area under the curve (AUC), revealed larger OPs in 4- and 8-month-old α-syn mice as compared to WT controls for light stimuli with high intensity. **(D,E)** Quantification of pSTR response did not reveal any differences at 4 months of age, yet a shorter pSTR latency time was observed in 18-month-old transgenic mice as compared to WTs. **(C,F)** L-DOPA treatment did not have an overt rescue effect on observed OP **(C)** and pSTR **(F)** differences in α-syn mice. Repeated measures Two-Way ANOVA **(A–C)** with Bonferroni's multiple comparisons *post hoc* test or unpaired *t*-test **(D–F)**: $*p < 0.05$; $**p < 0.01$; and $***p < 0.001$. Full ERG data is shown in **Supplementary Figure 1**.

PD diagnosis, monitoring and/or stratification, and will also aid research into novel retinal biomarkers. Animal research will remain an essential complement to the extensive clinical studies that are obviously needed, offering flexibility in study subjects and read-outs to dig into the cellular and molecular changes that characterize the PD retina and dictate the retinal biomarker results. Up till now, multiple studies have investigated the brain phenotype of PD animal models, yet retinal manifestations have received little attention (Santano et al., 2011; Normando et al., 2016; Price et al., 2016; Veys et al., 2019). Mammadova et al. investigated the retinal phenotype of the TgM83 mouse model. This transgenic mouse is characterized by α-syn accumulation mainly in the outer retina and p-α-syn pathology in both outer and inner retina, and thereby only partially mimics the inner retina pathology seen in PD patients (Mammadova et al., 2018, 2021). In addition, and in contrast to the Thy1-h[A30P]α-syn model, neuroinflammation, and photoreceptor cell loss were seen in the TgM83 model, again partially reflecting human disease – where also microglia reactivity was seen (Tansey and Goldberg, 2010; Ferreira and Romero-Ramos, 2018; Mammadova et al., 2018). Both in the Thy1-h[A30P]α-syn and TgM83 mice, and in contrast to reports on the human PD retina (Archibald et al., 2009; Mammadova et al., 2018; Ortuño-Lizarán et al., 2020), TH immunoreactivity was unaltered (**Table 1**). The lack of dopaminergic degeneration, even in end-stage animals (data not shown), highlights the limitations of the available transgenic mouse models in recapitulating the full complexity of human disease. Of note, this is in line with findings in the brain, where a lack of progressive neurodegeneration has been reported for several rodent PD models (Lim and Ng, 2009; Dawson et al., 2010; Kin et al., 2019). Furthermore, the diverging retinal manifestations observed in these two mouse models might result from the use of distinct promoters (Thy1 versus Prp) and/or different mutated forms of α-syn (A30P versus A53T), which might influence the aggregation process (Flagmeier et al., 2016). By examining the retina of the Thy1-h[A30P]α-syn PD mouse model, we aim to establish a research model with a retinal α-syn expression pattern that more closely resembles α-synucleinopathy in PD patients. We believe that such as model is valuable to investigate the retina-brain connection in PD and thereby propel retinal biomarker discovery and validation research and fundamental studies of the role of α-syn in health and disease.

We revealed that, from a young age onward, α-syn overexpression can be observed in the inner retina of α-syn mice, alongside a fraction of phosphorylated α-syn in RGC neurites and somata; an observation that complies with previously described (p)-α-syn localization in the retina of PD patients (**Table 1**; Ortuno-Lizaran et al., 2018a; Veys et al., 2019). Despite the lack of ThioS positive protein aggregates and accumulation of the Lewy body marker p62, α-syn overexpression did result in thinning of the inner retina in α-syn mice from the age of 12 months, similar to the inner retinal remodeling seen in PD patients (**Table 1**; Shrier et al., 2012; Adam et al., 2013;

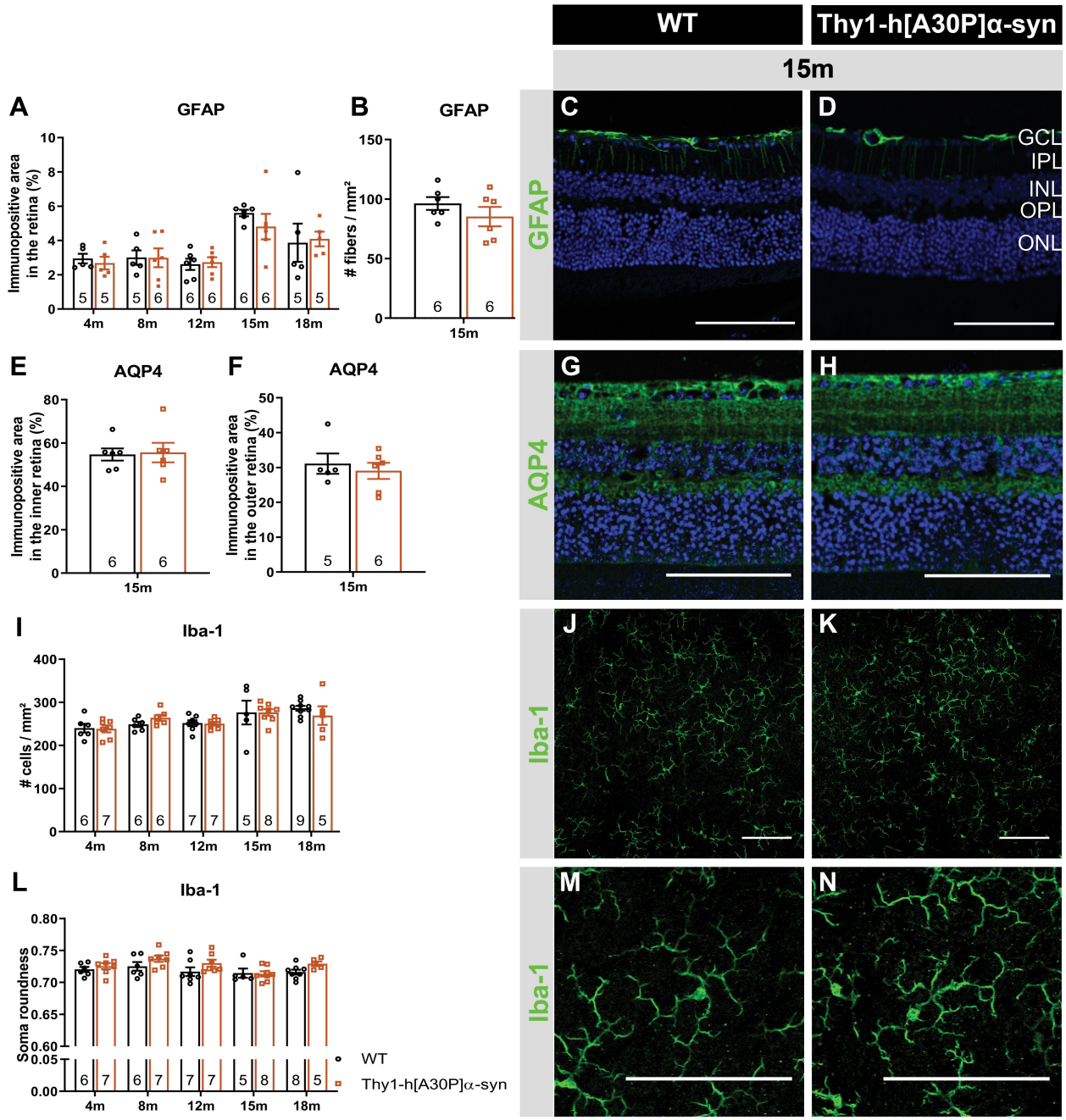

FIGURE 4 | Macroglia and microglia reactivity and water homeostasis appear normal in Thy1-h[A30P]α-syn mice. Representative images of retinal cross-sections stained for GFAP **(C,D)** and wholemounts stained for Iba-1 **(J,K,M,N)** and cross-sections stained for AQP4 **(G,H)** in 15-month-old α-syn and WT mice. **(A,B)** When measuring the GFAP immunopositive area and the number of radial fibers in the inner retina, no differences in macroglia reactivity were uncovered between transgenic and WT animals in any of the age groups. **(I,L)** No differences in Iba-1^{+} cell density and cell soma roundness, indicative of microgliosis, were observed. **(E,F)** AQP4 immunopositive area or localization in the inner versus outer retina of α-syn mice versus age-matched WT animals was similar. Two-Way ANOVA with Sidak's multiple comparisons *post hoc* test **(A,I,L)** or unpaired *t*-test **(B,E,F)**. Scale bar: 100 μm.

Spund et al., 2013; Lee et al., 2014; Bodis-Wollner et al., 2014b). Our data revealed that neurodegeneration of dopaminergic amacrine cells or melanopsin positive RGCs cannot account for this IPL thinning uncovered with OCT imaging. Instead, synapse loss may underlie this retinal atrophy. Indeed, significant changes in the density of Homer1+ postsynaptic -yet not VGLUT1+ presynaptic- terminals in the IPL underscore the OCT alterations. Postsynaptic terminals in the IPL come from RGCs and amacrine cells, neurons for which we also observed hα-syn overexpression and abnormal ERG responses (Connaughton,

TABLE 1 | Summary of the phenotypical alterations observed in the retina of PD patients, Thy1-h[A30P]α -syn mice.

PD patients	References	Thy1-h[A30P]α -syn mice	TgM83 mice
α-syn in GCL, IPL, and INL	Beach et al., 2014; Ho et al., 2014; Bodis-Wollner et al., 2014a	α-syn in GCL, IPL, and INL	α-syn in ONL and INL
p-α-syn positive cell bodies and neurites in GCL	Beach et al., 2014; Ortuno-Lizaran et al., 2018a	p-α-syn positive cell bodies and neurites in GCL	p-α-syn labeling in outer and inner retina p-Tau (Thr231) in OPL and GCL
Thinning of NFL, GCL, IPL, and INL (OCT)	Shrier et al., 2012; Adam et al., 2013; Spund et al., 2013; Lee et al., 2014; Bodis-Wollner et al., 2014b; Matlach et al., 2018	Thinning of IPL (OCT) Thickening of PL (OCT)	Thinning of ONL (histology)
Decreased TH levels and TH-positive cell density in INL Decreased TH + plexus complexity	Nguyen-Legros, 1988; Harnois and Di Paolo, 1990; Chorostecki et al., 2015; Ortuño-Lizarán et al., 2020	Preserved TH-positive cell density in INL Preserved TH + plexus size in IPL	Preserved TH levels in INL
Decreased melanopsin-positive cell density in GCL and dendritic tree complexity	Ortuno-Lizaran et al., 2018b	Preserved melanopsin-positive cell density in GCL	
Increased microglial reactivity (Iba-1)	Doorn et al., 2014; Ferreira and Romero-Ramos, 2018	No microglial reactivity (Iba-1)	Increased microglial reactivity (CD11b, CD68)
No macroglial reactivity (GFAP)	Mirza et al., 1999	No macroglial reactivity (GFAP)	Macroglial reactivity (GFAP)
RGC, bipolar and amacrine cell dysfunction (ERG): – diminished responses of the photopic b-wave, scotopic oscillatory potentials and P50 component of the pattern ERG reversed by L-DOPA – reversed by L-DOPA	Nightingale et al., 1986; Gottlob et al., 1987; Burguera et al., 1990; Ikeda et al., 1994; Peppe et al., 1992, 1995, 1998; Langheinrich et al., 2000; Sartucci et al., 2006; Garcia-Martin et al., 2014; Nowacka et al., 2015; Kashani et al., 2021	RGC and amacrine cell dysfunction (ERG): – supernormal responses of the scotopic oscillatory potentials and pSTR (starting at 4 and 8 months, respectively) – no overt response to L-DOPA	

Retinal manifestations on the TgM83 mouse model were described in Mammadova et al. (2018). OCT, optical coherence tomography; NFL, nerve fiber layer; GCL, ganglion cell layer; IPL, inner plexiform layer; INL, inner nuclear layer; ONL, outer nuclear layer; OPL, outer plexiform layer; PL, photoreceptor layer; ERG, electroretinography; OPs, oscillatory potentials; pSTR, positive scotopic threshold response; and TH: tyrosine hydroxylase.

1995). Furthermore, synapse loss has been shown to occur early in the neurodegenerative process, for example in the retina of glaucoma models and patients, or in the brain of AD or PD models and patients (Selkoe, 2002; Della Santina et al., 2013; Purro et al., 2014; Bellucci et al., 2016; Subramanian and Tremblay, 2021). More specifically, a decrease in synaptic volume in of pre- and post-synapses has been reported in the striatum of PD patients (Bellucci et al., 2016; Reeve et al., 2018; Gcwensa et al., 2021). Of note, an age-related decrease of postsynaptic retinal proteins was also observed in the plexiform layers of *Octodon degus,* the only rodent with naturally occurring AD (Chang et al., 2020).

The retinal atrophy and synapse loss observed in α-syn mice is accompanied by functional alterations, which were uncovered using ERG. These were striking for several reasons. First, amacrine cell responses were supernormal in α-syn mice. Although abnormal OPs are also typically seen in PD patients, these ERG alterations tend to decrease rather than increase in human patients (**Table 1**; Gottlob et al., 1987; Burguera et al., 1990; Ikeda et al., 1994; Nowacka et al., 2015). Remarkably, these supernormal ERG responses in α-syn mice coincide with a thickening of the PL, which might be caused by local edema or swelling of the photoreceptors (Devos et al., 2005; Archibald et al., 2009). Interestingly, this outer retinal swelling was also seen in the early disease stages of a rotenone-induced PD rat model, where it was suggested to be linked to increased mitochondrial biogenesis in the highly energy demanding photoreceptor cells (Normando et al., 2016). Outer retinal thickening has also been observed to co-occur with supernormal ERG measurements in the retina of the 3×Tg-AD Alzheimer's (Chiquita et al., 2019a). Furthermore, both supernormal scotopic ERG measurements and PL layer thickening have been related to a mild inflammatory phenotype in the early stages of retinal pathology linked to multiple sclerosis (Mirza and Jampol, 2013; Petzold, 2016). Yet, with the measurements used in this study, no abnormalities in AQP4 water channels and no inflammatory response of the macro- and microglia was detected. Second, an equally striking observation in this study is the increased conduction velocity of RGC electrophysiological responses in older animals, reminiscent of the RGC hyperactivity in early AD disease stages of 5×FAD mice (Araya et al., 2021). In AD models, amyloid-beta overproduction can lead to neuronal network hyperexcitability (Kazim et al., 2021). As AD and PD are both neurodegenerative proteinopathies and amyloid-beta and α-syn biology show many parallels, one could hypothesize that similar neuronal network hyperexcitability events might occur in PD too (Goedert, 2015). This hypothesis is supported by our data on synaptic integrity, which show preservation of presynaptic integrity yet loss of postsynaptic density. The postsynaptic density Homer1 proteins link metabotropic glutamate receptors to intracellular effectors, mediating the glutamate inducible effects in postsynaptic RGCs and amacrine cells (Connaughton, 1995). Dysregulation of extracellular glutamate concentrations at the synapse can lead to excess release of glutamate, which

is known to induce hyperexcitability in postsynaptic neurons (Gasparini and Griffiths, 2013). An alternative explanation for the supernormal ERG responses by RGCs might relate to the physiological role of α-syn at the synapse, where it is suggested to associate with synaptic vessels and to influence neurotransmitter release (Sulzer and Edwards, 2019). Since α-syn overexpression inhibits synaptic vesicle exocytosis, one could hypothesize that decreased exocytosis might disturb the tightly maintained balance that is involved in synaptic regulation (Sulzer and Edwards, 2019). Finally, the electrophysiological alterations observed in this study were, in contrast to ERG changes in PD patients, not reversed by L-DOPA treatment (**Table 1**; Archibald et al., 2009). Along with the observed lack of dopaminergic cell loss in the retina and the absence of hα-syn in dopaminergic amacrine cells in the α-syn mice, this suggests a dopamine-independent mechanism underlying the ERG alterations. Which neuronal subtype(s) account for the observed electrophysiological abnormalities should be elucidated in future research via more advanced electrophysiology studies, e.g., using patch clamping or microelectrode arrays (Obien et al., 2015; Chiquita et al., 2019b).

Besides generating insights into the (patho)physiological role of α-syn and the disease processes that lead to the retinal PD phenotype, we postulate that the α-syn mouse may also aid the

TABLE 2 | Overview of the reported phenotypical alterations in the brain and spinal cord of Thy1-h[A30P]α-syn mice, in relation to observations in the retina.

Observations in the brain and spinal cord	Time point of first observation	References	Own observations in the retina	Time point of first observation
Functional read-outs				
Decreased fine motor performance (beam transversal test)	2 months, worsens with age	Ekmark-Lewen et al., 2018		
Lower general activity and more risk-taking (multivariate concentric square field test)	8 months	Ekmark-Lewen et al., 2018		
Impaired spatial learning and memory (Morris water maze)	12 months	Freichel et al., 2007		
Impaired fear conditioning (freezing behavior after foot shock)	12 months	Freichel et al., 2007		
Higher locomotor activity	12 months	Freichel et al., 2007		
Impaired motor behavior (rotarod test)	17 months	Freichel et al., 2007		
(Hind limb) paralysis	18 months	Freichel et al., 2007		
Premature death	18 months	Freichel et al., 2007		
Decreased frequency of spontaneous excitatory postsynaptic currents (electrophysiology)	1 month	Chesselet et al., 2012	OP alterations (ERG)	4 months
			pSTR latency alterations (ERG)	18 months
Histopathology				
α-syn overexpression in neuronal cell bodies and neurites in the brain and spinal cord	6 month	Kahle et al., 2000	α-syn overexpression in neuronal cell bodies and neurites in the inner retina	4 months
p-α-syn positive neurons in spinal cord and brainstem	1 months	Freichel et al., 2007	p-α-syn positive neurons in GCL	4 months
Oligomeric α-syn in brainstem, midbrain and hippocampus	8 months	Ekmark-Lewen et al., 2018		
PK-resistant α-syn in brain	9 months	Neumann et al., 2002; Freichel et al., 2007		
Ubiquitin-positive inclusions in pontine reticular nuclei and ventral horn of the spinal cord	12 months	Neumann et al., 2002		
ThioS reactive species in brainstem	16 months	Schell et al., 2009	No ThioS reactivity detected	
Decreased TH immunoreactivity in central midbrain regions	8 months	Ekmark-Lewen et al., 2018	No changes in TH immunoreactivity	
Increased GFAP immunoreactivity in brainstem	8 months	Neumann et al., 2002; Ekmark-Lewen et al., 2018	No changes in GFAP immunoreactivity	
Limited inflammatory response (increase in $Mac2^+$ immune cells)	8 months	Ekmark-Lewen et al., 2018	No changes in Iba-1 immunoreactivity	
No reports of neurodegeneration			PL thickening (OCT)	4 months
			IPL thinning (OCT)	15 months

OCT, optical coherence tomography; PL, photoreceptor layer; IPL, inner plexiform layer; INL, inner nuclear layer; ERG, electroretinography; OPs, oscillatory potentials; pSTR, positive scotopic threshold response; TH, tyrosine hydroxylase; PK, proteinase K; and ThioS, thioflavin S.

understanding of the retina-brain connection. Indeed, the α-syn mouse is characterized by hα-syn overexpression in neuronal cell bodies and neurites in the brain and spinal cord (**Table 2**; Kahle et al., 2000; Freichel et al., 2007) and p-α-syn and oligomeric α-syn were detected in brainstem, midbrain, and hippocampus of 8-month-old transgenic mice. In addition, older mice also develop proteinase K-resistant α-syn deposits, ubiquitin-positive neuritic and cell body inclusions, and ThioS reactive α-syn species in various CNS regions (**Table 2**; Neumann et al., 2002; Schell et al., 2009). This synucleinopathy in the brain is accompanied by astrogliosis and dopaminergic neurodegeneration (Ekmark-Lewen et al., 2018), and led to a variety of behavioral changes in fine motor performance, learning, and memory, finally leading to paralysis and premature death around the age of 18 months (**Table 2**; Freichel et al., 2007; Ekmark-Lewen et al., 2018). We conclude that the rather subtle retinal phenotype stands in marked contrast to findings in the brain of these mice, exposing the organotypic heterogeneity of the retina compared to other brain structures. Notably, this heterogeneity may be exploited as a strength in future research, and aid the understanding of disease mechanisms and selective vulnerability in different locations in the CNS.

Irrespective of the differences in the retina versus brain phenotype of the α-syn mice, this study highlights the potential of the retina for *in vivo* imaging and electrophysiology measurements with non-invasive techniques, such as OCT and ERG. Especially OCT, which detected retinal thinning in the inner retina in our transgenic mice similar to what has been described in the human PD retina, has the potential to become a low-cost, non-invasive tool for diagnosis and follow-up of PD disease progression (Shrier et al., 2012; Adam et al., 2013; Spund et al., 2013; Lee et al., 2014; Bodis-Wollner et al., 2014b). Importantly, these techniques have the advantage of being suitable for both patient and preclinical research, thereby providing relevant endpoint measures and enhancing the translatability of this research to the clinic.

In conclusion, this study uncovered morphological and electrophysiological abnormalities in the α-syn mouse retina. While this mouse model does not display dopaminergic neurodegeneration or neuroinflammation, its retina is characterized by a decreased density of postsynaptic terminals that may reflect neurotransmitter dysregulation and as such is linked to the observed ERG changes and IPL thinning. These pathological changes resemble the loss of synapses and neuronal dysfunction that are typically observed during the earliest stages of neurodegenerative diseases and are in line with a multitude of OCT and ERG studies in PD patients and animal models. The methodologies and the α-syn mouse model used in this study thus constitute a toolbox for research of the early, preclinical/prodromal stages of PD, and may aid fundamental research of PD-associated retinal disease processes, such as α-syn mediated synaptic dysfunction, as well as retinal biomarker discovery and validation.

DATA AVAILABILITY STATEMENT

The raw data supporting the conclusions of this article will be made available by the authors, without undue reservation.

ETHICS STATEMENT

The animal study was reviewed and approved by KU Leuven institutional ethical committee.

AUTHOR CONTRIBUTIONS

LV and LD contributed to the conception of the study, elaborated on the study design, and wrote the manuscript. LV, JD, EL, LC, and MV performed the experimental work. LC edited the manuscript. All authors have read and approved the manuscript.

FUNDING

LV, MV, and LD are supported by the Research Foundation Flanders (fellowships 1S51718N, 1190320N, and 12I3817N). The funders had no role in study design, data collection and analysis, decision to publish, or preparation of the manuscript.

ACKNOWLEDGMENTS

We acknowledge support from Research Foundation Flanders (fellowships to LV, MV, and LD). We like to express our sincere thanks to Philipp J. Kahle for donating the Thy1-h[A30P]α-syn mice, and to Isabelle Etienne and Tine Van Bergen (Oxurion NV, Leuven, Belgium) for assistance with tissue processing.

SUPPLEMENTARY MATERIAL

The Supplementary Material for this article can be found online at: https://www.frontiersin.org/articles/10.3389/fnins.2021.726476/full#supplementary-material

REFERENCES

Adam, C. R., Shrier, E., Ding, Y., Glazman, S., and Bodis-Wollner, I. (2013). Correlation of inner retinal thickness evaluated by spectral-domain optical coherence tomography and contrast sensitivity in Parkinson disease. *J. Neuro Ophthalmol.* 33, 137–142. doi: 10.1097/WNO.0b013e31828c4e1a

Amann, B., Kleinwort, K. J. H., Hirmer, S., Sekundo, W., Kremmer, E., Hauck, S. M., et al. (2016). Expression and distribution pattern of aquaporin 4, 5 and 11 in retinas of 15 different species. *Int. J. Mol. Sci.* 17:1145. doi: 10.3390/ijms17071145

Araya, J., Bello, F., Shivashankar, G., Neira, D., Durán-Aniotz, C., Acosta, M. L., et al. (2021). Retinal ganglion cells functional changes in a mouse model of Alzheimer's disease are linked with neurotransmitter alterations. *J. Alzheimers Dis.* 82, S5–S18. doi: 10.3233/jad-201195

Archibald, N. K., Clarke, M. P., Mosimann, U. P., and Burn, D. J. (2009). The retina in Parkinson's disease. *Brain* 132, 1128–1145. doi: 10.1093/brain/awp068

Archibald, N. K., Clarke, M. P., Mosimann, U. P., and Burn, D. J. (2011). Visual symptoms in Parkinson's disease and Parkinson's disease dementia. *Mov. Disord.* 26, 2387–2395. doi: 10.1002/mds.23891

Armstrong, R. A. (2009). Alzheimer's disease and the eye. *J. Optom.* 2, 103–111. doi: 10.3921/joptom.2009.103

Armstrong, R. A. (2011). Visual symptoms in Parkinson's disease. *Parkinson Dis.* 2011:908306. doi: 10.4061/2011/908306

Aydin, T. S., Umit, D., Nur, O. M., Fatih, U., Asena, K., Nefise, O. Y., et al. (2018). Optical coherence tomography findings in Parkinson's disease. *Kaohsiung J. Med. Sci.* 34, 166–171. doi: 10.1016/j.kjms.2017.11.006

Barber, T. R., Klein, J. C., Mackay, C. E., and Hu, M. T. M. (2017). Neuroimaging in pre-motor Parkinson's disease. *NeuroImage Clin.* 15, 215–227. doi: 10.1016/j.nicl.2017.04.011

Beach, T. G., Carew, J., Serrano, G., Adler, C. H., Shill, H. A., Sue, L. I., et al. (2014). Phosphorylated alpha-synuclein-immunoreactive retinal neuronal elements in Parkinson's disease subjects. *Neurosci. Lett.* 571, 34–38. doi: 10.1016/j.neulet.2014.04.027

Bellucci, A., Mercuri, N. B., Venneri, A., Faustini, G., Longhena, F., Pizzi, M., et al. (2016). Parkinson's disease: from synaptic loss to connectome dysfunction. *Neuropathol. Appl. Neurobiol.* 42, 77–94. doi: 10.1111/nan.12297

Bertrand, J. A., Bedetti, C., Postuma, R. B., Monchi, O., Genier Marchand, D., Jubault, T., et al. (2012). Color discrimination deficits in Parkinson's disease are related to cognitive impairment and white-matter alterations. *Mov. Disord.* 27, 1781–1788. doi: 10.1002/mds.25272

Bodis-Wollner, I. (2013). Foveal vision is impaired in Parkinson's disease. *Parkinsonism Relat. Disord.* 19, 1–14. doi: 10.1016/j.parkreldis.2012.07.012

Bodis-Wollner, I., Kozlowski, P. B., Glazman, S., and Miri, S. (2014a). alpha-synuclein in the inner retina in Parkinson disease. *Ann. Neurol.* 75, 964–966. doi: 10.1002/ana.24182

Bodis-Wollner, I., Miri, S., and Glazman, S. (2014b). Venturing into the no-man's land of the retina in Parkinson's disease. *Mov. Disord.* 29, 15–22. doi: 10.1002/mds.25741

Boeke, A., Rosen, D., Mastrianni, J., Xie, T., and Bernard, J. (2016). Optical coherence tomography as potential biomarker in Parkinson's disease and Alzheimer's disease (P5.177). *Neurology* 86(16 Suppl.):P5.177.

Burguera, J. A., Vilela, C., Traba, A., Ameave, Y., and Vallet, M. (1990). [The electroretinogram and visual evoked potentials in patients with Parkinson's disease]. *Arch. Neurobiol.* 53, 1–7.

Cascella, R., Chen, S. W., Bigi, A., Camino, J. D., Xu, C. K., Dobson, C. M., et al. (2021). The release of toxic oligomers from α-synuclein fibrils induces dysfunction in neuronal cells. *Nat. Commun.* 12:1814. doi: 10.1038/s41467-021-21937-3

Chang, L. Y. L., Ardiles, A. O., Tapia-Rojas, C., Araya, J., Inestrosa, N. C., Palacios, A. G., et al. (2020). Evidence of synaptic and neurochemical remodeling in the retina of aging degus. *Front. Neurosci.* 14:161. doi: 10.3389/fnins.2020.00161

Chesselet, M. F., Richter, F., Zhu, C., Magen, I., Watson, M. B., and Subramaniam, S. R. (2012). A progressive mouse model of Parkinson's disease: the Thy1-aSyn ("Line 61") mice. *Neurotherapeutics* 9, 297–314. doi: 10.1007/s13311-012-0104-2

Chiquita, S., Campos, E. J., Castelhano, J., Ribeiro, M., Sereno, J., Moreira, P. I., et al. (2019a). Retinal thinning of inner sub-layers is associated with cortical atrophy in a mouse model of Alzheimer's disease: a longitudinal multimodal in vivo study. *Alzheimers Res. Ther.* 11:90. doi: 10.1186/s13195-019-0542-8

Chiquita, S., Rodrigues-Neves, A. C., Baptista, F. I., Carecho, R., Moreira, P. I., Castelo-Branco, M., et al. (2019b). The retina as a window or mirror of the brain changes detected in Alzheimer's disease: critical aspects to unravel. *Mol. Neurobiol.* 56, 5416–5435. doi: 10.1007/s12035-018-1461-6

Chorostecki, J., Seraji-Bozorgzad, N., Shah, A., Bao, F., Bao, G., George, E., et al. (2015). Characterization of retinal architecture in Parkinson's disease. *J. Neurol. Sci.* 355, 44–48. doi: 10.1016/j.jns.2015.05.007

Connaughton, V. (1995). *Glutamate and Glutamate Receptors in the Vertebrate Retina*. Salt Lake City, UT: University of Utah Health Sciences Center.

Davis, B. M., Salinas-Navarro, M., Cordeiro, M. F., Moons, L., and De Groef, L. (2017). Characterizing microglia activation: a spatial statistics approach to maximize information extraction. *Sci. Rep.* 7:1576. doi: 10.1038/s41598-017-01747-8

Dawson, T. M., Ko, H. S., and Dawson, V. L. (2010). Genetic animal models of Parkinson's disease. *Neuron* 66:646. doi: 10.1016/J.NEURON.2010.04.034

De Groef, L., and Cordeiro, M. F. (2018). Is the eye an extension of the brain in central nervous system disease? *J. Ocul. Pharmacol. Ther.* 34, 129–133. doi: 10.1089/jop.2016.0180

Della Santina, L., Inman, D. M., Lupien, C. B., Horner, P. J., and Wong, R. O. L. (2013). Differential progression of structural and functional alterations in distinct retinal ganglion cell types in a mouse model of glaucoma. *J. Neurosci.* 33, 17444–17457. doi: 10.1523/JNEUROSCI.5461-12.2013

Devos, D., Tir, M., Maurage, C. A., Waucquier, N., Defebvre, L., Defoort-Dhellemmes, S., et al. (2005). ERG and anatomical abnormalities suggesting retinopathy in dementia with Lewy bodies. *Neurology* 65, 1107–1110. doi: 10.1212/01.wnl.0000178896.44905.33

Djamgoz, M. B., Hankins, M. W., Hirano, J., and Archer, S. N. (1997). Neurobiology of retinal dopamine in relation to degenerative states of the tissue. *Vision Res.* 37, 3509–3529. doi: 10.1016/s0042-6989(97)00129-6

Doorn, K. J., Moors, T., Drukarch, B., van de Berg, W. D. J., Lucassen, P. J., and van Dam, A. M. (2014). Microglial phenotypes and toll-like receptor 2 in the substantia nigra and hippocampus of incidental Lewy body disease cases and Parkinson's disease patients. *Acta Neuropathol. Commun.* 2, 1–17. doi: 10.1186/s40478-014-0090-1

Ekmark-Lewen, S., Lindstrom, V., Gumucio, A., Ihse, E., Behere, A., Kahle, P. J., et al. (2018). Early fine motor impairment and behavioral dysfunction in (Thy-1)-h[A30P] alpha-synuclein mice. *Brain Behav.* 8:e00915. doi: 10.1002/brb3.915

Ferreira, S. A., and Romero-Ramos, M. (2018). Microglia response during Parkinson's disease: alpha-synuclein intervention. *Front. Cell. Neurosci.* 12:247. doi: 10.3389/fncel.2018.00247

Flagmeier, P., Meisl, G., Vendruscolo, M., Knowles, T. P. J., Dobson, C. M., Buell, A. K., et al. (2016). Mutations associated with familial Parkinson's disease alter the initiation and amplification steps of α-synuclein aggregation. *Proc. Natl. Acad. Sci. U.S.A.* 113, 10328–10333. doi: 10.1073/PNAS.1604645113

Foglio, E., and Luigi Fabrizio, R. (2010). Aquaporins and neurodegenerative diseases. *Curr. Neuropharmacol.* 8, 112–121. doi: 10.2174/157015910791233150

Forsaa, E. B., Larsen, J. P., Wentzel-Larsen, T., and Alves, G. (2010). What predicts mortality in Parkinson disease? A prospective population-based long-term study. *Neurology* 75, 1270–1276. doi: 10.1212/WNL.0b013e3181f61311

Freichel, C., Neumann, M., Ballard, T., Muller, V., Woolley, M., Ozmen, L., et al. (2007). Age-dependent cognitive decline and amygdala pathology in alpha-synuclein transgenic mice. *Neurobiol. Aging* 28, 1421–1435. doi: 10.1016/j.neurobiolaging.2006.06.013

Fukuda, A. M., and Badaut, J. (2012). Aquaporin 4: a player in cerebral edema and neuroinflammation. *J. Neuroinflammation* 9:279. doi: 10.1186/1742-2094-9-279

Garcia-Martin, E., Rodriguez-Mena, D., Satue, M., Almarcegui, C., Dolz, I., Alarcia, R., et al. (2014). Electrophysiology and optical coherence tomography to evaluate Parkinson disease severity. *Investig. Ophthalmol. Vis. Sci.* 55, 696–705. doi: 10.1167/iovs.13-13062

Gasparini, C. F., and Griffiths, L. R. (2013). The biology of the glutamatergic system and potential role in migraine. *Int. J. Biomed. Sci.* 9, 1–8.

Gcwensa, N. Z., Russell, D. L., Cowell, R. M., and Volpicelli-Daley, L. A. (2021). Molecular mechanisms underlying synaptic and axon degeneration in Parkinson's disease. *Front. Cell. Neurosci.* 15:44. doi: 10.3389/fncel.2021.626128

Goedert, M. (2015). NEURODEGENERATION. Alzheimer's and Parkinson's diseases: the prion concept in relation to assembled Abeta, tau, and alpha-synuclein. *Science* 349:1255555. doi: 10.1126/science.1255555

Gottlob, I., Schneider, E., Heider, W., and Skrandies, W. (1987). Alteration of visual evoked potentials and electroretinograms in Parkinson's disease. *Electroencephalogr. Clin. Neurophysiol.* 66, 349–357. doi: 10.1016/0013-4694(87)90032-0

Guo, L., Normando, E. M., Shah, P. A., De Groef, L., and Cordeiro, M. F. (2018). Oculo-visual abnormalities in Parkinson's disease: possible value as biomarkers. *Mov. Disord.* 33, 1390–1406. doi: 10.1002/mds.27454

Harnois, C., and Di Paolo, T. (1990). Decreased dopamine in the retinas of patients with Parkinson's disease. *Investig. Ophthalmol. Vis. Sci.* 31, 2473–2475.

Ho, C. Y., Troncoso, J. C., Knox, D., Stark, W., and Eberhart, C. G. (2014). Beta-amyloid, phospho-tau and alpha-synuclein deposits similar to those in the brain are not identified in the eyes of Alzheimer's and Parkinson's disease patients. *Brain Pathol.* 24, 25–32. doi: 10.1111/bpa.12070

Hustad, E., and Aasly, J. O. (2020). Clinical and imaging markers of prodromal Parkinson's disease. *Front. Neurol.* 11:395. doi: 10.3389/fneur.2020.00395

Ikeda, H., Head, G. M., and Ellis, C. J. (1994). Electrophysiological signs of retinal dopamine deficiency in recently diagnosed Parkinson's disease and a follow up study. *Vision Res.* 34, 2629–2638. doi: 10.1016/0042-6989(94)90248-8

Jankovic, J. (2008). Parkinson's disease: clinical features and diagnosis. *J. Neurol. Neurosurg. Psychiatry* 79, 368–376. doi: 10.1136/jnnp.2007.131045

Kahle, P. J., Neumann, M., Ozmen, L., Muller, V., Jacobsen, H., Schindzielorz, A., et al. (2000). Subcellular localization of wild-type and Parkinson's disease-associated mutant alpha -synuclein in human and transgenic mouse brain. *J. Neurosci.* 20, 6365–6373. doi: 10.1523/jneurosci.20-17-06365.2000

Kashani, A. H., Asanad, S., Chan, J. W., Singer, M. B., Zhang, J., Sharifi, M., et al. (2021). Past, present and future role of retinal imaging in neurodegenerative disease. *Prog. Retin. Eye Res.* 83:100938. doi: 10.1016/j.preteyeres.2020.100938

Kazim, S. F., Seo, J. H., Bianchi, R., Larson, C. S., Sharma, A., Wong, R. K. S., et al. (2021). Neuronal network excitability in Alzheimer's disease: the puzzle of similar versus divergent roles of amyloid β and tau. *Eneuro* 8:ENEURO.0418-20.2020. doi: 10.1523/ENEURO.0418-20.2020

Kin, K., Yasuhara, T., Kameda, M., and Date, I. (2019). Animal models for Parkinson's disease research: Trends in the 2000s. *Int. J. Mol. Sci.* 20 doi: 10.3390/ijms20215402

Langheinrich, T., Tebartz Van Elst, L., Lagrèze, W. A., Bach, M., Lücking, C. H., and Greenlee, M. W. (2000). Visual contrast response functions in Parkinson's disease: evidence from electroretinograms, visually evoked potentials and psychophysics. *Clin. Neurophysiol.* 111, 66–74. doi: 10.1016/S1388-2457(99)00223-0

Lashuel, H. A., Overk, C. R., Oueslati, A., and Masliah, E. (2013). The many faces of alpha-synuclein: from structure and toxicity to therapeutic target. *Nat. Rev. Neurosci.* 14, 38–48. doi: 10.1038/nrn3406

Lee, H. J., Suk, J. E., Patrick, C., Bae, E. J., Cho, J. H., Rho, S., et al. (2010). Direct transfer of α-synuclein from neuron to astroglia causes inflammatory responses in synucleinopathies. *J. Biol. Chem.* 285, 9262–9272. doi: 10.1074/jbc.M109.081125

Lee, J. Y., Kim, J. M., Ahn, J., Kim, H. J., Jeon, B. S., and Kim, T. W. (2014). Retinal nerve fiber layer thickness and visual hallucinations in Parkinson's disease. *Mov. Disord.* 29, 61–67. doi: 10.1002/mds.25543

Lim, K. L., and Ng, C. H. (2009). Genetic models of Parkinson disease. *Biochim. Biophys. Acta Mol. Basis Dis.* 1792, 604–615. doi: 10.1016/J.BBADIS.2008.10.005

London, A., Benhar, I., and Schwartz, M. (2013). The retina as a window to the brain-from eye research to CNS disorders. *Nat. Rev. Neurol.* 9, 44–53. doi: 10.1038/nrneurol.2012.227

Mahlknecht, P., Seppi, K., and Poewe, W. (2015). The concept of prodromal Parkinson's disease. *J. Parkinsons. Dis.* 5, 681–697. doi: 10.3233/JPD-150685

Mammadova, N., Baron, T., Verchère, J., Greenlee, J. J., and Greenlee, M. H. W. (2021). "Retina as a model to study in vivo transmission of α-synuclein in the A53T mouse model of Parkinson's disease," in *Mouse Genetics. Methods in Molecular Biology*, Vol. 2224, eds S. R. Singh, R. M. Hoffman, and A. Singh (New York, NY: Humana), 75–85. doi: 10.1007/978-1-0716-1008-4_5

Mammadova, N., Summers, C. M., Kokemuller, R. D., He, Q., Ding, S., Baron, T., et al. (2018). Accelerated accumulation of retinal alpha-synuclein (pSer129) and tau, neuroinflammation, and autophagic dysregulation in a seeded mouse model of Parkinson's disease. *Neurobiol. Dis.* 121, 1–16. doi: 10.1016/j.nbd.2018.09.013

Marsili, L., Rizzo, G., and Colosimo, C. (2018). Diagnostic criteria for Parkinson's disease: from James Parkinson to the concept of prodromal disease. *Front. Neurol.* 9:156. doi: 10.3389/fneur.2018.00156

Martínez-Lapiscina, E. H., Sanchez-Dalmau, B., Fraga-Pumar, E., Ortiz-Perez, S., Tercero-Uribe, A. I., Torres-Torres, R., et al. (2014). The visual pathway as a model to understand brain damage in multiple sclerosis. *Mult. Scler.* 20, 1678–1685. doi: 10.1177/1352458514542862

Matlach, J., Wagner, M., Malzahn, U., Schmidtmann, I., Steigerwald, F., Musacchio, T., et al. (2018). Retinal changes in Parkinson's disease and glaucoma. *Parkinsonism Relat. Disord.* 56, 41–46. doi: 10.1016/j.parkreldis.2018.06.016

Mazzarella, J., and Cole, J. (2016). All eyes on neurodegenerative diseases. *Rev. Optom.* 153, 42–52.

Mirza, B., Hadberg, H., Thomsen, P., and Moos, T. (1999). The absence of reactive astrocytosis is indicative of a unique inflammatory process in Parkinson's disease. *Neuroscience* 95, 425–432. doi: 10.1016/S0306-4522(99)00455-8

Mirza, R. G., and Jampol, L. M. (2013). *White Spot Syndromes and Related Diseases*. *Retin.* 5th Edn, 1337–1380. doi: 10.1016/B978-1-4557-0737-9.00076-X

Müller, L. P. D. S., Azar, S. S., de los Santos, J., and Brecha, N. C. (2017). Prox1 is a marker for AII amacrine cells in the mouse retina. *Front. Neuroanat.* 11:39. doi: 10.3389/FNANA.2017.00039

Neumann, M., Kahle, P. J., Giasson, B. I., Ozmen, L., Borroni, E., Spooren, W., et al. (2002). Misfolded proteinase K-resistant hyperphosphorylated alpha-synuclein in aged transgenic mice with locomotor deterioration and in human alpha-synucleinopathies. *J. Clin. Invest.* 110, 1429–1439. doi: 10.1172/jci15777

Nguyen-Legros, J. (1988). Functional neuroarchitecture of the retina: hypothesis on the dysfunction of retinal dopaminergic circuitry in Parkinson's disease. *Surg. Radiol. Anat.* 10, 137–144. doi: 10.1007/bf02307822

Nightingale, S., Mitchell, K. W., and Howe, J. W. (1986). Visual evoked cortical potentials and pattern electroretinograms in Parkinson's disease and control subjects. *J. Neurol. Neurosurg. Psychiatry* 49, 1280–1287. doi: 10.1136/jnnp.49.11.1280

Normando, E. M., Davis, B. M., De Groef, L., Nizari, S., Turner, L. A., Ravindran, N., et al. (2016). The retina as an early biomarker of neurodegeneration in a rotenone-induced model of Parkinson's disease: evidence for a neuroprotective effect of rosiglitazone in the eye and brain. *Acta Neuropathol. Commun.* 4:86. doi: 10.1186/s40478-016-0346-z

Nowacka, B., Lubiński, W., Honczarenko, K., Potemkowski, A., and Safranow, K. (2015). Bioelectrical function and structural assessment of the retina in patients with early stages of Parkinson's disease (PD). *Doc. Ophthalmol.* 131, 95–104. doi: 10.1007/s10633-015-9503-0

Obien, M. E. J., Deligkaris, K., Bullmann, T., Bakkum, D. J., and Frey, U. (2015). Revealing neuronal function through microelectrode array recordings. *Front. Neurosci.* 9:423. doi: 10.3389/fnins.2014.00423

Ortuno-Lizaran, I., Beach, T. G., Serrano, G. E., Walker, D. G., Adler, C. H., and Cuenca, N. (2018a). Phosphorylated alpha-synuclein in the retina is a biomarker of Parkinson's disease pathology severity. *Mov. Disord.* 33, 1315–1324. doi: 10.1002/mds.27392

Ortuno-Lizaran, I., Esquiva, G., Beach, T. G., Serrano, G. E., Adler, C. H., Lax, P., et al. (2018b). Degeneration of human photosensitive retinal ganglion cells may explain sleep and circadian rhythms disorders in Parkinson's disease. *Acta Neuropathol. Commun.* 6:90. doi: 10.1186/s40478-018-0596-z

Ortuño-Lizarán, I., Sánchez-Sáez, X., Lax, P., Serrano, G. E., Beach, T. G., Adler, C. H., et al. (2020). Dopaminergic retinal cell loss and visual dysfunction in Parkinson disease. *Ann. Neurol.* 88, 893–906. doi: 10.1002/ana.25897

Peppe, A., Stanzione, P., Pierantozzi, M., Semprini, R., Bassi, A., Santilli, A. M., et al. (1998). Does pattern electroretinogram spatial tuning alteration in Parkinson's disease depend on motor disturbances or retinal dopaminergic loss? *Electroencephalogr. Clin. Neurophysiol.* 106, 374–382. doi: 10.1016/s0013-4694(97)00075-8

Peppe, A., Stanzione, P., Pierelli, F., De Angelis, D., Pierantozzi, M., and Bernardi, G. (1995). Visual alterations in de novo Parkinson's disease: pattern electroretinogram latencies are more delayed and more reversible by levodopa than are visual evoked potentials. *Neurology* 45, 1144–1148. doi: 10.1212/WNL.45.6.1144

Peppe, A., Stanzione, P., Pierelli, F., Stefano, E., Rizzo, P. A., Tagliati, M., et al. (1992). Low contrast stimuli enhance PERG sensitivity to the visual dysfunction in Parkinson's disease. *Electroencephalogr. Clin. Neurophysiol.* 82, 453–457. doi: 10.1016/0013-4694(92)90051-i

Petzold, A. (2016). Retinal glymphatic system: an explanation for transient retinal layer volume changes? *Brain* 139, 2816–2819. doi: 10.1093/brain/aww239

Pisa, M., Croese, T., Dalla Costa, G., Guerrieri, S., Huang, S. C., Finardi, A., et al. (2021). Subclinical anterior optic pathway involvement in early multiple sclerosis and clinically isolated syndromes. *Brain* 144, 848–862. doi: 10.1093/brain/awaa458

Postuma, R. B., and Berg, D. (2017). The new diagnostic criteria for Parkinson's disease. *Int. Rev. Neurobiol.* 132, 55–78. doi: 10.1016/bs.irn.2017.01.008

Postuma, R. B., Berg, D., Adler, C. H., Bloem, B. R., Chan, P., Deuschl, G., et al. (2016). The new definition and diagnostic criteria of Parkinson's disease. *Lancet Neurol.* 15, 546–548. doi: 10.1016/S1474-4422(16)00116-2

Price, D. L., Rockenstein, E., Mante, M., Adame, A., Overk, C., Spencer, B., et al. (2016). Longitudinal live imaging of retinal alpha-synuclein::GFP deposits in a transgenic mouse model of Parkinson's disease/dementia with Lewy bodies. *Sci. Rep.* 6:29523. doi: 10.1038/srep29523

Price, M. J., Feldman, R. G., Adelberg, D., and Kayne, H. (1992). Abnormalities in color vision and contrast sensitivity in Parkinson's disease. *Neurology* 42, 887–890. doi: 10.1212/wnl.42.4.887

Purro, S. A., Galli, S., and Salinas, P. C. (2014). Dysfunction of Wnt signaling and synaptic disassembly in neurodegenerative diseases. *J. Mol. Cell Biol.* 6, 75–80. doi: 10.1093/jmcb/mjt049

Rahimi, J., Milenkovic, I., and Kovacs, G. G. (2015). Patterns of Tau and alpha-synuclein pathology in the visual system. *J. Parkinsons Dis.* 5, 333–340. doi: 10.3233/JPD-140485

Ramirez, A. I., de Hoz, R., Salobrar-Garcia, E., Salazar, J. J., Rojas, B., Ajoy, D., et al. (2017). The role of microglia in retinal neurodegeneration: Alzheimer's disease, Parkinson, and Glaucoma. *Front. Aging Neurosci.* 9:214. doi: 10.3389/fnagi.2017.00214

Reeve, A. K., Grady, J. P., Cosgrave, E. M., Bennison, E., Chen, C., Hepplewhite, P. D., et al. (2018). Mitochondrial dysfunction within the synapses of substantia nigra neurons in Parkinson's disease. *NPJ Parkinsons Dis.* 4:9. doi: 10.1038/s41531-018-0044-6

Roberts, H. L., and Brown, D. R. (2015). Seeking a mechanism for the toxicity of oligomeric α-synuclein. *Biomolecules* 5:282. doi: 10.3390/BIOM5020282

Santano, C., Perez de Lara, M., and Pintor, J. (2011). "Retinal disturbances in patients and animal models with Huntington's, Parkinson's and Alzheimer's disease," in *Oxidative Stress in Applied Basic Research and Clinical Practice – Studies on Experimental Models*, eds S. Basu and L. Wiklund (New York, NY: Humana Press), 221–250. doi: 10.1007/978-1-60761-956-7_10

Sartucci, F., Orlandi, G., Bonuccelli, U., Borghetti, D., Murri, L., Orsini, C., et al. (2006). Chromatic pattern-reversal electroretinograms (ChPERGs) are spared in multiple system atrophy compared with Parkinson's disease. *Neurol. Sci.* 26, 395–401. doi: 10.1007/s10072-006-0522-1

Schell, H., Hasegawa, T., Neumann, M., and Kahle, P. J. (2009). Nuclear and neuritic distribution of serine-129 phosphorylated α-synuclein in transgenic mice. *Neuroscience* 160, 796–804. doi: 10.1016/j.neuroscience.2009.03.002

Schindelin, J., Arganda-Carreras, I., Frise, E., Kaynig, V., Longair, M., Pietzsch, T., et al. (2012). Fiji: an open-source platform for biological-image analysis. *Nat. Methods* 9, 676–682. doi: 10.1038/nmeth.2019

Selkoe, D. J. (2002). Alzheimer's disease is a synaptic failure. *Science* 298, 789–791. doi: 10.1126/science.1074069

Sergeys, J., Etienne, I., Van Hove, I., Lefevere, E., Stalmans, I., Feyen, J. H. M., et al. (2019). Longitudinal in vivo characterization of the streptozotocin-induced diabetic mouse model: focus on early inner retinal responses. *Investig. Ophthalmol. Vis. Sci.* 60, 807–822. doi: 10.1167/iovs.18-25372

Shrier, E. M., Adam, C. R., Spund, B., Glazman, S., and Bodis-Wollner, I. (2012). Interocular asymmetry of foveal thickness in Parkinson disease. *J. Ophthalmol.* 2012:728457. doi: 10.1155/2012/728457

Spund, B., Ding, Y., Liu, T., Selesnick, I., Glazman, S., Shrier, E. M., et al. (2013). Remodeling of the fovea in Parkinson disease. *J. Neural Transm.* 120, 745–753. doi: 10.1007/s00702-012-0909-5

Subramanian, J., and Tremblay, M. È (2021). Editorial: synaptic loss and neurodegeneration. *Front. Cell. Neurosci.* 15:681029. doi: 10.3389/fncel.2021.681029

Sulzer, D., and Edwards, R. H. (2019). The physiological role of α-synuclein and its relationship to Parkinson's disease. *J. Neurochem.* 150, 475–486. doi: 10.1111/jnc.14810

Tansey, M. G., and Goldberg, M. S. (2010). Neuroinflammation in Parkinson's disease: its role in neuronal death and implications for therapeutic intervention. *Neurobiol. Dis.* 37, 510–518. doi: 10.1016/j.nbd.2009.11.004

Turcano, P., Chen, J. J., Bureau, B. L., and Savica, R. (2018). Early ophthalmologic features of Parkinson's disease: a review of preceding clinical and diagnostic markers. *J. Neurol.* 266, 2103–2111. doi: 10.1007/s00415-018-9051-0

Van Hove, I., De Groef, L., Boeckx, B., Modave, E., Hu, T. T., Beets, K., et al. (2020). Single-cell transcriptome analysis of the Akimba mouse retina reveals cell-type-specific insights into the pathobiology of diabetic retinopathy. *Diabetologia* 63, 2235–2248. doi: 10.1007/s00125-020-05218-0

Vandenabeele, M., Veys, L., Lemmens, S., Hadoux, X., Gelders, G., Masin, L., et al. (2021). The App NL-G-F mouse retina is a site for preclinical Alzheimer's disease diagnosis and research. *Acta Neuropathol. Commun.* 9:6. doi: 10.1186/s40478-020-01102-5

Veys, L., Vandenabeele, M., Ortuno-Lizaran, I., Baekelandt, V., Cuenca, N., Moons, L., et al. (2019). Retinal alpha-synuclein deposits in Parkinson's disease patients and animal models. *Acta Neuropathol.* 137, 379–395. doi: 10.1007/s00401-018-01956-z

Xia, F., Ha, Y., Shi, S., Li, Y., Li, S., Luisi, J., et al. (2021). Early alterations of neurovascular unit in the retina in mouse models of tauopathy. *Acta Neuropathol. Commun.* 9:51. doi: 10.1186/s40478-021-01149-y

Conflict of Interest: The authors declare that the research was conducted in the absence of any commercial or financial relationships that could be construed as a potential conflict of interest.

Publisher's Note: All claims expressed in this article are solely those of the authors and do not necessarily represent those of their affiliated organizations, or those of the publisher, the editors and the reviewers. Any product that may be evaluated in this article, or claim that may be made by its manufacturer, is not guaranteed or endorsed by the publisher.

frontiers in Neuroscience

REVIEW
published: 22 September 2021
doi: 10.3389/fnins.2021.731614

Retinal Vasculopathy in Alzheimer's Disease

*Haoshen Shi[1], Yosef Koronyo[1], Altan Rentsendorj[1], Dieu-Trang Fuchs[1], Julia Sheyn[1], Keith L. Black[1], Nazanin Mirzaei[1] and Maya Koronyo-Hamaoui[1,2]**

[1] Department of Neurosurgery, Maxine Dunitz Neurosurgical Research Institute, Cedars-Sinai Medical Center, Los Angeles, CA, United States, [2] Department of Biomedical Sciences, Cedars-Sinai Medical Center, Los Angeles, CA, United States

The retina has been increasingly investigated as a site of Alzheimer's disease (AD) manifestation for over a decade. Early reports documented degeneration of retinal ganglion cells and their axonal projections. Our group provided the first evidence of the key pathological hallmarks of AD, amyloid β-protein (Aβ) plaques including vascular Aβ deposits, in the retina of AD and mild cognitively impaired (MCI) patients. Subsequent studies validated these findings and further identified electroretinography and vision deficits, retinal (p)tau and inflammation, intracellular Aβ accumulation, and retinal ganglion cell-subtype degeneration surrounding Aβ plaques in these patients. Our data suggest that the brain and retina follow a similar trajectory during AD progression, probably due to their common embryonic origin and anatomical proximity. However, the retina is the only CNS organ feasible for direct, repeated, and non-invasive ophthalmic examination with ultra-high spatial resolution and sensitivity. Neurovascular unit integrity is key to maintaining normal CNS function and cerebral vascular abnormalities are increasingly recognized as early and pivotal factors driving cognitive impairment in AD. Likewise, retinal vascular abnormalities such as changes in vessel density and fractal dimensions, blood flow, foveal avascular zone, curvature tortuosity, and arteriole-to-venule ratio were described in AD patients including early-stage cases. A rapidly growing number of reports have suggested that cerebral and retinal vasculopathy are tightly associated with cognitive deficits in AD patients and animal models. Importantly, we recently identified early and progressive deficiency in retinal vascular platelet-derived growth factor receptor-β (PDGFRβ) expression and pericyte loss that were associated with retinal vascular amyloidosis and cerebral amyloid angiopathy in MCI and AD patients. Other studies utilizing optical coherence tomography (OCT), retinal amyloid-fluorescence imaging and retinal hyperspectral imaging have made significant progress in visualizing and quantifying AD pathology through the retina. With new advances in OCT angiography, OCT leakage, scanning laser microscopy, fluorescein angiography and adaptive optics imaging, future studies focusing on retinal vascular AD pathologies could transform non-invasive pre-clinical AD diagnosis and monitoring.

Keywords: cerebral amyloid angiopathy, vascular amyloidosis, eye, ocular disease, retinal imaging, blood retinal barrier, Alzheimer's disease, neurodegenerative disease

OPEN ACCESS

Edited by:
Tim Magnus,
University of Hamburg, Germany

Reviewed by:
Gareth R. Howell,
Jackson Laboratory, United States
Giovanni Luca Romano,
University of Catania, Italy

***Correspondence:**
Maya Koronyo-Hamaoui
maya.koronyo@csmc.edu

Specialty section:
This article was submitted to Neurodegeneration, a section of the journal Frontiers in Neuroscience

Received: *27 June 2021*
Accepted: *26 August 2021*
Published: *22 September 2021*

Citation:
Shi H, Koronyo Y, Rentsendorj A, Fuchs D-T, Sheyn J, Black KL, Mirzaei N and Koronyo-Hamaoui M (2021) Retinal Vasculopathy in Alzheimer's Disease. Front. Neurosci. 15:731614. doi: 10.3389/fnins.2021.731614

INTRODUCTION

Alzheimer's disease (AD) is the leading cause of senile dementia, accounting for 60–80% of total cases (Alzheimer's Association, 2020). By 2050, over six million Americans are projected to live with AD, which could lead to a staggering $355 billion national financial burden (National Institue on Aging, 2019; Alzheimer's Association, 2020). AD patients progressively develop irreversible cognitive loss due to neurodegeneration in the brain and other direct or indirect factors such as accumulation of toxic molecules, neuroinflammation, and vascular damage. The main pathological hallmarks of AD are amyloid β-protein (Aβ) accumulation and neurofibrillary tangles, mainly composed of hyperphosphorylated (p)tau deposits, that may exist inside or outside of neurons and in blood vessels (Bloom, 2014; Cisternas et al., 2019). Our group identified these hallmarks in the retina of postmortem and living AD and mild cognitively impaired (MCI) patients (Koronyo-Hamaoui et al., 2011; La Morgia et al., 2016; Koronyo et al., 2017). Investigation of CNS and fluid biomarkers has become an essential part of AD research. In 2018, the National Institute on Aging and Alzheimer's Association (NIA-AA) created an updated research framework for classifying pathological phases of AD based on detection of abnormal levels of molecular biomarkers Aβ (A), tau (T), and neurodegeneration [AT(N)], regardless of cognitive status in living patients (Jack et al., 2018). The ATN framework was also proposed to be expandable to include new AD biomarkers such as vascular biomarkers (ATNV) (Jack et al., 2018).

Vascular pathology in AD is an expanding subject and a growing number of studies show that vascular-related damage in the brain and retina can predict cognitive decline (Vidal and Mavet, 1989; Baker et al., 2007; Gharbiya et al., 2014; Boyle et al., 2015; Bulut et al., 2016, 2018; Cunha et al., 2017; McGrory et al., 2017; Planton et al., 2017; Cabrera DeBuc et al., 2018; Deal et al., 2018; Jiang et al., 2018; O'Bryhim et al., 2018; van der Flier et al., 2018; Iadecola et al., 2019; Jung et al., 2019; Montagne et al., 2020; Shi et al., 2020a; Li et al., 2021). Cerebral vascular damage such as ischemia leads to disturbed nutrient supply, induces oxidative stress and inflammatory activities, impedes Aβ clearance and/or alters amyloid-processing enzymes (Marchesi, 2011), all of which can contribute to neurodegeneration and cognitive decline. Studies have also proposed that the onset of clinical dementia may be preceded by reduced cerebral blood flow associated with insufficient Aβ clearance (Wolters et al., 2017; Govindpani et al., 2019). With new disease-modifying therapies on the horizon and emphasizing the need for early intervention (Tonda-Turo et al., 2018), the current challenge is to diagnose AD early and accurately in the clinical setting to allow for an effective outcome that could limit the damage and prevent further disease progression.

Vascular Damage in AD Brain

The brain is nourished by one of the human body's richest networks of blood vessels (Prensa, 2014), rendering its vascular network highly susceptible to aging and AD-related cerebral damage. Studies indicate that AD pathology is associated with severe effects on cerebral blood vessels, potentially by a wide range of complications (Govindpani et al., 2019). These include cerebral amyloid angiopathy (CAA) (Ellis et al., 1996; Arvanitakis et al., 2011; Viswanathan and Greenberg, 2011), vascular non-perfusion (Bonte et al., 1986; Hirsch et al., 1997; Binnewijzend et al., 2016), neurovascular unit (NVU) uncoupling and degeneration (Higuchi et al., 1987; Vinters et al., 1994; Claudio, 1996), angiogenesis (Desai et al., 2009; Biron et al., 2011), small blood vessel distortions (Hassler, 1965; Beskow et al., 1971; Fischer et al., 1990; Kalaria and Kroon, 1992), blood–brain barrier (BBB) breakdown and damage (Slemmon et al., 1994; Zipser et al., 2007; Bell and Zlokovic, 2009; Ryu and McLarnon, 2009; Sengillo et al., 2013; van de Haar et al., 2016a,b), vascular tau accumulation (Williams et al., 2005; Castillo-Carranza et al., 2017), dysregulated glucose metabolism (Kalaria and Harik, 1989; Harik, 1992), inflammation (Grammas and Ovase, 2001; Tripathy et al., 2007), hypertension (Launer, 2002; Gabin et al., 2017), hypercholesterolemia (Matsuzaki et al., 2011), and atherosclerosis (Alzheimer, 1911; Yarchoan et al., 2012).

Amyloid plaques are the most considerable hallmarks of AD, with 42 and 40 amino acid-long Aβ alloforms tightly associated with AD pathogenesis and vascular pathology (Blennow et al., 2015; Selkoe and Hardy, 2016). Nearly 85% of AD patients develop varying degrees of CAA complications (Arvanitakis et al., 2011; Viswanathan and Greenberg, 2011), defined by Aβ deposits inside walls of arteries, arterioles and capillaries (DeSimone et al., 2017). Accumulation of Aβ within blood vessels is associated with damage to muscular and elastic tissue, possibly replaced by Aβ fibrils, leading to lobar cerebral hemorrhage (ICH) or vascular non-perfusion (Mehndiratta et al., 2012; Keable et al., 2016). CAA can also trigger other pathogenic pathways, such as inflammation and oxidative stress, further leading to cerebral tissue damage (Ghiso et al., 2010).

Alzheimer's Retinopathy

Over the past decade, the retina has been extensively investigated as a top candidate site of AD manifestation beyond the brain, as it shares many structural, cellular, molecular, and functional similarities with the brain (Hinton et al., 1986; Purves, 2001; Patton et al., 2005; Koronyo-Hamaoui et al., 2011; Koronyo et al., 2012, 2017; Schon et al., 2012; Erskine and Herrera, 2014; Crair and Mason, 2016; Hart et al., 2016; La Morgia et al., 2016; den Haan et al., 2018a; Asanad et al., 2019; Grimaldi et al., 2019; Lee S. et al., 2020; Mirzaei et al., 2020; Schultz et al., 2020; Snyder et al., 2021). Given the parallel pathology in the brain and retina, the retina has the potential to become a non-invasive diagnostic window since it is not shielded by bone and is easily accessible by ophthalmic exams such as optical coherence tomography (OCT) and fundoscopy (including scanning laser ophthalmoscopy) with subcellular resolution. The retina is directly and indirectly connected to the brain through bundles of neuronal axons forming the optic nerve, and by retinal and cerebral blood vessels, which may facilitate transportation of abnormal Aβ and tau species

and further lead to the spread of AD pathology throughout the CNS (Morin et al., 1993). In addition, the discovery of dysfunctional lymphatic vessels within the brain of rodent models of AD implicates this CNS-specific lymphatic network, referred to as the glymphatic system (Jessen et al., 2015), as a culprit of insufficient cerebral amyloid clearance in AD (Louveau et al., 2015; Da Mesquita et al., 2018; Ahn et al., 2019). Recently, an ocular lymphatic drainage system was also identified in rodent models, which relies on an aquaporin-4-dependent pathway to clear fluid and metabolites (Wang et al., 2020). The roles of such lymphatic systems in retinal diseases and AD remain to be explored in future studies.

Studies conducted by OCT, electroretinogram (ERG), and histological examinations on cognitively impaired patients and laboratory animals have extensively described various retinal pathological and functional changes associated with AD development. In fact, the retina is heavily affected by AD pathology and displays a wide spectrum of retinopathy (reviewed in Mirzaei et al., 2020). This includes optic nerve degeneration and retinal neuronal and ganglion cell (RGC) loss (Hinton et al., 1986; Blanks et al., 1989, 1996; La Morgia et al., 2016; Koronyo et al., 2017; Asanad et al., 2019), retinal nerve fiber layer (NFL) thinning (Kergoat et al., 2001; Parisi et al., 2001; Berisha et al., 2007; Paquet et al., 2007; Moschos et al., 2012; Kirbas et al., 2013; Marziani et al., 2013; Moreno-Ramos et al., 2013; Kromer et al., 2014; Shi et al., 2014; Bayhan et al., 2015; Coppola et al., 2015; Gao et al., 2015; Liu et al., 2015; La Morgia et al., 2016), gliosis (Hinton et al., 1986; Curcio and Drucker, 1993; Blanks et al., 1996; Guo et al., 2010; Grimaldi et al., 2019), and vascular degeneration and injury (Patton et al., 2005; Frost et al., 2013; Cheung et al., 2014; Feke et al., 2015; Williams et al., 2015; Kapasi and Schneider, 2016; Shi et al., 2020b). This retinal damage can explain, at least in part, the visual dysfunctions (Sadun and Bassi, 1990; Armstrong and Syed, 1996; Risacher et al., 2020), sleep disturbances (La Morgia et al., 2016; Wang and Holtzman, 2020), and ERG abnormalities (Trick et al., 1989; Parisi et al., 2001; Moschos et al., 2012) documented in AD patients. Such findings have largely encouraged basic research in the AD retina and exploration of retinal imaging techniques for AD diagnosis.

Our group was the first to demonstrate the existence of Aβ accumulation, the hallmark AD pathology, in the retina of AD patients, including early-stage cases. In a study published in mid-2010, we revealed the aggregation of Aβ deposits in retinal flat-mounts isolated from 13 out of 13 neuropathologically confirmed AD and mild cognitively impaired (MCI) patients, which was minimally or undetected in 5 cognitively normal (CN) subjects negative for brain amyloid (Koronyo-Hamaoui et al., 2011). Further, this pioneer study demonstrated for the first time the ability to non-invasively detect curcumin-labeled Aβ deposits in live murine models of AD (Koronyo-Hamaoui et al., 2011). Importantly, similar reductions in retinal and brain Aβ plaques were detected *ex vivo* and *in vivo* in AD-model mice (Koronyo-Hamaoui et al., 2011; Koronyo et al., 2012) in response to immunomodulation therapies (Butovsky et al., 2006; Koronyo-Hamaoui et al., 2009; Bakalash et al., 2011; Koronyo et al., 2015; Rentsendorj et al., 2018; Doustar et al., 2020). Although a few studies failed to detect Aβ and/or (p)tau in the retina of AD patients, these reports included low case numbers (Schon et al., 2012; Ho et al., 2014; Williams et al., 2017) and only examined limited retinal regions in cross sections, focusing on less affected regions in these patients (La Morgia et al., 2016; Koronyo et al., 2017; Asanad et al., 2019; Shi et al., 2020b). It is possible this discrepancy in findings could also be due to differences in retinal tissue preservation, processing, and/or immunostaining protocols.

Subsequent studies by La Morgia et al. (2016), Lee S. et al. (2020), and others also demonstrated Aβ plaques and vascular-associated deposits in postmortem retinas of AD patient cohorts. Retinal amyloidosis in AD patients was in stark contrast to minimal pathology observed in the retinas of CN individuals (Tsai et al., 2014; La Morgia et al., 2016; den Haan et al., 2018a; Grimaldi et al., 2019; Lee S. et al., 2020; Qiu et al., 2020; Shi et al., 2020a; Cao et al., 2021). In 2017, Koronyo et al. (2017) published the development of more advanced human retinal extraction and histological techniques. Authors utilized immunofluorescence, anti-Aβ compound labeling, non-fluorescence immunostaining, and transmission electron microscopy (TEM) to measure $A\beta_{42}$ plaque burden, characterize retinal Aβ plaque subtypes and morphology including identifying retinal Aβ fibrils and protofibrils, and describe Aβ plaque topographical and layer distribution in a larger cohort of 23 AD patients vs. 14 age- and sex-matched CN patients (Koronyo et al., 2017). In this study, several Aβ-epitope labeling techniques including Gallyas silver stain, curcumin, thioflavin-S, congo red, as well as a combination of monoclonal antibodies against various N'-, C'- and center Aβ sequences were used to describe amyloidosis in the human AD retina. Hence, together with post-mortem detection by immunofluorescence staining, peroxidase-based staining, and TEM analysis on retinal flat-mounts and cross-sections, this study profoundly validated Aβ accumulation in the AD retina in comparison to CN controls. We also demonstrated a significant correlation between retinal and brain plaque burdens, and more importantly, provided the first proof-of-concept trial using curcumin labeling and a scanning laser ophthalmoscope to detect and quantify retinal Aβ plaques in living patients, (Koronyo et al., 2017).

Indeed, multiple biochemical and histological studies corroborated these findings of Aβ deposits in the human AD retina (den Haan et al., 2018a; Grimaldi et al., 2019; Lee S. et al., 2020; Qiu et al., 2020) and further described retinal pTau, $A\beta_{40}$ and $A\beta_{42}$ accumulation, inflammation, and correlations between retinal and cerebral Aβ levels in AD patients (Alexandrov et al., 2011; Schon et al., 2012; den Haan et al., 2018b; Grimaldi et al., 2019; Lee S. et al., 2020; Qiu et al., 2020; Schultz et al., 2020; Shi et al., 2020b). More recently, *in vivo* retinal amyloid imaging in living MCI and AD patients was achieved via either retinal curcumin-enhanced fluorescence and SLO imaging or hyperspectral imaging (Hadoux et al., 2019; More et al., 2019; Dumitrascu et al., 2020; Lemmens et al., 2020; Ngolab et al., 2021).

Recent studies by Chibhabha et al. (2020); Sidiqi et al. (2020), and Barton et al. (2021) in the $APP_{SWE}/PS1_{\Delta E9}$ transgenic mouse model further corroborated these findings via Aβ retinal curcumin imaging. In fact, numerous studies in AD rodent models have detected Aβ and its alloforms such as $Aβ_{40}$ and $Aβ_{42}$ in the AD retina (Inestrosa et al., 2005; Dutescu et al., 2009; Liu et al., 2009; Alexandrov et al., 2011; Ardiles et al., 2012; Schon et al., 2012; Williams et al., 2013; Yang et al., 2013; Zhao et al., 2013; Park et al., 2014; Tsai et al., 2014; Du et al., 2015; Parthasarathy et al., 2015; Chiasseu et al., 2017; Grimaldi et al., 2018; Harrison et al., 2019).

Retinal Vascular Aβ Deposits in AD Patients and Animal Models

An early study by Liu et al. (2009) in the Tg2576 transgenic murine model describes Aβ deposits within retinal microvessels by immunostaining against various Aβ epitopes, using mAbs clones 6E10, 12F4 and 5C3, in retinal cross-sections. Histological examinations by La Morgia et al. (2016) and Koronyo et al. (2017) of retinas from AD patients and age- and sex-matched cognitively normal controls provided evidence for retinal Aβ deposits inside blood vessel walls, perivascular and along blood vessels by immunostaining for 12F4-positive $Aβ_{42}$ in retinal flat-mounts and cross-sections. In the Koronyo et al. (2017) study, retinal vascular Aβ accumulation in retinal flat-mounts and cross-sections of AD patients was also validated by other techniques including congo red, Gallyas silver stain, curcumin, 11A50-B10-positive $Aβ_{40}$ immunostaining, as well as TEM analysis (Koronyo et al., 2017). In murine models of AD, a study by the same team demonstrated that following systemic administration of curcumin to $APP_{SWE}PS1_{\Delta E9}$ model mice, *ex vivo* examination of retinal flatmounts revealed double-labeling of curcumin with 4G8 for Aβ deposits inside retinal blood vessels (Koronyo-Hamaoui et al., 2011).

Amyloidosis in cerebral blood vessels predominately consists of $Aβ_{40}$ alloforms (Gravina et al., 1995). Accordingly, Shi et al. (2020b) conducted the first stereological quantification and mapping of $Aβ_{40}$ in retinal blood vessels by immunostaining of 11A50-B10 and JRF/cAβ 40/28—specific monoclonal antibodies detecting the $Aβ_{40}$ alloform—in retinal cross-sections and isolated retinal blood vessels from MCI and AD patients (see **Figures 1A–E,G,K,L** for retinal vascular amyloidosis). The pattern that was revealed by $Aβ_{40}$ immunoreactivity covered most vascular compartments including tunica media, adventitia, and intima, indicating retinal blood vessels may also be thoroughly affected by Aβ deposition (**Figure 1B**). Increased levels of $Aβ_{1-40}$ peptides in the retina of AD patients as compared with age- and sex-matched cognitively normal controls was further validated by a sandwich enzyme-linked

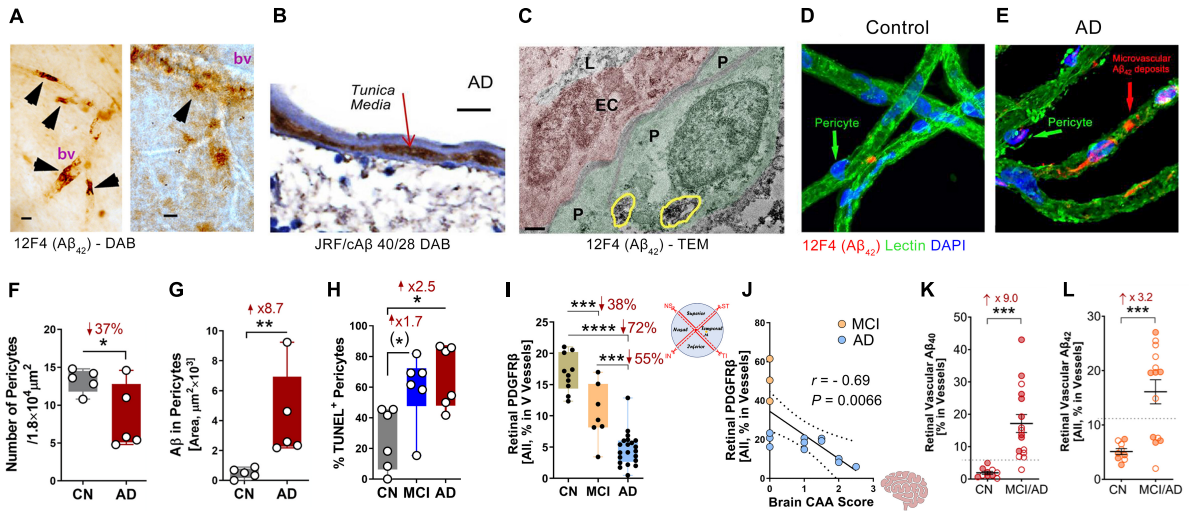

FIGURE 1 | Retinal vascular amyloidosis and pericyte loss in the retina of MCI and AD patients. **(A)** 3,3′-Diaminobenzidine (DAB) staining of $Aβ_{42}$ by 12F4 antibody in retinal blood vessels from flat-mount retina in an AD patient. Scale bar = 20 µm. **(B)** DAB staining of $Aβ_{40}$ by JRF/cAβ 40/28 antibody on a retinal cross-section sample from an AD patient. Scale bar = 20 µm. **(C)** Transmission electron microscopy (TEM) for $Aβ_{42}$ by 12F4 antibody staining in retinal blood vessels and pericytes. P, pericyte; EC, endothelial cell; L, lumen. Yellow circles indicate $Aβ_{42}$ staining. Scale bar = 0.5 µm. **(D,E)** Immunostaining of $Aβ_{42}$ by 12F4 antibody on retinal blood vessels isolated from an AD patient and control. Scale bars = 20 µm. **(F)** Quantification of pericytes in AD patients and cognitively normal (CN) controls based on isolated blood vessels. **(G)** Stereological quantification of Aβ in pericytes in AD patients and CN controls based on isolated blood vessels. **(H)** Quantification of terminal deoxynucleotidyl transferase-mediated dUTP nick-end labeling (TUNEL) positive pericytes on retinal cross-sections from CN, mild cognitively impaired (MCI), and AD patients. **(I)** Stereological quantification of PDGFRβ on retinal cross-sections from CN, MCI, and AD patients. **(J)** Pearson's (r) correlation between cerebral amyloidosis angiopathy (CAA) and retinal PDGFRβ from MCI and AD patients. **(K,L)** Stereological quantification of panel **(K)**. $Aβ_{40}$ and **(L)** $Aβ_{42}$ in CN versus MCI/AD patients. Filled circles represent males and clear circles represent females. Data from individual human donor as well as groups are shown as mean ± SEM. $^*p < 0.05$, $^{**}p < 0.01$, $^{***}p < 0.001$, $^{****}p < 0.0001$, by one-way ANOVA with Sidak's *post hoc* multiple comparison test (more than 2 groups) or unpaired 2-tailed Student's t test (2 groups). Fold and percentage changes are shown in red. Panel A reproduced from Koronyo et al. (2017) with permission of ASCI via Copyright Clearance Center. Panels B–L reproduced from Shi et al. (2020b) under terms of the Creative Commons Attribution 4.0 International License (http://creativecommons.org/licenses/by/4.0/).

immunosorbent (ELISA) analytical biochemistry assay (Shi et al., 2020b). When correlated with cerebral pathologies, levels of retinal $A\beta_{40}$ significantly associated with entorhinal cortex plaque load and had a trend of predicting cognitive decline and CAA. Retinal vascular $A\beta_{40}$ tightly associated with neuritic plaques in the entorhinal cortex and combined cerebral regions including hippocampus, frontal cortex, temporal cortex, and parietal cortex. A study by Schultz et al. (2020) also successfully correlated levels of retinal high molecular weight $A\beta_{42}$ and $A\beta_{40}$ with neurofibrillary tangles (NFT) and Aβ scores in the hippocampus of AD patients. Another notable finding was the downregulation of low-density lipoprotein receptor-related protein 1 (LRP1) in AD retina, suggesting compromised Aβ clearance (Shi et al., 2020b).

In a subsequent report, Shi et al. (2020a) detected $A\beta_{40}$ accumulation in retinal blood vessels of 8-month-old $APP_{SWE}PS1_{\Delta E9}$ mice. Another recent study by Habiba et al. (2021) revealed detectable levels of $A\beta_{40}$ and $A\beta_{42}$ oligomers in the retina and blood as early as in 3-month-old APP/PS1 mice, prior to their detection in the respective brain. It is important to note that the transgenic APP/PS1 mouse model is driven by increased production of human amyloidogenic Aβ peptides, and therefore does not fully represent the human disease. Nevertheless, this mouse model is known to develop Aβ plaques and intracellular soluble Aβ oligomers, (p)tau, pronounced micro- and astrogliosis, synaptic loss, as well as cognitive and visual decline (Jankowsky et al., 2003; Butovsky et al., 2006; Koronyo-Hamaoui et al., 2009; Bakalash et al., 2011; Koronyo et al., 2015; Rentsendorj et al., 2018; Doustar et al., 2020; Vit et al., 2021). Intriguingly, a recent study by Chintapaludi et al. (2020) detected early onset alterations of retinal inflammatory genes before cerebral amyloidosis. Nevertheless, more supporting evidence and validation is needed to further evaluate the feasibility to diagnose AD by retinal vascular amyloid imaging.

AD-Related Retinal Vasculopathy

Mounting evidence has demonstrated a wide range of retinal vascular abnormalities in both AD patients and animals, such as reduced macular microvascular density (O'Bryhim et al., 2018), decreased blood flow (Berisha et al., 2007; Feke et al., 2015; Einarsdottir et al., 2016), compromised microvascular network (Frost et al., 2013; Cheung et al., 2014; Williams et al., 2015; Einarsdottir et al., 2016; Cabrera DeBuc et al., 2018), damaged vascular branching complexity (Frost et al., 2013; Cheung et al., 2014), vein narrowing (Berisha et al., 2007; Frost et al., 2013; Cheung et al., 2014; Feke et al., 2015; Cabrera DeBuc et al., 2018), and increased vascular tortuosity (Cheung et al., 2014). Among these findings, several studies showed significant correlations between retinal vascular impairment and AD susceptibility, while others did not. Nevertheless, these discoveries have provided numerous potential retinal vascular targets for AD monitoring and diagnosis. Compared to the brain, a distinct feature of the retina is the existence of Müller glial cells, which are the principal retinal glial cell type that maintain neuronal activity by regulating extracellular concentration of neurotransmitters and neuroactive ions (Newman and Reichenbach, 1996). Indeed, a previously published report suggested that retinal Aβ is engulfed by these specialized Muller glial cells (den Haan et al., 2018b), warranting further research on the potential role of these retina-specific glial cells in AD pathogenesis. It is important to note that most investigations are still limited to cross-sectional observations. Future studies should seek to apply standardized protocols and design with longitudinal study methods.

Another similarity between the retina and brain is the blood-organ barrier: the blood–retinal barrier (BRB) is highly comparable to the BBB, both structurally and functionally (Campbell and Humphries, 2012; Zenaro et al., 2017; Cai et al., 2018). The BBB is composed of cerebral vascular endothelial cells with tight junctions (TJ), astrocyte end-feet and supporting pericytes, while the BRB is made of an inner barrier of retinal vascular endothelial cells and an outer barrier of retinal epithelial cells, both with TJ and supporting pericytes (Campbell and Humphries, 2012; Zenaro et al., 2017; Cai et al., 2018). The main functions of these barriers are to modulate the influx of ions, proteins and water, as well as curb the infiltration of circulating immune cells (Cunha-Vaz et al., 2011). In AD, a compromised BBB is viewed as one of the principal causes for cerebral amyloidosis due to its essential role in clearing abundant cerebral Aβ to the circulating blood via the vascular network (Zlokovic et al., 1993; DeMattos et al., 2002; Banks et al., 2003; Do et al., 2015; Zhao et al., 2015; Sweeney et al., 2018). Recently, the Zlokovic group has successfully connected the BBB-associated pericyte injury biomarker, soluble PDGFRβ, in cerebrospinal fluid (CSF) to cognitive decline in apolipoprotein E (APOE4) carriers even after controlling for Aβ and tau status (Montagne et al., 2020). These findings suggest that BBB biomarkers might be an option for next-generation AD diagnostics and therapeutics.

Recent investigation of BRB in MCI and AD patients by Shi et al. (2020b) has revealed early and progressive retinal vascular PDGFRβ deficiency and pericyte loss associated with retinal vascular $A\beta_{40}$ and $A\beta_{42}$ deposition in postmortem tissues from MCI and AD patients (**Figures 1D–J**). In a subset of patients with neuropathological reports, retinal vascular PDGFRβ expression significantly correlated with CAA and cognitive decline assessed by the Mini-Mental State Examination (MMSE). These data suggest that pericyte loss or PDGFRβ downregulation may precede AD progression. The retinal pericytes in cognitively impaired patients were found to accumulate $A\beta_{40}$ and $A\beta_{42}$ and undergo apoptosis, demonstrated by terminal deoxynucleotidyl transferase dUTP nick end labeling (TUNEL) assay and cleaved caspase-3 nuclear staining. Interestingly, a previous study detected increased neuronal apoptosis in the rat retina induced by intra-vitreous injection of $A\beta_{1\text{-}42}$ oligomers (Fisichella et al., 2016). In a subsequent study, the Koronyo-Hamaoui group further discovered significantly augmented capillary degeneration in 8-month-old $APP_{SWE}PS1_{\Delta E9}$ mice compared to wild type littermates that was further exacerbated in 12-month-old mice (**Figures 2A,B**; Shi et al., 2020a). Retinal capillary loss was associated with increased retinal vascular amyloidosis, indicating more BRB damage may be driven by vascular Aβ deposition and implicated in AD pathology (Shi et al., 2020a). Western blot analysis of whole retinal lysates revealed altered expression of key TJ molecules of the BRB, including claudin-1 and zonula occludens-1 (ZO-1) (**Figures 2C,D**). These changes

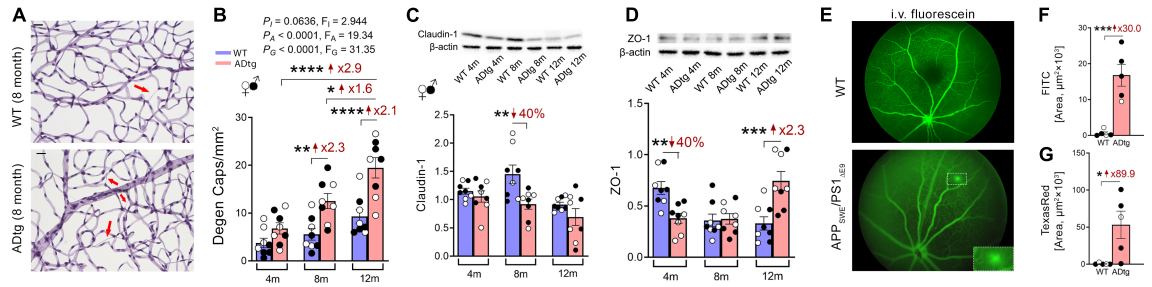

FIGURE 2 | Retinal vasculopathy in $APP_{SWE}PS1_{\Delta E9}$ (ADtg) mice. **(A,B)** Representative images of periodic acid-Schiff (PAS)-stained, hematoxylin-counterstained isolated retinal microvasculature from ADtg and matched wild type (WT) littermates. Acellular degenerated retinal capillaries are indicated by red arrows. **(B)** Numbers of degenerated retinal capillaries when mice are stratified by mouse genotypes, WT or ADtg, by age groups of 4, 8, and 12 months. **(C,D)** Western-Blot analysis of panel **(C)** claudin-1 and **(D)** ZO-1 in retinal lysates from 4, 8, and 12-month-old $APP_{SWE}PS1_{\Delta E9}$ mice and WT controls. **(E)** Images showing *in vivo* retinal microvascular imaging for leakage after intraperitoneal fluorescein injection in 12-month-old WT and ADtg mice. **(F,G)** Quantitative analysis of the panel **(D)** FITC (1,000 kDa) or **(E)** Texas Red (3 kDa)-stained area in retinal flat-mounts from WT or ADtg mice. Black-filled circles represent males and clear circles represent females. Data from individual mouse as well as groups are shown as mean ± SEM. $^{*}p < 0.05$, $^{**}p < 0.01$, $^{***}p < 0.001$, $^{****}p < 0.0001$, by 2-way ANOVA with Sidak's *post hoc* multiple comparison test (more than 2 groups) or unpaired 2-tailed Student's t test (2 groups). Fold and percentage changes are shown in red. Reproduced from Shi et al. (2020a) under terms of the Creative Commons Attribution 4.0 International License (http://creativecommons.org/licenses/by/4.0/).

were also accompanied by elevated NF-κB p65 phosphorylation in retinas of 12-month-old ADtg mice, implicating upregulated inflammation in the retina with increased vascular amyloidosis burden. Having found these changes in retinal blood vessels and capillaries of AD-model mice, the authors sought to explore how these vascular pathologies may have affected BRB permeability. *In vivo* fluorescein (332 Da) imaging of $APP_{SWE}PS1_{\Delta E9}$ mice showed live retinal vascular leakage in 12-month-old but not in 8-month-old mouse models of AD (**Figure 2E**). Intriguingly, intravenous injection of larger FITC-dextran (1,000 kDa) and Texas-Red-dextran (3 kDa) molecules in 6-month-old $APP_{SWE}PS1_{\Delta E9}$ mice followed by *ex vivo* postmortem retinal imaging and quantification of the fluorescent signal indicated a dramatic increase in retinal vascular leakage of both molecules (**Figures 2F,G**). These BRB permeability changes in transgenic AD mice occur even earlier than the respective cerebral leakage measured by the same molecules (Lahiri et al., 2019). The difference between *in vivo* and *ex vivo* observations is suggestive of a shift in molecular size-dependent transporting mechanisms through the BRB in the AD transgenic mice model. Accordingly, a recent study utilizing the C57BL/6 mouse revealed a decrease in plasma protein transport activity through the BBB in the aged brain, driven by transport shifting from ligand-specific receptor-mediated to non-specific caveolar transcytosis (Yang et al., 2020). Whether this also occurs in AD patients' BRB needs further validation. Overall, such discoveries have suggested that several BRB compartments are affected in AD disease progression that should be further evaluated as biomarkers for AD diagnosis.

Cerebral Imaging for AD

Recent developments in brain imaging modalities have significantly improved the ability to rule-in AD related cerebral pathologies in at-risk populations (Johnson et al., 2012). These include MRI (fMRI) (Smith et al., 1999; Machulda et al., 2003; Dickerson et al., 2004; Johnson et al., 2006, 2012), fluorodeoxyglucose (FDG) positron emission tomography (PET) (Foster et al., 1983; Hoffman et al., 2000; Engler et al., 2006), amyloid PET imaging (Drzezga et al., 2008; Ikonomovic et al., 2008), PET imaging of copper trafficking (Torres et al., 2016; Andreozzi et al., 2017), and transcranial Doppler (TCD) ultrasound (Roher et al., 2011). However, these techniques are still subject to a variety of limitations such as high cost, low availability, low spatial resolution, low specificity, or involving the use of unsafe radio isotopes (Johnson et al., 2012). Nevertheless, current imaging techniques do not provide a solution for large scale screening of pre-symptomatic at-risk populations, which is the main goal of current efforts to develop more sensitive ocular examination techniques for AD diagnosis.

Retinal OCT and OCT-A Imaging in MCI and AD Patients

Optical coherence tomography has been a pioneer technology in capturing retinal structural changes in living AD patients. This technology utilizes low-coherence light to acquire two- and three-dimensional images of retinal cross-sectional anatomy with micrometer resolution (Frohman et al., 2008; Popescu et al., 2011; Aumann et al., 2019). It provides non-invasive live measurements of retinal layer structure and is widely used in ophthalmic exanimations for diagnosis of glaucoma, age-related macular degeneration (AMD), diabetic retinopathy (DR), as well as other ocular diseases (Lang, 2007; Medical Advisory, 2009; Sathyan et al., 2012). Parisi et al. (2001) utilized this technology for the first time in AD patients, demonstrating a significant reduction in retinal nerve fiber layer (NFL) thickness as compared to healthy control individuals. Paquet et al. (2007) further described a significant reduction of retinal NFL thickness in MCI, mild AD, moderate AD, and severe AD patients compared to healthy controls. Subsequently, numerous studies verified these early studies and reported decreases in NFL, ganglion cell layer (GCL), and macula thickness correlating with cognitive decline (Kromer et al., 2014; Cunha et al., 2016; Doustar et al., 2017; Ferrari et al., 2017; Polans et al., 2017; Polo et al., 2017; Bulut et al., 2018;

Janez-Escalada et al., 2019; Salobrar-Garcia et al., 2019; Czako et al., 2020; Dumitrascu and Koronyo-Hamaoui, 2020; Mejia-Vergara et al., 2021; Yan et al., 2021). OCT-adaptive optics is a relatively newer advancement of this technology which provides ultra-high-resolution images, including of blood vessel walls, that warrants further testing in the AD retina (Snyder et al., 2021).

Among the many advances in OCT technology, OCT-angiography (OCTA) has been specifically developed for the investigation of retinal blood vessels, revolutionizing the diagnosis of retinal vascular-related disorders (de Carlo et al., 2015; Chalam and Sambhav, 2016; Hagag et al., 2017). It provides high-resolution motion-contrast images based on backscattered light from neuronal and vascular tissues in the retina (Kashani et al., 2017). This enables visualization of various retinal vascular abnormalities such as microaneurysms, neovascularization, retinal vascular non-perfusion, reduced vascular density, and modified foveal avascular zone (FAZ) (Kashani et al., 2017). OCT-A received FDA approval in 2016 and has been rigorously used in diagnosis of retinal vascular diseases including DR, uveitis, AMD, and others (Pichi et al., 2017; Khadamy et al., 2018; Schneider and Fowler, 2018; Tey et al., 2019). The significant potential of this technology has recently led to a surge of research activity related to its utility in exploring retinal biomarkers in AD. An early case-control study by Bulut et al. (2018) on a total of 52 AD patients and healthy controls described a significant decrease in retinal vascular density, reduced retinal and choroidal thickness, as well as enlarged FAZ area in the patients. Shortly after, Jiang et al. (2018) based on 52 participants demonstrated lower densities of retinal vascular network, superficial vascular plexus (SVP), and deep vascular plexus (DCP) in MCI and AD patients, while O'Bryhim et al. (2018) with 32 participants validated increased FAZ area in AD patients. To date, such OCTA case-controlled studies seem to be largely consistent in demonstrating retinal vascular density loss and increased FAZ area in AD patients but differ in identifying vascular areas affected, the superficial vs. deep, or parafoveal vs. perifoveal vessels (Lahme et al., 2018; Sadda et al., 2019; Yoon et al., 2019; Zabel et al., 2019; Zhang et al., 2019; Czako et al., 2020; Lee J. Y. et al., 2020; Wu et al., 2020; Rifai et al., 2021). Overall, these are indeed breakthrough findings that warrant further investigation, considering OCTA is a relatively new technology. It is also important to note that sample sizes in most of these studies are relatively small. To better evaluate OCTA as a diagnostic tool for AD, longitudinal studies with a standardized consistent protocol and large case numbers are needed.

Blood–retinal barrier permeability in laboratory animals is usually measured by injecting fluorescent dyes such as fluorescein (Do carmo et al., 1998) or Evans blue (Xu et al., 2001), followed by *in vivo* or *ex vivo* imaging for retinal vascular leakage. Fundus fluorescein angiography (FFA) was developed based on visualizing fluorescent dye by fundus camera that has been widely used to evaluate retinal vascular circulation and BRB integrity (Marmor and Ravin, 2011). Another modified OCT method, OCT-leakage, was recently developed to monitor retinal edema, thus evaluating BRB damage (Cunha-Vaz et al., 2016; Cunha-Vaz, 2017). This method applies a proprietary algorithm to identify sites of decreased optical reflectivity, then the system quantifies and detects the correlation of retinal extracellular space. The developer tested OCT-leakage on 28 patients and provided consistent output between FFA and OCT-leakage for BRB damage in diabetic retinopathy (Cunha-Vaz et al., 2017). Both FFA and OCT-leakage can potentially be tested in cognitively impaired patients to investigate the potential of BRB permeability monitoring for AD diagnosis.

CONCLUSION

In summary, recent advancements in retinal vascular research in AD patients and animal models have provided many potential candidate targets for non-invasive diagnosis by retinal vascular imaging. These include but are not limited to retinal vascular amyloidosis, FAZ area, vascular leakage, vascular blood flow and perfusion, TJ alteration, vascular density, pericyte and PDGFRβ loss, vascular branching complexity and others. Reports suggest that certain vascular abnormalities occur very early during AD progression and may predict cognitive decline in patients; thus, their detection may be critical for early diagnosis and prognosis prediction. However, since some of these vascular findings are commonly observed in retinal degenerative and inflammatory diseases, it is important to also consider AD-specific hallmark biomarkers such as Aβ and (p)tau for accurate diagnosis. Finally, with the recent development of retinal amyloid imaging (Koronyo et al., 2017; Dumitrascu et al., 2020; Ngolab et al., 2021), pericyte imaging (Schallek et al., 2013), OCTA and OCT-leakage (Cunha-Vaz et al., 2016; Cunha-Vaz, 2017), hyperspectral imaging (Hadoux et al., 2019; More et al., 2019; Lemmens et al., 2020), and FFA (Marmor and Ravin, 2011), future studies may pave a the way for next-generation non-invasive ophthalmic imaging technologies to facilitate AD monitoring and diagnosis.

AUTHOR CONTRIBUTIONS

HS and MK-H: draft manuscript and figures preparation. MK-H, HS, YK, AR, D-TF, NM, JS, and KB: manuscript editing. MK-H: study supervision. All authors read and approved the submitted version.

FUNDING

The work of MK-H was supported by the National Institute of Health (NIH)/NIA Grant Numbers: R01AG056478, R01 AG056478-04S1 and R01AG055865, as well as by the Haim Saban and Tom Gordon Private Foundations.

ACKNOWLEDGMENTS

We thank Mia Oviatt for help with manuscript editing. The authors dedicate the manuscript to the memory of Dr. Salomon Moni Hamaoui and Lillian Jones Black, who died of Alzheimer's disease.

REFERENCES

Ahn, J. H., Cho, H., Kim, J.-H., Kim, S. H., Ham, J.-S., Park, I., et al. (2019). Meningeal lymphatic vessels at the skull base drain cerebrospinal fluid. *Nature* 572, 62–66. doi: 10.1038/s41586-019-1419-5

Alexandrov, P. N., Pogue, A., Bhattacharjee, S., and Lukiw, W. J. (2011). Retinal amyloid peptides and complement factor H in transgenic models of Alzheimer's disease. *Neuroreport* 22, 623–627. doi: 10.1097/wnr.0b013e3283497334

Alzheimer, A. (1911). Über eigenartige Krankheitsfälle des späteren Alters. *Z. f. d. g. Neur. u. Psych.* 4:356. doi: 10.1007/bf02866241

Alzheimer's Association (2020). *What is Alzheimer's Disease?* [Online]. Available online at: https://www.alz.org/alzheimers-dementia/what-is-alzheimers (Accessed June 1, 2021).*

Andreozzi, E. M., Torres, J. B., Sunassee, K., Dunn, J., Walker-Samuel, S., Szanda, I., et al. (2017). Studies of copper trafficking in a mouse model of Alzheimer's disease by positron emission tomography: comparison of (64)Cu acetate and (64)CuGTSM. *Metallomics* 9, 1622–1633. doi: 10.1039/c7mt00227k

Ardiles, A. O., Tapia-Rojas, C. C., Mandal, M., Alexandre, F., Kirkwood, A., Inestrosa, N. C., et al. (2012). Postsynaptic dysfunction is associated with spatial and object recognition memory loss in a natural model of Alzheimer's disease. *Proc. Natl. Acad. Sci. U.S.A.* 109, 13835–13840. doi: 10.1073/pnas.1201209109

Armstrong, R. A., and Syed, A. B. (1996). Alzheimer's disease and the eye. *Ophthalmic Physiol. Opt.* 16(Suppl. 1), S2–S8.

Arvanitakis, Z., Leurgans, S. E., Wang, Z., Wilson, R. S., Bennett, D. A., and Schneider, J. A. (2011). Cerebral amyloid angiopathy pathology and cognitive domains in older persons. *Ann. Neurol.* 69, 320–327. doi: 10.1002/ana.22112

Asanad, S., Ross-Cisneros, F. N., Nassisi, M., Barron, E., Karanjia, R., and Sadun, A. A. (2019). The retina in alzheimer's disease: histomorphometric analysis of an ophthalmologic biomarker. *Invest. Ophthalmol. Vis. Sci.* 60, 1491–1500. doi: 10.1167/iovs.18-25966

Aumann, S., Donner, S., Fischer, J., and Muller, F. (2019). "Optical coherence tomography (OCT): principle and technical realization," in *High Resolution Imaging in Microscopy and Ophthalmology: New Frontiers in Biomedical Optics*, ed. J. F. Bille (Cham: Springer), 59–85. doi: 10.1007/978-3-030-16638-0_3

Bakalash, S., Pham, M., Koronyo, Y., Salumbides, B. C., Kramerov, A., Seidenberg, H., et al. (2011). Egr1 expression is induced following glatiramer acetate immunotherapy in rodent models of glaucoma and Alzheimer's disease. *Invest. Ophthalmol. Vis. Sci.* 52, 9033–9046. doi: 10.1167/iovs.11-7498

Baker, M. L., Marino Larsen, E. K., Kuller, L. H., Klein, R., Klein, B. E., Siscovick, D. S., et al. (2007). Retinal microvascular signs, cognitive function, and dementia in older persons: the cardiovascular health study. *Stroke* 38, 2041–2047. doi: 10.1161/strokeaha.107.483586

Banks, W. A., Robinson, S. M., Verma, S., and Morley, J. E. (2003). Efflux of human and mouse amyloid beta proteins 1-40 and 1-42 from brain: impairment in a mouse model of Alzheimer's disease. *Neuroscience* 121, 487–492. doi: 10.1016/s0306-4522(03)00474-3

Barton, S. M., To, E., Rogers, B. P., Whitmore, C., Uppal, M., Matsubara, J. A., et al. (2021). Inhalable Thioflavin S for the detection of amyloid beta deposits in the retina. *Molecules* 26:835. doi: 10.3390/molecules26040835

Bayhan, H. A., Aslan Bayhan, S., Celikbilek, A., Tanik, N., and Gurdal, C. (2015). Evaluation of the chorioretinal thickness changes in Alzheimer's disease using spectral-domain optical coherence tomography. *Clin. Exp. Ophthalmol.* 43, 145–151.

Bell, R. D., and Zlokovic, B. V. (2009). Neurovascular mechanisms and blood-brain barrier disorder in Alzheimer's disease. *Acta Neuropathol.* 118, 103–113. doi: 10.1007/s00401-009-0522-3

Berisha, F., Feke, G. T., Trempe, C. L., Mcmeel, J. W., and Schepens, C. L. (2007). Retinal abnormalities in early Alzheimer's disease. *Invest. Ophthalmol. Vis. Sci.* 48, 2285–2289.

Beskow, J., Hassler, O., and Ottosson, J. O. (1971). Cerebral arterial deformities in relation to senile deterioration. *Acta Psychiatr. Scand. Suppl.* 221, 111–119. doi: 10.1111/j.1600-0447.1971.tb02143.x

Binnewijzend, M. A., Benedictus, M. R., Kuijer, J. P., Van Der Flier, W. M., Teunissen, C. E., Prins, N. D., et al. (2016). Cerebral perfusion in the predementia stages of Alzheimer's disease. *Eur. Radiol.* 26, 506–514. doi: 10.1007/s00330-015-3834-9

Biron, K. E., Dickstein, D. L., Gopaul, R., and Jefferies, W. A. (2011). Amyloid triggers extensive cerebral angiogenesis causing blood brain barrier permeability and hypervascularity in Alzheimer's disease. *PLoS One* 6:e23789. doi: 10.1371/journal.pone.0023789

Blanks, J. C., Hinton, D. R., Sadun, A. A., and Miller, C. A. (1989). Retinal ganglion cell degeneration in Alzheimer's disease. *Brain Res.* 501, 364–372.

Blanks, J. C., Schmidt, S. Y., Torigoe, Y., Porrello, K. V., Hinton, D. R., and Blanks, R. H. (1996). Retinal pathology in Alzheimer's disease, II. Regional neuron loss and glial changes in GCL. *Neurobiol. Aging* 17, 385–395. doi: 10.1016/0197-4580(96)00009-7

Blennow, K., Mattsson, N., Scholl, M., Hansson, O., and Zetterberg, H. (2015). Amyloid biomarkers in Alzheimer's disease. *Trends Pharmacol. Sci.* 36, 297–309.

Bloom, G. S. (2014). Amyloid-beta and tau: the trigger and bullet in Alzheimer disease pathogenesis. *JAMA Neurol.* 71, 505–508. doi: 10.1001/jamaneurol.2013.5847

Bonte, F. J., Ross, E. D., Chehabi, H. H., and Devous, M. D. Sr. (1986). SPECT study of regional cerebral blood flow in Alzheimer disease. *J. Comput. Assist. Tomogr.* 10, 579–583. doi: 10.1097/00004728-198607000-00005

Boyle, P. A., Yu, L., Nag, S., Leurgans, S., Wilson, R. S., Bennett, D. A., et al. (2015). Cerebral amyloid angiopathy and cognitive outcomes in community-based older persons. *Neurology* 85, 1930–1936. doi: 10.1212/wnl.0000000000002175

Bulut, M., Kurtulus, F., Gozkaya, O., Erol, M. K., Cengiz, A., Akidan, M., et al. (2018). Evaluation of optical coherence tomography angiographic findings in Alzheimer's type dementia. *Br. J. Ophthalmol.* 102, 233–237. doi: 10.1136/bjophthalmol-2017-310476

Bulut, M., Yaman, A., Erol, M. K., Kurtuluş, F., Toslak, D., Doğan, B., et al. (2016). Choroidal thickness in patients with mild cognitive impairment and Alzheimer's type dementia. *J. Ophthalmol.* 2016:7291257.

Butovsky, O., Koronyo-Hamaoui, M., Kunis, G., Ophir, E., Landa, G., Cohen, H., et al. (2006). Glatiramer acetate fights against Alzheimer's disease by inducing dendritic-like microglia expressing insulin-like growth factor 1. *Proc. Natl. Acad. Sci. U.S.A.* 103, 11784–11789. doi: 10.1073/pnas.0604681103

Cabrera DeBuc, D., Somfai, G. M., Arthur, E., Kostic, M., Oropesa, S., and Mendoza Santiesteban, C. (2018). Investigating multimodal diagnostic eye biomarkers of cognitive impairment by measuring vascular and neurogenic changes in the retina. *Front. Physiol.* 9:1721. doi: 10.3389/fphys.2018.01721

Cai, Z., Qiao, P. F., Wan, C. Q., Cai, M., Zhou, N. K., and Li, Q. (2018). Role of blood-brain barrier in Alzheimer's Disease. *J. Alzheimers Dis.* 63, 1223–1234.

Campbell, M., and Humphries, P. (2012). The blood-retina barrier: tight junctions and barrier modulation. *Adv. Exp. Med. Biol.* 763, 70–84. doi: 10.1007/978-1-4614-4711-5_3

Cao, K. J., Kim, J. H., Kroeger, H., Gaffney, P. M., Lin, J. H., Sigurdson, C. J., et al. (2021). ARCAM-1 facilitates fluorescence detection of amyloid-containing deposits in the retina. *Transl. Vis. Sci. Technol.* 10:5. doi: 10.1167/tvst.10.7.5

Castillo-Carranza, D. L., Nilson, A. N., Van Skike, C. E., Jahrling, J. B., Patel, K., Garach, P., et al. (2017). Cerebral microvascular accumulation of tau oligomers in Alzheimer's Disease and related tauopathies. *Aging Dis.* 8, 257–266. doi: 10.14336/ad.2017.0112

Chalam, K. V., and Sambhav, K. (2016). Optical coherence tomography angiography in retinal diseases. *J. Ophthalmic. Vis. Res.* 11, 84–92.

Cheung, C. Y., Ong, Y. T., Ikram, M. K., Ong, S. Y., Li, X., Hilal, S., et al. (2014). Microvascular network alterations in the retina of patients with Alzheimer's disease. *Alzheimers Demen.* 10, 135–142. doi: 10.1016/j.jalz.2013.06.009

Chiasseu, M., Alarcon-Martinez, L., Belforte, N., Quintero, H., Dotigny, F., Destroismaisons, L., et al. (2017). Tau accumulation in the retina promotes early neuronal dysfunction and precedes brain pathology in a mouse model of Alzheimer's disease. *Mol. Neurodegener.* 12:58.

Chibhabha, F., Yang, Y., Ying, K., Jia, F., Zhang, Q., Ullah, S., et al. (2020). Non-invasive optical imaging of retinal Aβ plaques using curcumin loaded polymeric micelles in APP(swe)/PS1(ΔE9) transgenic mice for the diagnosis of Alzheimer's disease. *J. Mater Chem. B* 8, 7438–7452. doi: 10.1039/d0tb01101k

Chintapaludi, S. R., Uyar, A., Jackson, H. M., Acklin, C. J., Wang, X., Sasner, M., et al. (2020). Staging Alzheimer's Disease in the brain and retina of B6.APP/PS1 mice by transcriptional profiling. *J. Alzheimers Dis.* 73, 1421–1434. doi: 10.3233/jad-190793

Cisternas, P., Taylor, X., and Lasagna-Reeves, C. A. (2019). The Amyloid-Tau-Neuroinflammation axis in the context of cerebral amyloid angiopathy. *Int. J. Mol. Sci.* 20:6319. doi: 10.3390/ijms20246319

Claudio, L. (1996). Ultrastructural features of the blood-brain barrier in biopsy tissue from Alzheimer's disease patients. *Acta Neuropathol.* 91, 6–14. doi: 10.1007/s004010050386

Coppola, G., Di Renzo, A., Ziccardi, L., Martelli, F., Fadda, A., Manni, G., et al. (2015). Optical coherence tomography in Alzheimer's Disease: a meta-analysis. *PLoS One* 10:e0134750. doi: 10.1371/journal.pone.0134750

Crair, M. C., and Mason, C. A. (2016). Reconnecting eye to brain. *J. Neurosci.* 36, 10707–10722. doi: 10.1523/jneurosci.1711-16.2016

Cunha, J. P., Proença, R., Dias-Santos, A., Melancia, D., Almeida, R., Águas, H., et al. (2017). Choroidal thinning: Alzheimer's disease and aging. *Alzheimers Demen. (Amst.)* 8, 11–17.

Cunha, L. P., Almeida, A. L., Costa-Cunha, L. V., Costa, C. F., and Monteiro, M. L. (2016). The role of optical coherence tomography in Alzheimer's disease. *Int. J. Retina Vitreous* 2:24.

Cunha-Vaz, J. (2017). The blood-retinal barrier in the management of retinal disease: EURETINA award lecture. *Ophthalmologica* 237, 1–10. doi: 10.1159/000455809

Cunha-Vaz, J., Bernardes, R., and Lobo, C. (2011). Blood-retinal barrier. *Eur. J. Ophthalmol.* 21(Suppl. 6), S3–S9.

Cunha-Vaz, J., Santos, T., Alves, D., Marques, I., Neves, C., Soares, M., et al. (2017). Agreement between OCT leakage and fluorescein angiography to identify sites of alteration of the blood-retinal barrier in diabetes. *Ophthalmol. Retina* 1, 395–403. doi: 10.1016/j.oret.2017.02.002

Cunha-Vaz, J., Santos, T., Ribeiro, L., Alves, D., Marques, I., and Goldberg, M. (2016). OCT-Leakage: a new method to identify and locate abnormal fluid accumulation in diabetic retinal edema. *Invest. Ophthalmol. Vis. Sci.* 57, 6776–6783. doi: 10.1167/iovs.16-19999

Curcio, C. A., and Drucker, D. N. (1993). Retinal ganglion cells in Alzheimer's disease and aging. *Ann. Neurol.* 33, 248–257. doi: 10.1002/ana.410330305

Czako, C., Kovacs, T., Ungvari, Z., Csiszar, A., Yabluchanskiy, A., Conley, S., et al. (2020). Retinal biomarkers for Alzheimer's disease and vascular cognitive impairment and dementia (VCID): implication for early diagnosis and prognosis. *Geroscience* 42, 1499–1525. doi: 10.1007/s11357-020-00252-7

Da Mesquita, S., Louveau, A., Vaccari, A., Smirnov, I., Cornelison, R. C., Kingsmore, K. M., et al. (2018). Publisher correction: functional aspects of meningeal lymphatics in ageing and Alzheimer's disease. *Nature* 564:E7.

de Carlo, T. E., Romano, A., Waheed, N. K., and Duker, J. S. (2015). A review of optical coherence tomography angiography (OCTA). *Int. J. Retina Vitreous* 1:5.

Deal, J. A., Sharrett, A. R., Rawlings, A. M., Gottesman, R. F., Bandeen-Roche, K., Albert, M., et al. (2018). Retinal signs and 20-year cognitive decline in the Atherosclerosis Risk in Communities Study. *Neurology* 90, e1158–e1166.

DeMattos, R. B., Bales, K. R., Cummins, D. J., Paul, S. M., and Holtzman, D. M. (2002). Brain to plasma amyloid-beta efflux: a measure of brain amyloid burden in a mouse model of Alzheimer's disease. *Science* 295, 2264–2267. doi: 10.1126/science.1067568

den Haan, J., Morrema, T. H. J., Rozemuller, A. J., Bouwman, F. H., and Hoozemans, J. J. M. (2018a). Different curcumin forms selectively bind fibrillar amyloid beta in post mortem Alzheimer's disease brains: implications for in-vivo diagnostics. *Acta Neuropathol. Commun.* 6:75.

den Haan, J., Morrema, T. H. J., Verbraak, F. D., De Boer, J. F., Scheltens, P., Rozemuller, A. J., et al. (2018b). Amyloid-beta and phosphorylated tau in post-mortem Alzheimer's disease retinas. *Acta Neuropathol. Commun.* 6:147.

Desai, B. S., Schneider, J. A., Li, J. L., Carvey, P. M., and Hendey, B. (2009). Evidence of angiogenic vessels in Alzheimer's disease. *J. Neural. Transm. (Vienna)* 116, 587–597. doi: 10.1007/s00702-009-0226-9

DeSimone, C. V., Graff-Radford, J., El-Harasis, M. A., Rabinstein, A. A., Asirvatham, S. J., and Holmes, D. R. Jr. (2017). Cerebral amyloid angiopathy: diagnosis. clinical implications, and management strategies in atrial fibrillation. *J. Am. Coll. Cardiol.* 70, 1173–1182.

Dickerson, B. C., Salat, D. H., Bates, J. F., Atiya, M., Killiany, R. J., Greve, D. N., et al. (2004). Medial temporal lobe function and structure in mild cognitive impairment. *Ann. Neurol.* 56, 27–35. doi: 10.1002/ana.20163

Do carmo, A., Ramos, P., Reis, A., Proenca, R., and Cunha-Vaz, J. G. (1998). Breakdown of the inner and outer blood retinal barrier in streptozotocin-induced diabetes. *Exp. Eye Res.* 67, 569–575. doi: 10.1006/exer.1998.0546

Do, T. M., Dodacki, A., Alata, W., Calon, F., Nicolic, S., Scherrmann, J. M., et al. (2015). Age-Dependent regulation of the blood-brain barrier influx/efflux equilibrium of amyloid-beta peptide in a mouse model of Alzheimer's Disease (3xTg-AD). *J. Alzheimers Dis.* 49, 287–300. doi: 10.3233/jad-150350

Doustar, J., Rentsendorj, A., Torbati, T., Regis, G. C., Fuchs, D. T., Sheyn, J., et al. (2020). Parallels between retinal and brain pathology and response to immunotherapy in old, late-stage Alzheimer's disease mouse models. *Aging Cell* 19:e13246.

Doustar, J., Torbati, T., Black, K. L., Koronyo, Y., and Koronyo-Hamaoui, M. (2017). Optical coherence tomography in Alzheimer's Disease and other neurodegenerative diseases. *Front. Neurol.* 8:701. doi: 10.3389/fneur.2017.00701

Drzezga, A., Grimmer, T., Henriksen, G., Stangier, I., Perneczky, R., Diehl-Schmid, J., et al. (2008). Imaging of amyloid plaques and cerebral glucose metabolism in semantic dementia and Alzheimer's disease. *Neuroimage* 39, 619–633. doi: 10.1016/j.neuroimage.2007.09.020

Du, L. Y., Chang, L. Y., Ardiles, A. O., Tapia-Rojas, C., Araya, J., Inestrosa, N. C., et al. (2015). Alzheimer's Disease-related protein expression in the retina of octodon degus. *PLoS One* 10:e0135499. doi: 10.1371/journal.pone.0135499

Dumitrascu, O. M., and Koronyo-Hamaoui, M. (2020). Retinal vessel changes in cerebrovascular disease. *Curr. Opin. Neurol.* 33, 87–92. doi: 10.1097/wco.0000000000000779

Dumitrascu, O. M., Lyden, P. D., Torbati, T., Sheyn, J., Sherzai, A., Sherzai, D., et al. (2020). Sectoral segmentation of retinal amyloid imaging in subjects with cognitive decline. *Alzheimers Demen. (Amst.)* 12:e12109.

Dutescu, R. M., Li, Q. X., Crowston, J., Masters, C. L., Baird, P. N., and Culvenor, J. G. (2009). Amyloid precursor protein processing and retinal pathology in mouse models of Alzheimer's disease. *Graefes Arch. Clin. Exp. Ophthalmol.* 247, 1213–1221. doi: 10.1007/s00417-009-1060-3

Einarsdottir, A. B., Hardarson, S. H., Kristjansdottir, J. V., Bragason, D. T., Snaedal, J., and Stefansson, E. (2016). Retinal oximetry imaging in Alzheimer's disease. *J. Alzheimers Dis.* 49, 79–83. doi: 10.3233/jad-150457

Ellis, R. J., Olichney, J. M., Thal, L. J., Mirra, S. S., Morris, J. C., Beekly, D., et al. (1996). Cerebral amyloid angiopathy in the brains of patients with Alzheimer's disease: the CERAD experience, Part XV. *Neurology* 46, 1592–1596. doi: 10.1212/wnl.46.6.1592

Engler, H., Forsberg, A., Almkvist, O., Blomquist, G., Larsson, E., Savitcheva, I., et al. (2006). Two-year follow-up of amyloid deposition in patients with Alzheimer's disease. *Brain* 129, 2856–2866. doi: 10.1093/brain/awl178

Erskine, L., and Herrera, E. (2014). Connecting the retina to the brain. *ASN Neuro* 6:1759091414562107.

Feke, G. T., Hyman, B. T., Stern, R. A., and Pasquale, L. R. (2015). Retinal blood flow in mild cognitive impairment and Alzheimer's disease. *Alzheimers Demen. (Amst.)* 1, 144–151.

Ferrari, L., Huang, S. C., Magnani, G., Ambrosi, A., Comi, G., and Leocani, L. (2017). Optical coherence tomography reveals retinal neuroaxonal thinning in frontotemporal dementia as in Alzheimer's Disease. *J. Alzheimers Dis.* 56, 1101–1107. doi: 10.3233/jad-160886

Fischer, V. W., Siddiqi, A., and Yusufaly, Y. (1990). Altered angioarchitecture in selected areas of brains with Alzheimer's disease. *Acta Neuropathol.* 79, 672–679. doi: 10.1007/bf00294246

Fisichella, V., Giurdanella, G., Platania, C. B., Romano, G. L., Leggio, G. M., Salomone, S., et al. (2016). TGF-beta1 prevents rat retinal insult induced by amyloid-beta (1-42) oligomers. *Eur. J. Pharmacol.* 787, 72–77. doi: 10.1016/j.ejphar.2016.02.002

Foster, N. L., Chase, T. N., Fedio, P., Patronas, N. J., Brooks, R. A., and Di Chiro, G. (1983). Alzheimer's disease: focal cortical changes shown by positron emission tomography. *Neurology* 33, 961–965. doi: 10.1212/wnl.33.8.961

Frohman, E. M., Fujimoto, J. G., Frohman, T. C., Calabresi, P. A., Cutter, G., and Balcer, L. J. (2008). Optical coherence tomography: a window into the mechanisms of multiple sclerosis. *Nat. Clin. Pract. Neurol.* 4, 664–675.

Frost, S., Kanagasingam, Y., Sohrabi, H., Vignarajan, J., Bourgeat, P., Salvado, O., et al. (2013). Retinal vascular biomarkers for early detection and monitoring of Alzheimer's disease. *Transl. Psychiatry* 3:e233. doi: 10.1038/tp.2012.150

Gabin, J. M., Tambs, K., Saltvedt, I., Sund, E., and Holmen, J. (2017). Association between blood pressure and Alzheimer disease measured up to 27 years prior to diagnosis: the HUNT Study. *Alzheimers Res. Ther.* 9:37.

Gao, L., Liu, Y., Li, X., Bai, Q., and Liu, P. (2015). Abnormal retinal nerve fiber layer thickness and macula lutea in patients with mild cognitive impairment and Alzheimer's disease. *Arch. Gerontol. Geriatr.* 60, 162–167. doi: 10.1016/j.archger.2014.10.011

Gharbiya, M., Trebbastoni, A., Parisi, F., Manganiello, S., Cruciani, F., D'antonio, F., et al. (2014). Choroidal thinning as a new finding in Alzheimer's disease: evidence from enhanced depth imaging spectral domain optical coherence tomography. *J. Alzheimers Dis.* 40, 907–917. doi: 10.3233/jad-132039

Ghiso, J., Tomidokoro, Y., Revesz, T., Frangione, B., and Rostagno, A. (2010). Cerebral Amyloid Angiopathy And Alzheimer's Disease. *Hirosaki Igaku* 61, S111–S124.

Govindpani, K., Mcnamara, L. G., Smith, N. R., Vinnakota, C., Waldvogel, H. J., Faull, R. L., et al. (2019). Vascular dysfunction in Alzheimer's Disease: a prelude to the pathological process or a consequence of it? *J. Clin. Med.* 8:651. doi: 10.3390/jcm8050651

Grammas, P., and Ovase, R. (2001). Inflammatory factors are elevated in brain microvessels in Alzheimer's disease. *Neurobiol. Aging* 22, 837–842. doi: 10.1016/s0197-4580(01)00276-7

Gravina, S. A., Ho, L., Eckman, C. B., Long, K. E., Otvos, L. Jr., Younkin, L. H., et al. (1995). Amyloid beta protein (A beta) in Alzheimer's disease brain. Biochemical and immunocytochemical analysis with antibodies specific for forms ending at A beta 40 or A beta 42(43). *J. Biol. Chem.* 270, 7013–7016.

Grimaldi, A., Brighi, C., Peruzzi, G., Ragozzino, D., Bonanni, V., Limatola, C., et al. (2018). Inflammation, neurodegeneration and protein aggregation in the retina as ocular biomarkers for Alzheimer's disease in the 3xTg-AD mouse model. *Cell Death Dis.* 9:685.

Grimaldi, A., Pediconi, N., Oieni, F., Pizzarelli, R., Rosito, M., Giubettini, M., et al. (2019). Neuroinflammatory Processes. A1 astrocyte activation and protein aggregation in the retina of alzheimer's disease patients, possible biomarkers for early diagnosis. *Front Neurosci* 13:925. doi: 10.3389/fnins.2019.00925

Guo, L., Duggan, J., and Cordeiro, M. F. (2010). Alzheimer's disease and retinal neurodegeneration. *Curr. Alzheimer Res.* 7, 3–14. doi: 10.2174/156720510790274491

Habiba, U., Descallar, J., Kreilaus, F., Adhikari, U. K., Kumar, S., Morley, J. W., et al. (2021). Detection of retinal and blood Abeta oligomers with nanobodies. *Alzheimers Demen. (Amst.)* 13:e12193.

Hadoux, X., Hui, F., Lim, J. K. H., Masters, C. L., Pebay, A., Chevalier, S., et al. (2019). Non-invasive in vivo hyperspectral imaging of the retina for potential biomarker use in Alzheimer's disease. *Nat. Commun.* 10:4227.

Hagag, A. M., Gao, S. S., Jia, Y., and Huang, D. (2017). Optical coherence tomography angiography: technical principles and clinical applications in ophthalmology. *Taiwan J. Ophthalmol.* 7, 115–129. doi: 10.4103/tjo.tjo_31_17

Harik, S. I. (1992). Changes in the glucose transporter of brain capillaries. *Can. J. Physiol. Pharmacol.* 70(Suppl.), S113–S117.

Harrison, I. F., Whitaker, R., Bertelli, P. M., O'callaghan, J. M., Csincsik, L., Bocchetta, M., et al. (2019). Optic nerve thinning and neurosensory retinal degeneration in the rTg4510 mouse model of frontotemporal dementia. *Acta Neuropathol. Commun.* 7:4.

Hart, N. J., Koronyo, Y., Black, K. L., and Koronyo-Hamaoui, M. (2016). Ocular indicators of Alzheimer's: exploring disease in the retina. *Acta Neuropathol.* 132, 767–787. doi: 10.1007/s00401-016-1613-6

Hassler, O. (1965). Vascular changes in senile brains. A micro-angiographic study. *Acta Neuropathol.* 5, 40–53. doi: 10.1007/bf00689161

Higuchi, Y., Miyakawa, T., Shimoji, A., and Katsuragi, S. (1987). Ultrastructural changes of blood vessels in the cerebral cortex in Alzheimer's disease. *Jpn. J. Psychiatry Neurol.* 41, 283–290. doi: 10.1111/j.1440-1819.1987.tb00414.x

Hinton, D. R., Sadun, A. A., Blanks, J. C., and Miller, C. A. (1986). Optic-nerve degeneration in Alzheimer's disease. *N. Engl. J. Med.* 315, 485–487.

Hirsch, C., Bartenstein, P., Minoshima, S., Mosch, D., Willoch, F., Buch, K., et al. (1997). Reduction of regional cerebral blood flow and cognitive impairment in patients with Alzheimer's disease: evaluation of an observer-independent analytic approach. *Demen. Geriatr. Cogn. Disord.* 8, 98–104. doi: 10.1159/000106613

Ho, C. Y., Troncoso, J. C., Knox, D., Stark, W., and Eberhart, C. G. (2014). Beta-amyloid, phospho-tau and alpha-synuclein deposits similar to those in the brain are not identified in the eyes of Alzheimer's and Parkinson's disease patients. *Brain Pathol.* 24, 25–32. doi: 10.1111/bpa.12070

Hoffman, J. M., Welsh-Bohmer, K. A., Hanson, M., Crain, B., Hulette, C., Earl, N., et al. (2000). FDG PET imaging in patients with pathologically verified dementia. *J. Nucl. Med.* 41, 1920–1928.

Iadecola, C., Duering, M., Hachinski, V., Joutel, A., Pendlebury, S. T., Schneider, J. A., et al. (2019). Vascular cognitive impairment and dementia: JACC scientific expert panel. *J. Am. Coll. Cardiol.* 73, 3326–3344.

Ikonomovic, M. D., Klunk, W. E., Abrahamson, E. E., Mathis, C. A., Price, J. C., Tsopelas, N. D., et al. (2008). Post-mortem correlates of in vivo PiB-PET amyloid imaging in a typical case of Alzheimer's disease. *Brain* 131, 1630–1645. doi: 10.1093/brain/awn016

Inestrosa, N. C., Reyes, A. E., Chacon, M. A., Cerpa, W., Villalon, A., Montiel, J., et al. (2005). Human-like rodent amyloid-beta-peptide determines Alzheimer pathology in aged wild-type Octodon degu. *Neurobiol. Aging* 26, 1023–1028. doi: 10.1016/j.neurobiolaging.2004.09.016

Jack, C.R., Jr, Bennett, D. A., Blennow, K., Carrillo, M. C., Dunn, B., Haeberlein, S. B., et al. (2018). NIA-AA research framework: toward a biological definition of Alzheimer's disease. *Alzheimers Demen.* 14, 535–562. doi: 10.1016/j.jalz.2018.02.018

Janez-Escalada, L., Janez-Garcia, L., Salobrar-Garcia, E., Santos-Mayo, A., De Hoz, R., Yubero, R., et al. (2019). Spatial analysis of thickness changes in ten retinal layers of Alzheimer's disease patients based on optical coherence tomography. *Sci. Rep.* 9:13000.

Jankowsky, J. L., Xu, G., Fromholt, D., Gonzales, V., and Borchelt, D. R. (2003). Environmental enrichment exacerbates amyloid plaque formation in a transgenic mouse model of Alzheimer disease. *J. Neuropathol. Exp. Neurol.* 62, 1220–1227. doi: 10.1093/jnen/62.12.1220

Jessen, N. A., Munk, A. S., Lundgaard, I., and Nedergaard, M. (2015). The glymphatic system: a beginner's guide. *Neurochem. Res.* 40, 2583–2599.

Jiang, H., Wei, Y., Shi, Y., Wright, C. B., Sun, X., Gregori, G., et al. (2018). Altered macular microvasculature in mild cognitive impairment and Alzheimer Disease. *J. Neuroophthalmol.* 38, 292–298. doi: 10.1097/wno.0000000000000580

Johnson, K. A., Fox, N. C., Sperling, R. A., and Klunk, W. E. (2012). Brain imaging in Alzheimer disease. *Cold Spring Harb. Perspect. Med.* 2:a006213.

Johnson, S. C., Schmitz, T. W., Moritz, C. H., Meyerand, M. E., Rowley, H. A., Alexander, A. L., et al. (2006). Activation of brain regions vulnerable to Alzheimer's disease: the effect of mild cognitive impairment. *Neurobiol. Aging* 27, 1604–1612. doi: 10.1016/j.neurobiolaging.2005.09.017

Jung, N. Y., Han, J. C., Ong, Y. T., Cheung, C. Y., Chen, C. P., Wong, T. Y., et al. (2019). Retinal microvasculature changes in amyloid-negative subcortical vascular cognitive impairment compared to amyloid-positive Alzheimer's disease. *J. Neurol. Sci.* 396, 94–101. doi: 10.1016/j.jns.2018.10.025

Kalaria, R. N., and Harik, S. I. (1989). Reduced glucose transporter at the blood-brain barrier and in cerebral cortex in Alzheimer disease. *J. Neurochem.* 53, 1083–1088. doi: 10.1111/j.1471-4159.1989.tb07399.x

Kalaria, R. N., and Kroon, S. N. (1992). Expression of leukocyte antigen CD34 by brain capillaries in Alzheimer's disease and neurologically normal subjects. *Acta Neuropathol.* 84, 606–612.

Kapasi, A., and Schneider, J. A. (2016). Vascular contributions to cognitive impairment, clinical Alzheimer's disease, and dementia in older persons. *Biochim. Biophys. Acta* 1862, 878–886. doi: 10.1016/j.bbadis.2015.12.023

Kashani, A. H., Chen, C. L., Gahm, J. K., Zheng, F., Richter, G. M., Rosenfeld, P. J., et al. (2017). Optical coherence tomography angiography: a comprehensive review of current methods and clinical applications. *Prog. Retin. Eye Res.* 60, 66–100.

Keable, A., Fenna, K., Yuen, H. M., Johnston, D. A., Smyth, N. R., Smith, C., et al. (2016). Deposition of amyloid β in the walls of human leptomeningeal arteries in relation to perivascular drainage pathways in cerebral amyloid angiopathy. *Biochim. Biophys. Acta* 1862, 1037–1046. doi: 10.1016/j.bbadis.2015.08.024

Kergoat, H., Kergoat, M. J., Justino, L., Chertkow, H., Robillard, A., and Bergman, H. (2001). An evaluation of the retinal nerve fiber layer thickness by scanning laser polarimetry in individuals with dementia of the Alzheimer type. *Acta Ophthalmol. Scand.* 79, 187–191. doi: 10.1034/j.1600-0420.2001.079002187.x

Khadamy, J., Abri Aghdam, K., and Falavarjani, K. G. (2018). An update on optical coherence tomography angiography in diabetic retinopathy. *J. Ophthalmic. Vis. Res.* 13, 487–497.

Kirbas, S., Turkyilmaz, K., Anlar, O., Tufekci, A., and Durmus, M. (2013). Retinal nerve fiber layer thickness in patients with Alzheimer disease. *J. Neuroophthalmol.* 33, 58–61. doi: 10.1097/wno.0b013e318267fd5f

Koronyo, Y., Biggs, D., Barron, E., Boyer, D. S., Pearlman, J. A., Au, W. J., et al. (2017). Retinal amyloid pathology and proof-of-concept imaging trial in Alzheimer's disease. *JCI Insight* 2:e93621.

Koronyo, Y., Salumbides, B. C., Black, K. L., and Koronyo-Hamaoui, M. (2012). Alzheimer's disease in the retina: imaging retinal abeta plaques for early diagnosis and therapy assessment. *Neurodegener. Dis.* 10, 285–293. doi: 10.1159/000335154

Koronyo, Y., Salumbides, B. C., Sheyn, J., Pelissier, L., Li, S., Ljubimov, V., et al. (2015). Therapeutic effects of glatiramer acetate and grafted CD115(+) monocytes in a mouse model of Alzheimer's disease. *Brain* 138, 2399–2422. doi: 10.1093/brain/awv150

Koronyo-Hamaoui, M., Ko, M. K., Koronyo, Y., Azoulay, D., Seksenyan, A., Kunis, G., et al. (2009). Attenuation of AD-like neuropathology by harnessing peripheral immune cells: local elevation of IL-10 and MMP-9. *J. Neurochem.* 111, 1409–1424. doi: 10.1111/j.1471-4159.2009.06402.x

Koronyo-Hamaoui, M., Koronyo, Y., Ljubimov, A. V., Miller, C. A., Ko, M. K., Black, K. L., et al. (2011). Identification of amyloid plaques in retinas from Alzheimer's patients and noninvasive in vivo optical imaging of retinal plaques in a mouse model. *Neuroimage* 54(Suppl. 1), S204–S217.

Kromer, R., Serbecic, N., Hausner, L., Froelich, L., Aboul-Enein, F., and Beutelspacher, S. C. (2014). Detection of retinal nerve fiber layer defects in Alzheimer's Disease using SD-OCT. *Front Psychiatry* 5:22. doi: 10.3389/fpsyt.2014.00022

La Morgia, C., Ross-Cisneros, F. N., Koronyo, Y., Hannibal, J., Gallassi, R., Cantalupo, G., et al. (2016). Melanopsin retinal ganglion cell loss in Alzheimer disease. *Ann. Neurol.* 79, 90–109.

Lahiri, S., Regis, G. C., Koronyo, Y., Fuchs, D. T., Sheyn, J., Kim, E. H., et al. (2019). Acute neuropathological consequences of short-term mechanical ventilation in wild-type and Alzheimer's disease mice. *Crit. Care* 23:63.

Lahme, L., Esser, E. L., Mihailovic, N., Schubert, F., Lauermann, J., Johnen, A., et al. (2018). Evaluation of ocular perfusion in Alzheimer's Disease using optical coherence tomography angiography. *J. Alzheimers Dis.* 66, 1745–1752. doi: 10.3233/jad-180738

Lang, G. E. (2007). Optical coherence tomography findings in diabetic retinopathy. *Dev. Ophthalmol.* 39, 31–47. doi: 10.1159/000098498

Launer, L. J. (2002). Demonstrating the case that AD is a vascular disease: epidemiologic evidence. *Ageing Res. Rev.* 1, 61–77. doi: 10.1016/s0047-6374(01)00364-5

Lee, J. Y., Kim, J. P., Jang, H., Kim, J., Kang, S. H., Kim, J. S., et al. (2020). Optical coherence tomography angiography as a potential screening tool for cerebral small vessel diseases. *Alzheimers Res. Ther.* 12:73.

Lee, S., Jiang, K., Mcilmoyle, B., To, E., Xu, Q. A., Hirsch-Reinshagen, V., et al. (2020). Amyloid beta immunoreactivity in the retinal ganglion cell layer of the Alzheimer's Eye. *Front. Neurosci.* 14:758. doi: 10.3389/fnins.2020.00758

Lemmens, S., Van Craenendonck, T., Van Eijgen, J., De Groef, L., Bruffaerts, R., De Jesus, D. A., et al. (2020). Combination of snapshot hyperspectral retinal imaging and optical coherence tomography to identify Alzheimer's disease patients. *Alzheimers Res. Ther.* 12:144.

Li, M., Li, Y., Zuo, L., Hu, W., and Jiang, T. (2021). Increase of blood-brain barrier leakage is related to cognitive decline in vascular mild cognitive impairment. *BMC Neurol.* 21:159. doi: 10.1186/s12883-021-02189-6

Liu, B., Rasool, S., Yang, Z., Glabe, C. G., Schreiber, S. S., Ge, J., et al. (2009). Amyloid-peptide vaccinations reduce {beta}-amyloid plaques but exacerbate vascular deposition and inflammation in the retina of Alzheimer's transgenic mice. *Am. J. Pathol.* 175, 2099–2110. doi: 10.2353/ajpath.2009.090159

Liu, D., Zhang, L., Li, Z., Zhang, X., Wu, Y., Yang, H., et al. (2015). Thinner changes of the retinal nerve fiber layer in patients with mild cognitive impairment and Alzheimer's disease. *BMC Neurol.* 15:14. doi: 10.1186/s12883-015-0268-6

Louveau, A., Smirnov, I., Keyes, T. J., Eccles, J. D., Rouhani, S. J., Peske, J. D., et al. (2015). Structural and functional features of central nervous system lymphatic vessels. *Nature* 523, 337–341. doi: 10.1038/nature14432

Machulda, M. M., Ward, H. A., Borowski, B., Gunter, J. L., Cha, R. H., O'brien, P. C., et al. (2003). Comparison of memory fMRI response among normal, MCI, and Alzheimer's patients. *Neurology* 61, 500–506. doi: 10.1212/01.wnl.0000079052.01016.78

Marchesi, V. T. (2011). Alzheimer's dementia begins as a disease of small blood vessels, damaged by oxidative-induced inflammation and dysregulated amyloid metabolism: implications for early detection and therapy. *FASEB J.* 25, 5–13. doi: 10.1096/fj.11-0102ufm

Marmor, M. F., and Ravin, J. G. (2011). Fluorescein angiography: insight and serendipity a half century ago. *Arch. Ophthalmol.* 129, 943–948. doi: 10.1001/archophthalmol.2011.160

Marziani, E., Pomati, S., Ramolfo, P., Cigada, M., Giani, A., Mariani, C., et al. (2013). Evaluation of retinal nerve fiber layer and ganglion cell layer thickness in Alzheimer's disease using spectral-domain optical coherence tomography. *Invest. Ophthalmol. Vis. Sci.* 54, 5953–5958. doi: 10.1167/iovs.13-12046

Matsuzaki, T., Sasaki, K., Hata, J., Hirakawa, Y., Fujimi, K., Ninomiya, T., et al. (2011). Association of Alzheimer disease pathology with abnormal lipid metabolism: the Hisayama Study. *Neurology* 77, 1068–1075. doi: 10.1212/wnl.0b013e31822e145d

McGrory, S., Cameron, J. R., Pellegrini, E., Warren, C., Doubal, F. N., Deary, I. J., et al. (2017). The application of retinal fundus camera imaging in dementia: a systematic review. *Alzheimers Demen. (Amst.)* 6, 91–107. doi: 10.1016/j.dadm.2016.11.001

Medical Advisory, S. (2009). Optical coherence tomography for age-related macular degeneration and diabetic macular edema: an evidence-based analysis. *Ont. Health Technol. Assess. Ser.* 9, 1–22. doi: 10.1007/978-3-642-01467-3_1

Mehndiratta, P., Manjila, S., Ostergard, T., Eisele, S., Cohen, M. L., Sila, C., et al. (2012). Cerebral amyloid angiopathy-associated intracerebral hemorrhage: pathology and management. *Neurosurg. Focus* 32:E7.

Mejia-Vergara, A. J., Karanjia, R., and Sadun, A. A. (2021). OCT parameters of the optic nerve head and the retina as surrogate markers of brain volume in a normal population, a pilot study. *J. Neurol. Sci.* 420:117213. doi: 10.1016/j.jns.2020.117213

Mirzaei, N., Shi, H., Oviatt, M., Doustar, J., Rentsendorj, A., Fuchs, D.-T., et al. (2020). Alzheimer's retinopathy: seeing disease in the eyes. *Front. Neurosci.* 14:921. doi: 10.3389/fnins.2020.00921

Montagne, A., Nation, D. A., Sagare, A. P., Barisano, G., Sweeney, M. D., Chakhoyan, A., et al. (2020). APOE4 leads to blood-brain barrier dysfunction predicting cognitive decline. *Nature* 581, 71–76. doi: 10.1038/s41586-020-2247-3

More, S. S., Beach, J. M., Mcclelland, C., Mokhtarzadeh, A., and Vince, R. (2019). In vivo assessment of retinal biomarkers by hyperspectral imaging: early detection of Alzheimer's Disease. *ACS Chem. Neurosci.* 10, 4492–4501. doi: 10.1021/acschemneuro.9b00331

Moreno-Ramos, T., Benito-Leon, J., Villarejo, A., and Bermejo-Pareja, F. (2013). Retinal nerve fiber layer thinning in dementia associated with Parkinson's disease, dementia with Lewy bodies, and Alzheimer's disease. *J. Alzheimers Dis.* 34, 659–664. doi: 10.3233/jad-121975

Morin, P. J., Abraham, C. R., Amaratunga, A., Johnson, R. J., Huber, G., Sandell, J. H., et al. (1993). Amyloid precursor protein is synthesized by retinal ganglion cells, rapidly transported to the optic nerve plasma membrane and nerve terminals, and metabolized. *J. Neurochem.* 61, 464–473. doi: 10.1111/j.1471-4159.1993.tb02147.x

Moschos, M. M., Markopoulos, I., Chatziralli, I., Rouvas, A., Papageorgiou, S. G., Ladas, I., et al. (2012). Structural and functional impairment of the retina and optic nerve in Alzheimer's disease. *Curr. Alzheimer Res.* 9, 782–788. doi: 10.2174/156720512802455340

National Institue on Aging (2019). *Alzheimer's Disease Fact* Sheet. [Online].Available online at: https://www.nia.nih.gov/health/alzheimers-disease-fact-sheet (accessed May 22, 2019).

Newman, E., and Reichenbach, A. (1996). The Muller cell: a functional element of the retina. *Trends Neurosci.* 19, 307–312.

Ngolab, J., Donohue, M., Belsha, A., Salazar, J., Cohen, P., Jaiswal, S., et al. (2021). Feasibility study for detection of retinal amyloid in clinical trials: the Anti-Amyloid Treatment in Asymptomatic Alzheimer's Disease (A4) trial. *Alzheimers Dement (Amst).* 13:e12199. doi: 10.1002/dad2.12199

O'Bryhim, B. E., Apte, R. S., Kung, N., Coble, D., and Van Stavern, G. P. (2018). Association of preclinical Alzheimer Disease with optical coherence tomographic angiography findings. *JAMA Ophthalmol.* 136, 1242–1248. doi: 10.1001/jamaophthalmol.2018.3556

Paquet, C., Boissonnot, M., Roger, F., Dighiero, P., Gil, R., and Hugon, J. (2007). Abnormal retinal thickness in patients with mild cognitive impairment and Alzheimer's disease. *Neurosci. Lett.* 420, 97–99. doi: 10.1016/j.neulet.2007.02.090

Parisi, V., Restuccia, R., Fattapposta, F., Mina, C., Bucci, M. G., and Pierelli, F. (2001). Morphological and functional retinal impairment in Alzheimer's disease patients. *Clin. Neurophysiol.* 112, 1860–1867.

Park, S. W., Kim, J. H., Mook-Jung, I., Kim, K. W., Park, W. J., and Park, K. H. (2014). Intracellular amyloid beta alters the tight junction of retinal pigment epithelium in 5XFAD mice. *Neurobiol. Aging* 35, 2013–2020. doi: 10.1016/j.neurobiolaging.2014.03.008

Parthasarathy, R., Chow, K. M., Derafshi, Z., Fautsch, M. P., Hetling, J. R., Rodgers, D. W., et al. (2015). Reduction of amyloid-beta levels in mouse eye tissues by intra-vitreally delivered neprilysin. *Exp. Eye Res.* 138, 134–144. doi: 10.1016/j.exer.2015.06.027

Patton, N., Aslam, T., Macgillivray, T., Pattie, A., Deary, I. J., and Dhillon, B. (2005). Retinal vascular image analysis as a potential screening tool for cerebrovascular disease: a rationale based on homology between cerebral and retinal microvasculatures. *J. Anat.* 206, 319–348. doi: 10.1111/j.1469-7580.2005.00395.x

Pichi, F., Sarraf, D., Arepalli, S., Lowder, C. Y., Cunningham, E. T. Jr., Neri, P., et al. (2017). The application of optical coherence tomography angiography in uveitis and inflammatory eye diseases. *Prog. Retin. Eye Res.* 59, 178–201. doi: 10.1016/j.preteyeres.2017.04.005

Planton, M., Raposo, N., Albucher, J. F., and Pariente, J. (2017). Cerebral amyloid angiopathy-related cognitive impairment: the search for a specific neuropsychological pattern. *Rev. Neurol. (Paris)* 173, 562–565. doi: 10.1016/j.neurol.2017.09.006

Polans, J., Keller, B., Carrasco-Zevallos, O. M., Larocca, F., Cole, E., Whitson, H. E., et al. (2017). Wide-field retinal optical coherence tomography with wavefront sensorless adaptive optics for enhanced imaging of targeted regions. *Biomed. Opt. Express* 8, 16–37. doi: 10.1364/boe.8.000016

Polo, V., Rodrigo, M. J., Garcia-Martin, E., Otin, S., Larrosa, J. M., Fuertes, M. I., et al. (2017). Visual dysfunction and its correlation with retinal changes in patients with Alzheimer's disease. *Eye (Lond.)* 31, 1034–1041. doi: 10.1038/eye.2017.23

Popescu, D. P., Choo-Smith, L. P., Flueraru, C., Mao, Y., Chang, S., Disano, J., et al. (2011). Optical coherence tomography: fundamental principles, instrumental designs and biomedical applications. *Biophys. Rev.* 3:155. doi: 10.1007/s12551-011-0054-7

Prensa, L. (2014). *Alzheimer's Disease Risk And The Importance Of Brain Health* [Online]. Available online at: https://montgomery.pa.networkofcare.org/mh/news-article-detail.aspx?id=55601 (accessed Jun 7, 2021).

Purves, D. E. A. (ed.) (2001). "The Retina, Chapters 11 and 12," in *Neuroscience*, 2nd Edn (Sunderland, MA: Sinauer Associates).

Qiu, Y., Jin, T., Mason, E., and Campbell, M. C. W. (2020). Predicting thioflavin fluorescence of retinal amyloid deposits associated with Alzheimer's Disease from their polarimetric properties. *Transl. Vis. Sci. Technol.* 9:47. doi: 10.1167/tvst.9.2.47

Rentsendorj, A., Sheyn, J., Fuchs, D. T., Daley, D., Salumbides, B. C., Schubloom, H. E., et al. (2018). A novel role for osteopontin in macrophage-mediated amyloid-beta clearance in Alzheimer's models. *Brain Behav. Immun.* 67, 163–180. doi: 10.1016/j.bbi.2017.08.019

Rifai, O. M., Mcgrory, S., Robbins, C. B., Grewal, D. S., Liu, A., Fekrat, S., et al. (2021). The application of optical coherence tomography angiography in Alzheimer's disease: a systematic review. *Alzheimers Demen. (Amst.)* 13:e12149.

Risacher, S. L., Wudunn, D., Tallman, E. F., West, J. D., Gao, S., Farlow, M. R., et al. (2020). Visual contrast sensitivity is associated with the presence of cerebral amyloid and tau deposition. *Brain Commun.* 2:fcaa019.

Roher, A. E., Garami, Z., Tyas, S. L., Maarouf, C. L., Kokjohn, T. A., Belohlavek, M., et al. (2011). Transcranial doppler ultrasound blood flow velocity and pulsatility index as systemic indicators for Alzheimer's disease. *Alzheimers Dement.* 7, 445–455. doi: 10.1016/j.jalz.2010.09.002

Ryu, J. K., and McLarnon, J. G. (2009). A leaky blood-brain barrier, fibrinogen infiltration and microglial reactivity in inflamed Alzheimer's disease brain. *J. Cell Mol. Med.* 13, 2911–2925. doi: 10.1111/j.1582-4934.2008.00434.x

Sadda, S. R., Borrelli, E., Fan, W., Ebraheem, A., Marion, K. M., Harrington, M., et al. (2019). A pilot study of fluorescence lifetime imaging ophthalmoscopy in preclinical Alzheimer's disease. *Eye (Lond.)* 33, 1271–1279. doi: 10.1038/s41433-019-0406-2

Sadun, A. A., and Bassi, C. J. (1990). Optic nerve damage in Alzheimer's disease. *Ophthalmology* 97, 9–17. doi: 10.1016/s0161-6420(90)32621-0

Salobrar-Garcia, E., De Hoz, R., Ramirez, A. I., Lopez-Cuenca, I., Rojas, P., Vazirani, R., et al. (2019). Changes in visual function and retinal structure in the progression of Alzheimer's disease. *PLoS One* 14:e0220535. doi: 10.1371/journal.pone.0220535

Sathyan, P., Shilpa, S., and Anitha, A. (2012). Optical coherence tomography in glaucoma. *J. Curr. Glaucoma Pract.* 6, 1–5.

Schallek, J., Geng, Y., Nguyen, H., and Williams, D. R. (2013). Morphology and topography of retinal pericytes in the living mouse retina using in vivo adaptive optics imaging and ex vivo characterization. *Invest. Ophthalmol. Vis. Sci.* 54, 8237–8250.

Schneider, E. W., and Fowler, S. C. (2018). Optical coherence tomography angiography in the management of age-related macular degeneration. *Curr. Opin. Ophthalmol.* 29, 217–225.

Schon, C., Hoffmann, N. A., Ochs, S. M., Burgold, S., Filser, S., Steinbach, S., et al. (2012). Long-term in vivo imaging of fibrillar tau in the retina of P301S transgenic mice. *PLoS One* 7:e53547. doi: 10.1371/journal.pone.0053547

Schultz, N., Byman, E., Netherlands Brain, B., and Wennstrom, M. (2020). Levels of retinal amyloid-beta correlate with levels of retinal IAPP and hippocampal amyloid-beta in neuropathologically evaluated individuals. *J. Alzheimers Dis.* 73, 1201–1209. doi: 10.3233/jad-190868

Selkoe, D. J., and Hardy, J. (2016). The amyloid hypothesis of Alzheimer's disease at 25 years. *EMBO Mol. Med.* 8, 595–608.

Sengillo, J. D., Winkler, E. A., Walker, C. T., Sullivan, J. S., Johnson, M., and Zlokovic, B. V. (2013). Deficiency in mural vascular cells coincides with blood-brain barrier disruption in Alzheimer's disease. *Brain Pathol.* 23, 303–310. doi: 10.1111/bpa.12004

Shi, H., Koronyo, Y., Fuchs, D. T., Sheyn, J., Wawrowsky, K., Lahiri, S., et al. (2020a). Retinal capillary degeneration and blood-retinal barrier disruption in murine models of Alzheimer's disease. *Acta Neuropathol. Commun.* 8:202.

Shi, H., Koronyo, Y., Rentsendorj, A., Regis, G. C., Sheyn, J., Fuchs, D. T., et al. (2020b). Identification of early pericyte loss and vascular amyloidosis in Alzheimer's disease retina. *Acta Neuropathol.* 139, 813–836. doi: 10.1007/s00401-020-02134-w

Shi, Z., Wu, Y., Wang, M., Cao, J., Feng, W., Cheng, Y., et al. (2014). Greater attenuation of retinal nerve fiber layer thickness in Alzheimer's disease patients. *J. Alzheimers Dis.* 40, 277–283. doi: 10.3233/jad-131898

Sidiqi, A., Wahl, D., Lee, S., Ma, D., To, E., Cui, J., et al. (2020). In vivo retinal fluorescence imaging with curcumin in an alzheimer mouse model. *Front. Neurosci.* 14:713. doi: 10.3389/fnins.2020.00713

Slemmon, J. R., Hughes, C. M., Campbell, G. A., and Flood, D. G. (1994). Increased levels of hemoglobin-derived and other peptides in Alzheimer's disease cerebellum. *J. Neurosci.* 14, 2225–2235. doi: 10.1523/jneurosci.14-04-02225.1994

Smith, C. D., Andersen, A. H., Kryscio, R. J., Schmitt, F. A., Kindy, M. S., Blonder, L. X., et al. (1999). Altered brain activation in cognitively intact individuals at high risk for Alzheimer's disease. *Neurology* 53, 1391–1396. doi: 10.1212/wnl.53.7.1391

Snyder, P. J., Alber, J., Alt, C., Bain, L. J., Bouma, B. E., Bouwman, F. H., et al. (2021). Retinal imaging in Alzheimer's and neurodegenerative diseases. *Alzheimers Demen.* 17, 103–111.

Sweeney, M. D., Sagare, A. P., and Zlokovic, B. V. (2018). Blood-brain barrier breakdown in Alzheimer disease and other neurodegenerative disorders. *Nat. Rev. Neurol.* 14, 133–150. doi: 10.1038/nrneurol.2017.188

Tey, K. Y., Teo, K., Tan, A. C. S., Devarajan, K., Tan, B., Tan, J., et al. (2019). Optical coherence tomography angiography in diabetic retinopathy: a review of current applications. *Eye Vis. (Lond.)* 6:37.

Tonda-Turo, C., Origlia, N., Mattu, C., Accorroni, A., and Chiono, V. (2018). Current limitations in the treatment of parkinson's and Alzheimer's Diseases: state-of-the-art and future perspective of polymeric carriers. *Curr. Med. Chem.* 25, 5755–5771. doi: 10.2174/0929867325666180221125759

Torres, J. B., Andreozzi, E. M., Dunn, J. T., Siddique, M., Szanda, I., Howlett, D. R., et al. (2016). PET imaging of copper trafficking in a mouse model of Alzheimer Disease. *J. Nucl. Med.* 57, 109–114. doi: 10.2967/jnumed.115.162370

Trick, G. L., Barris, M. C., and Bickler-Bluth, M. (1989). Abnormal pattern electroretinograms in patients with senile dementia of the Alzheimer type. *Ann. Neurol.* 26, 226–231. doi: 10.1002/ana.410260208

Tripathy, D., Thirumangalakudi, L., and Grammas, P. (2007). Expression of macrophage inflammatory protein 1-alpha is elevated in Alzheimer's vessels and is regulated by oxidative stress. *J. Alzheimers Dis.* 11, 447–455. doi: 10.3233/jad-2007-11405

Tsai, Y., Lu, B., Ljubimov, A. V., Girman, S., Ross-Cisneros, F. N., Sadun, A. A., et al. (2014). Ocular changes in TgF344-AD rat model of Alzheimer's disease. *Invest. Ophthalmol. Vis. Sci.* 55, 523–534. doi: 10.1167/iovs.13-12888

van de Haar, H. J., Burgmans, S., Jansen, J. F., Van Osch, M. J., Van Buchem, M. A., Muller, M., et al. (2016a). Blood-brain barrier leakage in patients with early Alzheimer Disease. *Radiology* 281, 527–535. doi: 10.1148/radiol.2016152244

van de Haar, H. J., Jansen, J. F. A., Van Osch, M. J. P., Van Buchem, M. A., Muller, M., Wong, S. M., et al. (2016b). Neurovascular unit impairment in early Alzheimer's disease measured with magnetic resonance imaging. *Neurobiol. Aging* 45, 190–196. doi: 10.1016/j.neurobiolaging.2016.06.006

van der Flier, W. M., Skoog, I., Schneider, J. A., Pantoni, L., Mok, V., Chen, C. L. H., et al. (2018). Vascular cognitive impairment. *Nat. Rev. Dis. Primers* 4:18003.

Vidal, D., and Mavet, S. (1989). In vitro and in vivo toxicity of T-2 toxin, a fusarium mycotoxin, to mouse peritoneal macrophages. *Infect. Immun.* 57, 2260–2264. doi: 10.1128/iai.57.7.2260-2264.1989

Vinters, H. V., Secor, D. L., Read, S. L., Frazee, J. G., Tomiyasu, U., Stanley, T. M., et al. (1994). Microvasculature in brain biopsy specimens from patients with Alzheimer's disease: an immunohistochemical and ultrastructural study. *Ultrastruct. Pathol.* 18, 333–348. doi: 10.3109/01913129409023202

Viswanathan, A., and Greenberg, S. M. (2011). Cerebral amyloid angiopathy in the elderly. *Ann. Neurol.* 70, 871–880.

Vit, J. P., Fuchs, D. T., Angel, A., Levy, A., Lamensdorf, I., Black, K. L., et al. (2021). Color and contrast vision in mouse models of aging and Alzheimer's disease using a novel visual-stimuli four-arm maze. *Sci. Rep.* 11:1255.

Wang, C., and Holtzman, D. M. (2020). Bidirectional relationship between sleep and Alzheimer's disease: role of amyloid, tau, and other factors. *Neuropsychopharmacology* 45, 104–120. doi: 10.1038/s41386-019-0478-5

Wang, X., Lou, N., Eberhardt, A., Yang, Y., Kusk, P., Xu, Q., et al. (2020). An ocular glymphatic clearance system removes β-amyloid from the rodent eye. *Sci. Transl. Med.* 12:eaaw3210. doi: 10.1126/scitranslmed.aaw3210

Williams, E. A., Mcguone, D., Frosch, M. P., Hyman, B. T., Laver, N., and Stemmer-Rachamimov, A. (2017). Absence of Alzheimer Disease neuropathologic changes in eyes of subjects with alzheimer disease. *J. Neuropathol. Exp. Neurol.* 76, 376–383. doi: 10.1093/jnen/nlx020

Williams, M. A., Mcgowan, A. J., Cardwell, C. R., Cheung, C. Y., Craig, D., Passmore, P., et al. (2015). Retinal microvascular network attenuation in Alzheimer's disease. *Alzheimers Demen. (Amst.)* 1, 229–235. doi: 10.1016/j.dadm.2015.04.001

Williams, P. A., Thirgood, R. A., Oliphant, H., Frizzati, A., Littlewood, E., Votruba, M., et al. (2013). Retinal ganglion cell dendritic degeneration in a mouse model of Alzheimer's disease. *Neurobiol. Aging* 34, 1799–1806. doi: 10.1016/j.neurobiolaging.2013.01.006

Williams, S., Chalmers, K., Wilcock, G. K., and Love, S. (2005). Relationship of neurofibrillary pathology to cerebral amyloid angiopathy in Alzheimer's disease. *Neuropathol. Appl. Neurobiol.* 31, 414–421. doi: 10.1111/j.1365-2990.2005.00663.x

Wolters, F. J., Zonneveld, H. I., Hofman, A., Van Der Lugt, A., Koudstaal, P. J., Vernooij, M. W., et al. (2017). Cerebral perfusion and the risk of dementia: a population-based study. *Circulation* 136, 719–728. doi: 10.1161/circulationaha.117.027448

Wu, J., Zhang, X., Azhati, G., Li, T., Xu, G., and Liu, F. (2020). Retinal microvascular attenuation in mental cognitive impairment and Alzheimer's disease by optical coherence tomography angiography. *Acta Ophthalmol.* 98, e781–e787.

Xu, Q., Qaum, T., and Adamis, A. P. (2001). Sensitive blood-retinal barrier breakdown quantitation using evans blue. *Invest. Ophthalmol. Vis. Sci.* 42, 789–794.

Yan, Y., Wu, X., Wang, X., Geng, Z., Wang, L., Xiao, G., et al. (2021). The retinal vessel density can reflect cognitive function in patients with Alzheimer's disease: evidence from optical coherence tomography angiography. *J. Alzheimers Dis.* 79, 1307–1316. doi: 10.3233/jad-200971

Yang, A. C., Stevens, M. Y., Chen, M. B., Lee, D. P., Stahli, D., Gate, D., et al. (2020). Physiological blood-brain transport is impaired with age by a shift in transcytosis. *Nature* 583, 425–430. doi: 10.1038/s41586-020-2453-z

Yang, Y., Shiao, C., Hemingway, J. F., Jorstad, N. L., Shalloway, B. R., Chang, R., et al. (2013). Suppressed retinal degeneration in aged wild type and APPswe/PS1DeltaE9 mice by bone marrow transplantation. *PLoS One* 8:e64246. doi: 10.1371/journal.pone.0064246

Yarchoan, M., Xie, S. X., Kling, M. A., Toledo, J. B., Wolk, D. A., Lee, E. B., et al. (2012). Cerebrovascular atherosclerosis correlates with Alzheimer pathology in neurodegenerative dementias. *Brain* 135, 3749–3756.

Yoon, S. P., Grewal, D. S., Thompson, A. C., Polascik, B. W., Dunn, C., Burke, J. R., et al. (2019). Retinal microvascular and neurodegenerative changes in Alzheimer's disease and mild cognitive impairment compared with control participants. *Ophthalmol. Retina* 3, 489–499. doi: 10.1016/j.oret.2019.02.002

Zabel, P., Kaluzny, J. J., Wilkosc-Debczynska, M., Gebska-Toloczko, M., Suwala, K., Zabel, K., et al. (2019). Comparison of retinal microvasculature in patients with Alzheimer's disease and primary open-angle glaucoma by optical coherence tomography angiography. *Invest. Ophthalmol. Vis. Sci.* 60, 3447–3455. doi: 10.1167/iovs.19-27028

Zenaro, E., Piacentino, G., and Constantin, G. (2017). The blood-brain barrier in Alzheimer's disease. *Neurobiol. Dis.* 107, 41–56.

Zhang, Y. S., Zhou, N., Knoll, B. M., Samra, S., Ward, M. R., Weintraub, S., et al. (2019). Parafoveal vessel loss and correlation between peripapillary vessel density and cognitive performance in amnestic mild cognitive impairment and early Alzheimer's disease on optical coherence tomography angiography. *PLoS One* 14:e0214685. doi: 10.1371/journal.pone.0214685

Zhao, H., Chang, R., Che, H., Wang, J., Yang, L., Fang, W., et al. (2013). Hyperphosphorylation of tau protein by calpain regulation in retina of Alzheimer's disease transgenic mouse. *Neurosci. Lett.* 551, 12–16. doi: 10.1016/j.neulet.2013.06.026

Zhao, Z., Sagare, A. P., Ma, Q., Halliday, M. R., Kong, P., Kisler, K., et al. (2015). Central role for PICALM in amyloid-beta blood-brain barrier transcytosis and clearance. *Nat. Neurosci.* 18, 978–987. doi: 10.1038/nn.4025

Zipser, B. D., Johanson, C. E., Gonzalez, L., Berzin, T. M., Tavares, R., Hulette, C. M., et al. (2007). Microvascular injury and blood-brain barrier leakage in Alzheimer's disease. *Neurobiol. Aging* 28, 977–986.

Zlokovic, B. V., Ghiso, J., Mackic, J. B., Mccomb, J. G., Weiss, M. H., and Frangione, B. (1993). Blood-brain barrier transport of circulating Alzheimer's amyloid beta. *Biochem. Biophys. Res. Commun.* 197, 1034–1040. doi: 10.1006/bbrc.1993.2582

Conflict of Interest: YK, MK-H, and KB are co-founders and stockholders of NeuroVision Imaging, Inc., Sacramento, CA, United States. MK-H, HS, YK, and KB are inventors on Patent Application No. 62/970,083 filed February 4, 2020 entitled "Method of Detecting Cognitive Impairment."

The remaining authors declare that the research was conducted in the absence of any commercial or financial relationships that could be construed as a potential conflict of interest.

Publisher's Note: All claims expressed in this article are solely those of the authors and do not necessarily represent those of their affiliated organizations, or those of the publisher, the editors and the reviewers. Any product that may be evaluated in this article, or claim that may be made by its manufacturer, is not guaranteed or endorsed by the publisher.

frontiers in Neuroscience

ORIGINAL RESEARCH
published: 12 October 2021
doi: 10.3389/fnins.2021.761654

Retinal Oxygen Metabolism and Haemodynamics in Patients With Multiple Sclerosis and History of Optic Neuritis

*Martin Kallab[1], Nikolaus Hommer[1], Andreas Schlatter[1,2], Gabriel Bsteh[3], Patrick Altmann[3], Alina Popa-Cherecheanu[4,5], Martin Pfister[6,7], René M. Werkmeister[6], Doreen Schmidl[1], Leopold Schmetterer[1,6,8,9,10,11,12] and Gerhard Garhöfer[1]**

[1] Department of Clinical Pharmacology, Medical University of Vienna, Vienna, Austria, [2] Vienna Institute for Research in Ocular Surgery (VIROS), Karl Landsteiner Institute, Hanusch Hospital, Vienna, Austria, [3] Department of Neurology, Medical University of Vienna, Vienna, Austria, [4] Carol Davila University of Medicine and Pharmacy, Bucharest, Romania, [5] Department of Ophthalmology, University Emergency Hospital, Bucharest, Romania, [6] Center for Medical Physics and Biomedical Engineering, Medical University of Vienna, Vienna, Austria, [7] Institute of Applied Physics, Vienna University of Technology, Vienna, Austria, [8] Singapore Eye Research Institute, Singapore, Singapore, [9] Nanyang Technological University, Singapore, Singapore, [10] Ophthalmology and Visual Sciences Academic Clinical Program, Duke-NUS Medical School, Singapore, Singapore, [11] SERI-NTU Advanced Ocular Engineering (STANCE), Singapore, Singapore, [12] Institute of Molecular and Clinical Ophthalmology, Basel, Switzerland

OPEN ACCESS

Edited by:
Yuyi You,
Macquarie University, Australia

Reviewed by:
Sabrina Reinehr,
Ruhr-University Bochum, Germany
Lies De Groef,
KU Leuven, Belgium

***Correspondence:**
Gerhard Garhöfer
gerhard.garhoefer@meduniwien.ac.at

Specialty section:
This article was submitted to Neurodegeneration, a section of the journal Frontiers in Neuroscience

Received: *20 August 2021*
Accepted: *22 September 2021*
Published: *12 October 2021*

Citation:
Kallab M, Hommer N, Schlatter A, Bsteh G, Altmann P, Popa-Cherecheanu A, Pfister M, Werkmeister RM, Schmidl D, Schmetterer L and Garhöfer G (2021) Retinal Oxygen Metabolism and Haemodynamics in Patients With Multiple Sclerosis and History of Optic Neuritis. Front. Neurosci. 15:761654. doi: 10.3389/fnins.2021.761654

Vascular changes and alterations of oxygen metabolism are suggested to be implicated in multiple sclerosis (MS) pathogenesis and progression. Recently developed in vivo retinal fundus imaging technologies provide now an opportunity to non-invasively assess metabolic changes in the neural retina. This study was performed to assess retinal oxygen metabolism, peripapillary capillary density (CD), large vessel density (LVD), retinal nerve fiber layer thickness (RNFLT) and ganglion cell inner plexiform layer thickness (GCIPLT) in patients with diagnosed relapsing multiple sclerosis (RMS) and history of unilateral optic neuritis (ON). 16 RMS patients and 18 healthy controls (HC) were included in this study. Retinal oxygen extraction was modeled using O_2 saturations and Doppler optical coherence tomography (DOCT) derived retinal blood flow (RBF) data. CD and LVD were assessed using optical coherence tomography (OCT) angiography. RNFLT and GCIPLT were measured using structural OCT. Measurements were performed in eyes with (MS+ON) and without (MS-ON) history for ON in RMS patients and in one eye in HC. Total oxygen extraction was lowest in MS+ON (1.8 ± 0.2 µl O_2/min), higher in MS-ON (2.1 ± 0.5 µl O_2/min, $p = 0.019$ vs. MS+ON) and highest in HC eyes (2.3 ± 0.6 µl O_2/min, $p = 0.002$ vs. MS, ANOVA $p = 0.031$). RBF was lower in MS+ON (33.2 ± 6.0 µl/min) compared to MS-ON (38.3 ± 4.6 µl/min, $p = 0.005$ vs. MS+ON) and HC eyes (37.2 ± 4.7 µl/min, $p = 0.014$ vs. MS+ON, ANOVA $p = 0.010$). CD, LVD, RNFLT and GCIPL were significantly lower in MS+ON eyes. The present data suggest that structural alterations in the retina of RMS patients

are accompanied by changes in oxygen metabolism, which are more pronounced in MS+ON than in MS-ON eyes. Whether these alterations promote MS onset and progression or occur as consequence of disease warrants further investigation.

Clinical Trial Registration: ClinicalTrials.gov registry, NCT03401879.

Keywords: multiple sclerosis, retinal blood flow, retinal oxygen saturation, microcirculation, optical coherence tomography angiography

INTRODUCTION

Multiple sclerosis (MS) is a demyelinating disease of the central nervous system with a global median prevalence of approximately 33 people per 100,000 and one of the major reasons for permanent disability in young adults (Reich et al., 2018). Although there is general agreement that MS is an immune-mediated process, there is compelling evidence that vascular factors and metabolic alterations such as mitochondrial dysfunction (Dutta et al., 2006; Mahad et al., 2008) or hypoxia (Davies et al., 2013; Yang and Dunn, 2015; Johnson et al., 2016) play an essential role in the pathogenesis and progression of the disease. As such, it has been shown that local oxygen supply insufficiency leads to hypoxic damage, resulting in neuroinflammation and demyelination of nerve fibers with the known clinical consequences, while in turn neuroinflammation per se can also trigger hypoxia (Yang and Dunn, 2019; Halder and Milner, 2021). Thus, more knowledge on the oxygen metabolism may help to get a better understanding of the pathophysiological mechanisms involved in the disease progression and develop new therapeutic strategies.

Currently, studying microvascular and metabolic changes in MS is hampered by a paucity of available non-invasive methods to measure oxygen metabolism in the human brain. In this context, the anterior visual system – mainly the neural retina and the optic nerve – offers unique possibilities to non-invasively gain insight into the metabolic and microvascular processes in unprecedented resolution. Recent development in retinal imaging allows for the non-invasive determination of oxygen saturation in retinal vessels (Hammer et al., 2008) as well as for the quantitative assessment of perfusion (Werkmeister et al., 2008) and microvascular density (Tan et al., 2020). Further, as a part of the central nervous system, the retina is a highly metabolically active tissue, which is frequently affected by MS. More specifically, in 15–20% of patients diagnosed with MS, the symptom leading to clinical investigation is optic neuritis (ON) (Confavreux et al., 2000). Further, as much as 70% of patients with MS are affected by ON at some time during the disease (Toosy et al., 2014).

The current study takes advantage of recently developed imaging techniques to assess retinal oxygen metabolism, retinal perfusion and capillary density in patients with diagnosed relapsing MS (RMS) and history of unilateral ON and to compare these parameters with a healthy control group. Retinal oxygen extraction is measured based on Doppler optical coherence tomography (DOCT) (Werkmeister et al., 2008) and non-invasive determination of oxygen saturation via reflectometry (Hammer et al., 2008). This approach has been validated and recently successfully used to investigate metabolic changes under pathological conditions such as diabetes (Fondi et al., 2017). Further, structural changes were assessed using optical coherence tomography (OCT) and OCT angiography (OCTA).

The aim of this observer-masked cross-sectional study was to investigate potential metabolic and vascular alterations of the retina in patients with MS.

MATERIALS AND METHODS

Study Subjects

MS patients as well as age- and sex-matched healthy subjects were recruited between February 2018 and January 2021. The study was conducted in accordance with the Declaration of Helsinki and the Good Clinical Practice (GCP) guidelines of the International Council for Harmonisation of Technical Requirements for Pharmaceuticals for Human Use (ICH). Written informed consent was obtained from all participants before any study related procedures and the Ethics Committee of the Medical University of Vienna approved the study with all its procedures before initiation.

In/Exclusion Criteria

Inclusion criteria for MS patients were age $\geq$18 years, diagnosis of relapsing multiple sclerosis (RMS) according to McDonald criteria (revision 2017), history of unilateral ON with unaffected contralateral eye, ON more than one year ago, adequate visual and auditory acuity to allow ocular blood flow measurements, stable doses of concomitant medications for at least 30 days prior inclusion if considered relevant by the investigator, normal ophthalmologic findings apart from MS- or ON-related alterations and ametropia $<$ 6 Dpt.

Exclusion criteria for MS patients were presence or history of a severe medical condition other than MS as judged by the clinical investigator, history of neuromyelitis optica spectrum disorder (NMOSD), history of any inflammatory or infectious disease of the central nervous system other than MS, any other significant and clinically relevant neurological disease as judged by the investigator, untreated arterial hypertension and diabetes. Further, patients with ocular diseases or presence of any abnormality preventing reliable measurements in the study eyes as judged by the investigator, best-corrected visual acuity (BCVA) $<$ 0.5 Snellen, pregnancy or planned pregnancy and alcoholism or substance abuse were excluded.

Inclusion criteria for healthy subjects were age over 18 years, normal findings in the medical history (or clinically irrelevant

as judged by the investigator), normal ophthalmic findings and ametropia <6 Dpt. Exclusion criteria for healthy subjects were: history of any disease of the central nervous system, presence or history of any severe medical condition as judged by the investigator, untreated arterial hypertension, presence of any abnormalities preventing reliable measurements in the study eye as judged by the investigator, family history of MS, ON, or NMOSD, BCVA < 0.5 Snellen, pregnancy or planned pregnancy and alcoholism or substance abuse.

Experimental Paradigm

Before inclusion into the study, a screening examination was performed to assess eligibility. It comprised the following procedures: detailed medical history including assessment of current MS-related symptoms (in MS patients) and concomitant medication, pregnancy testing in women with childbearing potential, measurement of systemic haemodynamics, BCVA, visual field (VF) testing using standard automated perimetry (SAP; Humphrey 30-2 SITA-Standard, Carl Zeiss Meditec Inc., Dublin, Ireland), measurement of axial eye length using an IOL-Master (Carl Zeiss Meditec Inc.), slit-lamp examination including dilated funduscopy and measurement of intraocular pressure (IOP) using applanation tonometry.

Upon confirmation of eligibility, patients and healthy subjects were included into the study. One drop of tropicamide was administered to the study eye(s) and a 20-min resting period was scheduled to obtain stable haemodynamic conditions. Then, an ONH-centered 50° fundus image was taken using a retinal vessel analyzer (RVA; Imedos Systems, Jena, Germany) to measure vessel diameters and O_2 saturations, before retinal blood flow was assessed using a previously described custom built dual-beam DOCT system (Werkmeister et al., 2008; Doblhoff-Dier et al., 2014). Finally, a 3.5 diameter circumpapillary OCT ring scan, a 20°×20° macular volume scan and a 15°×15° peripapillary OCTA volume scan (384 B-Scans and 384 A-Scans/B-Scan) using the commercial Heidelberg Spectralis OCT(A) (Heidelberg Engineering, Heidelberg, Germany) were performed. In MS patients, both the eye with (MS+ON) and without (MS-ON) history for ON were measured, in healthy subjects one randomly chosen eye was measured.

Methods

Noninvasive Measurement of Systemic Haemodynamics

Measurements of systemic haemodynamics were performed on the upper arm by an automated oscillometric device (Infinity Delta; Dräger, Vienna, Austria). This device recorded systolic, diastolic and mean arterial pressures (SBP, DBP, MAP), pulse rate (HR) and peripheral oxygen saturation using a fingertip pulse oximeter.

Intraocular Pressure

A slit-lamp mounted Goldmann applanation tonometer was used to assess IOP at the screening examination. One drop of oxybuprocainhydrochloride combined with sodium fluorescein was used for anesthesia of the cornea before each measurement.

Circumpapillary Optical Coherence Tomography, Macular Optical Coherence Tomography and Peripapillary Optical Coherence Tomography Angiography

Circumpapillary OCT scans were analyzed using the segmentation and analysis software of the Spectralis glaucoma module and global RNFL-thickness (RNFLT) in μm was extracted for every measurement.

Macular OCT scans were used to measure the ganglion cell layer and inner plexiform layer thickness (GCIPL) as previously described using the standard Spectralis software segmentation of GCL and IPL (Bsteh et al., 2021). In short, GCL and IPL thicknesses in the inner quadrants (3 mm) of the macula-centered ETDRS grid were averaged and GCIPL was calculated as the sum of the averaged GCL and IPL thicknesses.

Peripapillary OCTA scans were processed using standard segmentation and slab settings of the Spectralis OCTA module. Superficial vascular complex (SVC) slabs were exported to the Fiji distribution of ImageJ (Schindelin et al., 2012). Major retinal vessels were separated from the capillary bed using a Hessian-based large vessel detection algorithm (Sato et al., 1998) as frequently applied in the analysis of retinal OCTA scans (Tan et al., 2020). In short, a Hessian-based filter captures tubular structures of a certain caliber range and the output was used to create a binary vessel mask.

For capillary-specific analysis, this mask was applied to remove major retinal vessels before an optic disc-centered ring-shaped region of interest (ROI) with an inner diameter of 2.5 mm and an outer diameter of 4 mm was defined. The ring-shaped, capillary-specific ROI was binarized by mean values and capillary density (CD) was calculated as percentage of white pixels. For large vessel-specific analysis, the inverted vessel mask was applied to remove the capillaries before ROI definition, thresholding and density calculation was done as described for the capillary-specific analysis to determine the large vessel density (LVD).

Retinal Vessel Diameter and Oxygen Saturation

The RVA system allows for the evaluation of retinal vessel diameters and oxygen saturation (Hammer et al., 2008; Garhofer et al., 2010). For this purpose, a computer-coupled fundus camera is used.

Applying the VesselMap software to the ONH-centered fundus image as acquired by the RVA, all peripapillary arteries and veins branching from the central retinal artery (CRA) and central retinal vein (CRV) were selected and the CRA- and CRV-equivalent (CRAE and CRVE) and arterio-venous ratio (AVR) were calculated by the software as proposed previously (Hubbard et al., 1999).

Fundus images as taken using the RVA device were also used to estimate oxygen saturations of all retinal arteries ($SaO_{2,A}$) and veins ($SaO_{2,V}$) using a reflectometric approach (Hammer et al., 2008, 2009). In short, two images with different wavelengths are simultaneously taken (610 and 545 nm) and oxygen saturation is estimated based on the fact that hemoglobin exerts different light absorption characteristics depending on its level of oxygenation. While this effect is greatest at around 610 nm, the isosbestic wavelength for hemoglobin i.e., the

wavelength at which deoxygenated and oxygenated hemoglobin show identical absorption characteristics is 548 nm. Using the differences of these two images, $SaO_{2,A}$ or $SaO_{2,V}$ are estimated in all retinal vessels.

Total Retinal Blood Flow Measurement

For TRBF calculation, measurements of the above-mentioned fundus-camera coupled DOCT device were used. As described previously, a peripapillary scanning pattern including horizontal and vertical scans was applied to ensure coverage of all retinal arteries and veins and blood flow was assessed in all vessels with a diameter of 40 μm or larger (Doblhoff-Dier et al., 2014). Each scan consisted of repetitive B-scans at the same position and lasted for several seconds to ensure averaging of parameters over a minimum of one full pulse cycle. The background and details of single vessel velocity, diameter and flow extraction have been extensively described in numerous previous publications (Werkmeister et al., 2012a,b, 2015; Doblhoff-Dier et al., 2014; Fondi et al., 2017; Bata et al., 2019). In reference to these papers, we confine ourselves to a short summary: two orthogonally polarized superluminescent diode beams separated by the known angle $\Delta\alpha$ are focused onto one retinal spot. Due to the two different angles α_1 and $\alpha_2(\Delta\alpha = \alpha_1 - \alpha_2)$ at which the two probe beams impinge onto the vessel of interest, the phase shifts $\Phi_1$and Φ_2 induced into the probing light reflected by moving particles (e.g., red blood cells) are different. This difference ($\Delta\Phi(\Delta\Phi = \Phi_1 - \Phi_2)$ between the two probe beams in combination with $\Delta\alpha$, several device and physiological constants (λ = OCT light source central wavelength, τ = time interval between two recordings dependent on acquisition rate, n = group refractive index of blood) and the angle β (angle between the detection plane spanned by the two probe beams and the velocity vector) can be used to calculate absolute blood velocity using the following equation (Eq. 1):

$$V_{abs} = \Delta\Phi * \frac{\lambda}{4\pi * n * \tau * \Delta\alpha * \cos\beta} \quad (1)$$

Vessel diameter (D) is extracted from the DOCT scans using a caliper in the analysis software and absolute flood flow (Q_{abs}) is calculated using Eq. 2

$$Q = \frac{D^2}{4} * \pi * V_{abs} \quad (2)$$

Summing up single vessel flow results for all arteries and veins gives arterial and venous TRBFs ($TRBF_A$ and $TRBF_V$). TRBF measurements have been recently evaluated for reproducibility and repeatability (Szegedi et al., 2020b). TRBFs presented in this study are the means of $TRBF_A$ and $TRBF_V$.

Oxygen Content and Retinal Oxygen Extraction

The model to calculate the oxygen content and retinal oxygen extraction based on $SaO_{2,A}$ and $SaO_{2,V}$ was profoundly described and discussed previously by Werkmeister et al. (2015) and has since been applied in further studies in healthy subjects as well as in patients with ocular diseases (Fondi et al., 2017; Bata et al., 2019; Hommer et al., 2021). In short, $SaO_{2,A}$ and $SaO_{2,V}$ are corrected for the distance of their measurement point to the CRA or CRV merging point. By calculating the mean of the corrected $SaO_{2,A}$ values ($cSaO_{2,A}$), oxygen saturation in the central retinal artery ($SaO_{2,CRA}$) can be directly obtained. For calculation of oxygen saturation in the central retinal vein ($SaO_{2,CRV}$), an additional step taking the flow in each individual vessel as weighting factor into account is necessary as the venous blood in the CRV is a mixture of all merging retinal veins. In a next step, the oxygen content of the CRA ($cO_{2,CRA}$) and CRV ($cO_{2,CRV}$) are estimated considering the fact that not only hemoglobin bound oxygen needs to be considered but also the oxygen dissolved in plasma.

Finally retinal oxygen extraction ($extO_2$) is calculated using Eq. 3, where $cO_{2,CRA}$ and $cO_{2,CRV}$ are the oxygen contents of CRA and CRV, respectively and Q is the TRBF as described above.

$$extO_2 = \left(cO_{2,CRA} - cO_{2,CRV}\right) * Q \quad (3)$$

Statistical Analysis

Statistical analysis was performed using IBM SPSS Statistics (Version 27, IBM, Armonk, NY, United States). All values are presented as means ± standard deviations. Normal distribution was confirmed using the Kolmogorov-Smirnov test. Descriptive statistics are reported for all values obtained. A one-way ANOVA model was used to assess overall differences between the three groups (MS+ON, MS-ON and healthy eyes). For those that turned out to be significant in the ANOVA model for three groups, contrasts between two groups (MS+ON vs. MS-ON, MS+ON vs. healthy eyes and MS-ON vs. healthy eyes) were defined. Prior to calculating contrasts for planned comparison between groups, a Levene's test to assess equality of variances was carried out. Plots for the figures were produced using GraphPad Prism 9.2.0 (GraphPad Software Inc., CA, United States). A p-value <0.05 was considered as the level of significance.

RESULTS

A total of 34 subjects were included in the present study, of which 16 had MS and 18 were healthy age- and sex-matched controls. As both eyes were measured in MS patients with history of unilateral ON a total of 16 MS+ON, 16 MS-ON and 18 healthy eyes were enrolled in this study. The demographics and baseline characteristics of the two study groups are shown in **Table 1**. There was no difference between groups in terms of age, sex or systemic haemodynamics.

Eleven (11) out of 16 MS patients were currently medicated with a disease-modifying therapy, of which five took glatiramer acetate, three dimethyl fumurate and one each fingolimod, natalizumab or interferon beta.

Seven (7) patients reported no current MS-related symptoms, 6 reported one and 3 reported more than one symptom. The most frequent symptoms were upper/lower limb paresthesia, gait disorder, fatigue and vertigo.

Retinal Vessel Diameters

CRAE was significantly different between the three groups ($p = 0.015$), with CRAE being significantly lower in MS+ON eyes

TABLE 1 | Baseline characteristics of the two study groups.

	Healthy subjects	Patients with MS		*p*-value
Age (years)	41 ± 16	43 ± 13		0.698
Gender (m/f)	4/14	4/12		0.583
Years since diagnosis of MS (years)	N/A	9 ± 8		N/A
Time elapsed since ON (years)	N/A	8 ± 7		N/A
Systolic blood pressure (mmHg)	117 ± 14	123 ± 13		0.197
Diastolic blood pressure (mmHg)	72 ± 8	76 ± 8		0.128
Heart rate (bpm)	66 ± 9	69 ± 12		0.446
Mean arterial pressure (mmHg)	90 ± 12	96 ± 10		0.145
Intraocular pressure (mmHg)	13 ± 2	15 ± 3 (MS+ON)	15 ± 3 (MS-ON)	0.062
Best corrected visual acuity (Snellen decimal)	1.2 ± 0.5	1.2 ± 0.3 (MS+ON)	1.2 ± 0.2 (MS-ON)	0.937
Visual field mean deviation (dB)	−0.5 ± 1.2	−1.8 ± 3.2 (MS+ON)	−1.0 ± 2.9 (MS-ON)	0.333

Values are presented as mean ± standard deviation.
ON, optic neuritis; MS, multiple sclerosis.
p-values are calculated by one-way ANOVA.

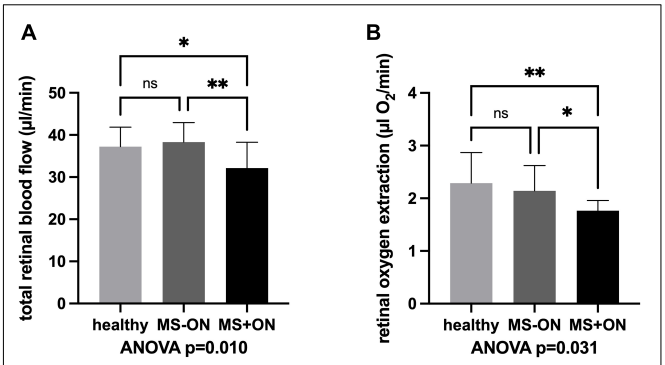

FIGURE 1 | Total retinal blood flow **(A)** and retinal oxygen extraction **(B)** in eyes with history of acute optic neuritis (MS+ON), in contralateral eyes with no history of ON (MS-ON) and healthy control eyes are significantly different between the study groups upon ANOVA analysis. MS+ON eyes showed significantly reduced total retinal blood flow and oxygen extraction as compared to MS-ON and healthy eyes. Data are presented as means ± standard deviation. *$p < 0.05$, **$p < 0.01$, ns, not significant.

(182 ± 13 µm) and MS-ON eyes (182 ± 16 µm) compared to healthy eyes (196 ± 18 µm, $p = 0.014$ for MS+ON vs. healthy and $p = 0.011$ for MS-ON vs. healthy). In contrast, no significant difference between groups was found for CRVE (222 ± 15 µm in MS+ON eyes, 223 ± 13 µm in MS-ON eyes and 227 ± 14 µm in healthy eyes ($p = 0.649$ between groups). AVR was also significantly different between groups ($p = 0.034$). It was significantly reduced in eyes with MS+ON compared to healthy eyes (0.82 ± 0.06 vs. 0.87 ± 0.07, $p = 0.047$) as well as in MS-ON eyes compared to healthy eyes (0.81 ± 0.06 vs. 0.87 ± 0.07, $p = 0.015$).

Oxygen Extraction and Total Retinal Blood Flow

A statistically significant difference between the three groups was found for TRBF ($p = 0.010$, **Figure 1A**) and calculated oxygen extraction ($p = 0.031$, **Figure 1B**). Calculated oxygen extraction was lowest in MS+ON eyes (1.8 ± 0.2 µl O2/min), higher in MS-ON eyes (2.1 ± 0.5 µl O2/min; $p = 0.019$ for MS+ON vs. MS-ON, **Figure 1B**) and highest in healthy eyes (2.3 ± 0.6 µl O2/min; $p = 0.002$ for MS+ON vs. healthy, **Figure 1B**). TRBF was lower in MS+ON eyes (33.2 ± 6.0 µl/min) as compared to MS-ON eyes (38.3 ± 4.6 µl/min) and healthy eyes (37.2 ± 4.7 µl/min; $p = 0.005$ for MS+ON vs. MS-ON eyes, $p = 0.014$ for MS+ON vs. healthy eyes, $p = 0.560$ for MS-ON vs. healthy eyes, **Figure 1A**).

Retinal Nerve Fiber Layer Thickness, Ganglion Cell Inner Plexiform Layer Thickness, Capillary Density and Large Vessel Density

RNFLT and GCIPL were significantly different between the three groups ($p < 0.001$ each). RNFLT was significantly lower in MS+ON eyes (80.7 ± 14.0 µm) compared to MS-ON eyes (96.8 ± 8.9 µm) and eyes of healthy controls (100.0 ± 9.5 µm; $p < 0.001$ between MS+ON and MS-ON or healthy eyes, $p = 0.311$ between MS-ON and healthy eyes). This was also similar for GCIPL which was significantly lower in MS+ON eyes (73.7 ± 14.6 µm) compared to MS-ON eyes (92.2 ± 9.4 µm, $p < 0.001$ vs. MS+ON eyes) or healthy eyes (93.8 ± 7.2 µm, $p < 0.001$ vs. MS+ON eyes; $p = 0.665$ vs. MS-ON eyes).

Peripapillary CD without large vessels as assessed by OCTA was significantly different between the three groups ($p < 0.001$). In particular, it was lower in MS+ON eyes (46.0 ± 4.7 %) compared to MS-ON eyes (49.1 ± 3.5 %, $p = 0.037$ vs. MS+ON eyes) and compared to healthy eyes (51.7 ± 2.9 %, $p < 0.001$ vs. MS+ON eyes). No statistically significant difference was found between MS-ON eyes and healthy eyes ($p = 0.069$, **Figure 2A**). LVD also showed a significant difference between the three groups ($p = 0.014$). It was significantly reduced in MS+ON eyes compared to healthy eyes (14.0 ± 2.0% vs. 16.3 ± 2.3%, $p = 0.004$), but no significant differences were found between MS+ON and MS-ON eyes (14.0 ± 2.0% vs. 15.4 ± 1.8%, $p = 0.075$) or MS-ON and healthy eyes ($p = 0.236$, **Figure 2B**).

No statistically significant correlations were found between changes in hemodynamic parameters and RNFL/GCIPL loss in neither MS+ON nor MS-ON eyes (data not shown).

DISCUSSION

To the best of our knowledge, the data from our study shows for the first time that retinal oxygen extraction is reduced in patients with MS and history of unilateral ON when compared to healthy subjects, suggesting an impaired oxygen metabolism in patients with MS and ON. Further, our results indicate that these impairments are more pronounced in the ON eye compared to the fellow eye without history of ON and paralleled by a decrease

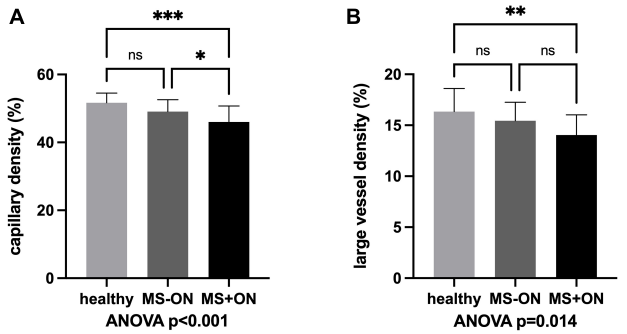

FIGURE 2 | Capillary density **(A)** and large vessel density **(B)** in eyes with history of acute optic neuritis (MS+ON), in contralateral eyes with no history of ON (MS-ON) and healthy control eyes are significantly different between the study groups upon ANOVA analysis. MS+ON eyes showed a significantly reduced capillary density as compared to MS-ON and healthy eyes while large vessel density was significantly different between healthy and MS+ON eyes, only. Data are presented as means ± standard deviation. $^{*}p < 0.05$, $^{**}p < 0.01$, $^{***}p < 0.001$, ns, not significant.

in retinal blood flow. Finally, our data confirms previous evidence for microvascular rarefication in patients with MS compared to healthy controls.

As the eye offers ideal opportunities to observe microvascular changes in-vivo, extensive research has been performed to investigate changes in the retinal neural tissue in patients with MS (Petzold et al., 2017; Britze and Frederiksen, 2018; Kleerekooper et al., 2020). As such, early post-mortem studies indicate that the anterior visual pathway is involved in 90% of patients with MS (Toussaint et al., 1983). More recently, OCT has been used as a non-invasive technique to assess potential neurodegenerative changes in different layers of the neural retina (Petzold et al., 2017). This was done in an effort to investigate whether this technique might provide potential novel biomarkers for neurodegeneration in patients with MS (Garcia-Martin et al., 2017; Britze and Frederiksen, 2018). Interestingly, the latter studies indicate that retinal thinning is present in patients with MS, independently of a history of ON and with the most pronounced differences in the peripapillary RNFL and macular ganglion cell layer and inner plexiform layer (Petzold et al., 2017). Although these anatomic changes in the retina of patients with MS are well described, there is only sparse knowledge on functional changes. Although recent reports indicate impaired perfusion in patients with MS (Wang et al., 2018; Liu et al., 2019), the question whether TRBF or oxygen metabolism is altered in patients with MS is not yet answered.

The present study provides in-vivo evidence that retinal oxygen metabolism is compromised in patients with MS. In particular, we found that retinal oxygen extraction was lowest in MS+ON eyes, higher in MS-ON eyes and highest in healthy eyes. The reason for this reduction of oxygen extraction is not entirely clear, but may be related to a reduced oxygen demand in particular of the inner retina caused by neurodegenerative changes of retinal neurons.

However, when discussing these findings, the complex oxygen supply of the retina needs to be considered. The retina is nourished by two distinct vascular beds: the retinal circulation, which supplies the inner retina including the ganglion cells and their associated axons and the choroidal circulation, which provides oxygen and other nutrients mainly to the photoreceptors of the outer retina. As the oxygen diffusion from the choroid to the inner retina is assumed to be negligible under physiological conditions, changes in the oxygen extraction of the retinal circulation can be mainly attributed to inner retinal oxygen consumption (Linsenmeier and Zhang, 2017). Hence, our findings may be at least partially explained by the reduced number of retinal neural cells and their axons, which are nourished via the retinal circulation. Along this line of thought, we have recently shown that oxygen extraction as measured by the model used in the current study correlates with the RNFLT as measured using structural OCT, and the total number of retinal ganglion cells in healthy subjects (Bata et al., 2019). This indicates that a loss of retinal neural cells may lead to a reduced oxygen demand of the tissue and consequently to a reduced oxygen extraction. This hypothesis is also supported by the results of the current study. Our results show a reduced GCIPL and RNFLT as well as reduced capillary density and arteriolar narrowing in patients with MS, indicative for a structural loss in this groups of patients. Further, these findings are also in keeping with previous results reporting that eyes of patients with MS and ON show a reduced RNFLT and GCIPL (Walter et al., 2012; Fernandes et al., 2013; Hokazono et al., 2013; Balk et al., 2014; Knier et al., 2016; Bsteh et al., 2020). Interestingly, both parameters can serve as biomarkers for disability progression, with suggested advantages for the latter (Bsteh et al., 2019a,b, 2021). In this context it needs to be noted that although there was a clear tendency toward a decrease in GCIPL and RNFLT in patients with MS-ON when compared to healthy control subjects, this effect did not reach level of significance. As previously mentioned, larger studies consistently report reduced GCIPL and RNFLT in patients with MS-ON, it is reasonable to suggest that the lack of statistical significance is related to the relatively small sample size of the current study (Oberwahrenbrock et al., 2012; Britze et al., 2017; Alonso et al., 2018; Balci et al., 2020; Farci et al., 2020).

Secondly, our results show that TRBF is lower in MS+ON eyes compared to MS-ON and healthy eyes. This clearly indicates that patients with a history of ON have compromised blood flow and supports the hypothesis that impaired blood flow and hypoperfusion may be an essential factor in patients with ON and MS (Kleerekooper et al., 2020). Again, our results are also in keeping with previous reports: Using a retinal function imager, Liu et al. showed that retinal perfusion is decreased in patients with relapsing MS when compared to healthy subjects (Liu et al., 2019). However, the latter study is limited by the fact that the authors did not differentiate between MS+ON and MS-ON eyes and the instrument used was not capable to provide data regarding TRBF. In another study, the same group of investigators assessed inter-eye correlations and potential differences of the retinal blood velocity in patients with MS (Jiang et al., 2016). The authors concluded that patients with

MS show lower blood velocities as compared to healthy subjects (Jiang et al., 2016). Although the latter study measured only velocities but not volumetric blood flow as in the current study, this again supports our findings that blood flow is compromised in patients with MS. In addition, our finding of reduced blood flow is also compatible with the data of retinal vessel analysis as measured in the current study, showing a reduced AVR mainly caused by reduced CRAE. This, in turn, indicates pronounced arterial constriction in the major retinal vessels, which is in line with data on upregulation of endothelin-1 in MS lesions and elevated serum and CSF levels of this vasoconstrictive peptide (Speciale et al., 2000; Haufschild et al., 2001; Halder and Milner, 2021).

Finally, the finding of impaired volumetric blood flow in patients with MS is also compatible with the OCTA data of the current study. Our results show a pronounced decrease of capillary density in patients with MS, which again is more pronounced in MS+ON eyes compared to MS-ON eyes or healthy controls. This is also in keeping with previously published studies, which consistently reported a rarefication of the macular and/or peripapillary microvasculature in patients with MS (Feucht et al., 2019; Murphy et al., 2020; Yilmaz et al., 2020). Although OCTA does not allow for direct measurement of volumetric blood flow, it supports the hypothesis that microvascular perfusion may be impaired in patients with MS.

There is increasing evidence that mitochondrial dysfunction plays an important role in several neurodegenerative disorders, including MS (Mao and Reddy, 2010; Barcelos et al., 2019). Given the high metabolic rate of the neural tissue, an impairment of intracellular energy metabolism may easily translate to metabolic stress with the ultimate consequence of neurodegeneration (Mao and Reddy, 2010). Currently, there is no evidence regarding a direct interaction of MS-related mitochondrial dysfunction and decreased retinal oxygen extraction as observed in the current study. However, reduced oxygen metabolism in the retina might be an early sign of an impairment of neural function and may therefore serve as an additional retinal biomarker for disease progression complementing the purely structural parameters such as RNFLT and GCIPL.

Altered retinal oxygen metabolism has consistently been reported also for other neurodegenerative diseases than MS, such as mild cognitive impairment or Alzheimer's disease (Olafsdottir et al., 2018; Stefánsson et al., 2019; Szegedi et al., 2020a), accompanied by a reduction of blood flow (Szegedi et al., 2020a) and microvascular dysfunction (Chua et al., 2020). This supports the hypothesis that oxygen extraction is related to neuronal degeneration or an impairment of neural function. Along this line of thought is has been shown that there is an age-dependent decline of retinal oxygen extraction correlated to the physiological age-dependent ganglion cell loss (Bata et al., 2019).

Our study has several strengths and limitations that warrant further discussion. The strength of our study is the use of a combination of state-of-the-art technology that allows us to draw direct conclusions regarding the oxygen metabolism of the retina. We have successfully used the same approach to assess oxygen extraction in healthy subjects (Palkovits et al., 2014; Werkmeister et al., 2015) as well as in patients with systemic diseases such as diabetes (Fondi et al., 2017), showing for the latter a reduction of oxygen extraction already in early disease stage.

Some limitations need to be addressed as well: First, our study is cross sectional in design. Therefore, based on the current results, it cannot be determined whether decreased blood flow and reduced oxygen extraction of the retinal neural tissue is a causative factor in the pathogenesis of the disease making the eye more vulnerable to damage or a consequence of retinal nerve fiber loss and a reduced oxygen demand of the tissue. Longitudinal studies would be necessary to finally get insight in this question and could also elucidate whether the assessed parameters are subject to temporal change and/or are associated with disease progression. Secondly, the study population is limited to a total number of 34 subjects. A larger study population would increase the power and allow for the detection of mores subtle changes in anatomical and functional properties of the retina especially in MS-ON patients. However, as the equipment used in the current study is not commercially available and requires particular training for the investigator, larger multicenter trials will be dependent on the future commercial availability of devices for measurement of ocular blood flow.

In summary, our data indicates that structural alterations found in the retinal tissue of patients with MS are accompanied by metabolic changes. Both oxygen metabolism and retinal blood flow seem to be impaired in patients with MS and history of ON. Whether this is a cause or a consequence of the disease has yet to be investigated.

DATA AVAILABILITY STATEMENT

The raw data supporting the conclusions of this article will be made available by the authors, without undue reservation.

ETHICS STATEMENT

The studies involving human participants were reviewed and approved by Ethics Committee of the Medical University of Vienna. The patients/participants provided their written informed consent to participate in this study.

AUTHOR CONTRIBUTIONS

MK, DS, and GG contributed to conception and design of the study and drafted the manuscript. MK, NH, AS, GB, and PA were involved in acquisition of data. MK, GB, PA, AP-C, MP, RW, DS, LS, and GG performed the data analysis and interpreted the data. All authors contributed to manuscript revision and approved the submitted version.

FUNDING

Support by the Austrian Science Fund (grant numbers KLI 721 and KLI 529) is gratefully acknowledged.

REFERENCES

Alonso, R., Gonzalez-Moron, D., and Garcea, O. (2018). Optical coherence tomography as a biomarker of neurodegeneration in multiple sclerosis: a review. *Mult. Scler. Relat. Disord.* 22, 77–82. doi: 10.1016/j.msard.2018.03.007

Balci, S., Yildiz, M. B., Ozcelik Kose, A., Suer, D., Turan Vural, E., Emir, C., et al. (2020). Optic Nerve Head Changes in Patients with Optic Neuritis Secondary to Multiple Sclerosis: a Comparison of the Affected and Fellow Healthy Eyes. *Medeni. Med. J.* 35, 330–337.

Balk, L. J., Twisk, J. W., Steenwijk, M. D., Daams, M., Tewarie, P., Killestein, J., et al. (2014). A dam for retrograde axonal degeneration in multiple sclerosis? *J. Neurol. Neurosurg. Psychiatry* 85, 782–789. doi: 10.1136/jnnp-2013-306902

Barcelos, I. P., Troxell, R. M., and Graves, J. S. (2019). Mitochondrial Dysfunction and Multiple Sclerosis. *Biology* 8:37. doi: 10.3390/biology8020037

Bata, A. M., Fondi, K., Szegedi, S., Aschinger, G. C., Hommer, A., Schmidl, D., et al. (2019). Age-Related Decline of Retinal Oxygen Extraction in Healthy Subjects. *Invest. Ophthalmol. Vis. Sci.* 60, 3162–3169. doi: 10.1167/iovs.18-26234

Britze, J., and Frederiksen, J. L. (2018). Optical coherence tomography in multiple sclerosis. *Eye* 32, 884–888.

Britze, J., Pihl-Jensen, G., and Frederiksen, J. L. (2017). Retinal ganglion cell analysis in multiple sclerosis and optic neuritis: a systematic review and meta-analysis. *J. Neurol.* 264, 1837–1853. doi: 10.1007/s00415-017-8531-y

Bsteh, G., Berek, K., Hegen, H., Altmann, P., Wurth, S., Auer, M., et al. (2021). Macular ganglion cell-inner plexiform layer thinning as a biomarker of disability progression in relapsing multiple sclerosis. *Mult. Scler.* 27, 684–694. doi: 10.1177/1352458520935724

Bsteh, G., Hegen, H., Altmann, P., Auer, M., Berek, K., Zinganell, A., et al. (2020). Validation of inter-eye difference thresholds in optical coherence tomography for identification of optic neuritis in multiple sclerosis. *Mult. Scler. Relat. Disord.* 45:102403. doi: 10.1016/j.msard.2020.102403

Bsteh, G., Hegen, H., Teuchner, B., Amprosi, M., Berek, K., Ladstatter, F., et al. (2019a). Peripapillary retinal nerve fibre layer as measured by optical coherence tomography is a prognostic biomarker not only for physical but also for cognitive disability progression in multiple sclerosis. *Mult. Scler.* 25, 196–203. doi: 10.1177/1352458517740216

Bsteh, G., Hegen, H., Teuchner, B., Berek, K., Wurth, S., Auer, M., et al. (2019b). Peripapillary retinal nerve fibre layer thinning rate as a biomarker discriminating stable and progressing relapsing-remitting multiple sclerosis. *Eur. J. Neurol.* 26, 865–871. doi: 10.1111/ene.13897

Chua, J., Hu, Q., Ke, M., Tan, B., Hong, J., Yao, X., et al. (2020). Retinal microvasculature dysfunction is associated with Alzheimer's disease and mild cognitive impairment. *Alzheimers Res. Ther.* 12:161.

Confavreux, C., Vukusic, S., Moreau, T., and Adeleine, P. (2000). Relapses and progression of disability in multiple sclerosis. *N. Engl. J. Med.* 343, 1430–1438. doi: 10.1056/nejm200011163432001

Davies, A. L., Desai, R. A., Bloomfield, P. S., Mcintosh, P. R., Chapple, K. J., Linington, C., et al. (2013). Neurological deficits caused by tissue hypoxia in neuroinflammatory disease. *Ann. Neurol.* 74, 815–825. doi: 10.1002/ana.24006

Doblhoff-Dier, V., Schmetterer, L., Vilser, W., Garhofer, G., Groschl, M., Leitgeb, R. A., et al. (2014). Measurement of the total retinal blood flow using dual beam Fourier-domain Doppler optical coherence tomography with orthogonal detection planes. *Biomed. Opt. Express* 5, 630–642.

Dutta, R., Mcdonough, J., Yin, X., Peterson, J., Chang, A., Torres, T., et al. (2006). Mitochondrial dysfunction as a cause of axonal degeneration in multiple sclerosis patients. *Ann. Neurol.* 59, 478–489. doi: 10.1002/ana.20736

Farci, R., Carta, A., Cocco, E., Frau, J., Fossarello, M., and Diaz, G. (2020). Optical coherence tomography angiography in multiple sclerosis: a cross-sectional study. *PLoS One* 15:e0236090. doi: 10.1371/journal.pone.0236090

Fernandes, D. B., Raza, A. S., Nogueira, R. G., Wang, D., Callegaro, D., Hood, D. C., et al. (2013). Evaluation of inner retinal layers in patients with multiple sclerosis or neuromyelitis optica using optical coherence tomography. *Ophthalmology* 120, 387–394. doi: 10.1016/j.ophtha.2012.07.066

Feucht, N., Maier, M., Lepennetier, G., Pettenkofer, M., Wetzlmair, C., Daltrozzo, T., et al. (2019). Optical coherence tomography angiography indicates associations of the retinal vascular network and disease activity in multiple sclerosis. *Mult. Scler.* 25, 224–234. doi: 10.1177/1352458517750009

Fondi, K., Wozniak, P. A., Howorka, K., Bata, A. M., Aschinger, G. C., Popa-Cherecheanu, A., et al. (2017). Retinal oxygen extraction in individuals with type 1 diabetes with no or mild diabetic retinopathy. *Diabetologia* 60, 1534–1540. doi: 10.1007/s00125-017-4309-0

Garcia-Martin, E., Ara, J. R., Martin, J., Almarcegui, C., Dolz, I., Vilades, E., et al. (2017). Retinal and Optic Nerve Degeneration in Patients with Multiple Sclerosis Followed up for 5 Years. *Ophthalmology* 124, 688–696. doi: 10.1016/j.ophtha.2017.01.005

Garhofer, G., Bek, T., Boehm, A. G., Gherghel, D., Grunwald, J., Jeppesen, P., et al. (2010). Use of the retinal vessel analyzer in ocular blood flow research. *Acta Ophthalmol.* 88, 717–722. doi: 10.1111/j.1755-3768.2009.01587.x

Halder, S. K., and Milner, R. (2021). Hypoxia in multiple sclerosis; is it the chicken or the egg? *Brain* 144, 402–410. doi: 10.1093/brain/awaa427

Hammer, M., Vilser, W., Riemer, T., Mandecka, A., Schweitzer, D., Kuhn, U., et al. (2009). Diabetic patients with retinopathy show increased retinal venous oxygen saturation. *Graefes Arch. Clin. Exp. Ophthalmol.* 247, 1025–1030. doi: 10.1007/s00417-009-1078-6

Hammer, M., Vilser, W., Riemer, T., and Schweitzer, D. (2008). Retinal vessel oximetry-calibration, compensation for vessel diameter and fundus pigmentation, and reproducibility. *J. Biomed. Opt.* 13:054015. doi: 10.1117/1.2976032

Haufschild, T., Shaw, S. G., Kesselring, J., and Flammer, J. (2001). Increased endothelin-1 plasma levels in patients with multiple sclerosis. *J. Neuroophthalmol.* 21, 37–38. doi: 10.1097/00041327-200103000-00011

Hokazono, K., Raza, A. S., Oyamada, M. K., Hood, D. C., and Monteiro, M. L. (2013). Pattern electroretinogram in neuromyelitis optica and multiple sclerosis with or without optic neuritis and its correlation with FD-OCT and perimetry. *Doc. Ophthalmol.* 127, 201–215. doi: 10.1007/s10633-013-9401-2

Hommer, N., Schmidl, D., Kallab, M., Bauer, M., Werkmeister, R. M., Schmetterer, L., et al. (2021). The Effect of Orally Administered Low-Dose Dronabinol on Retinal Blood Flow and Oxygen Metabolism in Healthy Subjects. *J. Ocul. Pharmacol. Ther.* 37, 360–366. doi: 10.1089/jop.2020.0131

Hubbard, L. D., Brothers, R. J., King, W. N., Clegg, L. X., Klein, R., Cooper, L. S., et al. (1999). Methods for evaluation of retinal microvascular abnormalities associated with hypertension/sclerosis in the Atherosclerosis Risk in Communities Study. *Ophthalmology* 106, 2269–2280. doi: 10.1016/s0161-6420(99)90525-0

Jiang, H., Delgado, S., Tan, J., Liu, C., Rammohan, K. W., Debuc, D. C., et al. (2016). Impaired retinal microcirculation in multiple sclerosis. *Mult. Scler.* 22, 1812–1820. doi: 10.1177/1352458516631035

Johnson, T. W., Wu, Y., Nathoo, N., Rogers, J. A., Wee Yong, V., and Dunn, J. F. (2016). Gray Matter Hypoxia in the Brain of the Experimental Autoimmune Encephalomyelitis Model of Multiple Sclerosis. *PLoS One* 11:e0167196. doi: 10.1371/journal.pone.0167196

Kleerekooper, I., Petzold, A., and Trip, S. A. (2020). Anterior visual system imaging to investigate energy failure in multiple sclerosis. *Brain* 143, 1999–2008. doi: 10.1093/brain/awaa049

Knier, B., Berthele, A., Buck, D., Schmidt, P., Zimmer, C., Muhlau, M., et al. (2016). Optical coherence tomography indicates disease activity prior to clinical onset of central nervous system demyelination. *Mult. Scler.* 22, 893–900. doi: 10.1177/1352458515604496

Linsenmeier, R. A., and Zhang, H. F. (2017). Retinal oxygen: from animals to humans. *Prog. Retin. Eye Res.* 58, 115–151. doi: 10.1016/j.preteyeres.2017.01.003

Liu, Y., Delgado, S., Jiang, H., Lin, Y., Hernandez, J., Deng, Y., et al. (2019). Retinal Tissue Perfusion in Patients with Multiple Sclerosis. *Curr. Eye Res.* 44, 1091–1097. doi: 10.1080/02713683.2019.1612444

Mahad, D., Ziabreva, I., Lassmann, H., and Turnbull, D. (2008). Mitochondrial defects in acute multiple sclerosis lesions. *Brain* 131, 1722–1735. doi: 10.1093/brain/awn105

Mao, P., and Reddy, P. H. (2010). Is multiple sclerosis a mitochondrial disease? *Biochim. Biophys. Acta* 1802, 66–79.

Murphy, O. C., Kwakyi, O., Iftikhar, M., Zafar, S., Lambe, J., Pellegrini, N., et al. (2020). Alterations in the retinal vasculature occur in multiple sclerosis and exhibit novel correlations with disability and visual function measures. *Mult. Scler.* 26, 815–828. doi: 10.1177/1352458519845116

Oberwahrenbrock, T., Schippling, S., Ringelstein, M., Kaufhold, F., Zimmermann, H., Keser, N., et al. (2012). Retinal Damage in Multiple Sclerosis Disease Subtypes Measured by High-Resolution Optical Coherence Tomography. *Mult. Scler. Int.* 2012:530305.

Olafsdottir, O. B., Saevarsdottir, H. S., Hardarson, S. H., Hannesdottir, K. H., Traustadottir, V. D., Karlsson, R. A., et al. (2018). Retinal oxygen metabolism in patients with mild cognitive impairment. *Alzheimers Dement.* 10, 340–345. doi: 10.1016/j.dadm.2018.03.002

Palkovits, S., Told, R., Boltz, A., Schmidl, D., Popa Cherecheanu, A., Schmetterer, L., et al. (2014). Effect of increased oxygen tension on flicker-induced vasodilatation in the human retina. *J. Cereb. Blood Flow Metab.* 34, 1914–1918. doi: 10.1038/jcbfm.2014.161

Petzold, A., Balcer, L. J., Calabresi, P. A., Costello, F., Frohman, T. C., Frohman, E. M., et al. (2017). Retinal layer segmentation in multiple sclerosis: a systematic review and meta-analysis. *Lancet Neurol.* 16, 797–812.

Reich, D. S., Lucchinetti, C. F., and Calabresi, P. A. (2018). Multiple Sclerosis. *N. Engl. J. Med.* 378, 169–180.

Sato, Y., Nakajima, S., Shiraga, N., Atsumi, H., Yoshida, S., Koller, T., et al. (1998). Three-dimensional multi-scale line filter for segmentation and visualization of curvilinear structures in medical images. *Med. Image Anal.* 2, 143–168. doi: 10.1016/s1361-8415(98)80009-1

Schindelin, J., Arganda-Carreras, I., Frise, E., Kaynig, V., Longair, M., Pietzsch, T., et al. (2012). Fiji: an open-source platform for biological-image analysis. *Nat. Methods* 9, 676–682. doi: 10.1038/nmeth.2019

Speciale, L., Sarasella, M., Ruzzante, S., Caputo, D., Mancuso, R., Calvo, M. G., et al. (2000). Endothelin and nitric oxide levels in cerebrospinal fluid of patients with multiple sclerosis. *J. Neurovirol.* 6, S62–S66.

Stefánsson, E., Olafsdottir, O. B., Eliasdottir, T. S., Vehmeijer, W., Einarsdottir, A. B., Bek, T., et al. (2019). Retinal oximetry: metabolic imaging for diseases of the retina and brain. *Prog. Retin. Eye Res.* 70, 1–22. doi: 10.1016/j.preteyeres.2019.04.001

Szegedi, S., Hommer, N., Kallab, M., Puchner, S., Schmidl, D., Werkmeister, R. M., et al. (2020b). Repeatability and Reproducibility of Total Retinal Blood Flow Measurements Using Bi-Directional Doppler OCT. *Transl. Vis. Sci. Technol.* 9:34.

Szegedi, S., Dal-Bianco, P., Stögmann, E., Traub-Weidinger, T., Rainer, M., Masching, A., et al. (2020a). Anatomical and functional changes in the retina in patients with Alzheimer's disease and mild cognitive impairment. *Acta Ophthalmol.* 98, e914–e921.

Tan, B., Sim, R., Chua, J., Wong, D. W. K., Yao, X., Garhofer, G., et al. (2020). Approaches to quantify optical coherence tomography angiography metrics. *Ann. Transl. Med.* 8:1205. doi: 10.21037/atm-20-3246

Toosy, A. T., Mason, D. F., and Miller, D. H. (2014). Optic neuritis. *Lancet Neurol.* 13, 83–99.

Toussaint, D., Perier, O., Verstappen, A., and Bervoets, S. (1983). Clinicopathological study of the visual pathways, eyes, and cerebral hemispheres in 32 cases of disseminated sclerosis. *J. Clin. Neuroophthalmol.* 3, 211–220.

Walter, S. D., Ishikawa, H., Galetta, K. M., Sakai, R. E., Feller, D. J., Henderson, S. B., et al. (2012). Ganglion cell loss in relation to visual disability in multiple sclerosis. *Ophthalmology* 119, 1250–1257. doi: 10.1016/j.ophtha.2011.11.032

Wang, L., Kwakyi, O., Nguyen, J., Ogbuokiri, E., Murphy, O., Caldito, N. G., et al. (2018). Microvascular blood flow velocities measured with a retinal function imager: inter-eye correlations in healthy controls and an exploration in multiple sclerosis. *Eye Vis.* 5:29.

Werkmeister, R. M., Dragostinoff, N., Palkovits, S., Told, R., Boltz, A., Leitgeb, R. A., et al. (2012a). Measurement of absolute blood flow velocity and blood flow in the human retina by dual-beam bidirectional Doppler fourier-domain optical coherence tomography. *Invest. Ophthalmol. Vis. Sci.* 53, 6062–6071. doi: 10.1167/iovs.12-9514

Werkmeister, R. M., Palkovits, S., Told, R., Groschl, M., Leitgeb, R. A., Garhofer, G., et al. (2012b). Response of retinal blood flow to systemic hyperoxia as measured with dual-beam bidirectional Doppler Fourier-domain optical coherence tomography. *PLoS One* 7:e45876. doi: 10.1371/journal.pone.0045876

Werkmeister, R. M., Dragostinoff, N., Pircher, M., Gotzinger, E., Hitzenberger, C. K., Leitgeb, R. A., et al. (2008). Bidirectional Doppler Fourier-domain optical coherence tomography for measurement of absolute flow velocities in human retinal vessels. *Opt. Lett.* 33, 2967–2969. doi: 10.1364/ol.33.002967

Werkmeister, R. M., Schmidl, D., Aschinger, G., Doblhoff-Dier, V., Palkovits, S., Wirth, M., et al. (2015). Retinal oxygen extraction in humans. *Sci. Rep.* 5:15763.

Yang, R., and Dunn, J. F. (2015). Reduced cortical microvascular oxygenation in multiple sclerosis: a blinded, case-controlled study using a novel quantitative near-infrared spectroscopy method. *Sci. Rep.* 5:16477.

Yang, R., and Dunn, J. F. (2019). Multiple sclerosis disease progression: contributions from a hypoxia-inflammation cycle. *Mult. Scler.* 25, 1715–1718. doi: 10.1177/1352458518791683

Yilmaz, H., Ersoy, A., and Icel, E. (2020). Assessments of vessel density and foveal avascular zone metrics in multiple sclerosis: an optical coherence tomography angiography study. *Eye* 34, 771–778. doi: 10.1038/s41433-019-0746-y

Conflict of Interest: The authors declare that the research was conducted in the absence of any commercial or financial relationships that could be construed as a potential conflict of interest.

Publisher's Note: All claims expressed in this article are solely those of the authors and do not necessarily represent those of their affiliated organizations, or those of the publisher, the editors and the reviewers. Any product that may be evaluated in this article, or claim that may be made by its manufacturer, is not guaranteed or endorsed by the publisher.

frontiers in Neuroscience

REVIEW
published: 29 October 2021
doi: 10.3389/fnins.2021.725187

Role of Multifocal Visually Evoked Potential as a Biomarker of Demyelination, Spontaneous Remyelination, and Myelin Repair in Multiple Sclerosis

Alexandr Klistorner[1,2]* *and Stuart L. Graham*[2]

[1] Department of Ophthalmology, The University of Sydney, Darlington, NSW, Australia, [2] Department of Ophthalmology, Macquarie University, Sydney, NSW, Australia

Multiple sclerosis (MS) is a complex disease of the central nervous system (CNS), characterized by inflammation, demyelination, neuro-axonal loss, and gliosis. Inflammatory demyelinating lesions are a hallmark of the disease. Spontaneous remyelination, however, is often incomplete and strategies that promote remyelination are needed. As a result, accurate and sensitive *in vivo* measures of remyelination are necessary. The visual pathway provides a unique opportunity for *in vivo* assessment of myelin damage and repair in the MS-affected brain since it is highly susceptible to damage in MS and is a very frequent site of MS lesions. The visually evoked potential (VEP), an event-related potential generated by the striate cortex in response to visual stimulation, is uniquely placed to serve as a biomarker of the myelination along the visual pathway. The multifocal VEP (mfVEP) represents a most recent addition to the array of VEP stimulations. This article provides a current view on the role of mfVEP as a biomarker of demyelination, spontaneous remyelination, and myelin repair in MS.

Keywords: multiple sclerosis, demyelination, remyelination, visual evoked cortical potentials, clinical trial

OPEN ACCESS

Edited by:
Tim Magnus,
University of Hamburg, Germany

Reviewed by:
Alessandro d'Ambrosio,
University of Campania Luigi Vanvitelli, Italy
Elena Gonzalez-Rey,
Instituto de Parasitología y Biomedicina López-Neyra (IPBLN), Spain

***Correspondence:**
Alexandr Klistorner
sasha.klistorner@sydney.edu.au

Specialty section:
This article was submitted to Neurodegeneration, a section of the journal Frontiers in Neuroscience

Received: *15 June 2021*
Accepted: *01 October 2021*
Published: *29 October 2021*

Citation:
Klistorner A and Graham SL (2021) Role of Multifocal Visually Evoked Potential as a Biomarker of Demyelination, Spontaneous Remyelination, and Myelin Repair in Multiple Sclerosis. Front. Neurosci. 15:725187. doi: 10.3389/fnins.2021.725187

Multiple sclerosis (MS) is a complex disease of the central nervous system (CNS), characterized by inflammation, demyelination, neuro-axonal loss, and gliosis. Inflammatory demyelinating lesions are a hallmark of the disease. The acute stage of lesion formation initially results in a complete block of conduction (and associated functional deficit) along the axons affected by the inflammation. Axonal conduction (and function), however, typically recovers within a few weeks, during which inflammation subsides, ion channels are reconstructed and conduction in surviving but demyelinated axons resumes, although often in a slower, continuous mode (Smith and Waxman, 2005). This restoration of conduction along the demyelinated axons is due to appearance of more widely distributed sodium channels that are diffusely deployed along demyelinated axolemma (Felts et al., 1997; Waxman, 2005).

Permanent demyelination, however, may contribute to accelerated degeneration of surviving axons by rendering them vulnerable to physiological stress (Kornek et al., 2000; Bruck et al., 2003). Chronic demyelination increases the energy demands of axonal conduction, ultimately compromising axoplasmic adenosine triphosphate (ATP) production, leading to an ionic imbalance and Ca^{2+}-mediated axonal degeneration (Correale et al., 2017). In addition, lack

of trophic support from myelin or oligodendrocytes and disruption of normal axon–myelin interactions may result in degeneration of chronically demyelinated axons (Trapp et al., 1999; Peterson and Fujinami, 2007).

While spontaneous remyelination was first described in MS in 1965 (Périer and Grégoire, 1965) and is now believed to be an early and frequent phenomenon occurring in MS (Raine and Wu, 1993; Patrikios et al., 2006), it is often incomplete (Prineas et al., 1989; Bramow et al., 2010) and strategies that promote remyelination are needed. A number of approaches to promote myelin repair have made significant progress in experimental models (Suhs et al., 2012) and it is now emerging as a new target for neuroprotective strategies, making its way into human clinical trials (see Cunniffe and Coles, 2019; Lubetzki et al., 2020 for review). Therefore, accurate and sensitive *in vivo* measures that can assess and verify the therapeutic and biological efficacy of putative remyelinating treatments are necessary in order for a transition to clinical therapy.

A number of imaging techniques have been suggested as potential surrogate biomarkers of myelin damage and repair in MS brain. There are several recent reviews examining the potential use of various imaging biomarkers in remyelination trials (Barkhof et al., 2009; Mallik et al., 2014; Oh et al., 2019). In this review, however, we concentrate on electrophysiological assessment of de/remyelination in MS patients.

The visual pathway provides a unique opportunity for *in vivo* assessment of myelin damage and repair in the MS-affected brain. Firstly, the visual system is highly susceptible to damage in MS and is a very frequent site of MS lesions. Optic neuritis (ON) is the presenting symptom of MS in approximately 20% of MS patients and evidence of previous ON is typically detected in half of the relapsing-remitting (RR) MS population, while optic radiation (OR) lesions are seen in about two-thirds (**Figure 1**; Hornabrook et al., 1992; Jenkins et al., 2010; Klistorner et al., 2015).

Secondly, the strictly hierarchical structure of the visual system provides an opportunity to follow the effect of MS damage along several levels of inter-connected neurons. Thirdly, with the advent of tractography [based on diffusion magnetic resonance imaging (MRI)], the entire length of the visual pathway, including the OR, can now be visualized and its structural damage can be quantified (**Figure 2**; Sherbondy et al., 2008).

In addition, contrary to many other white matter pathways, the visual pathway allows study of the dynamics of myelin alteration in both acute and chronic lesions. This is due to the fact that, while OR lesions are typically silent, lesions of the anterior visual pathway are clinically apparent.

Furthermore, accurate and quantifiable measures of visual system function, such as visual acuity [and low contrast visual acuity (LCVA) in particular], are readily available (Balcer et al., 2017).

Finally, the visually evoked potential (VEP), an event-related potential generated by the striate cortex in response to visual stimulation (Fahle and Bach, 2006), is uniquely placed to serve as a biomarker of the myelination along the visual pathway based on the following rationale. The VEP represents an electrical signal generated at the level of striate cortex by the combined activity of post-synaptic potentials in response to visual stimulation (Creutzfeldt et al., 1969; Fahle and Bach, 2006). As a result, its magnitude ("amplitude") and timing ("latency") are affected by pathological changes (such, for example, as MS lesions) along the entire visual pathway. Thus, it was suggested that amplitude of the VEP reflects the number of functional fibers along the visual pathway and is determined by the severity of inflammation in the acute stage of MS lesion and subsequent axonal degeneration in later stages (Jones and Brusa, 2003). Latency, on the other hand, is related to the speed of conduction. Since the slowing of conduction affects only the demyelinated portion of the axons (Smith and Waxman, 2005; Waxman, 2005), the extent of demyelinated area is likely to be proportional to the delay of VEP arrival to the visual cortex, i.e., delay of VEP latency. As a result, in contrast to most brain lesions, the effect of myelin loss

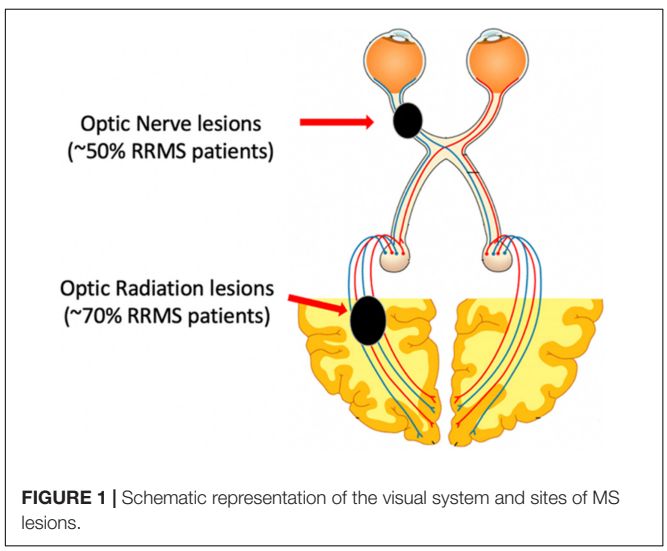

FIGURE 1 | Schematic representation of the visual system and sites of MS lesions.

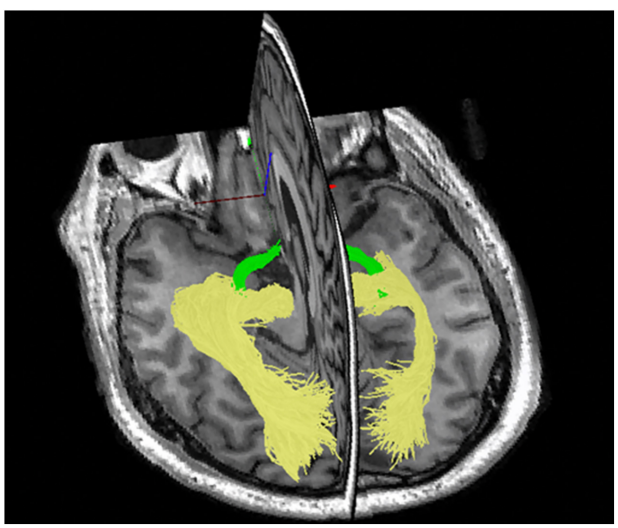

FIGURE 2 | Tractography of the optic tract (green) and optic radiation using ConTrack software.

and recovery can be qualitatively measured by the latency delay (Halliday et al., 1972).

This close association between VEP latency delay and degree of visual pathway demyelination has been confirmed by clinical and experimental studies. For example, van der Walt et al. (2015) demonstrated a high degree of concordance between the length of optic nerve lesion and relative latency delay of the VEP derived from stimulation of corresponding eye (**Figure 3**). Similar relationships have been found in animal studies (You et al., 2011; Heidari et al., 2019). A study by Alshowaeir et al. (2014) also revealed a close relationship between VEP latency delay and lesion volume in posterior visual pathway.

Since the VEP is generated at the level of striate cortex, it is affected by pathological changes along the entire visual pathway. Therefore, latency delay of the VEP reflects the combined effect of demyelination in the entire visual system including optic nerve and OR. However, due to the unique topographic anatomy of the visual system (i.e., post-chiasmal crossing and projection of fibers subserving similar parts of the visual field of both eyes to the same area of the cortex), the effect of optic nerve and OR demyelination on VEP can be differentiated. Thus, demyelinating lesions of OR typically produce a similar delay of the VEP response in both eyes. Conversely, since lesions of the optic nerve in MS are, as a rule, unilateral, optic nerve demyelination only affects VEP recorded in response to stimulation of the affected eye. Furthermore, the monocular nature of ON allows comparison of VEP parameters recorded from the affected eye with data obtained from the fellow (unaffected) eye. Using this inter-eye latency difference (asymmetry) significantly reduces between-subject variability, providing a very accurate measure of optic nerve de/remyelination (Graham et al., 2000; Hood et al., 2000b; Klistorner et al., 2018).

There are several stimulating modalities that are employed to generate the VEP. Flash stimuli are typically used in animal studies and to record VEP response from non-cooperative patients or young children, while pattern-reversal full or half-field VEPs are commonly used in adults (Fahle and Bach, 2006). The multifocal VEP (mfVEP) represents a most recent addition to the array of VEP stimulations. The multifocal technique was initially developed by Sutter and Tran (1992); Baseler et al. (1994), Baseler and Sutter (1997) and later modified and improved to study cortical responses, first in glaucoma and later in demyelinating diseases (Klistorner et al., 1998, 2010; Hood et al., 2000a; Fraser et al., 2006).

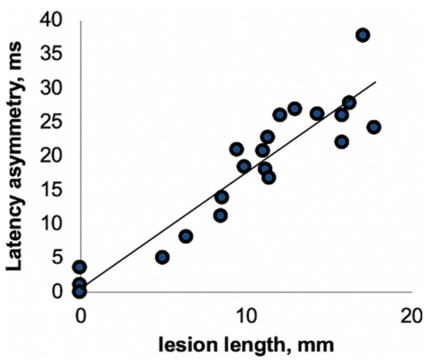

FIGURE 3 | Correlation between optic nerve lesion and mfVEP latency delay [from van der Walt et al. (2015)].

There are several advantages of mfVEP over full-field stimulation (**Table 1**).

The conventional full-field VEP provides a summed response of all neuronal elements stimulated and is greatly dominated by the macular region due to its cortical overrepresentation (Daniel and Whittridge, 1961). It has been estimated that 65% of the total full-field VEP response represents the central 2°of the visual field (Riggs and Wooten, 1972; Yiannikas and Walsh, 1983). A small unified check size, which is commonly used for full-field pattern stimulation, is another factor that tends to bias the central response (Harter, 1970).

In addition, being the vector sum of numerous differently oriented dipoles (caused by projection of upper and lower hemifields to oppositely oriented banks of the calcarine sulcus, which is further exacerbated by local cortical convolution), the waveform of the full-field VEP is prone to unpredictable change depending on the part of the nerve/visual field affected, leading sometimes to detection of apparent rather than real amplitude and latency change (Halliday et al., 1979; Klistorner et al., 1998). This is particularly apparent in case of OR lesions.

In contrast, the mfVEP simultaneously stimulates numerous small areas (typically 56) of the visual field using pseudorandom sequences and is able to extract individual responses from each stimulated area independently and at the same time (Sutter and Tran, 1992; Klistorner et al., 1998). This, together with cortical scaling of the stimulating areas, provides a much larger field of examination, which typically extends to 25° of eccentricity. In addition, larger check size at more peripheral locations produces an optimal mfVEP response from different parts of the visual field (**Figure 4A**; Balachandran et al., 2002). The introduction of orthogonally oriented bipolar recording channels straddling the inion (Klistorner and Graham, 2000) also enhanced the ability of mfVEP to detect signals from all parts of the visual field regardless of the orientation of the underlying striate cortex dipole (**Figure 4B**).

Furthermore, stimulation of small areas of the visual field eliminates the cancelation effect of various dipole orientation caused by the opposite position of upper and lower banks of calcarine sulcus (subserving the upper and lower hemifields) and cortical convolution, which is a serious limitation for the full-field VEP.

Since it was established that signals derived from the peripheral areas of the visual fields are less delayed and recover faster than responses derived from the central areas of the visual fields, this may also contribute to cancelation or distortion of the full-field VEP as it is a summed response (Klistorner et al., 2007).

There are various ways to measure mfVEP latency. Individual segments can be assessed independently and a retinotopically organized plot of latency delay can be constructed (both as absolute value of latency delay and deviation from a normative database) (**Figure 5**).

TABLE 1 | Comparison between full-field and multifocal VEP.

	Full-field VEP	Multifocal VEP
Retinal topography of the response	Dominated by the macular region	Equally distributed within central 48° of the visual field
Number of stimulating fields	Single	Multiple (up to 56)
Number of responses in individual recording	Single combined response	Independent responses from multiple small areas of the visual field
Ability to assess retinal topography of the response	No	Yes
Susceptible to cancelation between upper and lower hemifields	Yes	No
Cortically scaled stimulation	No	Yes

Alternatively, an averaged value of latency across all areas of the stimulated eye can be used. However, contrary to full-field VEP, averaging of mfVEP areas does not result in cancelation or distortion of the total signal since numerical values of latency not waveforms are averaged.

In summary, the mfVEP better reflects the true state of the conductivity along the visual pathway by including information from fibers subserving more peripheral parts of the visual field and eliminating cancelation effects of differently oriented dipoles. Simultaneous recording from a plurality of visual field locations and use of orthogonal channels also results in higher spatial resolution of the mf VEP technique, allowing independent assessment of multiple regions.

While a number of imaging techniques such as magnetization transfer ratio, diffusion tensor imaging, and myelin water fraction have been recently suggested as potential biomarkers for de/remyelination in MS lesions (Jelescu et al., 2016; van der Weijden et al., 2020; Klistorner S. A. et al., 2021), there is no current consensus on an issue of which one should be selected. There are also no clinical studies to compare sensitivity and specificity between imaging and electrophysiological (and VEP in particular) techniques in assessing de/remyelination.

ACUTE LESIONS OF THE VISUAL PATHWAY

The majority of new white matter lesions in MS are clinically silent and, as a result, are typically detected during routine MRI examination long after the acute inflammatory stage. Optic nerve lesions, on the other hand, are usually clinically apparent from the onset and, therefore, provide a unique platform to study spontaneous remyelination, as well as treatment-induced myelin repair in the early post-acute period using VEP latency as a biomarker (Hood et al., 2000a; Klistorner et al., 2010; Cadavid et al., 2017; Klistorner A. et al., 2021).

Furthermore, since precise timing of ON onset is known, the ON model also offers an opportunity to investigate the effect of the lesion's age on remyelinating capacity of any potential treating agent by studying patients with different post-ON intervals.

This is of particular importance since it is believed that remyelination is more likely to succeed in the acute or recent MS lesion, while the environment for successful remyelination may become less permissive in longstanding lesions (Chari and Blakemore, 2002; Ruffini et al., 2004). The "window of opportunity" for the process of remyelination to be successful (Blakemore et al., 2002) may be related to pro-reparative interactions between various cell populations and cytokines within the early MS lesion (Chari and Blakemore, 2002; Foote and Blakemore, 2005; Zhao et al., 2005). This critical period may open following sufficient expansion and differentiation of perilesional and lesional oligodendrocyte precursor cells and end with the conversion of acute to chronic inflammation status (Kotter et al., 2011). This age effect on the lesion is therefore likely to influence both spontaneous and treatment-induced remyelination that may be achieved.

Multifocal Visually Evoked Potential Studies of Spontaneous Remyelination of Acute Lesions

Both experimental and clinical studies have demonstrated that after a brief block of conduction caused by acute inflammation, the surviving, but chronically demyelinated axons largely recover the ability to conduct (Smith and Waxman, 2005; Klistorner et al., 2010). This general pattern is well reflected in clinical and electrophysiological recovery after an episode of acute ON. It was shown that after the resolution of acute inflammation that typically occurs within 1–2 weeks from the onset of ON, the conduction along the demyelinated part of the affected axons resumes, resulting in restoration of vision and recovery of VEP amplitude. However, similar to full-field VEP, immediately after recovery of the conduction block, the latency of mfVEP often displays significant prolongation. We have previously demonstrated that this latency delay is highly proportional to the length of the acute demyelinated area along the optic nerve (**Figure 3**; Klistorner et al., 2010) and, therefore, reflects the degree of initial myelin loss (Hood et al., 2000a; Jones and Brusa, 2003; Klistorner et al., 2010; van der Walt et al., 2015).

Subsequent shortening of mfVEP latency, which is frequently observed after this initial delay, is thought to represent the process of spontaneous remyelination (Hood et al., 2000a; Klistorner et al., 2010; van der Walt et al., 2015). The mfVEP latency improvement, however, is limited in magnitude and restricted in time (Klistorner et al., 2010). Thus, the speed of latency recovery is fastest during first 3 months after an acute episode of ON, but gradually decelerates in the following months

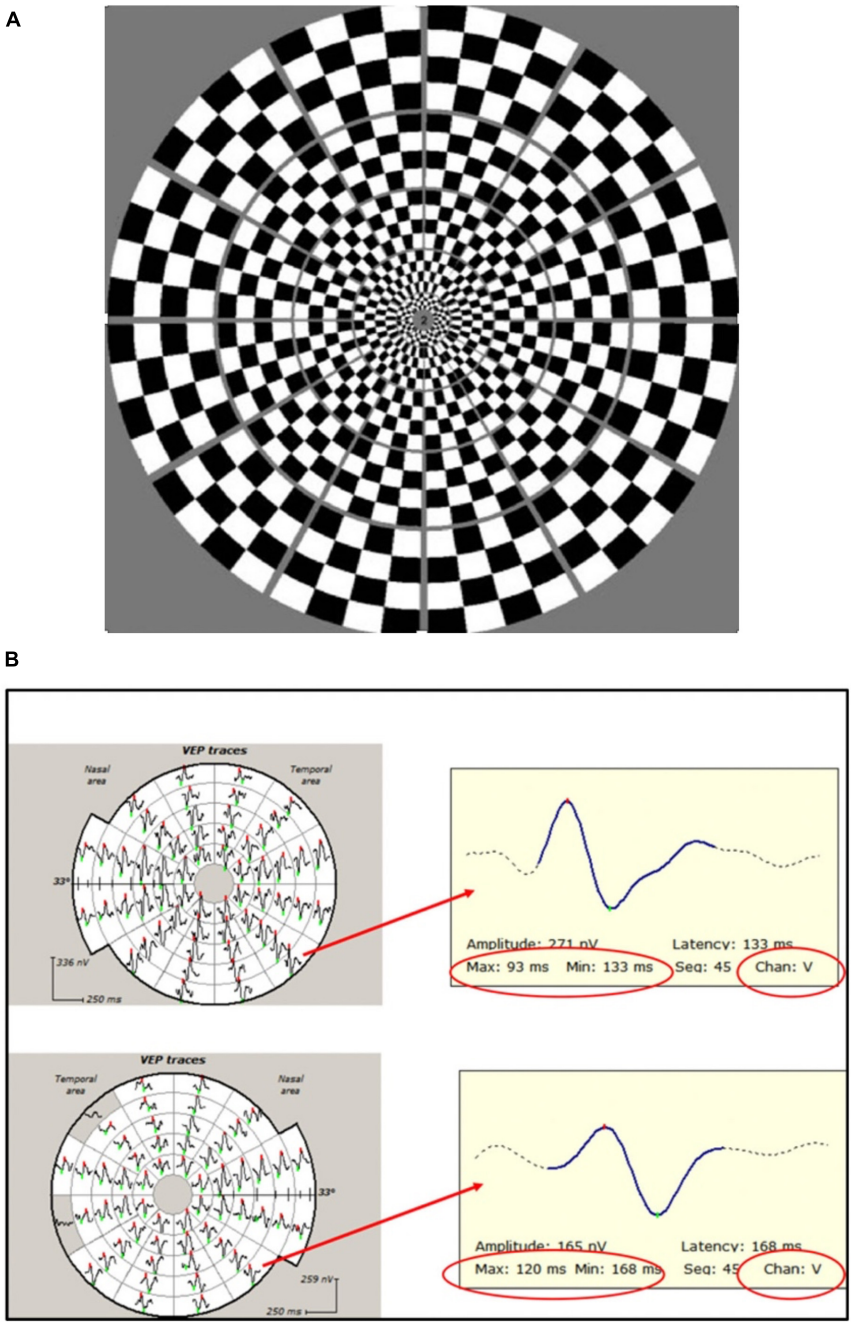

FIGURE 4 | (A) Dartboard stimulus used in mfVEP recording. **(B)** Example of mfVEP recording from ON (bottom row) and fellow (upper row) eyes. Individual travels from corresponding segments magnified to demonstrate latency measurement. Note that the same channel (vertical) is selected for inter-eye comparison.

and finally ceases by the end of the first year, remaining stable thereafter (Klistorner et al., 2010, Klistorner et al., 2020).

In addition, it was demonstrated that, at least in the optic nerve, the magnitude of post-acute latency shortening (i.e., spontaneous remyelination) is largely independent of initial latency delay (presumed size of the initial demyelinated lesion). For example, while in some cases initial (4 weeks after ON onset) latency delay of the mfVEP exceeds 35–40 ms (indicating almost total demyelination of the optic nerve), latency improvement does not usually go beyond 10–15 ms (average latency recovery 11.3 $\pm$ 3 ms) (Klistorner et al., 2010), indicating disproportionately small remyelination of large lesions (**Figure 6**). This partial recovery of mfVEP latency (van der Walt et al., 2015) reflects the limited nature of spontaneous remyelination, which is well documented in experimental and pathological studies (see Cunniffe and Coles, 2019 for review).

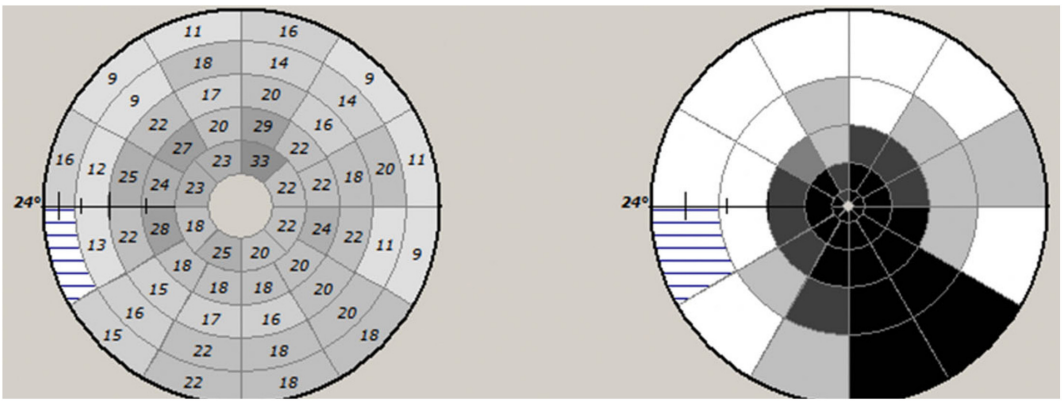

FIGURE 5 | Example of mfVEP latency asymmetry values of individual segments (left) and plot of probability values of deviation from normative database.

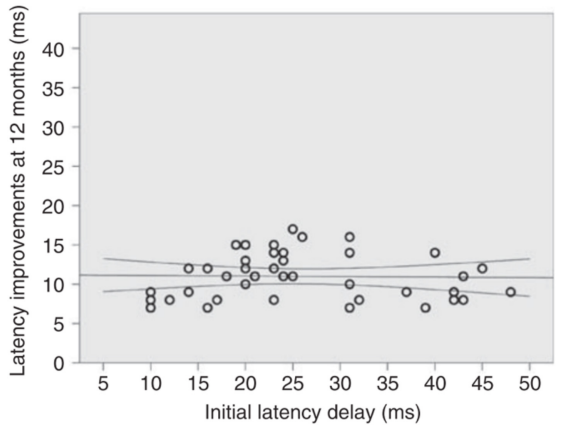

FIGURE 6 | Absolute latency recovery values at 12 months plotted against baseline latency delay [from Klistorner et al. (2010)].

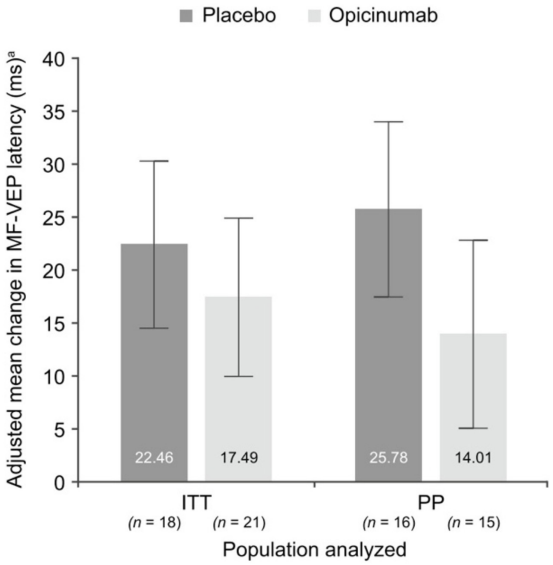

FIGURE 7 | Mean change in mfVEP latency, adjusted for the baseline latency of unaffected fellow eye, at week 24 in the affected eye compared with the unaffected fellow eye at baseline in the substudy ITT and PP populations [from Klistorner et al. (2018)].

Multifocal Visually Evoked Potential Studies of Treatment-Induced Remyelination of Acute Lesions

The acute ON model is becoming a method of choice for clinical trials aimed at myelin repair (Tsakiri et al., 2012; Galetta et al., 2015; Cadavid et al., 2017; Klistorner et al., 2018).

The mfVEP has recently been used to study remyelination in a clinical trial of monoclonal antibody opicinumab, which previously shows remyelinating activity in pre-clinical studies (RENEW and RENEWED). In the RENEW study, patients were treated with 100 mg/kg opicinumab for 20 weeks and assessed up to week 32, while the RENEWED study was designed as a follow-up study at 2 years after the last visit of RENEW study.

In the RENEW study, both the conventional full-field VEP (which was the primary endpoint of the study) and the mfVEP latency demonstrated a larger improvement in ON eyes of patients treated with opicinumab compared to placebo (Cadavid et al., 2017; Klistorner et al., 2018), although this only reached borderline significance. The average latency improvement in treated eyes compared to placebo was 7.6 ms in full-field VEP and 11.8 ms in mfVEP in the per-protocol population (**Figure 7**). The mfVEP result, however, was achieved with half of the sample size compared to full-field VEP (39 vs. 82 patients). The sample size advantage of using mfVEP was confirmed by a *post hoc* comparison of estimated effect size for change in mfVEP and full-field VEP latency for opicinumab versus placebo at week 24 in the intention-to-treat population, which showed that the mfVEP demonstrated a larger treatment effect size than full-field VEP (Klistorner et al., 2018).

Furthermore, while the high variability of full-field VEP precluded any meaningful assessment of amplitude, analysis of

mfVEP demonstrated evidence that fellow eye amplitude loss occurs after ON but can potentially be prevented by opicinumab treatment (Klistorner et al., 2018).

The RENEWED study also demonstrated higher sensitivity of mfVEP in monitoring treatment-induced remyelination compared to full-field VEP. The average difference between latency recovery of mfVEP in the treated vs. placebo group increased from 14.4 to 19.6 ms over the 2 years after treatment was terminated, while full-field VEP demonstrated reduction of latency recovery from 9.4 to 6.0 ms during the same period (Aktas et al., 2020).

Further analysis of mfVEP revealed that in the opicinumab group, there was a strong association between the degree of latency delay at baseline (as measured at week 4) and the latency recovery at RENEWED day 1 (r^2 = 0.72, p = 0.004, Pearson correlation coefficient). Conversely, the magnitude of mfVEP latency recovery was limited in the placebo group and did not correlate with initial degree of latency delay (p = 0.2) (Klistorner et al., 2020), which was consistent with the results of the "natural history" study of spontaneous optic nerve remyelination following an episode of acute ON reported earlier (Klistorner et al., 2010).

Therefore, in the presumed treatment-induced (opicinumab) remyelination following acute ON, the degree of myelin recovery was highly proportional to the extent of initial myelin loss (Klistorner et al., 2020).

It must be noted that while the degree of acute demyelination cannot often be assessed because of frequent incidence of edema and conduction block, continuous conduction along the demyelinated part of the affected axons typically resumes by 3–4 weeks, which still provides a good indication of the extent of original demyelination (van der Walt et al., 2015).

CHRONIC LESIONS OF THE VISUAL PATHWAY

While the clinical potential for remyelination of chronic lesions is more challenging (see discussion related to "window of opportunity" above), it is also extremely important since the diagnosis of MS is typically delayed (Klistorner et al., 2017) due to the fact that majority of MS lesions are clinically silent. As a result, it is exceedingly difficult to identify acute lesions. In addition, by the time of MS diagnosis, the patient often presents with a number of chronic brain lesions.

The visual system can also be used to monitor myelin alteration in chronic lesions. As stated above, since mfVEP is generated at the level of primary (striate) visual cortex but reflects the integrity of the full visual pathway, it is affected by the speed of conduction and, therefore, degree of de/remyelination along the entire pathway, including optic nerve and OR. Accordingly, delay of mfVEP latency in non-acute ON patients does reflect the combined effect of chronic demyelination in both optic nerve and OR. Since the effect of a chronic optic nerve lesion on mfVEP is usually monocular, while OR lesions will yield binocular latency delay due to partial chiasmal crossing of visual pathway, this provides a point of differentiation.

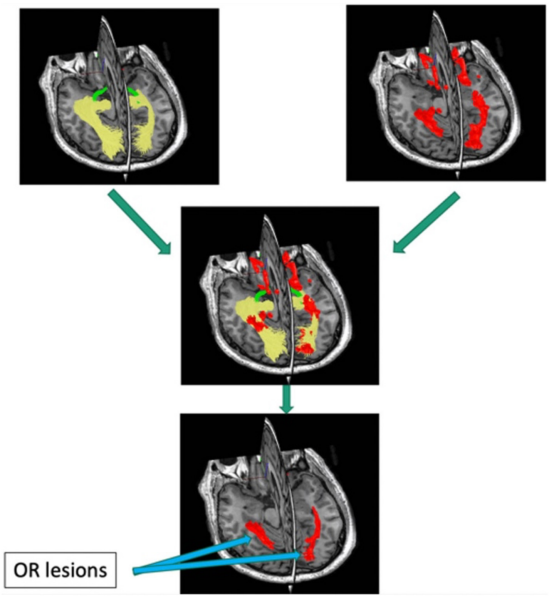

FIGURE 8 | Pipeline for detecting optic radiation lesions. Optic radiation (determined by tractography in yellow) is intersected with brain lesion mask (red).

Quantitative investigation of the association between mfVEP latency delay and MS-related damage of posterior visual pathway was aided by the relatively recent development of diffusion-based tractography, which enabled identification and segmentation of major white matter tracts including ORs (Sherbondy et al., 2008). Intersection of the brain lesion mask with OR mask obtained using brain white matter tractography (**Figure 8**) enabled accurate volumetric assessment of the OR lesions and demonstrated significant association between structural MRI-based estimation and electrophysiological measurement of OR demyelination (Alshowaeir et al., 2014), and confirmed the above relationship between OR lesions and binocular latency delays.

Multifocal Visually Evoked Potential Studies of Treatment-Induced Remyelination of Chronic Lesions

The mfVEP has also recently been employed as a biomarker for clinical trials to examine possible remyelination in chronic lesions, in combination with MRI. The utility of the mfVEP is further strengthened by our longitudinal analysis, which demonstrated the remarkably stable nature of mfVEP latency after 12 months in the absence of new lesional activity in the visual pathway (Klistorner et al., 2020).

While patient recruitment within a short window after symptom onset represents a limiting factor for acute ON trials, selection of patients for remyelinating trials based on chronic visual pathway lesions is less challenging. The main enrollment

criteria for such trials are the presence of measurable mfVEP signal (includes ∼95% of RRMS population) and significant latency delay indicating chronic demyelination along the visual pathway (includes ∼70% of RRMS population). Furthermore, the sample size calculated for 12 months in a clinical trial of a potential remyelinating agent based on latency of the mfVEP revealed that a relatively small sample size would be required to demonstrate efficacy of remyelination therapy (Klistorner et al., 2020). This approach has been tested in a substudy of the large clinical trial of opicinumab (SYNERGY, Biogen) and is currently employed in the VISIONARY-MS trial to test the efficacy of gold nanoparticles (Clene Nanomedicine, United States) and the CCMR Two trial to test the combination of metformin and clemastine (University of Cambridge, United States) in remyelination of chronic MS lesions.

Multifocal Visually Evoked Potential in Other Neurological Conditions

While mfVEP has also been used in monitoring other neurological conditions, such as neurofibromatosis, Leber's optic neuropathy, chronic inflammatory demyelinating polyneuropathy, optic disc drusen, chiasmal decompression, compressive optic neuropathy, and schizophrenia (Semela et al., 2009; Yamada et al., 2011; Raz et al., 2015; Ziccardi et al., 2015; Malmqvist et al., 2017; Graf et al., 2018; Jayanetti et al., 2018), its application is sporadic and clinical usefulness is limited.

AUTHOR CONTRIBUTIONS

Both authors listed have made a substantial, direct and intellectual contribution to the work, and approved it for publication.

FUNDING

This study was supported by NMSS- Grant RG 4716A7/3, Sydney Hospital Foundation and Sydney Medical Research Foundation.

REFERENCES

Aktas, O., Ziemssen, F., Ziemssen, T., Comi, G., Butzkueven, H., Izquierdo, G., et al. (2020). *RENEWED: Long-Term Electrophysiological and Clinical Outcomes in Participants Previously Enrolled in the Opicinumab Phase 2 Study RENEW*. Philadelphia, PA: Wolters Kluwer Health, Inc.

Alshowaeir, D., Yiannikas, C., Garrick, R., Parratt, J., Barnett, M. H., Graham, S. L., et al. (2014). Latency of multifocal visual evoked potentials in nonoptic neuritis eyes of multiple sclerosis patients associated with optic radiation lesions. *Invest. Ophthalmol. Vis. Sci.* 55, 3758–3764. doi: 10.1167/iovs.14-14571

Balachandran, C., Klistorner, A., and Graham, S. L. (2002). Effect of stimulus check size on multifocal visual evoked potentials. *Doc. Ophthalmol.* 106, 183–188.

Balcer, L. J., Raynowska, J., Nolan, R., Galetta, S. L., Kapoor, R., Benedict, R., et al. (2017). Validity of low-contrast letter acuity as a visual performance outcome measure for multiple sclerosis. *Mult. Scler.* 23, 734–747. doi: 10.1177/1352458517690822

Barkhof, F., Calabresi, P. A., Miller, D. H., and Reingold, S. C. (2009). Imaging outcomes for neuroprotection and repair in multiple sclerosis trials. *Nat. Rev. Neurol.* 5, 256–266. doi: 10.1038/nrneurol.2009.41

Baseler, H. A., and Sutter, E. E. (1997). M and P components of the VEP and their visual field contribution. *Vis. Res.* 37, 675–790. doi: 10.1016/S0042-6989(96)00209-X

Baseler, H. A., Sutter, E. E., Klein, S. A., and Carney, T. (1994). The topography of visual evoked response properties across the visual field. *Electroencephal. Clin. Neurophysiol.* 90, 65–81. doi: 10.1016/0013-4694(94)90114-7

Blakemore, W. F., Chari, D. M., Gilson, J. M., and Crang, A. J. (2002). Modelling large areas of demyelination in the rat reveals the potential and possible limitations of transplanted glial cells for remyelination in the CNS. *Glia* 38, 155–168. doi: 10.1002/glia.10067

Bramow, S., Frischer, J. M., Lassmann, H., Koch-Henriksen, N., Lucchinetti, C. F., Sorensen, P. S., et al. (2010). Demyelination versus remyelination in progressive multiple sclerosis. *Brain* 133, 2983–2998. doi: 10.1093/brain/awq250

Bruck, W., Kuhlmann, T., and Stadelmann, C. (2003). Remyelination in multiple sclerosis. *J. Neurol. Sci.* 206, 181–185. doi: 10.1016/S0022-510X(02)00191-0

Cadavid, D., Balcer, L., Galetta, S., Aktas, O., Ziemssen, T., Vanopdenbosch, L., et al. (2017). Safety and efficacy of opicinumab in acute optic neuritis (RENEW): a randomised, placebo-controlled, phase 2 trial. *Lancet Neurol.* 16, 189–199. doi: 10.1016/S1474-4422(16)30377-5

Chari, D. M., and Blakemore, W. F. (2002). New insights into remyelination failure in multiple sclerosis: implications for glial cell transplantation. *Mult. Scler.* 8, 271–277. doi: 10.1191/1352458502ms842oa

Correale, J., Gaitán, M. I., Ysrraelit, M. C., and Fiol, M. P. (2017). Progressive multiple sclerosis: from pathogenic mechanisms to treatment multiple sclerosis. *Brain* 140, 527–546. doi: 10.1093/brain/aww258

Creutzfeldt, O., Maekawa, K., and Hosli, L. (1969). Forms of spontaneous and evoked postsynaptic potentials of cortical nerve cells. *Prog. Brain Res.* 31, 265–273. doi: 10.1016/S0079-6123(08)63245-8

Cunniffe, N., and Coles, A. (2019). Promoting remyelination in multiple sclerosis. *J. Neurol.* 268, 30–44. doi: 10.1007/s00415-019-09421-x

Daniel, P. M., and Whittridge, D. (1961). The representation of the visual field on the cerebral cortex in monkeys. *J. Physiol.* 159, 203–221. doi: 10.1113/jphysiol.1961.sp006803

Fahle, M., and Bach, M. (2006). "Origin of the visual evoked potentials," in *Principles and Practice of Clinical Electrophysiology of Vision*, eds J. R. Heckenlively and G. B. Arden (Cambridge: The Mit Press), 207–234.

Felts, P. A., Baker, T. A., and Smith, K. J. (1997). Conduction in segmentally demyelinated mammalian central axons. *J. Neurosci.* 17, 7267–7277. doi: 10.1523/JNEUROSCI.17-19-07267.1997

Foote, A. K., and Blakemore, W. F. (2005). Inflammation stimulates remyelination in areas of chronic demyelination. *Brain* 128, 528–539. doi: 10.1093/brain/awh417

Fraser, C., Klistorner, A., Graham, S. L., Garrick, R., Billson, F., and Grigg, J. R. (2006). Multifocal visual evoked potential latency analysis: predicting progression to multiple sclerosis. *Arch. Neurol.* 63, 847–850. doi: 10.1001/archneur.63.6.847

Galetta, S. L., Villoslada, P., Levin, N., Shindler, K., Ishikawa, H., Parr, E., et al. (2015). Acute optic neuritis: unmet clinical needs and model for new therapies. *Neurol. Neuroimmunol. Neuroinflamm.* 2:e135. doi: 10.1212/NXI.0000000000000135

Graf, J., Jansen, L., Ingwersen, J., Ringelstein, M., Harmel, J., Rybak, J., et al. (2018). Multifocal visual evoked potentials in chronic inflammatory demyelinating polyneuropathy. *Ann. Clin. Trans. Neurol.* 5, 952–961. doi: 10.1002/acn3.593

Graham, S. L. L., Klistorner, A. I. I., Grigg, J. R. R., and Billson, F. A. (2000). Objective vep perimetry in glaucoma: asymmetry analysis to identify early deficits. *J. Glaucoma* 9, 10–19. doi: 10.1097/00061198-200002000-00004

Halliday, A. M., Darbett, G., Blumhardt, L. D., and Kriss, A. (1979). "The macular and submacular subcomponents of the pattern evoked response," in *Human Evoked Potentials*, ed. B. LDaG (New York, NY: Plenum Publishing), 135–151. doi: 10.1007/978-1-4684-3483-5_10

Halliday, A. M., McDonald, W. I., and Mushin, J. (1972). Delayed visual evoked response in optic neuritis. *Lancet* 1, 982–985. doi: 10.1016/S0140-6736(72)91155-5

Harter, M. R. (1970). Evoked cortical responses to checkerboard patterns: effect of check-size as a function of retinal eccentricity. *Vis. Res.* 10, 1365–1376. doi: 10.1016/0042-6989(70)90088-X

Heidari, M., Radcliff, A. B., McLellan, G. S., Ver Hoeve, J. N., Chan, K., Kiland, J. A., et al. (2019). Evoked potentials as a biomarker of remyelination. *Proc. Natl. Acad. Sci. U.S.A.* 116, 27074–27083. doi: 10.1073/pnas.1906358116

Hood, D. C., Odel, J. G., and Zhang, X. (2000a). Tracking the Recovery of Local Optic Nerve Function after Optic Neuritis:A Multifocal VEP Study. *Invest. Ophthalmol. Vis. Sci.* 41, 4032–4038.

Hood, D. C., Zhang, X., Greenstein, V. C., Kangovi, S., Odel, J. G., Liebmann, J. M., et al. (2000b). an interocular comparison of the multifocal VEP: a possible technique for detecting local damage to the optic nerve. *Invest. Ophthalmol. Vis. Sci.* 41, 1580–1587.

Hornabrook, R. S., Miller, D., Newton, M. R., MacManus, D. G., du Boulay, G. H., Halliday, A. M., et al. (1992). frequent involvement of optic radiation in patients with acute isolated optic neuritis. *Neurology* 42, 77–79. doi: 10.1212/WNL.42.1.77

Jayanetti, V., Klistorner, A., Graham, S. L., Dexter, M., Flaherty, M. P., Jones, K., et al. (2018). Monitoring of optic nerve function in neurofibromatosis 2 children with optic nerve sheath meningiomas using multifocal visual evoked potentials. *J. Clin. Neurosci.* 50, 262–267. doi: 10.1016/j.jocn.2018.01.012

Jelescu, I. O., Zurek, M., Winters, K. V., Veraart, J., Rajaratnam, A., Kim, N. S., et al. (2016). In vivo quantification of demyelination and recovery using compartment-specific diffusion MRI metrics validated by electron microscopy. *NeuroImage* 132, 104–114. doi: 10.1016/j.neuroimage.2016.02.004

Jenkins, T., Ciccarelli, O., Toosy, A., Miszkiel, K., Wheeler-Kingshott, C., Altmann, D., et al. (2010). Dissecting structure-function interactions in acute optic neuritis to investigate neuroplasticity. *Hum. Brain Map.* 31, 276–286. doi: 10.1002/hbm.20863

Jones, S. J., and Brusa, A. (2003). Neurophysiological evidence for long-term repair of MS lesions: implications for axon protection. *J. Neurol. Sci.* 206, 193–198. doi: 10.1016/S0022-510X(02)00428-8

Klistorner, A. I. I., Graham, S. L. L., Grigg, J. R. R., and Billson, F. A. (1998). Multifocal topographic visual evoked potential: improving objective detection of local visual field defects. *Invest. Ophthalmol. Vis. Sci.* 39, 937–950.

Klistorner, A., and Graham, S. L. L. (2000). Objective perimetry in glaucoma. *Ophthalmology* 107, 2283–2299. doi: 10.1016/S0161-6420(00)00367-5

Klistorner, A., Arvind, H., Garrick, R., Yiannikas, C., Paine, M., and Graham, S. L. (2010). Remyelination of optic nerve lesions: spatial and temporal factors. *Mult. Scler.* 16, 786–795. doi: 10.1177/1352458510371408

Klistorner, A., Chai, Y., Leocani, L., Albrecht, P., Aktas, O., Butzkueven, H., et al. (2018). Assessment of opicinumab in acute optic neuritis using multifocal visual evoked potential. *CNS Drugs* 32, 1159–1171. doi: 10.1007/s40263-018-0575-8

Klistorner, A., Graham, E. C., Yiannikas, C., Barnett, M., Parratt, J., Garrick, R., et al. (2017). Progression of Retinal Ganglion Cell Loss in Multiple Sclerosis Is Associated with New Lesions in the Optic Radiations. *Eur. J. Neurol.* 24, 1392–1398. doi: 10.1111/ene.13404

Klistorner, A., Graham, S., Fraser, C., Garrick, R., Nguyen, T., Paine, M., et al. (2007). Electrophysiological evidence for heterogeneity of lesions in optic neuritis. *Invest Ophthalmol. Vis. Sci.* 48, 4549–4556. doi: 10.1167/iovs.07-0381

Klistorner, A., Naylor, M., and Zhu, B. (2020). RENEWED: long-term mfvep latency outcomes in participants previously enrolled in the opicinumab phase 2 study RENEW. *Mult. Scler. J.* 26, 492. doi: 10.1177/1352458520974937

Klistorner, A., Triplett, J. D., Barnett, M. H., Yiannikas, C., Barton, J., Parratt, J., et al. (2021). Latency of multifocal visual evoked potential in multiple sclerosis. *J. Clin. Neurophysiol.* 38, 186–191.

Klistorner, A., Vootakuru, N., Wang, C., Yiannikas, C., Graham, S. L., Parratt, J., et al. (2015). Decoding diffusivity in multiple sclerosis: analysis of optic radiation lesional and non-lesional white matter. *PLoS One* 10:e0122114. doi: 10.1371/journal.pone.0122114

Klistorner, S. A., Barnett, M. H., Wasserthal, J., Yiannikas, C., Barton, J., Parratt, J., et al. (2021). Differentiating axonal loss and demyelination in chronic MS lesions: a novel approach using single streamline diffusivity analysis. *PLoS One* 16:e0244776. doi: 10.1371/journal.pone.0244766

Kornek, B., Storch, M. K., Weissert, R., Wallstroem, E., Stefferl, A., Olsson, T., et al. (2000). Multiple sclerosis and chronic autoimmune encephalomyelitis: a comparative study of axonal injury in active, inactive and remyelinated lesons. *Am. J. Pathol.* 157, 267–276. doi: 10.1016/S0002-9440(10)64537-3

Kotter, M. R., Stadelmann, C., and Hartung, H. P. (2011). Enhancing remyelination in disease–can we wrap it up? *Brain* 134(Pt 7), 1882–1900. doi: 10.1093/brain/awr014

Lubetzki, C., Zalc, B., Williams, A., Stadelmann, C., and Stankoff, B. (2020). Remyelination in multiple sclerosis: from basic science to clinical translation. *Lancet Neurol.* 19, 678–688. doi: 10.1016/S1474-4422(20)30140-X

Mallik, S., Samson, R. S., Wheeler-Kingshott, C. A., and Miller, D. H. (2014). Imaging outcomes for trials of remyelination in multiple sclerosis. *J. Neurol. Neurosurg. Psychiatry* 85, 1396–1404. doi: 10.1136/jnnp-2014-307650

Malmqvist, L., de Santiago, L., Boquete, L., and Hamann, S. (2017). Multifocal visual evoked potentials for quantifying optic nerve dysfunction in patients with optic disc drusen. *Acta Ophthalmol.* 95, 357–362. doi: 10.1111/aos.13347

Oh, J., Ontaneda, D., Azevedo, C., Klawiter, E. C., Absinta, M., Arnold, D. L., et al. (2019). Imaging outcome measures of neuroprotection and repair in MS: a consensus statement from NAIMS. *Neurology* 12, 519–533. doi: 10.1212/WNL.0000000000007099

Patrikios, P., Stadelmann, C., Kutzelnigg, A., Rauschka, H., Schmidbauer, M., Laursen, H., et al. (2006). remyelination is extensive in a subset of multiple sclerosis patients. *Brain* 129, 3165–3172. doi: 10.1093/brain/awl217

Périer, O., and Grégoire, A. (1965). Electron microscopic features of multiple sclerosis lesions. *Brain* 88, 937–952. doi: 10.1093/brain/88.5.937

Peterson, L. K., and Fujinami, R. S. (2007). Inflammation, demyelination, neurodegeneration and neuroprotectionin the pathogenesis of multiple sclerosis. *J. Neuroimunol.* 184, 37–44. doi: 10.1016/j.jneuroim.2006.11.015

Prineas, J. W., Kwon, E. E., Goldenberg, P. Z., Ilyas, A. A., Quarles, R. H., Benjamins, J. A., et al. (1989). Multiple sclerosis. oligodendrocyte proliferation and differentiation in fresh lesions. *Lab. Invest.* 61, 489–503.

Raine, C. S., and Wu, E. (1993). Multiple sclerosis: remyelination in acute lesions. *J. Neuropathol. Exp. Neurol.* 52, 199–204. doi: 10.1097/00005072-199305000-00003

Raz, N., Bick, A. S., Klistorner, A., Spektor, S., Reich, D. S., Ben-Hur, T., et al. (2015). Physiological correlates and predictors of functional recovery after chiasmal decompression. *J. Neuroophthalmol.* 35, 348–352. doi: 10.1097/WNO.0000000000000266

Riggs, L. A., and Wooten, B. R. (1972). "Electrical measures and psychophysical data on human vision," in *Handbook of Sensory Physiology*, eds D. Jameson and L. M. Hurvich (New York, NY: Springer-Verlag), 690–731. doi: 10.1007/978-3-642-88658-4_27

Ruffini, F., Kennedy, T. E., and Antel, J. P. (2004). Inflammation and remyelination in the central nervous system. *Am. J. Pathol.* 164, 1519–1522. doi: 10.1016/S0002-9440(10)63709-1

Semela, L., Yang, E. B., THedges, R., Vuong, L., Odel, J. G., and Hood, D. C. (2009). Multifocal visual-evoked potential in unilateral compressive optic neuropathy. *Invest. Ophtal. Vis. Sci.* 50, 4199–4204.

Sherbondy, A. J., Dougherty, R. F., Napel, S., and Wandell, B. A. (2008). Identifying the human optic radiation using diffusion imaging and fiber tractography. *J. Vis.* 8, 12.1–1211. doi: 10.1167/8.10.12

Smith, K. J., and Waxman, S. G. (2005). "The conduction properties of demyelinated and remyelinated axons," in *Multiple Sclerosis as Neuronal Disease*, ed. S. G. Waxman (Amsterdam: Elsevier Academic Press), 85–100. doi: 10.1016/B978-012738761-1/50007-9

Suhs, K. W., Hein, K., Sattler, M. B., Gorlitz, A., Ciupka, C., Scholz, K., et al. (2012). A randomized, double-blind, phase 2 study of erythropoietin in optic neuritis. *Ann. Neurol.* 72, 199–210. doi: 10.1002/ana.23573

Sutter, E. E., and Tran, D. (1992). The field topography of ERG components in man - 1. The photopic luminance response. *Vis. Res.* 32, 433–446. doi: 10.1016/0042-6989(92)90235-B

Trapp, B. D., Ransohoff, R., Fisher, E., and Rudick, R. (1999). Neurodegeneration in multiple sclerosis: relationship to neurological disability. *Neuroscientist* 5, 48–57. doi: 10.1177/107385849900500107

Tsakiri, A., Kallenbach, K., Fuglø, D., Wanscher, B., Larsson, H., and Frederiksen, J. (2012). Simvastatin improves final visual outcome in acute optic neuritis:

a randomized study. *Mult. Scler.* 18, 72–81. doi: 10.1177/1352458511415452

van der Walt, A., Kolbe, S., Mitchell, P., Wang, Y., Butzkueven, H., Egan, G., et al. (2015). Parallel changes in structural and functional measures of optic nerve myelination after optic neuritis. *PLoS One* 10:e0121084. doi: 10.1371/journal.pone.0121084

van der Weijden, C. W. J., García, D. V., Borra, R. J. H., Thurner, P., Meilof, J. F., van Laar, P. J., et al. (2020). Myelin quantification with MRI: a systematic review of accuracy and reproducibility. *NeuroImage* 226:117561. doi: 10.1016/j.neuroimage.2020.117561

Waxman, S. G. (2005). "Altered distributions and functions of multiple sodium channel subtypes in multiple sclerosis and its models," in *Multiple Sclerosis as a Neuronal Disease*, ed. S. G. Waxman (Amsterdam: Elsevier). doi: 10.1016/B978-012738761-1/50008-0

Yamada, M., Yukawa, E., Yakerani, F., Matsuura, T., and Hara, Y. (2011). Multifocal visual-evoked potentials in patients with schizophrenia during treatment. *Acta Neuropsychiatr.* 23, 31–34. doi: 10.1111/j.1601-5215.2010.00509.x

Yiannikas, C., and Walsh, J. C. (1983). The variation of the pattern shift visual evoked response with the size of the stimulus field. *Electroencephalogr. Clin. Neurophysiol.* 55, 427–435. doi: 10.1016/0013-4694(83)90131-1

You, Y., Klistorner, A., Thie, J., and Graham, S. L. (2011). Latency delay of visual evoked potential is a real measurement of demyelination in a rat model of optic neuritis. *Invest. Ophthalmol. Vis. Sci.* 52, 6911–6918. doi: 10.1167/iovs.11-7434

Zhao, C., Fancy, S., Kotter, M. R., Li, W. Y., and Franklin, R. (2005). Mechanisms of CNS remyelination-the key to therapeutic advances. *J. Neurol. Sci.* 233, 87–91. doi: 10.1016/j.jns.2005.03.008

Ziccardi, L., Parisi, V., Giannini, D., Sadun, F., De Negri, A. M., Barboni, P., et al. (2015). Multifocal VEP provide electrophysiological evidence of predominant dysfunction of the optic nerve fibers derived from the central retina in leber's hereditary optic neuropathy. *Graefes. Arch. Clin. Exp. Ophthalmol.* 253, 1591–2015. doi: 10.1007/s00417-015-2979-1

Conflict of Interest: The authors declare that the research was conducted in the absence of any commercial or financial relationships that could be construed as a potential conflict of interest.

Publisher's Note: All claims expressed in this article are solely those of the authors and do not necessarily represent those of their affiliated organizations, or those of the publisher, the editors and the reviewers. Any product that may be evaluated in this article, or claim that may be made by its manufacturer, is not guaranteed or endorsed by the publisher.

frontiers in Neuroscience

ORIGINAL RESEARCH
published: 05 November 2021
doi: 10.3389/fnins.2021.728905

Conditional Deletion of Activating Rearranged During Transfection Receptor Tyrosine Kinase Leads to Impairment of Photoreceptor Ribbon Synapses and Disrupted Visual Function in Mice

Wei-Hao Peng[1], Meng-Lin Liao[2], Wan-Chun Huang[2], Pei-Kang Liu[3,4,5,6], Sarah R. Levi[6], Yun-Ju Tseng[6], Chia-Ying Lee[7], Lung-Kun Yeh[7,8], Kuan-Jen Chen[7,8], Chung-Liang Chien[2†] and Nan-Kai Wang[6*†]*

[1] School of Medicine for International Students, College of Medicine, I-Shou University, Kaohsiung, Taiwan, [2] Department of Anatomy and Cell Biology, College of Medicine, National Taiwan University, Taipei, Taiwan, [3] Department of Ophthalmology, Kaohsiung Medical University Hospital, Kaohsiung Medical University, Kaohsiung, Taiwan, [4] School of Medicine, College of Medicine, Kaohsiung Medical University, Kaohsiung, Taiwan, [5] Institute of Biomedical Sciences, National Sun Yat-sen University, Kaohsiung, Taiwan, [6] Department of Ophthalmology, Edward S. Harkness Eye Institute, Columbia University Irving Medical Center, Columbia University, New York, NY, United States, [7] Department of Ophthalmology, Chang Gung Memorial Hospital, Taoyuan, Taiwan, [8] College of Medicine, Chang Gung University, Taoyuan, Taiwan

Purpose: The rearranged during transfection (RET) receptor tyrosine kinase plays a key role in transducing signals related to cell growth and differentiation. *Ret* mutant mice show abnormal retinal activity and abnormal levels and morphology of bipolar cells, yet die on the 21st day after birth as a result of renal underdevelopment. To extend the observation period, we generated the *Ret* conditional knockout *Chx10-Cre;C-Ret*$^{lx/lx}$ mouse model and analyzed the retinal function and morphological changes in mature and aging *Chx10-Cre;C-Ret*$^{lx/lx}$ mice.

Methods: Retina-specific depletion of *Ret* was achieved using mice with floxed alleles of the *Ret* gene with CHX10-driven Cre recombinase; floxed mice without Cre expression were used as controls. Retinal function was examined using electroretinography (ERG), and 2-, 4-, 12-, and 24-month-old mice were analyzed by hematoxylin staining and immunohistochemistry to evaluate retinal morphological alterations. The ultrastructure of photoreceptor synapses was evaluated using electron microscopy.

Results: The results of the ERG testing showed that b-wave amplitudes were reduced in *Chx10-Cre;C-Ret*$^{lx/lx}$ mice, whereas a-waves were not affected. A histopathological analysis revealed a thinner and disorganized outer plexiform layer at the ages of 12 and 24 months in *Chx10-Cre;C-Ret*$^{lx/lx}$ mice. Moreover, the data provided by immunohistochemistry showed defects in the synapses of photoreceptor cells. This

OPEN ACCESS

Edited by:
Jianhai Du,
West Virginia University, United States

Reviewed by:
Wallace B. Thoreson,
University of Nebraska Medical Center, United States
Yoshihiko Tsukamoto,
Hyogo College of Medicine, Japan

***Correspondence:**
Chung-Liang Chien
chien@ntu.edu.tw
Nan-Kai Wang
nw2189@cumc.columbia.edu

† These authors have contributed equally to this work

Specialty section:
This article was submitted to Neurodegeneration, a section of the journal Frontiers in Neuroscience

Received: *30 June 2021*
Accepted: *11 October 2021*
Published: *05 November 2021*

Citation:
Peng W-H, Liao M-L, Huang W-C, Liu P-K, Levi SR, Tseng Y-J, Lee C-Y, Yeh L-K, Chen K-J, Chien C-L and Wang N-K (2021) Conditional Deletion of Activating Rearranged During Transfection Receptor Tyrosine Kinase Leads to Impairment of Photoreceptor Ribbon Synapses and Disrupted Visual Function in Mice. Front. Neurosci. 15:728905. doi: 10.3389/fnins.2021.728905

result was confirmed at the ultrastructural level, thus supporting the participation of *Ret* in the morphological changes of the synaptic ribbon.

Conclusion: Our results provide evidence of the role of *Ret* in maintaining the function of the retina, which was essential for preserving the structure of the synaptic ribbon and supporting the integrity of the outer plexiform layer.

Keywords: GDNF family of ligands (GFL), rearranged during transfection (RET), mouse retina, ribbon synapses, Cre-loxP knockout mice

INTRODUCTION

The retina receives light signals at levels that span several orders of magnitude. Adaptive changes to different light levels occur at multiple sites within the retinal signal transmission and act together in processing the light information. In contrast to conventional neurons, photoreceptors do not signal via action potentials; rather, they continuously translate light into a graded transmitter release, with the highest exocytosis rates in the dark. To accomplish this task, photoreceptors and retinal bipolar cells contain a specialized type of synapse, the so-called ribbon synapse. The ribbon synapse is a specialized synaptic structure located in the outer plexiform layer (OPL) of the retina in which a synaptic "triad" is formed between the axonal pedicles of rods and cones and the dendrites of horizontal and bipolar cells. Through this special synapse, visual signals are transmitted from photoreceptors to bipolar and horizontal cells (Heidelberger et al., 2005). Morphologically, ribbon synapses are anchored to the plasma membrane in close vicinity to voltage-gated Ca^{2+} channels and are typically surrounded by a large number of synaptic vesicles (Sterling and Matthews, 2005). A previous study showed that the lack of active-zone-anchored synaptic ribbons reduced the presynaptic readily releasable vesicle pool and impaired synchronous visual signaling, thus affecting visual function (LoGiudice and Matthews, 2009). Therefore, photoreceptor ribbon synapses play an important role in visual function.

To protect central nervous system (CNS) cells, mutation-independent neuroprotective strategies—such as the glial-cell-line-derived neurotrophic factor (GDNF), the brain-derived neurotrophic factor (BDNF), the nerve growth factor (NGF), and the ciliary neurotrophic factor (CNTF)—have been applied to, and their therapeutic potential has been demonstrated in, the management of retinal impairment in various animal models (Chinskey et al., 2014). GDNF is a distant member of the transforming growth factor β (TGF-β) superfamily and a founder protein of the GDNF-family ligands (GFLs), which include neurturin (NRTN), artemin (ARTN), and persephin (PSPN) (Airaksinen and Saarma, 2002). All four GFLs (GDNF, NRTN, ARTN, and PSPN) signal via the activation of the rearranged during transfection (RET) receptor tyrosine kinase, a single-pass transmembrane protein that contains four cadherin-like repeats in the extracellular domain and a typical intracellular tyrosine kinase domain (Durbec et al., 1996). These GFLs promote the survival of various neurons, including peripheral neurons and central motor and dopamine neurons, and have been suggested as candidate therapeutic agents for neurodegenerative diseases (Takahashi, 2001).

The function of GDNF in the nervous system has been investigated in many studies. GDNF promotes the differentiation and survival of rat midbrain dopamine neurons and increases the outgrowth of neurites and dopamine uptake *in vitro* (Lin et al., 1993). Moreover, GDNF stimulates the formation of new axon terminals in dopamine neurons, which has led to an increased interest in the therapeutic potential of GDNF for the management of Parkinson's disease (Bourque and Trudeau, 2000). In addition, a previous study showed that GDNF supports the survival of spinal motoneurons (Henderson et al., 1994). In the eye, GDNF is mainly expressed in the retina and has potential therapeutic value by providing neuroprotection in the context of retinal degeneration (Koeberle and Ball, 1998). Moreover, GDNF was reported to be able to rescue retinal ganglion cells after axotomy (Yan et al., 1999) and to be very effective in retarding photoreceptor degeneration in the retinal degeneration 1 (*rd1*) mouse model (Frasson et al., 1999). Subretinal injection of GDNF decreased the loss of photoreceptors and provided a significant functional rescue, as demonstrated by recordable electroretinography (ERG) (Frasson et al., 1999). These studies suggest that GDNF-mediated RET signaling affects retinal function.

GDNF was shown to be a RET ligand, and extensive studies of intracellular signaling through RET have been performed. Specifically, mice carrying loss-of-function mutations in a variety of GFLs or in their receptors exhibited either a loss of sensory neuron populations or a loss of specific types of neurons (Airaksinen and Saarma, 2002; Ernsberger, 2008). Moreover, GDNF/RET signaling plays crucial roles in renal development (Costantini and Shakya, 2006) and the regulation of spermatogonia differentiation (Meng et al., 2000). In addition, RET mutations have been found to cause several human diseases, such as papillary thyroid carcinoma, multiple endocrine neoplasia types 2A and 2B, and Hirschsprung's disease. *Ret*-knockout mice exhibit a lack of enteric neurons and superior cervical ganglia, as well as renal agenesis or dysgenesis (Schuchardt et al., 1994;

Abbreviations: ARTN, artemin; BDNF, brain-derived neurotrophic factor; CNTF, ciliary neurotrophic factor; ERG, electroretinography; GDNF, glial-cell-line-derived neurotrophic factor; GFLs, GDNF-family ligands; INL, inner nuclear layer; IPL, inner plexiform layer; NGF, nerve growth factor; NRTN, neurturin; ONL, outer nuclear layer; OPL, outer plexiform layer; PSPN, persephin; RT, room temperature; TGF-β, transforming growth factor β; WT, wild-type.

Moore et al., 1996). Furthermore, a previous study demonstrated that abnormal retinal activity in NRTN- or *Ret*-deficient mice was associated with abnormal process extension of horizontal cells and bipolar cells into the outer nuclear layer (ONL), as well as a severely disrupted OPL with very sparse dendrites and axons of horizontal cells (Brantley et al., 2008). These results suggest that RET signaling is involved in retinal development. However, *Ret*-deficient mice die before postnatal day 21; thus, further evaluation of their retinal phenotype in adulthood is lacking in the literature (Schuchardt et al., 1994).

The Cre-loxP system is widely used as a powerful genetic tool for generating conditional knockout mice. Researchers can use this system to investigate genes of interest in a tissue/cell- (spatial control) and/or time- (temporal control) specific manner when straight knockout of the genes of interest causes embryonic lethality. In this study, we aimed to investigate the function of *Ret* in the retina by generating conditional knockout mice using the Cre-loxP system. Although conditional $Ret^{RETfloxEGFP/RETfloxEGFP}$*:Six3* Cre knockout mice have been reported, the long-term effect of this intervention on the retina remains unknown (Brantley et al., 2008). To overcome this limitation, we deleted *Ret* exclusively in the retina by crossing homozygous *Ret* conditional knockout mice (i.e., $Ret^{lx/lx}$ mice) with mice expressing Cre recombinase under the control of the *Chx10* gene. The *Chx10* gene is specifically expressed in the retinal progenitor cells at the early stage of eye development (E11.5), followed by a restricted expression in the bipolar cells as the progenitor cells differentiate and exit the cell cycle (Rowan and Cepko, 2004). We analyzed the retinal network in mature and aged *Chx10-Cre;C-*$Ret^{lx/lx}$ mice and investigated the alteration in the ultrastructure of synaptic ribbons in *Chx10-Cre;C-*$Ret^{lx/lx}$ mice specifically.

MATERIALS AND METHODS

Animals

All animal procedures were performed according to the guidelines of the Association for Research in Vision and Ophthalmology Statement for the Use of Animals in Ophthalmic and Vision Research and were approved by the Institutional Animal Care and Use Committee of the National Taiwan University. $Ret^{Ret\ <\ tm1.1Kln\ >}$ mice were generated by Dr. Klein (Kramer et al., 2007) by targeting a construct encompassing exons 11–13 of the *Ret* gene with Lox P sites flanking exon 12 (**Figure 1A**) (termed *C-*$Ret^{lx/lx}$ mice hereafter). The generation of conditional knockout mice with *Ret* gene deletion in the retina was achieved by crossing *C-*$Ret^{lx/lx}$ mice carrying LoxP sites flanking exon 12 of the *Ret* gene (Kramer et al., 2006) with mice expressing *Chx10-Cre* specifically in the retina (JAX: Stock No. 005105). All mice were housed in groups of four to five animals per cage in a room that was kept at 23 ± 1°C and 55% ± 5% humidity with a 12-h light/dark cycle, and were given *ad libitum* access to food and water. All mice used in our experiments were genotyped to confirm the absence of the *rd8* and *rd1* mutations as they may be present in vendor lines and subsequently confound ocular-induced mutant phenotypes (Errijgers et al., 2007; Mattapallil et al., 2012).

Mouse Genotyping

Mice were genotyped and verified using polymerase chain reaction (PCR) analysis. For genotyping, genomic DNA was isolated from a section of mouse tail, optic nerve and retina using an Aquadien™ kit (Bio-Rad, Richmond, CA, United States) according to the manufacturer's instructions. Mice homozygous for *C-*$Ret^{lx/lx}$ were identified using the C-*Ret* forward (5′-*CCA ACA GTA GCC TCT GTG TAA CCC C*-3′) and reverse (5′-*GCA GTC TCT CCA TGG ACA TGG TAG CC*-3′) primers span the loxP in intron 12 (**Figure 1A**, top). Optic atrophy type 1 *(Opa1)* forward (5′-*GAG CTG AGA GGG AGT GAA GAG AGG*-3′) and reverse (5′-*CCC AAA ACT CCT TTA TCC CAG TGA C*-3′) primers could serve as the positive control. Furthermore, the *Chx10-Cre* mice carried *EGFP* fused with Cre recombinase; therefore, primers that amplify *EGFP* were also used to detect the presence of Cre recombinase. The thermal cycling conditions consisted of 30 cycles of 30 s at 94°C, 30 s at 55°C, and 50 s at 72°C. Reactions contained 200 ng of template DNA, 0.5 μM primers, 100 μM dNTPs, 9% glycerol, 2.5 U of *Taq* polymerase, 1.8 mM $MgCl_2$, and 1× PCR buffer (GIBCO BRL) in a volume of 20 μL. The PCR products were resolved via 2% agarose gel electrophoresis using Gel Red (Invitrogen/Life Technologies) as the visualizing dye. The DNA bands were visualized using a ChemiDoc Imaging System (Bio-Rad).

Electroretinography

Electroretinography was performed as described previously (Wang et al., 2010). After 12 h of adaptation in the dark, the mice were prepared for the ERG recordings using an Espion ERG System (Diagnosys LLC; Lowell, MA, United States) under dim red light. The animals were kept on a heating pad (Mycoal, Tochigi, Japan) during the ERG recordings, to maintain a constant body temperature. Mice were anesthetized via intraperitoneal injection of 0.1 mL of a mixed solution (1 mL of ketamine at 100 mg/mL and 0.1 mL of xylazine at 20 mg/mL in 8.9 mL of PBS) per 10 g of body weight, and pupils were dilated with topical 2.5% phenylephrine hydrochloride and 1% tropicamide. The test protocol consisted of 11 dark-adapted and nine light-adapted steps. The light intensities of the stimuli used for scotopic serial intensity ERG were −3.6, −3.2, −2.8, −2.4, −2.0, −1.6, −1.2, −0.6, 0.0, 0.4, and 0.9 log cd.s/m^2 in sequence. The intervals between each stimulus varied from 2 to 30 s, and the number of repeats varied from 10 to 4 times. After the completion of dark-adapted recordings, the animals were exposed to a full-field 30 cd/m^2 white background for 10 min; subsequent steps were delivered on top of this continuous background. The single-flash stimuli applied after light adaptation consisted of −0.1, 0.1, 0.3, 0.8, 1.0, 1.2, and 1.47 log cd.s/m^2. The intervals between each stimulus varied from 1 to 10 s, and the number of repeats varied from 3 to 10 times. A digital band-pass filter ranging from 0.3 to 300 Hz was used to isolate signals after the waves were recorded. The a-wave amplitude was measured from the baseline to the trough of the a-wave, and the b-wave

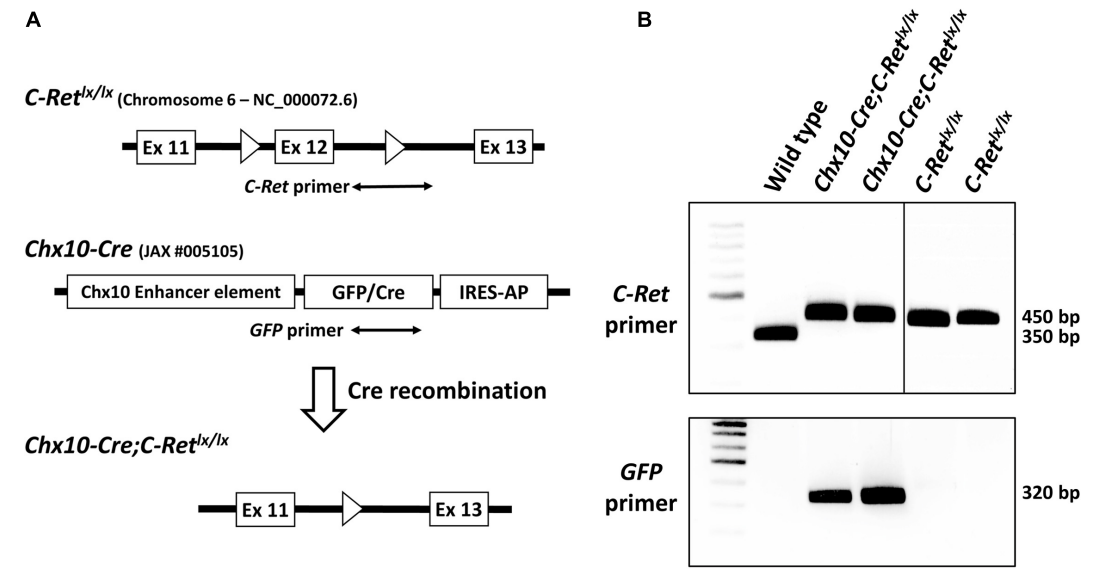

FIGURE 1 | Targeting strategy for the generation of conditional *Ret*-knockout mice and genotyping of *C-Ret*$^{lx/lx}$ and *Chx10-Cre;C-Ret*$^{lx/lx}$ mice using polymerase chain reaction (PCR). The Cre-loxP system was used to generate conditional *Ret*-knockout mice. In *C-Ret*$^{lx/lx}$ mice, the target, exon 12, of the *C-Ret* gene is flanked by two loxP sites (**A**, top). The Chx10-Cre mouse model (JAX #005105) was generated by Chx10 BAC transgenes using a GFP/Cre translational fusion protein combined with internal ribosome entry sequence-human placental alkaline phosphatase cassette (IRES-AP) under the control of Chx10 enhancer elements (**A**, middle). In *Chx10-Cre;C-Ret*$^{lx/lx}$ mice, Cre recognizes the loxP sites and excises the target exon 12 together with one loxP sequence while recombining the two ends of the remaining sequences, thus causing the permanent deletion of the target *C-Ret* gene. Exons are depicted as white boxes and *loxP* sites are shown as white triangles (**A**, bottom). A PCR analysis of all three genotypes (wild-type, *C-Ret*$^{lx/lx}$, and *Chx10-Cre;C-Ret*$^{lx/lx}$) using the *C-Ret* primers (**A**, top) showed that a 350 bp signal was detected in the wild-type (WT) mice and 450 bp signals were observed in *C-Ret*$^{lx/lx}$ and *Chx10-Cre;C-Ret*$^{lx/lx}$ mice (**B**, top). The PCR amplification of *GFP* (**A**, middle), which was detected as a 320 bp fragment, was observed exclusively in *Chx10-Cre;C-Ret*$^{lx/lx}$ mice (**B**, bottom).

was measured from the trough of the a-wave to the peak of the b-wave.

Tissue Preparation

Mice were sacrificed at 2, 4, 12, and 24 months of age and their eyes were enucleated and fixed in 4% paraformaldehyde (PFA) in PBS for 1 h at room temperature (RT). For a better retinal infiltration of 4% PFA, corneas were partially removed and then placed in 4% PFA at 4°C for ∼1 h. After washing in PBS three times, the tissues were incubated in a 30% sucrose solution in PBS at 4°C for 3 days. Tissues were embedded in optimum cutting temperature (OCT) compound (Thermo, Pittsburgh, PA, United States), snap frozen in liquid nitrogen, and immediately stored at –80°C. Cryosections (14 μm in thickness) were cut and collected on slides (Matsunami, Osaka, Japan). All slides were stored at –80°C before use. Before any staining process, the slides were air dried for 15 min and washed in PBS.

Hematoxylin Staining

Sections were stained with hematoxylin for 1 min, then washed with running water for 5 min. The stained sections were mounted with an aqueous mounting medium (EMS, Hatfield, PA, United States) and viewed under a microscope (Olympus CH-2 system, Tokyo, Japan). The brightness and contrast of photomicrographs were adjusted for maximum clarity using Adobe Photoshop CS5 (Adobe Systems, San Jose, CA, United States). The retinas of three mice in each group underwent further histological analysis.

Immunohistochemistry

Sections were blocked with blocking buffer [5% fetal bovine serum (FBS) in PBS containing 0.1% Triton X-100] for 1 h at RT, followed by incubation with the primary antibodies (**Table 1**) diluted in 3% FBS in PBS at 4°C overnight. The sections were subsequently incubated with the secondary antibodies for 1 h at RT. After washing three times in PBS, they were mounted with mounting medium (EMS, Hatfield, PA, United States) and viewed under a Leica DM6000 Confocal Fluorescence Imaging Microscope (Leica Microsystems, Wetzlar, Germany).

Transmission Electron Microscopy and Quantification

Retinas were isolated and fixed in 2% glutaraldehyde and 2% PFA in 0.1 M PB at 4°C overnight. After postfixing in 1% osmium tetroxide for 1 h, tissue samples were dehydrated in a graded ethanol series and embedded in epoxy resin (EMS, Hatfield, PA, United States). Ultrathin sections (70 nm in thickness) were collected on copper grids and stained with uranyl acetate and lead citrate before examination under a Hitachi H-7100 electron microscope (Hitachi, Tokyo, Japan) equipped with a Gatan 832 digital camera (Gatan, Inc., Pleasanton, CA, United States).

For the quantification of synaptic ribbon conditions, images of the OPL were taken at a magnification of 40,000X. Approximately

TABLE 1 | List of antibodies applied for immunohistochemistry.

Antigen	Antiserum	Cell type	Source	Catalog	Dilution factor
α-internexin	Mouse anti-internexin, α, C-terminus, clone 2E3	Horizontal cell and ganglion cell	Millipore	MAB5224	1:100
PKC-α	Mouse anti-PKC-α (H-7)	Rod bipolar cell	Santa Cruz Biotechnology	Sc-8393	1:100
PKC-α	Rabbit anti-PKC-α (H-300)	Rod bipolar cell	Santa Cruz Biotechnology	Sc-10800	1:100
Synaptophysin	Rabbit anti-synaptophysin	Photoreceptor	Abcam	Ab-14692	1:100
Calbindin	Rabbit anti-calbindin	Horizontal cell	Invitrogen	PA1-931	1:500
PSD-95	Mouse anti-PSD95	Photoreceptor	NeuroMab	75-028	1:500
EGFP	Rabbit anti-(GFP)	GFP expressing cells	Millipore	Ab-3080	1:500
Mouse IgG	Goat anti-mouse IgG Alexa 488 and 594		Invitrogen	A11001 A11005	1:200
Rabbit IgG	Goat anti-rabbit IgG Alexa 488 and 594		Invitrogen	A11008 A11012	1:200

500 photoreceptor terminals for each age were examined and classified into different categories of rod-shaped ribbon profiles.

Histological Quantification

The thickness of the ONL and inner nuclear layer (INL) was quantified from single optical sections. Images were taken at a distance of 200 μm from the optic disc and within fields with a size of 300 × 800 μm^2, which was modified from previous studies that chose the area of approximately 200–500 μm away from the optic nerve for quantification (Berger et al., 2014; Mead et al., 2014). Five images per retina were analyzed in three mice per group.

Statistical Analysis

All experimental data were assessed by an operator blinded to the genetic condition. The results were presented as the mean ± standard error of the mean (SEM) and statistical significance was determined by independent Student's *t*-test. $P < 0.05$ was considered significant. All analyses were performed using SPSS (IBM SPSS Statistics for Windows, Version 21.0, IBM Corp. Armonk, NY, United States) and GraphPad Prism 5.0a (GraphPad Software Inc., San Diego, CA, United States).

RESULTS

Generation of Conditional Knockout Mice

To detect the *C-Ret*$^{lx/lx}$ allele in both *Chx10-Cre*;*C-Ret*$^{lx/lx}$ and *C-Ret*$^{lx/lx}$ mice, total DNA from wild-type (WT) and transgenic mice was subjected to PCR analysis with *C-Ret* primers spanning the intron 12 loxP sequence (**Figure 1A**, top). In WT mice (without the loxP insertion), the 350 bp amplicon was detected using the C-*Ret* primers. In contrast, given that *C-Ret*$^{lx/lx}$ and *Chx10-Cre;C-Ret*$^{lx/lx}$ mice contained loxP sequences, they yielded an amplicon of 450 bp instead (**Figure 1B**, top). Because the *Chx10-Cre* mouse model (JAX: Stock No. 005105) was generated by Chx10 BAC transgenes using a "GFP/Cre translational fusion protein" (**Figure 1A**, middle), we used GFP primers to determine the presence of Cre. Consequently, we found that a 320 bp fragment was detected exclusively in *Chx10-Cre;C-Ret*$^{lx/lx}$ mice, and not in WT or *C-Ret*$^{lx/lx}$ mice (**Figure 1B**, bottom).

Conditional Knockout *C-Ret* in Retina and Expression of *Chx10-Cre*

To validate whether exon 12 of the *C-Ret gene* was deleted in the retina of *Chx10-Cre;C-Ret*$^{lx/lx}$ mice, we performed PCR analysis using *C-Ret* primers on DNA extracted from retina and optic nerve of *C-Ret*$^{lx/lx}$ and *Chx10-Cre;C-Ret*$^{lx/lx}$ mice. We found that PCR could amplify *C-Ret* in *C-Ret*$^{lx/lx}$ retina, but barely in *Chx10-Cre;C-Ret*$^{lx/lx}$ retina, indicating that exon 12 of the *C-Ret* gene was deleted in most of the retina cells of *Chx10-Cre;C-Ret*$^{lx/lx}$ mice (**Figure 2A**, top). On the other hand, PCR could amplify *C-Ret* from optic nerves in both *C-Ret*$^{lx/lx}$ and *Chx10-Cre;C-Ret*$^{lx/lx}$ mice. In addition, PCR amplification with *Opa1* primers was used to make sure the DNA was successfully extracted from different regions of eyeball and equally loading DNA amount for each lane (**Figure 2A**, bottom). To further validate the expression of Cre expression in *Chx10-Cre* mice, we did immunohistochemistry to label rod bipolar cells and GFP expressing cells using anti-PKC-α and anti-EGFP antibodies. Because the Cre protein on its own has the capacity to cross the membrane and translocate to the nucleus (Will et al., 2002), the IHC results showed GFP expression only in the nuclei of *Chx10-Cre;C-Ret*$^{lx/lx}$ bipolar cells, while PKC-α expression was identified in the cytoplasm of bipolar cells in both *C-Ret*$^{lx/lx}$ and *Chx10-Cre;C-Ret*$^{lx/lx}$ mice (**Figure 2B**). Based on PCR and IHC analysis, *Chx10-Cre;C-Ret*$^{lx/lx}$ mice were conditionally deleted the exon 12 of *C-Ret gene* in the retina.

In vivo Analyses of Retinal Function and Morphology in *Chx10-Cre;C-Ret*$^{lx/lx}$ Mice

To determine the effect of *Ret* deficiency on retinal function, ERG was performed in 12-month-old *Chx10-Cre;C-Ret*$^{lx/lx}$ and *C-Ret*$^{lx/lx}$ mice (**Figure 3**). The *C-Ret*$^{lx/lx}$ mice showed a normal ERG pattern of series intensity stimulation. As the flash intensity of the scotopic phase increased, the amplitude of the a-wave and b-wave increased. The a-wave represents the activity of the photoreceptors, whereas the b-wave reflects bipolar cell activity. The scotopic ERG of *Chx10-Cre;C-Ret*$^{lx/lx}$ mice revealed a selective reduction of b-waves, with relative preservation of

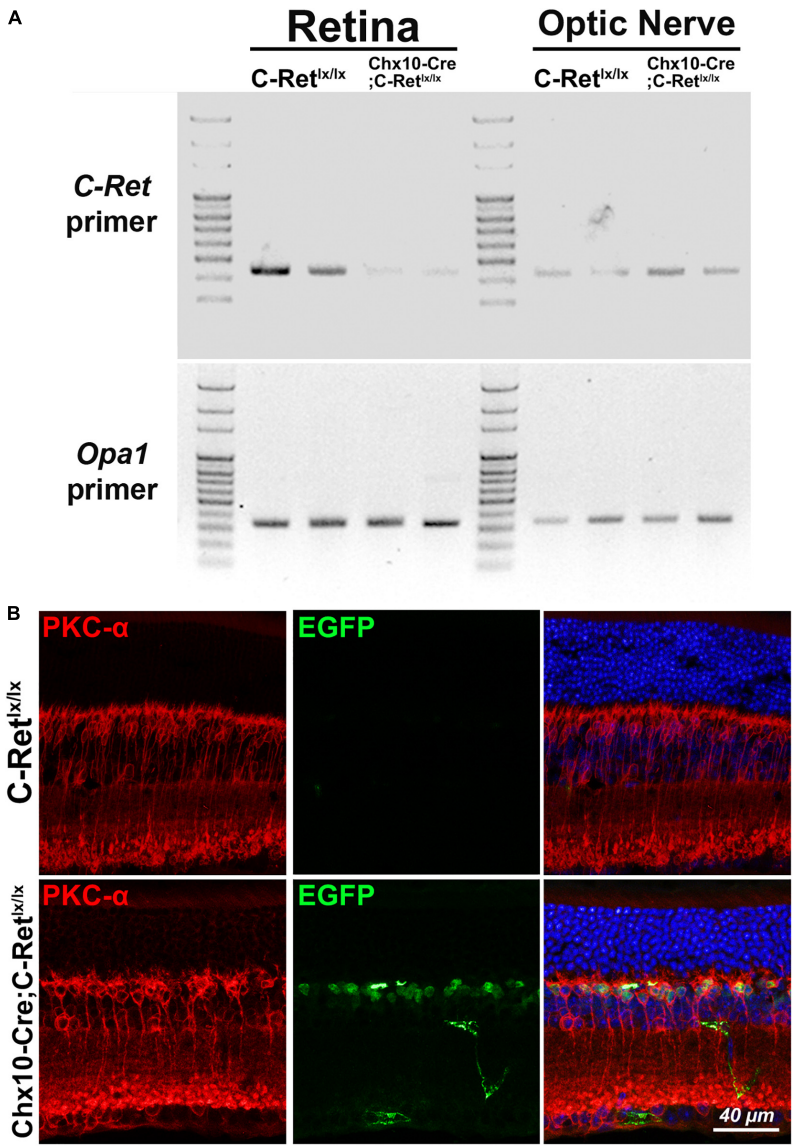

FIGURE 2 | Amplification of *C-Ret* gene and immunohistochemistry of GFP in *C-Ret*$^{lx/lx}$ and *Chx10-Cre;C-Ret*$^{lx/lx}$ mice. (**A**, top) Polymerase chain reaction (PCR) was performed using *C-Ret* primers to screen the presence of exon 12 within the *C-Ret* gene. The results showed that barely any amplification occurred in the retinae of *Chx10-Cre;C-Ret*$^{lx/lx}$ mice compared to that in the retinae of *C-Ret*$^{lx/lx}$ mice. PCR was able to amplify *C-Ret* gene from optic nerve in both *C-Ret*$^{lx/lx}$ and *Chx10-Cre;C-Ret*$^{lx/lx}$ mice. (**A**, bottom) PCR analysis using *Opa1* primers showed equally amplification between *C-Ret*$^{lx/lx}$ and *Chx10-Cre;C-Ret*$^{lx/lx}$ mice in retinae and optic nerve tissue. **(B)** Retinal sections of animals aged 12 months were immunostained with anti-PKC-α (red) and anti-EGFP (green) antibodies to label rod bipolar and GFP expressing cells, respectively, followed by counterstaining with Hoechst dye, to indicate cell nuclei (blue). PKC-α (red) was expressed in cytoplasm of bipolar cells in *C-Ret*$^{lx/lx}$ and *Chx10-Cre;C-Ret*$^{lx/lx}$ mice; however, the GFP was only expressed in the nucleus of bipolar cells of *Chx10-Cre;C-Ret*$^{lx/lx}$ mice due to fusion with Cre protein, which has the capacity to cross the membrane and translocate to the nucleus.

a-waves in the scotopic phase (**Figures 3A,B**). The implicit times of a- and b- waves were more delayed in *Chx10-Cre;C-Ret*$^{lx/lx}$ mice (**Figure 3B**) ($n = 6$; $^*P < 0.05$). In photopic serial intensity ERG, there were reductions in amplitude of a- and b- waves in *Chx10-Cre;C-Ret*$^{lx/lx}$ mice, which were statistically significant in some intensities of b-waves. However, there was no obvious difference in the implicit time of a- and b- waves in photopic responses between *Chx10-Cre;C-Ret*$^{lx/lx}$ and *C-Ret*$^{lx/lx}$ mice. The ERG recordings suggested that the *Chx10-Cre;C-Ret*$^{lx/lx}$ mice may exhibit a greater effect on the function of bipolar cells. Furthermore, these tracings were similar to those of an electronegative ERG corresponding to inner retinal dysfunction.

Hematoxylin staining was used to examine whether the *Chx10-Cre;C-Ret*$^{lx/lx}$ mice had morphological alterations in the retina (**Figure 4**). We observed that, compared with *C-Ret*$^{lx/lx}$ mice (**Figures 4A–D**), the retinas of *Chx10-Cre;C-Ret*$^{lx/lx}$ mice seemed to exhibit a progressive decrease in the thickness of the ONL, OPL, INL, and inner plexiform layer (IPL) (**Figures 4E–H**).

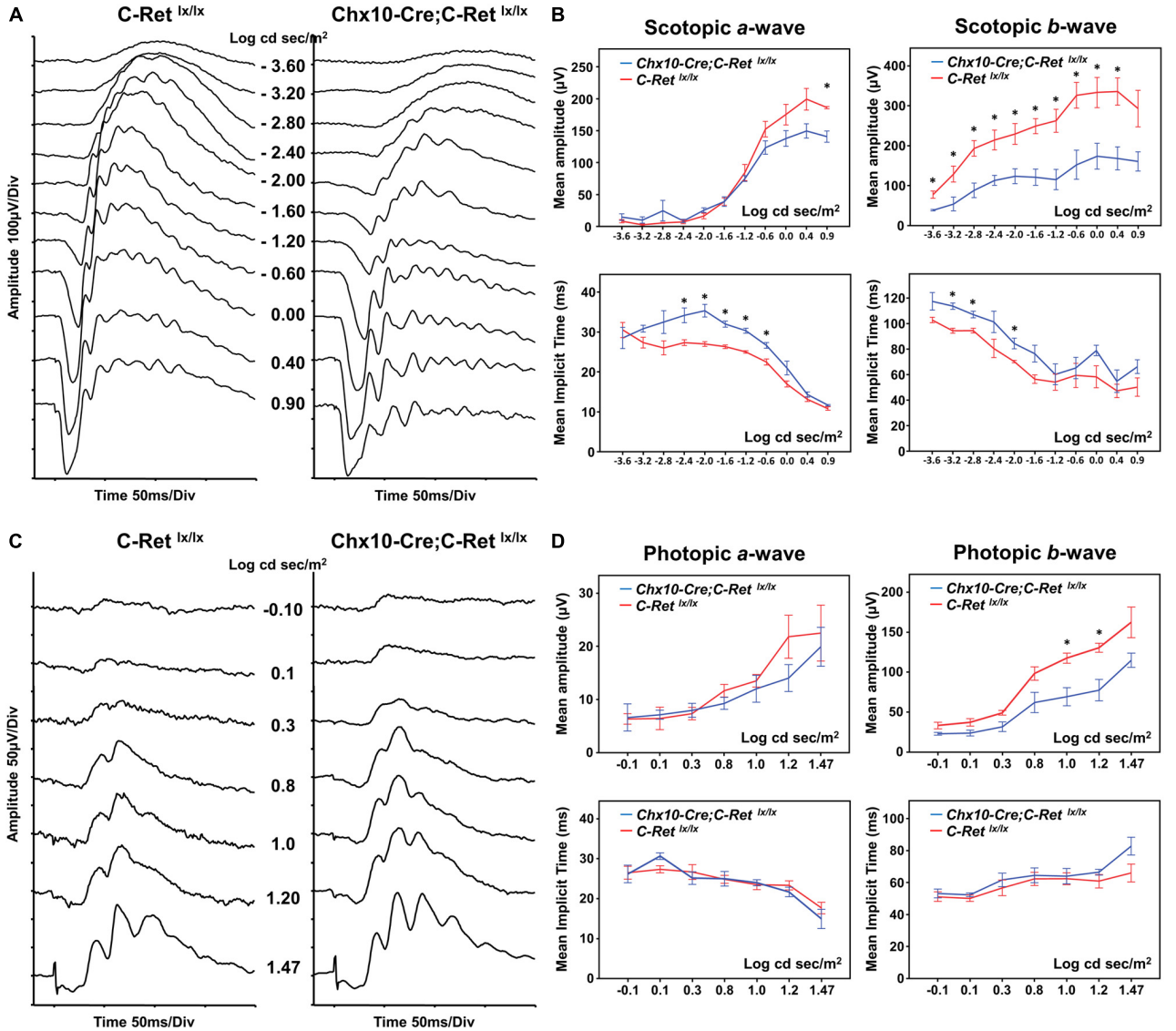

FIGURE 3 | Electroretinography (ERG) of *C-Ret*$^{lx/lx}$ and *Chx10-CRE;C-Ret*$^{lx/lx}$ mice. **(A)** Representative ERG waveforms were recorded from 12-month-old *C-Ret*$^{lx/lx}$ and *Chx10-Cre;C-Ret*$^{lx/lx}$ mice at increasing stimulus intensities in the scotopic phase. In *Chx10-Cre;C-Ret*$^{lx/lx}$ mice, a decrease in the b-wave and a relative preservation of the a-wave were observed. **(B)** The b-wave amplitudes were significantly larger in *C-Ret*$^{lx/lx}$ mice than they were in *Chx10-Cre;C-Ret*$^{lx/lx}$ mice at most of the different intensities of the scotopic phase, whereas the a-wave amplitudes were similar between *C-Ret*$^{lx/lx}$ and *Chx10-Cre;C-Ret*$^{lx/lx}$ mice. There were some delays in the implicit time of a- and b- waves in *Chx10-Cre;C-Ret*$^{lx/lx}$ mice as compared to the implicit times in *C-Ret*$^{lx/lx}$ mice at some flash intensities. **(C)** Representative photopic ERG waveforms were recorded from 12-month-old *C-Ret*$^{lx/lx}$ and *Chx10-Cre;C-Ret*$^{lx/lx}$ mice at increasing stimulus intensities. **(D)** In *Chx10-Cre;C-Ret*$^{lx/lx}$ mice, there were reductions in b-wave amplitudes, while no significant decrease in the amplitude occurred in the a-wave. There were no significant delays in the a- and b- waves in photopic serial intensities. The electronegative ERG result indicated inner retinal dysfunction in *Chx10-Cre;C-Ret*$^{lx/lx}$ mice ($n = 6$; $^*P < 0.05$).

Some nuclei in the ONL invaded the OPL in *Chx10-Cre;C-Ret*$^{lx/lx}$ mice at 12 months of age, which became more obvious in these animals at the age of 24 months. We then quantified the thickness of the ONL (**Figure 4I**) and INL (**Figure 4J**) using morphometric measurements. Although there was no statistically significant difference in the thickness of the ONL and INL between the *Chx10-Cre;C-Ret*$^{lx/lx}$ and *C-Ret*$^{lx/lx}$ retinas, we found that the thickness of the ONL in *Chx10-Cre;C-Ret*$^{lx/lx}$ mice showed a 15.4% reduction at 12 months and a 16.3% reduction at 24 months. This observation suggests that the retinal morphology in *Chx10-Cre;C-Ret*$^{lx/lx}$ mice is altered at older ages.

Immunohistochemistry of Horizontal Cells and Rod Bipolar Cells in *Chx10-Cre;C-Ret*$^{lx/lx}$ Mice

To identify the components that are potentially altered in the OPL, IHC was performed to label the horizontal cells and

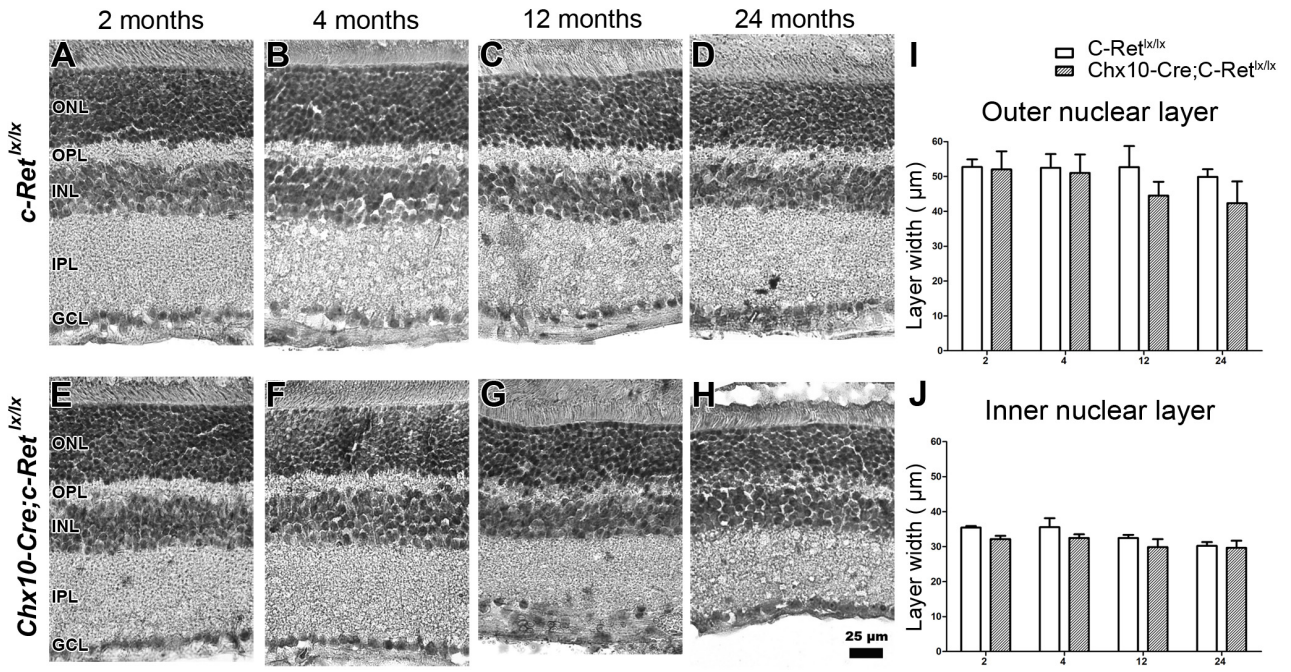

FIGURE 4 | Morphological examination of *C-Ret*$^{lx/lx}$ and *Chx10-Cre;C-Ret*$^{lx/lx}$ mice. Hematoxylin staining of the retinas of *C-Ret*$^{lx/lx}$ **(A–D)** and *Chx10-Cre;C-Ret*$^{lx/lx}$ **(E–H)** mice was performed at 2, 4, 12, and 24 months of age. At the age of 2 and 4 months, the OPL in *Chx10-Cre;C-Ret*$^{lx/lx}$ retinas was slightly thinner than that in *C-Ret*$^{lx/lx}$ mice **(A,B,E,F)**. Furthermore, this phenomenon was detected in the OPL of *Chx10-Cre;C-Ret*$^{lx/lx}$ retinas which became worse, and their retina even showed disorganization at the ages of 12 and 24 months **(C,D,G,H)**. The thickness of the ONL and INL was measured in three animals per group at the ages of 2, 4, 12, and 24 months **(I,J)**. The ONL in *Chx10-Cre;C-Ret*$^{lx/lx}$ retinas was thinner than that in *C-Ret*$^{lx/lx}$ retinas at the ages of 12 and 24 months, albeit with no statistical significance at either of the stages **(I)**. Similarly, the INL in *Chx10-Cre;C-Ret*$^{lx/lx}$ retinas was slightly thinner (albeit not significantly) than that in *C-Ret*$^{lx/lx}$ retinas **(J)**. An independent *t*-test was used in this analysis, and significance was set at $P < 0.05$. ONL, outer nuclear layer; OPL, outer plexiform layer; INL, inner nuclear layer; IPL, inner plexiform layer; GCL, ganglion cell layer. Scale bar, 25 μm.

rod bipolar cells in mouse retinas. Bipolar cells and horizontal cells are the second−order neurons that form synapses with photoreceptor terminals in the OPL. A previous study indicated that α-internexin is expressed in horizontal cells and may be used as a marker of these cells in the study of the mouse retina (Chien and Liem, 1995). Therefore, an anti-α-internexin antibody was used to detect the processes of horizontal cells (**Figures 5A–H**). In *C-Ret*$^{lx/lx}$ mice, horizontal cells possessed arborizing processes in the OPL of mice aged 2–24 months (**Figures 5A–D**). In contrast, the processes of horizontal cells in *Chx10-Cre;C-Ret*$^{lx/lx}$ mice were reduced at the ages of 2 and 4 months (**Figures 5E,F**), followed by a dramatic decrease at the ages of 12 and 24 months (**Figures 5G,H**). In order to obtain a second confirmation of changes in horizontal cells, the anti-calbindin antibody was applied to the sections, revealing a similar immunoreactivity pattern to that of α-internexin (**Supplementary Figure 1**). These results demonstrated that horizontal cells were affected in the conditional *Ret*-knockout mice.

The retinal rod bipolar cells expressed protein kinase C alpha (PKC-α), the distribution of which, within cells, is reportedly activity-dependent in the rat model (Gabriel et al., 2001). Thus, vertical sections of retinas were immunostained for PKC-α (**Figures 5I–P**). The immunoreactivity of PKC-α in *C-Ret*$^{lx/lx}$ mice showed that the bipolar cells had their cell bodies and the cytosolic compartments in the INL, the dendritic processes in the OPL, and the axon terminals in the innermost sublamina of the IPL (**Figures 5I–L**). A subpopulation of bipolar cells with axons terminating close to the ganglion cell layer was also observed. In *Chx10-Cre;C-Ret*$^{lx/lx}$ mice, bipolar cells exhibited a normal organization pattern, as in *C-Ret*$^{lx/lx}$ mice, and had well-preserved processes at the ages of 2 and 4 months (**Figures 5M,N**). However, at the ages of 12 and 24 months, some bipolar cells exhibited abnormal processes that sprouted into the ONL (**Figures 5O,P**). Furthermore, the aberrant processes tended to become longer and more numerous in aged *Chx10-Cre;C-Ret*$^{lx/lx}$ mice. According to these observations, bipolar cells may also be altered in conditional *Ret*-knockout mice.

Alteration of Pre- and Post-synaptic Structures in *Chx10-Cre;C-Ret*$^{lx/lx}$ Retinas

To determine whether the dendritic extensions of the rod bipolar cells change in synapses with photoreceptors, double IHC was performed. Given that synaptophysin is an integral membrane protein of synaptic vesicles, it is used to label synaptic structures in the terminals of photoreceptors (Nag and Wadhwa, 2001). Double immunohistochemistry using anti-PKC-α and anti-synaptophysin antibodies demonstrated that PKC-α-positive processes lay among synaptophysin-positive terminals in

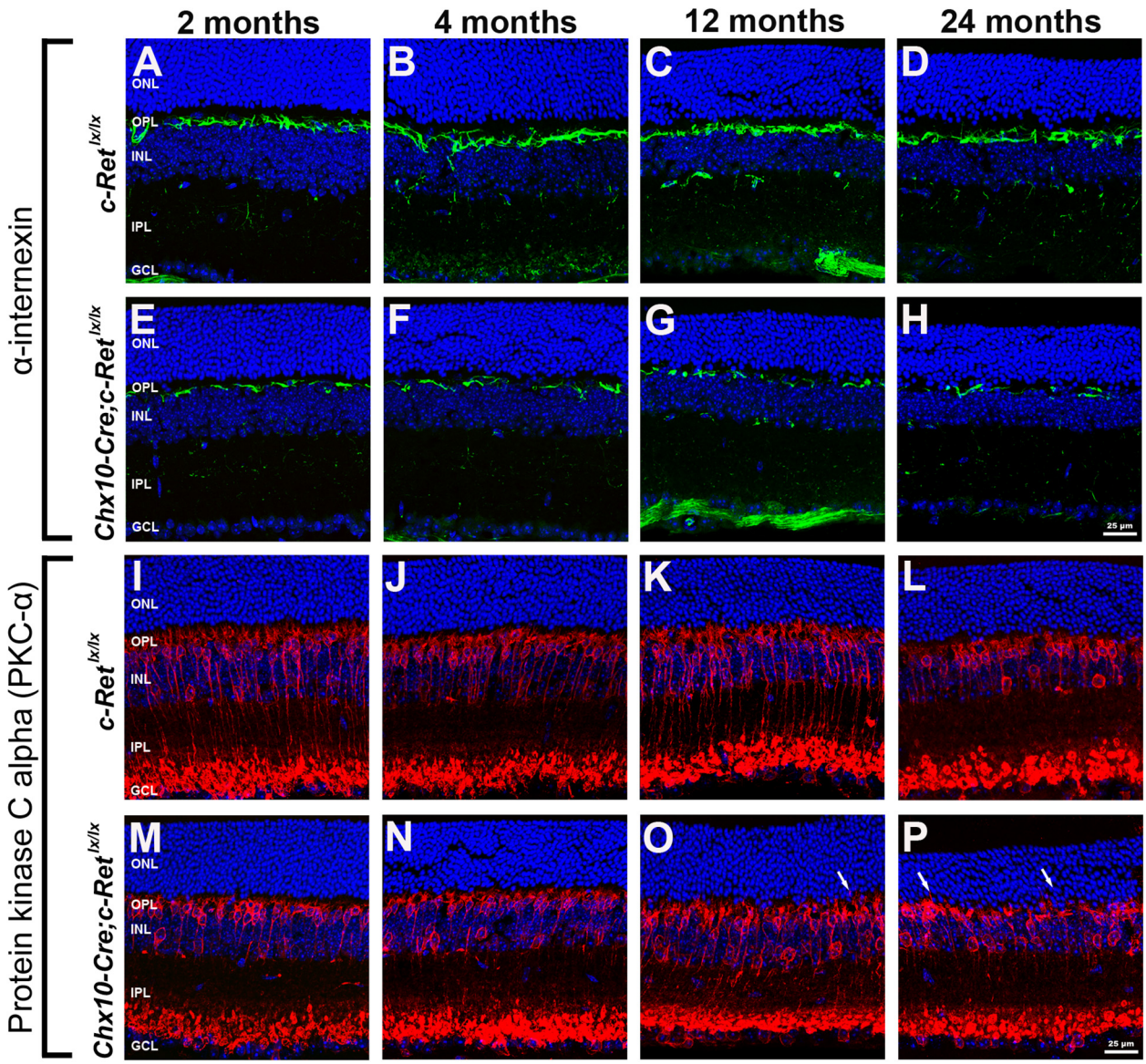

FIGURE 5 | Immunohistochemistry of horizontal cells and rod bipolar cells in *C-Ret*$^{lx/lx}$ and *Chx10-Cre;C-Ret*$^{lx/lx}$ retinas. Retinal sections of mice aged 2, 4, 12, and 24 months were immunostained with an anti-α-internexin antibody (green, **A–H**) or an anti-PKC-α antibody (green, **I–P**), to label horizontal cells and rod bipolar cells, respectively, followed by counterstaining with Hoechst dye, to reveal cell nuclei (blue). Compared with *C-Ret*$^{lx/lx}$ mice **(A–D)**, the processes of horizontal cells were sparse and discontinuous in *Chx10-Cre;C-Ret*$^{lx/lx}$ mice and were even more deteriorated at the ages of 12 and 24 months **(E–H)**. The processes of rod bipolar cells were similar between *C-Ret*$^{lx/lx}$ **(I–L)** and *Chx10-Cre;C-Ret*$^{lx/lx}$ **(M–P)** mice aged 2, 4, 12, and 24 months. However, some processes of rod bipolar cells extended into the ONL at the ages of 12 and 24 months in *Chx10-Cre;C-Ret*$^{lx/lx}$ mice (**O,P**, arrows), which was not observed in *C-Ret*$^{lx/lx}$ mice. ONL, outer nuclear layer; OPL, outer plexiform layer; INL, inner nuclear layer; IPL, inner plexiform layer; GCL, ganglion cell layer. Scale bar, 25 μm.

the OPL of *C-Ret*$^{lx/lx}$ mice (**Figures 6A–D**). A similar pattern was observed in *Chx10-Cre;C-Ret*$^{lx/lx}$ mice aged 2 and 4 months that processes, i.e., most of the rod bipolar cells labeled by the anti-PKC-α antibody were associated with synaptophysin-labeled rod axon terminals in the OPL (**Figures 6E,F**). However, in *Chx10-Cre;C-Ret*$^{lx/lx}$ mice aged 12 and 24 months, some PKC-α- and synaptophysin-positive processes were mislocalized in the ONL and synaptophysin-positive processes were also decreased (**Figures 6G,H**). In addition, the post-synaptic density protein 95 (PSD-95) was detected in the OPL (**Supplementary Figure 2**). A significant decrease of PSD-95 expression was found in *Chx10-Cre;C-Ret*$^{lx/lx}$ mice aged 12 and 24 months, compared to *C-Ret*$^{lx/lx}$ mice. The IHC results indicated that the synapses between rod bipolar cells and photoreceptors were affected in conditional *Ret*-knockout mice.

To further confirm the morphological changes observed in the OPL of *Chx10-Cre;C-Ret*$^{lx/lx}$ mice, we performed TEM observations and identified ribbon synapses at the outer retina

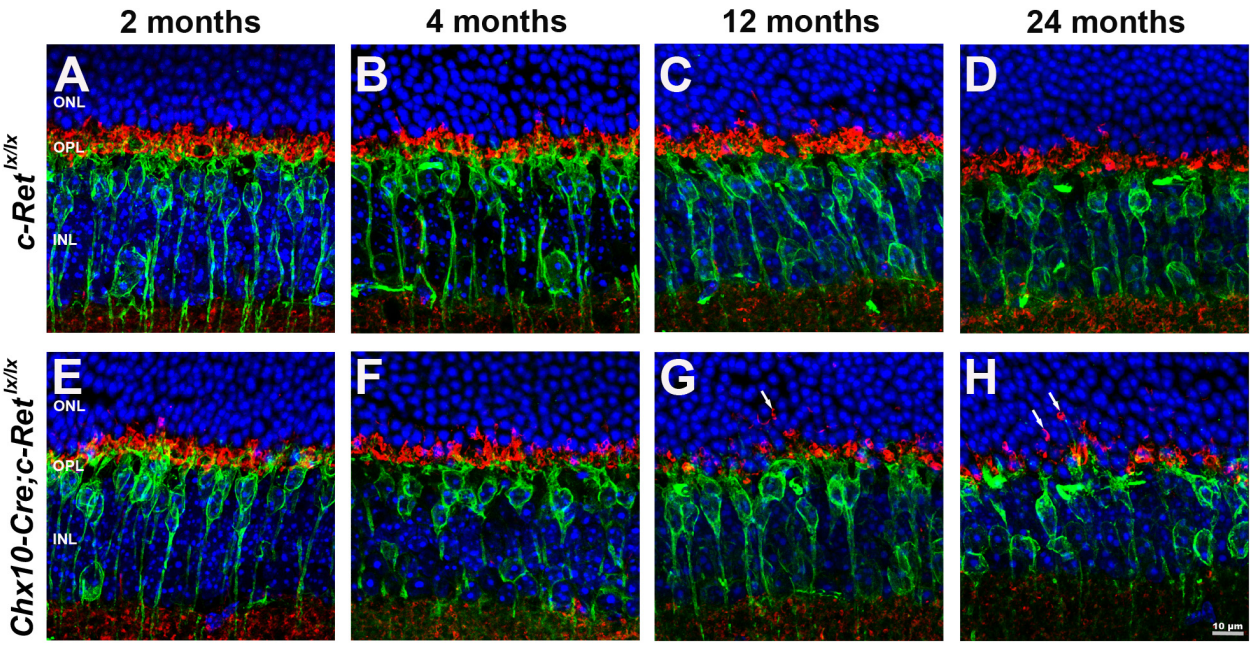

FIGURE 6 | Immunohistochemistry of pre- and postsynaptic structures in *C-Ret*$^{lx/lx}$ and *Chx10-Cre;C-Ret*$^{lx/lx}$ retinas. Retinal sections of animals aged 2, 4, 12, and 24 months were immunostained with an anti-PKC-α antibody (green) and an anti-synaptophysin antibody (red), to label rod bipolar cells and the synapses of photoreceptors, respectively, followed by counterstaining with Hoechst dye, to indicate cell nuclei (blue) **(A–H)**. The processes of rod bipolar cells formed synapses with photoreceptors in the OPL of *C-Ret*$^{lx/lx}$ mice at all ages **(A–D)** and *Chx10-Cre;C-Ret*$^{lx/lx}$ mice at the ages of 2 and 4 months **(E–F)**. Ectopic synapses in the ONL were observed in 12- and 24-month-old *Chx10-Cre;C-Ret*$^{lx/lx}$ mice (**G,H**, arrows). ONL, outer nuclear layer; OPL, outer plexiform layer; INL, inner nuclear layer. Scale bar, 10 μm.

of *C-Ret*$^{lx/lx}$ and *Chx10-Cre;C-Ret*$^{lx/lx}$ mice aged 2 months (**Figure 7**) and 12 months (**Figure 8**). The photoreceptor ribbon synapses of *C-Ret*$^{lx/lx}$ mice exhibited a varying number of rod-shaped profiles in photoreceptor terminals (**Figures 7A,B**). Ribbon ultrastructure was defined by the central presynaptic ribbon opposed by two postsynaptic horizontal cell processes. The synaptic ribbon displayed its typical plate-like shape, extending perpendicular to the presynaptic membrane into the cytoplasm. Although, plentiful synaptic ribbons in *Chx10-Cre;C-Ret*$^{lx/lx}$ mice aged 2 months, having roughly the same length and appearance as those in *C-Ret*$^{lx/lx}$ terminals, were observed, they were usually found to be "floating" in the cytoplasm instead of anchored to other synaptic structures (**Figures 7C–E**). Besides, the number of "Medusa-like' ribbons seemed to be increased and the synaptic ribbons were observed reduced in height and swollen shaped (**Figures 7E,F**). Therefore, the synaptic ribbon is surrounded by a halo of synaptic vesicles, as they do in the *C-Ret*$^{lx/lx}$ retina.

Furthermore, the appearance of the ribbon synaptic complexes in the 12-month *Chx10-Cre;C-Ret*$^{lx/lx}$ mice retinae differed significantly from those in the *C-Ret*$^{lx/lx}$ retinae. Normally, a rod synaptic terminal in *C-Ret*$^{lx/lx}$ retina contained a single ribbon synaptic site (**Figure 8A**), where glutamate was released onto the postsynaptic elements, horizontal cell processes and rod bipolar cell dendrites. The postsynaptic elements invaginated into the rod terminal and formed a triadic or tetradic configuration adjacent to the ribbon site (**Figure 8B**). However, most of the ribbons in the retinae of 12-month-old *Chx10-Cre;C-Ret*$^{lx/lx}$ mice were not docked at the synaptic site (i.e., they floated freely in the cytoplasm) (**Figures 8C,D**). Many empty rod terminals without presynaptic ribbons and postsynaptic invaginating elements were found in *Chx10-Cre;C-Ret*$^{lx/lx}$ mice (**Figure 8E**). In addition, the number of synaptic vesicles was decreased near synapses (**Figure 8D**) and found in clumps rather than distributed evenly in the pedicle (**Figure 8F**). Following these observations, we classified the synaptic ribbons into two categories: rod-shaped and non-rod-shaped, based on their general morphological features; this was followed by quantification of the synaptic ribbons. Representative examples of the rod-shaped ribbons anchored at the active zone, where exocytosis of synaptic vesicles occurred, are shown in **Figure 9A** and the quantitative data are summarized in **Figure 9B**. 87.1 and 86.3% of rod photoreceptor ribbon profiles were presynaptically anchored and rod-shaped in *C-Ret*$^{lx/lx}$ mice aged 2 and 12 months, respectively. In contrast, a significant decrease was found in the *Chx10-Cre;C-Ret*$^{lx/lx}$ mice whereby only 62.4% of rod photoreceptor ribbon profiles were presynaptically anchored and rod-shaped at the age of 2 months; this proportion only worsened at the age of 12 months (54.2% of rod photoreceptor ribbons). The aforementioned TEM results suggest that the loss of *Ret* causes a structural defect in the synaptic connection between photoreceptors and bipolar cells. Ultimately, this finding may underlie the abnormal ERG b-wave observed in *Chx10-Cre;C-Ret*$^{lx/lx}$ mice.

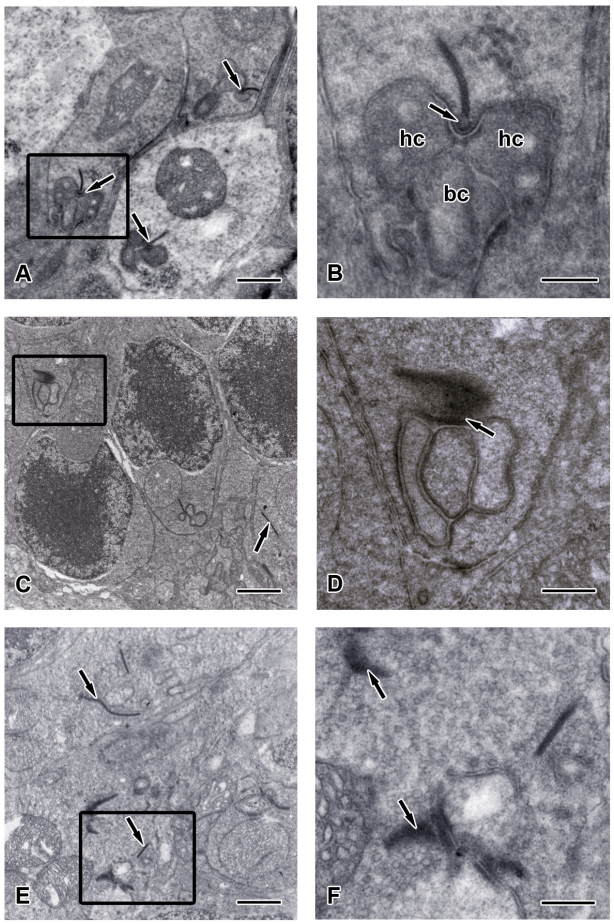

FIGURE 7 | Ultrastructure of the synaptic ribbons in *C-Ret*$^{lx/lx}$ and *Chx10-Cre;C-Ret*$^{lx/lx}$ retinas at the age of 2 months. Transmission electron microscopy (TEM) images showed the outer plexiform layer of *C-Ret*$^{lx/lx}$ **(A,B)** and *Chx10-Cre;C-Ret*$^{lx/lx}$ **(C–F)** mice at the age of 2 months. **(A)** Three typical rod-like synaptic ribbon profiles (arrows) with several mitochondria were observed in the pedicle of *C-Ret*$^{lx/lx}$ mice. **(B)** Higher magnification of the TEM image is shown in the rectangle of **(A)**. The electron dense synaptic ribbon was surrounded by a halo of synaptic vesicles. The arciform density (arrows) was positioned between the base of the ribbon and the plasma membrane. Three post-synaptic processes, two dendritic tips of horizontal cells (hc) and one dendritic tips of bipolar cells (bc), were closely apposed to the photoreceptor near the ribbon. **(C,E)** Most synaptic ribbons (arrows) in the rod spherules appeared to float in the cytoplasm, unassociated with an arciform density and the presynaptic membrane. **(D)** Higher magnification of the TEM image is shown in the rectangle of **(C)**. Synaptic structure in pedicle (arrow) of *Chx10-Cre;C-Ret*$^{lx/lx}$ retina was found to be dramatically different from that in the *C-Ret*$^{lx/lx}$ retina. **(F)** Higher magnification of the TEM image is shown in the rectangle of **(E)**. "Medusa-like" ribbons (arrows) were observed in which they displayed fewer postsynaptic processes that appeared to invaginate into a photoreceptor terminal. Scale bars: **(A,C,E)**, 1 μm; **(B,D,F)**, 300 nm.

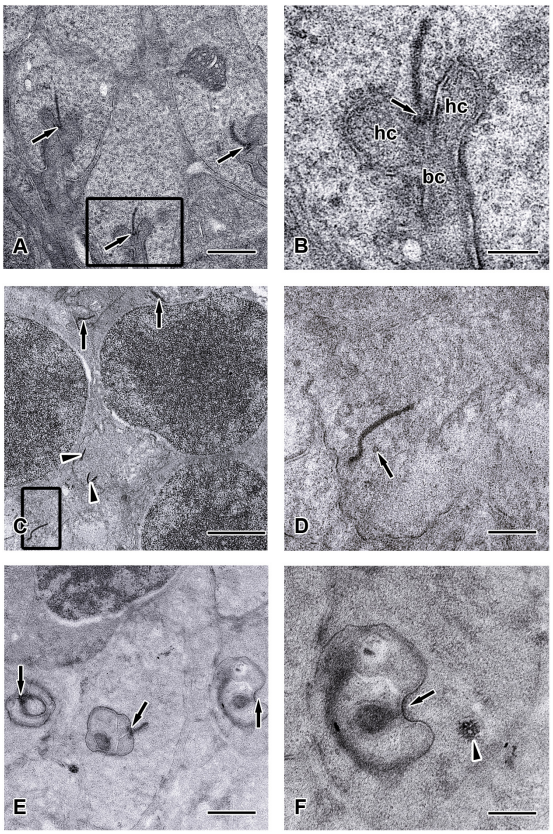

FIGURE 8 | Ultrastructure of the synaptic ribbons in *C-Ret*$^{lx/lx}$ and *Chx10-Cre;C-Ret*$^{lx/lx}$ retinas at the age of 12 months. TEM images showed the outer plexiform layer (ONL) of *C-Ret*$^{lx/lx}$ **(A,B)** and *Chx10-Cre;C-Ret*$^{lx/lx}$ **(C–F)** mice at the age of 12 months. **(A)** Three typical rod-like synaptic ribbon profiles (arrows) with several mitochondria were observed in the rod spherules of *C-Ret*$^{lx/lx}$ mice. **(B)** Higher magnification of the TEM image is shown in the rectangle of **(A)**. The large presynaptic terminals were filled with numerous synaptic vesicles, and the active zone was characterized by specialized presynaptic densities, the arciform densities (arrows). Opposite to the active zones were the dendritic tips of horizontal cells (hc) and bipolar cells (bc), which contained ionotropic and metabotropic glutamate receptors for signaling. **(C–E)** Electron micrographs showed different examples of rod terminals and the ultrastructural appearance of the ribbon synaptic complex in the *Chx10-Cre;C-Ret*$^{lx/lx}$ retina. **(C)** Some synaptic ribbons (arrows) were found to be mislocalized between cell nuclei in ONL, which were supposed to be found in outer plexiform layer. All other synaptic ribbons were found floating in the cytoplasm (arrowheads) and did not associate with an arciform density nor with the presynaptic membrane. **(D)** Higher magnification of the TEM images is shown in the rectangle of **(C)**. Orphan presynaptic density surrounded by synaptic vesicles (arrow) and irregularly shaped floating ribbons were shown in *Chx10-Cre;C-Ret*$^{lx/lx}$ retinae. **(E)** Three ultrastructural appearance of the ribbon synaptic complexes (arrows) of photoreceptor terminals were shown. **(F)** Higher magnification of the TEM images, shown in the rectangles of **(E)**, displayed an abnormal terminal with postsynaptic elements but without presynaptic ribbon (arrow). Although synaptic vesicles could still be observed, they seemed to be aggregated (arrowhead) rather than in their typical, individual form. Scale bars: **(A,E)**, 1 μm; **(B,D,F)**, 300 nm; **(C)**, 2 μm.

DISCUSSION

In this study, we generated retinal *Ret*-specific knockout mice using the Cre/loxP system and demonstrated a possible role for *Ret* in retinal function. First, we found severely abnormal ERG patterns, especially those of b-waves, in conditional *Ret*-knockout retinas. Second, we identified gradually reduced levels of immunoreactivity for α-internexin—a marker of processes of horizontal cells—as *Chx10-Cre;C-Ret*$^{lx/lx}$ mice increased in age.

Third, deficiency of *Ret* in the retina caused the mislocalization of synapses in the ONL, as demonstrated by immunostaining for PKC-α and synaptophysin. Finally, ultrastructural observations of conditional *Ret*-knockout retinas revealed that the synaptic ribbons were immature and not fully assembled, which may explain the abnormal ERG results.

The function of *Ret* in the retina was well assessed by full-field ERG in previous studies. *Ret* hypomorphic mice, which exhibit severely reduced *Ret* activity, do not survive beyond 3 weeks and display significantly reduced scotopic a-waves, b-waves, and photopic b-waves at postnatal day 18 (Brantley et al., 2008). In this study, the *Chx10-Cre;C-Ret*$^{lx/lx}$ mice, which had conditional retinal *Ret* deficiency, exhibited a prolonged survival time and a selective reduction in b-waves, but normal a-waves, on ERG performed at 12 months of age. As such, this waveform was deemed an electronegative ERG and suggested a dysfunction of the ON bipolar cells. In addition to bipolar cells, it was also hypothesized that reduced b-waves could result from the impaired horizontal cells if their inhibition to bipolar cells was switched off (Goetze et al., 2010). Taken together, these results indicate that sufficient *Ret* expression is required for normal retinal function and development.

GDNF and other GFLs (ARTN, NRTN, and PSPN) share the RET receptor tyrosine kinase as their common signaling receptor. A previous study revealed a thinner and disorganized OPL in *NRTN*$^{-/-}$ mice, suggesting that the aberrant morphology of photoreceptors, bipolar cells, and horizontal cells was caused by NRTN deficiency (Brantley et al., 2008). Moreover, GDNF can increase the proliferation, promote the differentiation, and prevent the programmed death of chicken rod photoreceptors, as assessed using re-aggregated retinal spheroids as an *in vitro* assay model (Rothermel and Layer, 2003). Another GDNF-family receptor alpha-4 (GFRα4)-deficient retinal culture study showed a decrease in the number of amacrine cells, horizontal cells, and blue-sensitive cone photoreceptors in this system (Rothermel et al., 2006). In our study, the immunoreactivities of α-internexin and PKC-α were altered in *Chx10-Cre;C-Ret*$^{lx/lx}$ mice. These results indicate that *Ret* dysfunction may trigger an abnormal morphology in horizontal cells and bipolar cell processes, and provided evidence that GFLs, GDNF-family receptors (GFRs), or the RET receptor tyrosine kinase can specifically affect distinct photoreceptors and other retinal cell subpopulations.

It was reported that GDNF can be produced by glial cells to increase the survival rate of a retinal ganglion or photoreceptor cells in different experimental models, such as the rescue of retinal ganglion cells after axotomy (Koeberle and Ball, 1998), the delivery of a protective effect in mice with glaucoma (Johnson et al., 2011), or the protection of photoreceptors in the *rd1* mouse (Frasson et al., 1999). Furthermore, GDNF also moderately protected the rat retina from ischemia–reperfusion injury, possibly by preventing apoptosis in retinal cells (Wu et al., 2004). These previous studies suggested that, in the absence of GDNF, retinal cells lose a protective factor, which might lead to serious retinal dysfunction or degeneration. In addition, a previous study demonstrated that GDNF partially restored ureteric branching morphogenesis in *Ret*-deficient mice with severe renal hypodysplasia, possibly through the induction of Met phosphorylation, rather than through RET signaling (Popsueva et al., 2003). This implies that it is also possible that GDNF partially signals independently of RET through the GDNF-family receptor alpha-1 (GFRα1) and Met phosphorylation in the retina. In fact, the GFL–GFRα1 complex activates Met kinase indirectly via Src kinases in the absence of RET kinase (Popsueva et al., 2003). The GFLs can also interact directly with heparan sulfate proteoglycans to activate Met kinase, which might be mediated by a neural cell adhesion molecule (N-CAM) (Sariola and Saarma, 2003). Our results revealed that the thickness of the ONL was decreased at the stage of 12 and 24 months; however, there were no significant differences between *C-Ret*$^{lx/lx}$ and *Chx10-Cre;C-Ret*$^{lx/lx}$ mice. Moreover, the processes of horizontal cells were significantly reduced, and the immunoreactivities of synaptophysin and PKC-α demonstrated the presence of mislocalized synapses in the ONL. Despite these alterations, the retinas of *Chx10-Cre;C-Ret*$^{lx/lx}$ mice did not show severe disorganization. We speculated that GDNF signaling independently of RET and via GFRα1 might explain why the retinas of *Chx10-Cre;C-Ret*$^{lx/lx}$ mice failed to show severe dysfunction or disorganization.

GDNF is also known as one of the neurotrophic factors that play key roles in the development and survival of neurons. Neurotrophic factors generally include the neurotrophin family [NGF, BDNF, neurotrophin-3 (NT-3), and NT-4/5], the GDNF family (GDNF, NRTN, ARTN, and PSPN), and the CNTF, which is a member of the interleukin 6 (IL-6) family of cytokines. Different factors can act in a sequential, simultaneous, additive (synergistical), or mutual-inhibition fashion. For instance, subpopulations of developing sensory and motor neurons are dependent on the simultaneous action of GDNF and BDNF (Henderson, 1996). Moreover, a combination of GDNF and CNTF was reported to afford higher protection to photoreceptors in a retinal degeneration (rd) mouse (Ogilvie et al., 2000). In our study, *Chx10-Cre;C-Ret*$^{lx/lx}$ mouse retinas had deletion of RET, which is the canonical GDNF receptor, but did not show severe dysfunction or disorganization. According to the studies mentioned above, another explanation for the resulting mild dysfunction following RET deletion is that the remaining neurotrophic factors—which remained unaffected—compensated for the effects of knocking out the RET signaling pathway. However, this study did not investigate the neurotrophic factors or possible signaling pathways independent of RET that may play roles in the retinas of *Chx10-Cre;C-Ret*$^{lx/lx}$ mice. Therefore, further research is required to clarify the mechanisms underlying these observations.

The ribbon complex of retinal photoreceptor synapses represents a specialization of the cytomatrix at the active zone that is present at conventional synapses. The active zones of synapses are highly organized structures designed for the regulated and site-specific release of neurotransmitters. The function of photoreceptor ribbons was suggested to be the continuous shuttling of vesicles to the active zone, for fusion and the release of glutamate (Lenzi and von Gersdorff, 2001). In a previous study, ribbons in *Bassoon (Bsn)*-mutant mouse retinas did not attach to the active zone, thus potentially

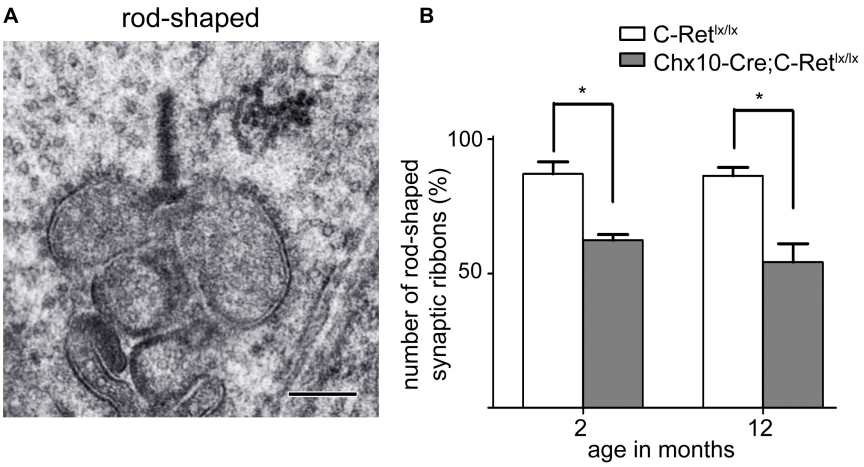

FIGURE 9 | Rod-shaped synaptic ribbons of photoreceptors disintegrated in *Chx10-Cre;C-Ret*$^{lx/lx}$ mice. **(A)** A typical rod-shaped synaptic ribbon is shown in the large presynaptic terminal. Scale bar: 300 nm. **(B)** Quantification was performed to investigate the number of rod-shaped synaptic ribbons in retinae of *C-Ret*$^{lx/lx}$ and *Chx10-Cre;C-Ret*$^{lx/lx}$ mice at the age of 2 and 12 months. The histogram was plotted using mean values ± standard error of the mean (SEM). * Denotes $p < 0.05$ in Student's *t*-test ($n = 3$).

resulting in the failure of synaptic transmission. Moreover, the a-waves of the ERG recordings performed in the *Bsn*-mutant mouse were not affected, whereas their b-waves, representing the response of the ON bipolar cells, were significantly reduced in amplitude and prolonged in implicit time (Dick et al., 2003). Our ultrastructural observation revealed the inappropriate assembly of synaptic ribbons, which then failed to anchor themselves to the active zone. Moreover, a severely affected ERG was recorded in the retinas of *Chx10-Cre;C-Ret*$^{lx/lx}$ mice, implying that conditional deletion of *Ret* in the retina may cause a dysfunction in synaptic transmission. In addition, other findings demonstrated that the co-administration of the fibroblast growth factor 2 (FGF-2) and GDNF can promote the long-term survival of target-deprived adult mouse spiral ganglion neurons (Wei et al., 2007). Furthermore, GDNF was shown to contribute to synaptic development and maturation in ventral midbrain dopaminergic neurons and spinal cord motoneurons (Bourque and Trudeau, 2000). Therefore, conditional deletion of *Ret*, the canonical GDNF receptor, may affect retinal development and cause morphological and physiological alterations in *Chx10-Cre;C-Ret*$^{lx/lx}$ mouse retinas.

Our study has documented dendritic sprouting in aging Ret-deficient mouse retinae. The outgrowth of bipolar cell dendrites was reported to be observed under some pathologic conditions, such as retinal detachment (Fisher et al., 2005), the nob2 mouse with a calcium channel Cav1.4 null mutation (Bayley and Morgans, 2007) and Bsn mice lacking functional Bassoon protein (Dick et al., 2003). A study of the RCS rat whose retina underwent progressive photoreceptor degeneration also demonstrated dendritic sprouting of rod bipolar cells (Cuenca et al., 2005). Furthermore, NRTN-deficient mice—a model deficit in one of GDNF family ligands—also showed abnormally located synapses in the ONL (Brantley et al., 2008). This study also suggested that the abnormal synapse formation in the ONL caused deficits in the signaling of photoreceptor to bipolar cell and contributed to the ERG defects which was similar to what we have observed at 2–24 month of *Chx10-Cre;C-Ret*$^{lx/lx}$ mice. However, a previous study indicated that the dendrites of rod bipolar cells, normally confined to the OPL, were found to extend into the ONL in normal aging retina and tended to increase in length and incidence with the age (Liets et al., 2006). Although the effect of aging could not be excluded in the abnormal synaptic formation of the Ret-deficient retina, the results of our ERG recordings, comparing *C-Ret*$^{lx/lx}$ and *Chx10-Cre;C-Ret*$^{lx/lx}$ mice at the age of 12 months, indicated that the *Chx10-Cre;C-Ret*$^{lx/lx}$ mice may have dysfunctional bipolar cells. Additionally, a previous study speculated that reduced synaptic efficacy may induce new neuronal growth and the formation of ectopic synapses in *Basson* mutant mice (Dick et al., 2003). Therefore, combining our ERG and morphological results, we deduced that inadequate Ret expression may increase the formation of ectopic synapses and exacerbate these to a dysfunctional level. While not evaluated here, further studies should look to investigate the specific molecular mechanisms mediating the genesis and function of ectopic synapses in Ret-deficient mice.

CONCLUSION

In conclusion, our results provide evidence of the role of *Ret* in retinal development, which is essential to maintain the processes of horizontal cells and preserve the integrity of the OPL by stabilizing the structure of the synaptic ribbons. The *Chx10-Cre;C-Ret*$^{lx/lx}$ mice developed in this study provided a valuable model in which to study *Ret* function in the retina and enhanced the understanding of *Ret* function in postnatal development and later stages. Finally, these conditional *Ret*-knockout mice might be useful for investigating the importance of GFL-mediated RET

activation in the retina of animal models of other diseases, such as neurodegenerative diseases or genetic disorders.

DATA AVAILABILITY STATEMENT

The raw data supporting the conclusions of this article will be made available by the authors, without undue reservation.

ETHICS STATEMENT

The animal study was reviewed and approved by the National Taiwan University Animal Ethics Committee.

AUTHOR CONTRIBUTIONS

W-HP conceived of the study, carried out the ultrastructure observation, drafted the manuscript, and final approval of the manuscript submission. M-LL participated in the design of the experiment and edited the manuscript. W-CH and C-YL carried out the antibody sensitivity test, immunohistochemical staining, and PCR experiment. SL edited the manuscript. Y-JT contributed with the electroretinography and data analysis. L-KY and K-JC contributed with the data analysis and interpretation. C-LC and N-KW designed the study, revised the work critically for important intellectual content, and gave their final approval of the version to be published. All the authors contributed to and approved the final manuscript.

FUNDING

This research was supported by grants to C-LC (106-2312-B-002-003 and 105-2320-B-002-008-MY3) from the Ministry of Science and Technology, Taiwan; a grant to W-HP (Isu-108-01-16A) from I-Shou University; grants to N-KW (NSC 102-2314-B-182-102-MY3) between 2013 and 2016 from the Ministry of Science and Technology, Taiwan; Vagelos College of Physicians & Surgeons Grants Program to N-KW from Columbia University Irving Medical Center, grants from National Eye Institute to N-KW (R01EY031354) and to Core Support for Vision Research (5P30EY019007). The content is solely the responsibility of the authors and does not necessarily represent the official views of the National Institutes of Health.

ACKNOWLEDGMENTS

We thank the staff of the imaging core at the First Core Labs, National Taiwan University College of Medicine, for technical assistance. We would also like to acknowledge Dr. Rüdiger Klein, director and scientific member at the Max Planck Institute of Neurobiology, for kindly providing the $Ret^{Ret\ <\ tm1.1Kln\ >}$ mice.

SUPPLEMENTARY MATERIAL

The Supplementary Material for this article can be found online at: https://www.frontiersin.org/articles/10.3389/fnins.2021.728905/full#supplementary-material

Supplementary Figure 1 | Calbindin staining of horizontal cells in *C-Ret*$^{lx/lx}$ and *Chx10-Cre;C-Ret*$^{lx/lx}$ retinas. Immunostaining against calbindin (green), a specific marker for horizontal cells, followed by counterstaining with Hoechst dye to indicate cell nuclei (blue) is shown. Compared to those of *C-Ret*$^{lx/lx}$ mice **(A–D)**, confocal microscopic images of horizontal cells at 2 month **(E)**, 4 months **(F)**, 12 months **(G)**, and 24 months **(H)** of *Chx10-Cre;C-Ret*$^{lx/lx}$ mice displayed a progressed decrease in calbindin-positive immunoreactivity with an increase in age. ONL, outer nuclear layer; OPL, outer plexiform layer; INL, inner nuclear layer; IPL, inner plexiform layer; GCL, ganglion cell layer. Scale bar, 25 μm.

Supplementary Figure 2 | Mislocalization of photoreceptor synaptic terminals observed in *Chx10-Cre;C-Ret*$^{lx/lx}$ mice. Retinal sections of animals aged 2, 4, 12, and 24 months were immunostained with an anti-PKC-α antibody (green) and an anti-PSD95 antibody (red), to label rod bipolar cells and the synapses of photoreceptors, respectively, followed by counterstaining with Hoechst dye, to indicate cell nuclei (blue) **(A–H)**. The processes of rod bipolar cells formed synapses with photoreceptors in the OPL of *C-Ret*$^{lx/lx}$ mice at all ages **(A–D)** and *Chx10-Cre;C-Ret*$^{lx/lx}$ mice at the ages of 2 and 4 months **(E–F)**. However, extended rod bipolar cell dendrites and ectopic photoreceptor terminals (arrows) in the ONL were observed in 12- and 24-month-old *Chx10-Cre;C-Ret*$^{lx/lx}$ mice **(G,H)**. ONL, outer nuclear layer; OPL, outer plexiform layer; INL, inner nuclear layer. Scale bar, 10 μm.

REFERENCES

Airaksinen, M. S., and Saarma, M. (2002). The GDNF family: signalling, biological functions and therapeutic value. *Nat. Rev. Neurosci.* 3, 383–394. doi: 10.1038/nrn812

Bayley, P. R., and Morgans, C. W. (2007). Rod bipolar cells and horizontal cells form displaced synaptic contacts with rods in the outer nuclear layer of the nob2 retina. *J. Comp. Neurol.* 500, 286–298. doi: 10.1002/cne.21188

Berger, A., Cavallero, S., Dominguez, E., Barbe, P., Simonutti, M., Sahel, J.-A., et al. (2014). Spectral-domain optical coherence tomography of the rodent eye: highlighting layers of the outer retina using signal averaging and comparison with histology. *PLoS One* 9:e96494. doi: 10.1371/journal.pone.0096494

Bourque, M. J., and Trudeau, L. E. (2000). GDNF enhances the synaptic efficacy of dopaminergic neurons in culture. *Eur. J. Neurosci.* 12, 3172–3180. doi: 10.1046/j.1460-9568.2000.00219.x

Brantley, M. A. Jr., Jain, S., Barr, E. E., Johnson, E. M. Jr., and Milbrandt, J. (2008). Neurturin-mediated ret activation is required for retinal function. *J. Neurosci.* 28, 4123–4135. doi: 10.1523/JNEUROSCI.0249-08.2008

Chien, C. L., and Liem, R. K. (1995). The neuronal intermediate filament, alpha-internexin is transiently expressed in amacrine cells in the developing mouse retina. *Exp. Eye Res.* 61, 749–756. doi: 10.1016/s0014-4835(05)80026-0

Chinskey, N. D., Besirli, C. G., and Zacks, D. N. (2014). Retinal cell death and current strategies in retinal neuroprotection. *Curr. Opin. Ophthalmol.* 25, 228–233. doi: 10.1097/ICU.0000000000000043

Costantini, F., and Shakya, R. (2006). GDNF/Ret signaling and the development of the kidney. *Bioessays* 28, 117–127. doi: 10.1002/bies.20357

Cuenca, N., Pinilla, I., Sauvé, Y., and Lund, R. (2005). Early changes in synaptic connectivity following progressive photoreceptor degeneration in RCS rats. *Eur. Neurosci.* 22, 1057–1072. doi: 10.1111/j.1460-9568.2005.04300.x

Dick, O., Tom Dieck, S., Altrock, W. D., Ammermüller, J., Weiler, R., Garner, C. C., et al. (2003). The presynaptic active zone protein bassoon is essential for photoreceptor ribbon synapse formation in the retina. *Neuron* 37, 775–786. doi: 10.1016/s0896-6273(03)00086-2

Durbec, P., Marcos-Gutierrez, C. V., Kilkenny, C., Grigoriou, M., Wartiowaara, K., Suvanto, P., et al. (1996). GDNF signalling through the Ret receptor tyrosine kinase. *Nature* 381, 789–793. doi: 10.1038/381789a0

Ernsberger, U. (2008). The role of GDNF family ligand signalling in the differentiation of sympathetic and dorsal root ganglion neurons. *Cell Tissue Res.* 333, 353–371. doi: 10.1007/s00441-008-0634-4

Errijgers, V., Van Dam, D., Gantois, I., Van Ginneken, C. J., Grossman, A. W., D'Hooge, R., et al. (2007). FVB.129P2-Pde6b(+) Tyr(c-ch)/Ant, a sighted variant of the FVB/N mouse strain suitable for behavioral analysis. *Genes Brain Behav.* 6, 552–557. doi: 10.1111/j.1601-183X.2006.00282.x

Fisher, S. K., Lewis, G. P., Linberg, K. A., and Verardo, M. R. (2005). Cellular remodeling in mammalian retina: results from studies of experimental retinal detachment. *Prog. Retin. Eye Res.* 24, 395–431. doi: 10.1016/j.preteyeres.2004.10.004

Frasson, M., Picaud, S., Leìveillard, T., Simonutti, M., Mohand–Said, S., Dreyfus, H., et al. (1999). Glial cell line–derived neurotrophic factor induces histologic and functional protection of rod photoreceptors in the rd/rd mouse. *Investig. Ophthalmol. Vis. Sci.* 40, 2724–2734.

Gabriel, R., Lesauter, J., Silver, R., Garcia-Espana, A., and Witkovsky, P. (2001). Diurnal and circadian variation of protein kinase C immunoreactivity in the rat retina. *J. Comp. Neurol.* 439, 140–150. doi: 10.1002/cne.1338

Goetze, B., Schmidt, K. F., Lehmann, K., Altrock, W. D., Gundelfinger, E. D., and Lowel, S. (2010). Vision and visual cortical maps in mice with a photoreceptor synaptopathy: reduced but robust visual capabilities in the absence of synaptic ribbons. *Neuroimage* 49, 1622–1631. doi: 10.1016/j.neuroimage.2009.10.019

Heidelberger, R., Thoreson, W. B., and Witkovsky, P. (2005). Synaptic transmission at retinal ribbon synapses. *Prog. Retin. Eye Res.* 24, 682–720. doi: 10.1016/j.preteyeres.2005.04.002

Henderson, C. E. (1996). Role of neurotrophic factors in neuronal development. *Curr. Opin. Neurobiol.* 6, 64–70. doi: 10.1016/s0959-4388(96)80010-9

Henderson, C. E., Phillips, H. S., Pollock, R. A., Davies, A. M., Lemeulle, C., Armanini, M., et al. (1994). GDNF: a potent survival factor for motoneurons present in peripheral nerve and muscle. *Science (New York, NY)* 266, 1062–1064. doi: 10.1126/science.7973664

Johnson, T. V., Bull, N. D., and Martin, K. R. (2011). Neurotrophic factor delivery as a protective treatment for glaucoma. *Exp. Eye Res.* 93, 196–203. doi: 10.1016/j.exer.2010.05.016

Koeberle, P. D., and Ball, A. K. (1998). Effects of GDNF on retinal ganglion cell survival following axotomy. *Vision Res.* 38, 1505–1515. doi: 10.1016/s0042-6989(97)00364-7

Kramer, E. R., Aron, L., Ramakers, G. M., Seitz, S., Zhuang, X., Beyer, K., et al. (2007). Absence of Ret signaling in mice causes progressive and late degeneration of the nigrostriatal system. *PLoS Biol.* 5:e39. doi: 10.1371/journal.pbio.0050039

Kramer, E. R., Knott, L., Su, F., Dessaud, E., Krull, C. E., Helmbacher, F., et al. (2006). Cooperation between GDNF/Ret and ephrinA/EphA4 signals for motor-axon pathway selection in the limb. *Neuron* 50, 35–47. doi: 10.1016/j.neuron.2006.02.020

Lenzi, D., and von Gersdorff, H. (2001). Structure suggests function: the case for synaptic ribbons as exocytotic nanomachines. *Bioessays* 23, 831–840. doi: 10.1002/bies.1118

Liets, L. C., Eliasieh, K., van der List, D. A., and Chalupa, L. M. (2006). Dendrites of rod bipolar cells sprout in normal aging retina. *Proc. Natl. Acad. Sci. U.S.A.* 103:12156. doi: 10.1073/pnas.0605211103

Lin, L. F., Doherty, D. H., Lile, J. D., Bektesh, S., and Collins, F. (1993). GDNF: a glial cell line-derived neurotrophic factor for midbrain dopaminergic neurons. *Science (New York, NY)* 260, 1130–1132. doi: 10.1126/science.8493557

LoGiudice, L., and Matthews, G. (2009). The role of ribbons at sensory synapses. *Neuroscientist* 15, 380–391. doi: 10.1177/1073858408331373

Mattapallil, M. J., Wawrousek, E. F., Chan, C. C., Zhao, H., Roychoudhury, J., Ferguson, T. A., et al. (2012). The Rd8 mutation of the Crb1 gene is present in vendor lines of C57BL/6N mice and embryonic stem cells, and confounds ocular induced mutant phenotypes. *Invest. Ophthalmol. Vis. Sci.* 53, 2921–2927. doi: 10.1167/iovs.12-9662

Mead, B., Thompson, A., Scheven, B. A., Logan, A., Berry, M., and Leadbeater, W. (2014). Comparative evaluation of methods for estimating retinal ganglion cell loss in retinal sections and wholemounts. *PLoS One* 9:e110612. doi: 10.1371/journal.pone.0110612

Meng, X., Lindahl, M., Hyvonen, M. E., Parvinen, M., de Rooij, D. G., Hess, M. W., et al. (2000). Regulation of cell fate decision of undifferentiated spermatogonia by GDNF. *Science (New York, NY)* 287, 1489–1493. doi: 10.1126/science.287.5457.1489

Moore, M. W., Klein, R. D., Farinas, I., Sauer, H., Armanini, M., Phillips, H., et al. (1996). Renal and neuronal abnormalities in mice lacking GDNF. *Nature* 382, 76–79. doi: 10.1038/382076a0

Nag, T. C., and Wadhwa, S. (2001). Differential expression of syntaxin-1 and synaptophysin in the developing and adult human retina. *J. Biosci.* 26, 179–191. doi: 10.1007/BF02703642

Ogilvie, J. M., Speck, J. D., and Lett, J. M. (2000). Growth factors in combination, but not individually, rescue rd mouse photoreceptors in organ culture. *Exp. Neurol.* 161, 676–685. doi: 10.1006/exnr.1999.7291

Popsueva, A., Poteryaev, D., Arighi, E., Meng, X., Angers-Loustau, A., Kaplan, D., et al. (2003). GDNF promotes tubulogenesis of GFRalpha1-expressing MDCK cells by Src-mediated phosphorylation of Met receptor tyrosine kinase. *J. Cell. Biol.* 161, 119–129. doi: 10.1083/jcb.200212174

Rothermel, A., and Layer, P. G. (2003). GDNF regulates chicken rod photoreceptor development and survival in reaggregated histotypic retinal spheres. *Invest. Ophthalmol. Vis. Sci.* 44, 2221–2228. doi: 10.1167/iovs.02-0915

Rothermel, A., Volpert, K., Burghardt, M., Lantzsch, C., Robitzki, A. A., and Layer, P. G. (2006). Knock-down of GFRalpha4 expression by RNA interference affects the development of retinal cell types in three-dimensional histiotypic retinal spheres. *Invest. Ophthalmol. Vis. Sci.* 47, 2716–2725. doi: 10.1167/iovs.05-1472

Rowan, S., and Cepko, C. L. (2004). Genetic analysis of the homeodomain transcription factor Chx10 in the retina using a novel multifunctional BAC transgenic mouse reporter. *Dev. Biol.* 271, 388–402. doi: 10.1016/j.ydbio.2004.03.039

Sariola, H., and Saarma, M. (2003). Novel functions and signalling pathways for GDNF. *J. Cell. Sci.* 116(Pt 19), 3855–3862. doi: 10.1242/jcs.00786

Schuchardt, A., D'Agati, V., Larsson-Blomberg, L., Costantini, F., and Pachnis, V. (1994). Defects in the kidney and enteric nervous system of mice lacking the tyrosine kinase receptor Ret. *Nature* 367, 380–383. doi: 10.1038/367380a0

Sterling, P., and Matthews, G. (2005). Structure and function of ribbon synapses. *Trends Neurosci.* 28, 20–29. doi: 10.1016/j.tins.2004.11.009

Takahashi, M. (2001). The GDNF/RET signaling pathway and human diseases. *Cytokine Growth Factor Rev.* 12, 361–373. doi: 10.1016/s1359-6101(01)00012-0

Wang, N. K., Tosi, J., Kasanuki, J. M., Chou, C. L., Kong, J., Parmalee, N., et al. (2010). Transplantation of reprogrammed embryonic stem cells improves visual function in a mouse model for retinitis pigmentosa. *Transplantation* 89, 911–919. doi: 10.1097/TP.0b013e3181d45a61

Wei, D., Jin, Z., Jarlebark, L., Scarfone, E., and Ulfendahl, M. (2007). Survival, synaptogenesis, and regeneration of adult mouse spiral ganglion neurons in vitro. *Dev. Neurobiol.* 67, 108–122. doi: 10.1002/dneu.20336

Will, E., Klump, H., Heffner, N., Schwieger, M., Schiedlmeier, B., Ostertag, W., et al. (2002). Unmodified Cre recombinase crosses the membrane. *Nucleic Acids Res.* 30, e59. doi: 10.1093/nar/gnf059

Wu, W. C., Lai, C. C., Chen, S. L., Sun, M. H., Xiao, X., Chen, T. L., et al. (2004). GDNF gene therapy attenuates retinal ischemic injuries in rats. *Mol. Vis.* 10, 93–102.

Yan, Q., Wang, J., Matheson, C. R., and Urich, J. L. (1999). Glial cell line-derived neurotrophic factor (GDNF) promotes the survival of axotomized retinal ganglion cells in adult rats: comparison to and combination with brain-derived neurotrophic factor (BDNF). *J. Neurobiol.* 38, 382–390. doi: 10.1002/(sici)1097-4695(19990215)38:3<382::aid-neu7<3.0.co;2-5

Conflict of Interest: The authors declare that the research was conducted in the absence of any commercial or financial relationships that could be construed as a potential conflict of interest.

Publisher's Note: All claims expressed in this article are solely those of the authors and do not necessarily represent those of their affiliated organizations, or those of the publisher, the editors and the reviewers. Any product that may be evaluated in this article, or claim that may be made by its manufacturer, is not guaranteed or endorsed by the publisher.

Advantages of publishing in Frontiers

OPEN ACCESS
Articles are free to read for greatest visibility and readership

FAST PUBLICATION
Around 90 days from submission to decision

HIGH QUALITY PEER-REVIEW
Rigorous, collaborative, and constructive peer-review

TRANSPARENT PEER-REVIEW
Editors and reviewers acknowledged by name on published articles

Frontiers
Avenue du Tribunal-Fédéral 34
1005 Lausanne | Switzerland

Visit us: www.frontiersin.org
Contact us: frontiersin.org/about/contact

REPRODUCIBILITY OF RESEARCH
Support open data and methods to enhance research reproducibility

DIGITAL PUBLISHING
Articles designed for optimal readership across devices

FOLLOW US
@frontiersin

IMPACT METRICS
Advanced article metrics track visibility across digital media

EXTENSIVE PROMOTION
Marketing and promotion of impactful research

LOOP RESEARCH NETWORK
Our network increases your article's readership